NUREG/CR-3318
HEDL-TME 84-1

LWR PRESSURE VESSEL SURVEILLANCE DOSIMETRY IMPROVEMENT PROGRAM:

PCA EXPERIMENTS, BLIND TEST, AND PHYSICS-DOSIMETRY SUPPORT FOR THE PSF EXPERIMENTS

Hanford Engineering Development Laboratory

Edited by:
W.N. McElroy

Prepared for U.S. Nuclear Regulatory Commission

NUREG/CR-3318
HEDL-TME 84-1
R5

LWR PRESSURE VESSEL SURVEILLANCE DOSIMETRY IMPROVEMENT PROGRAM:

PCA EXPERIMENTS, BLIND TEST, AND PHYSICS-DOSIMETRY SUPPORT FOR THE PSF EXPERIMENTS

Hanford Engineering Development Laboratory

Operated by Westinghouse Hanford Company
P.O. Box 1970 Richland, WA 99352
A Subsidiary of Westinghouse Electric Corporation

Edited by:
W.N. McElroy

Manuscript Completed: August 1984
Date Published: September 1984

Prepared for
Office of Nuclear Regulatory Research
U.S. Nuclear Regulatory Commission
Washington, DC 20555
NRC FIN B5988

ACKNOWLEDGMENTS

The success of the LWR Pressure Vessel Surveillance Dosimetry Improvement Program (LWR-PV-SDIP) continues to depend on the efforts and the free exchange of ideas and views by representatives of a large number of research, service, regulatory, vendor, architect/engineer, and utility organizations. The information reported herein could not have been developed without the continuing support of the respective funding organizations and their management and technical staffs. Special acknowledgment is due to C. Z. Serpan of NRC for having identified the need for an international program such as the LWR-PV-SDIP and for making it possible by taking a strong overall support and management lead.

The dedication and professional skill of the PCA operations team at ORNL contributed significantly to the success of the experimental program. The authors are indebted to staff members of the ORNL Operating Division Technical Service Group for their contributions and for their support to individual experimenters.

Additional acknowledgment is due to B. R. Hayward, R. L. Knecht, W. F. Sheely, and H. H. Yoshikawa of HEDL for their constructive comments and help in the preparation and review of program documentation. Very special acknowledgment is given to J. M. Dahlke and N. E. Kenny who edited this document, and to HEDL Publications and Communications, Word Processing, Graphics, and Duplicating personnel, who contributed to its preparation. Last but not least the credit is due to D. C. Smith of the HEDL Irradiation Environment Group, who assisted in the preparation and typing of the HEDL contributions for this document.

NUREG/CR-3318
HEDL-TME 84-1
R5

LWR PRESSURE VESSEL SURVEILLANCE DOSIMETRY IMPROVEMENT PROGRAM: PCA EXPERIMENTS, BLIND TEST, AND PHYSICS-DOSIMETRY SUPPORT FOR THE PSF EXPERIMENTS

Edited by

W. N. McElroy

FOREWORD

To account for neutron radiation damage in setting pressure-temperature limits and making fracture analyses, neutron-induced changes in fracture toughness and embrittlement for power reactor pressure vessel steels must be predicted, then checked by extrapolation of surveillance program data during the vessel's service life. Uncertainties in the predicting methodology can be significant. The main variables of concern are associated with:

1) *Steel chemical composition and microstructure*
2) *Steel irradiation temperature*
3) *Power plant configurations and dimensions - core edge to surveillance to vessel wall to support structure positions*
4) *Core power distribution*
5) *Reactor operating history*
6) *Reactor physics computations*
7) *Selection of neutron exposure units*
8) *Dosimetry measurements*
9) *Neutron spectral effects*
10) *Neutron dose rate effects*

Variables associated with the physical measurement of pressure vessel steel property changes are not considered here.

This and the previous "PCA Experiments and Blind Test" report have been prepared to:

1) *Serve as a general reference document containing benchmarked experimental and theoretical data and information required to determine and certify the accuracy of the experimental and analytical methods and data that are recommended in a series of ASTM LWR pressure vessel surveillance standards and are associated with the variables 3), 4), 6), 7), 8) and 9).*

2) *Provide detailed experimental and theoretical results to determine the limiting accuracy of transport theory calculations for predicting dosimetry sensor reaction rates and derived values of neutron exposure parameters (total fluence, fluence greater than 0.1 and 1.0 MeV, and dpa) for LWR pressure vessel benchmark fields simulating steel-water configurations of commercial power reactors.*

3) *Assess the accuracy of the methodology used to translate measured pressure vessel steel damage and exposure data (and the corresponding uncertainties) obtained at surveillance locations to the pressure vessel beltline region.*

4) *Provide PCA 4/12 and 4/12 SSC configurations' experimental and theoretical physics-dosimetry results in support of the "PSF Experiments and Blind Test."*

After an executive summary, a description of the PCA experimental test facility is provided in Section 1 followed by the presentation and discussion of experimental measurements and data in Sections 2, 3 and 4. The results of neutronic calculations by participants are given and referenced in Section 5. Current PCA specifications for transport theory validation are given in Section 6. The comparison and evaluation of measured and derived data are considered in Section 7.

CONTENTS

CONTENTS (Cont'd)

CONTENTS (Cont'd)

CONTENTS (Cont'd)

ACRONYMS

AEEW	Atomic Energy Establishment, Winfrith, UK
AERE	Atomic Energy Research Establishment, Winfrith, UK
ASTM	American Society for Testing and Materials
BNL	Brookhaven National Laboratory
B&W	Babcock & Wilcox Co.
BSR	Bulk Shielding Reactor
BWR	Boiling Water Reactor
CE	Combustion Engineering, Inc.
C/E	Calculated-to-Experimental
CEA	Atomic Energy Commission, France
CEN/SCK or SCK/CEN	Center for the Study of Nuclear Energy, Mol, Belgium
dpa	Displacements per atom
dps	Displacements per second
DT	Dead-time
EFPY	Effective full-power years
ENDF/B-IV & V	Evaluated Nuclear Data Files, Versions IV and V
EOL	End-of-Life
EPRI	Electric Power Research Institute, Palo Alto, CA
ESP	Emulsion Scanning Processor
ETZ	Extrapolations-to-Zero
FET	Field Effect Transistor
FSAR	Final Safety Analysis Report
FWHM	Full Width Half Maximum
HAFM	Helium Accumulation Fluence Monitor

ACRONYMS (Cont'd)

HEDL	Hanford Engineering Development Laboratory
HFIR	High Flux Isotope Reactor
ILRR	Interlaboratory Reaction Rate (Program)
KFA	Kernforshungsanlage (Nuclear Research Center)
LWR	Light Water Reactor
MTR	Material Test Reactor
NBS	National Bureau of Standards
NESDIP	NESTOR Reactor Surveillance Dosimetry Improvement Program Facility, Winfrith, UK
NRC	US Nuclear Regulatory Commission
NRE	Nuclear Research Emulsions
NRL	Naval Research Laboratory
ORNL	Oak Ridge National Laboratory
ORR	Oak Ridge (Research) Reactor
PCA	Pool Critical Assembly at ORNL
PSF	Poolside Facility of the ORR at ORNL
PV	Pressure Vessel
PVF	Pressure Vessel Front or Front of the Pressure Vessel Simulator
PVS	Pressure Vessel Simulator
PWR	Pressurized Water Reactor
RC	Resistive-Capacitive
RM	Radiometric
RMS	Root Mean Square
RPV	Reactor Pressure Vessel

ACRONYMS (Cont'd)

RTS	Rise-Time Spectra
SDMF	Surveillance Dosimetry Measurement Facility
SSC	Simulated Surveillance Capsule
SSTR	Solid State Track Recorder
TEC	Thermoelectric Cooler
TLD	Thermoluminescent Dosimeter
TS	Thermal Shield
TSB	Thermal Shield Back
TSF	Thermal Shield Front
UK	United Kingdom
US	United States
VB	Void Box
VENUS	Critical Facility, Mol, Belgium
1/4 T, 1/2 T, 3/4 T	Depths in a pressure vessel simulator block of total thickness, T
8/7, 12/13	PCA Blind Test Configurations (Actual dimensions given in Mc81, Sections 1.1 and 8.1)
4/12 SSC	PCA Engineering Mockup of PSF Metallurgical PV Test Facility (Actual dimensions given in Mc81, Section 8.1)
4/12	The above mockup without SSC

S.0 EXECUTIVE SUMMARY

W. N. McElroy (HEDL), F. B. K. Kam (ORNL), J. A. Grundl and E. D. McGarry (NBS), A. Fabry (CEN/SCK), and C. Z. Serpan (NRC)

S.1 OVERVIEW OF LWR PRESSURE VESSEL SURVEILLANCE

S.1.1 Surveillance Programs and ASTM Standards

The United States Nuclear Regulatory Commission (NRC) established the Light Water Reactor Pressure Vessel (LWR-PV) Surveillance Dosimetry Improvement Program in 1977 to improve, standardize and maintain dosimetry, damage correlation and the associated reactor analysis procedures and data used for predicting the integrated effects of neutron exposure to LWR-PVs (Se80).

The main focus of the research efforts presently underway is the LWR power reactor surveillance program in which metallurgical test specimens of the reactor PV and dosimetry sensors are placed in three to five surveillance capsules at or near the reactor PV inner wall. They are then irradiated in a temperature and neutron flux-spectrum environment as similar as possible to the PV itself for periods of time of about 1.5 to 15 effective full-power years (EFPY), with removal of the last capsule at a fluence corresponding to the 30- to 40-year plant end-of-life (EOL) fluence.

The surveillance capsule metallurgical and dosimetry results are used to verify and/or adjust the final safety analysis report's (FSAR) current and EOL projections of changes in the fracture toughness and embrittlement condition of the PV steel. The derived plant specific PV steel condition, in turn, determines the pressure-temperature operating curve used for the continued operation of the power plant.

The research underway has resulted in a series of American Society for Testing and Materials (ASTM) Standard Practices, Guides and Methods (see Figure S.1*) (As83,Mc84). These standards, and the recommended procedures and data contained therein, are to be used for:

- Calculating neutron flux-spectra and exposure parameters (total fluence, thermal fluence (E < 0.4 eV) (T), intermediate fluence (0.4 eV < E < 1.0 MeV) (I), fluences greater than 0.1 (FP1), 1.0 MeV (F1), and 6.0 MeV (F6) and dpa).

---

*These standards are identified and discussed in the ASTM Standard E706, "Master Matrix for LWR Pressure Vessel Surveillance Standards," Reference As83. The 1984 Annual Book of ASTM Standards will contain an updated version of the E706 Standard.

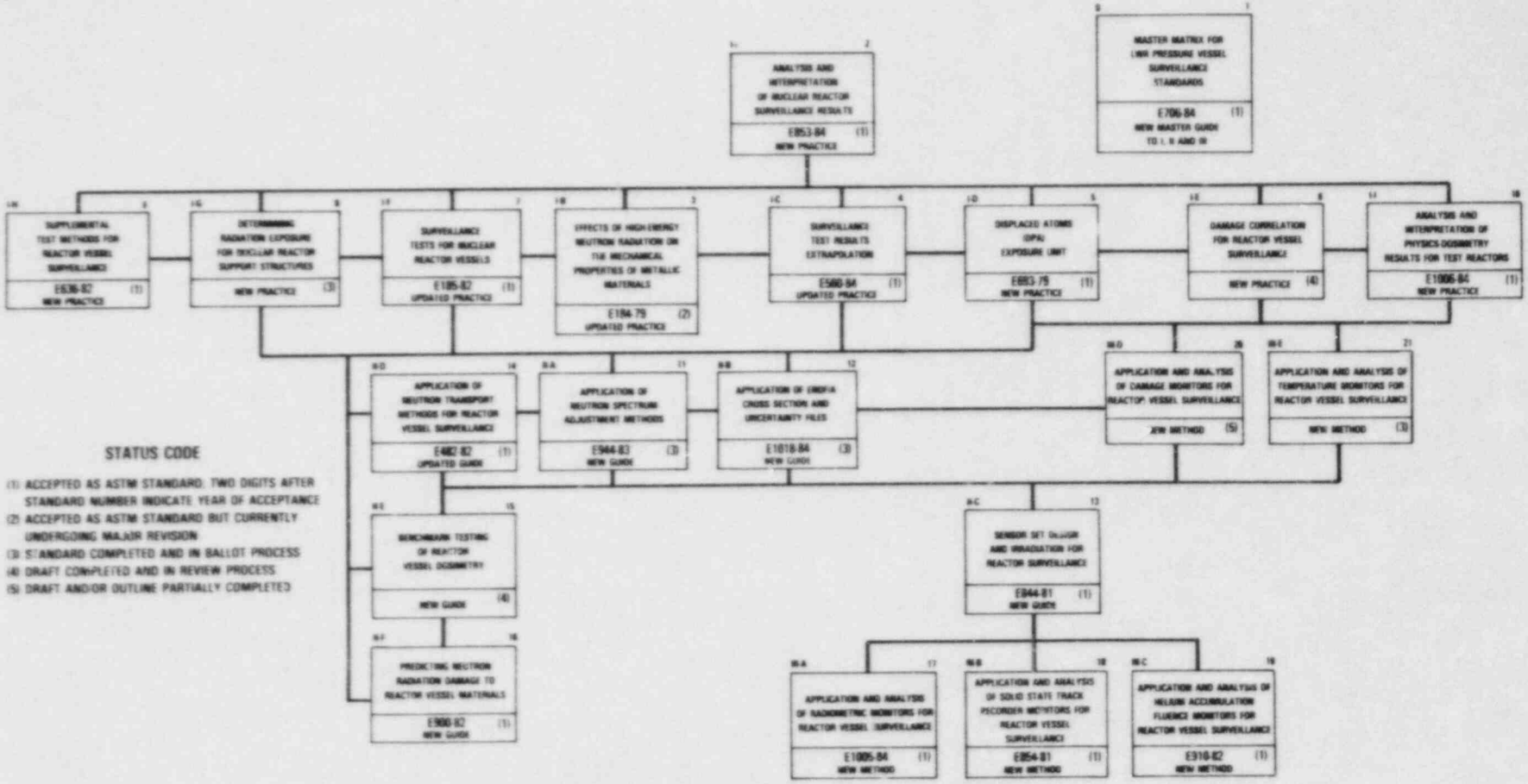

FIGURE S.1. ASTM Standards for Surveillance of LWR Nuclear Reactor Pressure Vessels and Their Support Structures.

- Performing and analyzing neutron dosimetry.
- Evaluating and correlating the neutron-induced radiation damage measured in surveillance capsule metallurgical specimens.
- Applying the results to current and EOL projections of the condition of LWR-PV and support structure steel materials and components.

A vigorous research effort attacking the same measurement and analysis problems exists worldwide, and strong cooperative links between the NRC supported activities at HEDL, ORNL, NBS and MEA-ENSA and those supported by CEN/SCK (Mol, Belgium), EPRI (Palo Alto, USA), KFA (Jülich, Germany) and several UK laboratories have been extended to a number of other countries and laboratories (Mc80,Mc81,Mc81a,Mc82,Mc82a,Mc84). These cooperative links have been strengthened by the active membership of the scientific staff of many of the participating countries and laboratories in the ASTM E10 Committee on Nuclear Technology and Applications, a number of whose subcommittees are responsible for the preparation of LWR-PV surveillance standards (He82).

S.1.2 Facilities and Programs

S.1.2.1 Summary Overview

In order to meet the needs of the LWR-PV-SDIP, simulated LWR-PV environments have been established throughout the world. Tables S-1 and S-2 provide summary information on research reactor and commercial PWR and BWR neutron/gamma-ray benchmark field facilities, respectively. Each of the highly specialized research reactor and the commercial facilities has been established to address specific LWR-PV-SDIP problem areas of importance to PWR and BWR reactor design, operation, safety, and licensing and regulatory issues. Description and use of these benchmark field facilities in the LWR-PV-SDIP have been adequately described elsewhere. The reader is referred to the LWR-PV-SDIP 1984 Annual Report (Mc84) for summary and updated program information on most of these facilities (As83,Al83,Au82,Au82a,Au83,Br82a, Fa79,Fa80a,Fa82,Fa82a,Fa83,Fa83a,Gr75b,G477a,Gr77b,Gr78,Gr78a,Gr81,Gr82, Ka82a,Ma81a,Ma81c,Ma81d,Ma82b,Mc81,Mc82a,Mc84,Se82,Sn82,St83a,St83b,Ti80, Ts82).

S.1.2.2 PCA Replica

To obtain additional experimental data for clarifying anomalies found in the PCA analysis and for validating techniques under development at RR&A Ltd and Winfrith in estimating RPV damage parameters, a PCA REPLICA experiment has been carried out at Winfrith. The REPLICA experiment duplicates precisely the PCA 12/13 configuration with the important exception that the reactor

TABLE S.1

LWR-PV BENCHMARK FIELD FACILITIES*

Benchmark Field Facility	Location	Anticipated Operation Schedule	Main Purpose
$^{252}Cf/^{235}U$	NBS, US	1975-Open	Standard fields for c oss-section testing and validation; emphasis is on equivalent fission flux calibrations and RM fluence counting standard.
PCA-PV	ORNL, US	1978-84	Data base for the "PCA Physics-Dosimetry Blind Test": Low-power experimental/calculational benchmark for different LWR-PV configurations; emphasis is on verification of radial neutron exposure gradients and lead factors; i.e., confirmation of radial through-wall fracture toughness and embrittlement predictions.
PSF-PV	ORNL, US	1980-84	Data base for the "PSF Physics-Dosimetry-Metallurgy Blind Test": High-power LWR-PV physics-dosimetry-metallurgical test; emphasis is on high-temperature and high-fluence simulation of PWR environmental conditions and verification of neutron damage gradients; i.e., confirmation of radial through-wall fracture toughness and embrittlement predictions.
PSF-SDMF	ORNL, US	1979-Open	High-power LWR-PV benchmark: Emphasis is on verification of surveillance capsule perturbations; specific RM, SSTR, HAFM, and DM verification tests, and quality assurance evaluations of commercial dosimetry materials and services; i.e., confirmation of the physics-dosimetry methods, procedures, and data recommended for in-situ in- and ex-vessel surveillance programs.
VENUS	CEN/SCK, Mol, Belgium	1982-Open	Low-power LWR-PV core source boundary benchmark: Emphasis is on verification of effects of new and old fuel management schemes and accuracy of azimuthal lead factors; i.e., confirmation of azimuthal PV-wall fracture toughness and embrittlement predictions.
NESDIP	AEEW, Winfrith, UK	1982-Open	Low-power LWR-PV cavity benchmark: Emphasis is on different PWR configurations and verification, via cavity measurements, of neutron exposure gradients and lead factors; i.e., confirmation of radial through-wall fracture toughness and embrittlement predictions.
DOMPAC	CEA, Fontenay, France	1980-1983	Low-fluence experimental/calculational benchmark for a specific PWR configuration: Emphasis is on verification of surveillance capsule perturbations and PV-wall neutron exposure and damage gradients; i.e., confirmation of radial PV-wall fracture toughness and embrittlement predictions.

*Acronyms:
- AEEW - Atomic Energy Establishment (Winfrith, UK).
- CEA - Commissariat a l' Energie Atomique (France).
- CEN/SCK - Centre d' Etude de l'Energie Nucleaire-Studiecentrum voor Kernernergie (Mol, Belgium).
- DOMPAC - Triton Reactor Thermal Shield and Pressure Vessel Mockup (Fontenay-aux-Roses, France).
- UK - United Kingdom.
- NBS - National Bureau of Standards, US.
- PCA-PV - Pool Critical Assembly Physics-Dosimetry Pressure Vessel Mockup (ORNL).
- ORNL - Oak Ridge National Laboratory.
- PSF-PV - Oak Ridge Research (ORR) Reactor Pool Side Facility Physics-Dosimetry-Metallurgy Pressure Vessel Mockup.
- PSF-SDMF - PSF Simulated Dosimetry Measurement Facility at the ORR.
- VENUS - Critical Facility (Mol, Belgium).
- NESDIP - NESTOR Reactor Surveillance Dosimetry Improvement Program Facility (Winfrith, UK).
- PWR - Pressurized Water Reactor.

TABLE S.2

POWER REACTORS BEING USED BY LWR-PV-SDIP PARTICIPANTS TO BENCHMARK PHYSICS-DOSIMETRY PROCEDURES AND DATA FOR PRESSURE VESSELS AND SUPPORT STRUCTURE SURVEILLANCE*

(Plant name; reactor type/supplier; reactor operator; ex-vessel cavity (C) and in-vessel (V) surveillance positions available)

Energy Range (MeV)	Type of Dosimeter	Dosimetry Reaction	Nuclear One-1 PWR/B&W Arkansas Power & Light		Nuclear One-2 PWR/CE Arkansas Power & Light		Brown's Ferry-3 BWR/GE Tennessee Valley Authority		H.B. Robinson PWR/WEC Carolina Power & Light		Maine Yankee PWR/CE Maine Yankee Atomic Power		Point Beach-2 PWR/WEC Wisconsin Electric Power		McGuire PWR/WEC Duke Power		CR or DB PWR/B&W [1]		Oconee 1,2&3 PWR/B&W Duke Power [1]		BR-3 PWR/WEC Belgium	
			C	V	C	V	C	V	C	V	C	V	C	V	C	V	C	V	C	V	C	V
>1.5	RMs	$^{63}Cu(n,\alpha)^{60}Co$ [f]	Y		Y	Y	Y	Y	Y	Y	Y	Y		Y	Y	Y	P	Y	P		Y	Y
		$^{46}Ti(n,p)^{46}Sc$ [f]	Y		Y	Y	Y	Y	Y	Y	Y	Y			Y		P	P	PYJ		Y	Y
		$^{54}Fe(n,p)^{54}Mn$ [f]	Y	Y	Y	Y	Y	Y	Y	Y	Y	Y		Y	Y	Y	P	Y	PY	Y	Y	Y
		$^{58}Ni(n,p)^{58}Co$ [f]	Y	Y	Y	Y	Y	Y	Y	Y	Y	Y		Y	Y	Y	P	Y	PY	Y	Y	Y
		$^{238}U(n,f)^{140}Ba$-La	Y	(N)	Y	(N)	Y	Y	(N)	(N)	(N)	(N)	(N)	(N)	(N)	(N)	(N)	(N)	(N)	(N)	(N)	(N)
		$^{238}U(n,f)^{103}Ru$	(Y)	Y	(Y)	(Y)	Y	Y	Y	Y	Y	Y			Y	Y	P	Y	P	Y	Y	Y
		$^{238}U(n,f)^{95}Zr$-Nb	(Y)	Y	(Y)	(Y)	Y	Y	Y	Y	Y	Y			Y	Y	P	Y	P	Y	Y	Y
		$^{238}U(n,f)^{137}Cs$	(Y)	Y	(Y)	Y	Y	Y	Y	Y	Y	Y			Y	Y	P	Y	P	Y	Y	Y
		$^{232}Th(n,f)^{140}Ba$-La		(N)		(N)	(N)	(N)	(N)	(N)	(N)	(N)	(N)	(N)	(N)	(N)	(N)	(N)	(N)	(N)	(N)	
		$^{232}Th(n,f)^{95}Zr$-Nb					Y	Y									P	P				
		$^{232}Th(n,f)^{137}Cs$					Y	Y									P	P				
		$^{237}Np(n,f)^{140}Ba$-La	Y	(N)	Y	(N)	Y	Y	(N)	(N)	(N)	(N)	(N)	(N)	(N)	(N)	P	(N)	(N)	(N)		(N)
>0.4		$^{237}Np(n,f)^{103}Ru$	(Y)	Y	(Y)	(Y)	Y	Y	Y	Y	Y	Y			Y	Y	P	Y	P	Y		Y
		$^{237}NP(n,f)^{95}Zr$-Nb	(Y)	Y	(Y)	(Y)	Y	Y	Y	Y	Y	Y			Y	Y	P	Y	P	Y		Y
		$^{237}Np(n,f)^{137}Cs$	(Y)	Y	(Y)	Y	Y	Y	Y	Y	Y	Y			Y	Y	P	Y	P	Y		Y
		$^{93}Nb(n,n')^{93m}Nb$							Y	Y	Y	Y		Y	Y	Y	P	P	P			Y
		$^{59}Co(n,\gamma)^{60}Co$ [e]	Y	Y	Y	Y	Y	Y	Y	Y	Y	Y		Y	Y	Y	P	Y	PY	Y	Y	Y
		$^{109}Ag(n,\gamma)^{110m}Ag$ [e]	Y		Y	Y	Y	Y	Y	Y	Y	Y			Y		P	P	P		Y	Y
		$^{58}Fe(n,\gamma)^{59}Fe$	Y	Y	Y	Y	Y	Y	Y	Y	Y	Y			Y		P	Y	PY	Y	Y	Y
5×10^{-7}		$^{45}Sc(n,\gamma)^{46}Sc$ [e]	Y		Y	Y	Y	Y	Y		Y	Y			Y		P	P	PY		Y	Y
to 0.5 [b]		$^{235}U(n,f)^{140}Ba$-La	Y	(N)	Y	(N)	Y	Y	(N)	(N)	(N)	(N)	(N)	(N)	(N)		(N)	(N)	(N)	(N)		(N)
		$^{235}U(n,f)^{103}Ru$	(Y)		(Y)		Y	Y	Y	Y	Y	Y			Y		P	P	P			Y
		$^{235}U(n,f)^{95}Zr$-Nb	(Y)		(Y)		Y	Y	Y	Y	Y	Y			Y		P	P	P			Y
		$^{235}U(n,f)^{137}Cs$	(Y)		(Y)		Y	Y	Y	Y	Y	Y			Y		P	P	P			Y
As Above [a]	SSTRs [g]	$^{238}U(n,f)FP$					Y		Y	Y	Y	Y			Y		P	P	P			
		$^{232}Th(n,f)FP$					Y								Y		P	P	P			
		$^{237}Np(n,f)FP$					Y		Y	Y	Y	Y			Y		P	P	P			
		$^{235}U(n,f)FP$					Y		Y	Y	Y	Y			Y		P	P	P			
		$^{239}Pu(n,f)FP$					Y														Y	
<0.1		$^{6}Li(n,\alpha)$															P	P	P			
		$^{10}B(n,\alpha)$															P	P	P			
>0.3		H(n,p) as CR-39		N		N		N		N		N	(N)	N		N	(P)	N	(P)			N
>4	RMs, HRFMs [d]	Ni(n,He) as metal [f]							(Y)	Y	(Y)	Y		Y	(Y)	Y	(P)	P	(Y)		(Y)	(Y)
		Al(n,He) as metal [f]	N		N		N		N	Y	(N)	Y		Y	N	Y	N	P	N		N	(Y)
		Cu(n,He) as metal [f]	N		N		N		N	Y	(N)	Y		Y	N	Y	N	P	N		N	(Y)
		Fe(n,He) as metal [f,h]	N		N		N		N	Y	(N)	Y		Y	N	Y	N	P	N		N	(Y)
>0.1 [b]		$^{7}Li(n,He)$ as LiF															P	P				
		Be(n,He) as metal								Y	Y						P	P				(Y)
		S(n,He) as PbS									Y						P	P				
		F(n,He) as PbF_2									Y						P	P				
		Ca(n,He) as CaF_2									Y						P	P				
		N(n,He) as MoN or TiN									Y						P	P				(Y)
		Cl(n,He) as $PbCl_2$									Y						P	P				
		O(n,He) as GeO_2															P	P				
<0.1		$^{6}Li(n,He)$ as LiF or alloy								Y	Y						P	P				(Y)
		$^{10}B(n,He)$ nat. or alloy								Y	Y						P	P				(Y)
>0.1	DMs [c]	Quartz															P	P				
		Sapphire								Y							P	P				
		A302B [f,k]								Y				Y			P	P				
		A533B [f,k]								Y				(Y)		Y	P	P				
		Other Steel [f]								Y		Y				Y	P	P				P

FOOTNOTES* for Table S.2

[a]Energy ranges for the solid state track recorders (SSTRs) are the same as those given for the fissionable radiometric sensors.

[b]Generally these reactions are used with cadmium, cadmium-oxide or gadolinium filters to eliminate their sensitivity to neutrons having energies less than 0.5 eV. The cavity measurements in the Arkansas Power & Light reactors have also included intermediate-energy measurements using thick (1.65 g/cm^2) ^{10}B filters (shells) for the ^{235}U, ^{238}U and ^{237}Np-fission sensors.

[c]DM means damage monitors (damage to the sensor crystal lattice, such as sapphire, A302B and A533B or other steels with high copper and nickel content and high sensitivity to damage).

[d]HAFM means helium accumulation fluence monitors.

[e]Generally cobalt and silver are included as dilute alloys with aluminum. Scandium is normally Sc_2O_3, and more recently is included as a ~0.1% Sc_2O_3-MgO ceramic wire.

[f]Frequently when there is no specific HAFM dosimetry package, some radiometric sensors and some steel damage monitors serve as HAFMs after they have been analyzed for their principal function.

[g]Ni and/or Fe gradient disks were also included in the SSTR capsule, as required.

[h]Iron is from RM sensors or Charpy specimens. Postirradiation determination of the boron content of these sensors has been noted to permit direct measurement of the thermal fluence.

[i]CR means power plant Crystal River-3 (Florida Power Corp.) and DB means Davis Besse-1 (Toledo Edison Co.)

[j]The Y following the P refers to a previous Oconee 2 test.

[k]This is surveillance capsule reference correlation material (ASTM reference steel plates).

[l]The determination (or feasibility) of using any of the Oconee plants for future benchmark studies has yet to be made.

GE - General Electric
WEC - Westinghouse Electric Company
B&W - Babcock and Wilcox
CE - Combustion Engineering

Y - Yes, this type of dosimetry has been used.
P - This type is planned for use.
N - This type is not desired or cannot be used.
( ) - There is some doubt about any of the letters enclosed in parentheses.

source of the latter was replaced by a thin fission-plate of enriched uranium alloyed with aluminum whose shape and dimensions matched the projection of the PCA source onto the front shield member. Extensive work was carried out, but it seems likely that the simpler source configuration of the Replica experiment can more easily be calibrated with a high degree of accuracy. In addition to this advantage the Replica provides a completely independent check of the findings of the PCA experiment and, if the experiments are found to be consistent, the increased weight of experimental evidence will aid in an understanding of the problem of calculating side shield penetrations.

As indicated above, the Replica experiment described in (Bu84) provides a completely independent complement to the collaborative PCA experiments carried out at Oak Ridge and reported herein and in (Mc81). In the Replica, agreement between calculation and the Winfrith measurements* is excellent at all positions up to the 1/4 T position in the RPV. There is some disagreement between measured and predicted attenuations through the RPV (in view of the use of measurements for diagnostics in the cavities of operating reactors as diagnostics, this discrepancy merits close attention). Additional summary statements from (Bu84) are:

- The tentative suggestion that the iron inelastic scattering cross section used is too large near the threshold energy is consistent with evidence from the Winfrith Iron Benchmark experiment (Ca80), for which a preliminary unpublished analysis indicated reductions of some 15% to 20%.

- The difference between predicted and measured reaction-rate attenuations across the RPV is the only disturbing feature of the calculations that, in general, agree very well with measurements.

- A critical comparison of the Replica and PCA experiments is clearly of value and, following further calculations for the PCA, this will be presented in the Part II Replica Report.

- The accurate prediction of events in an RPV is, of course, a more formidable exercise in an operating reactor than in a tightly controlled benchmark experiment; nevertheless, the latter does enable us to assess, and also minimize, sources of error in the former caused by calculational method and data.

---

*HEDL and other LWR-PV-SDIP program participants' calculational and experimental results will be documented in the Part II Replica Report (see Mc84, Section 2.1.2).

S.2 PCA EXPERIMENTS AND BLIND TEST

S.2.1 · Description of Experiment

As discussed both in (Mc81) and in Section 1, four clean, low neutron flux benchmark arrangements of a simulated LWR Thermal Shield (TS) and PV have been realized and extensively investigated at the PCA. These PCA 8/7, 12/13, 4/12, and 4/12 SSC configurations [X/Y: Water gaps (in cm) from the core edge to the TS/TS-to-vessel] have been the focus of international studies on transport theory methods in LWR-PV physics-dosimetry-metallurgy applications. Further, the PCA 8/7 and 12/13 configurations were the focus of an international Blind Test of transport theory methods (Mc81).

The PCA 4/12 and 4/12 SSC configurations are the focus of an international study of transport theory results in support of the two-year PSF Physics-Dosimetry-Metallurgy Experiment and the PSF Blind Test. Summary information on the PSF Experiment and the Physics-Dosimetry-Metallurgy Blind Test is provided in (Mc84).

Eleven laboratories in the PCA Blind Test, including vendors of power reactors, calculated the neutron flux-spectra and reaction rates of dosimetry sensors for specified locations in the PCA Benchmark. For eight of the laboratories, this was done without prior knowledge of the results of dosimetry measurements performed in the same configurations. Information on the results obtained and the methods used by individual laboratories are documented in (Mc81). The majority of the laboratories used a two-dimensional x-y geometry with some form of leakage correction. Two participants also submitted results from one-dimensional calculations, and one participant used cylindrical geometry for the calculation. One Monte Carlo calculation was also submitted.

As discussed in (Mc81) and in Sections 2 through 4, a large number of dosimetry integral and differential experiments were performed in four different PCA configurations [8/7, 12/13, 4/12, and 4/12 SSC; see (Mc81) and Section 1.0]. Measurements of $^{235}U(n,f)$ Bare and Cd-Covered, $^{237}Np(g,f)$, $^{103}Rh(n,n')$, $^{115}In(n,n')$, $^{238}U(n,f)$, $^{232}Th(n,f)$, $^{58}Ni(n,p)$, and/or $^{27}Al(n,\alpha)$ reaction rates are available at the different experimental locations (see Figures 1.1.2, 1.1.3, 1.1.4, and 1.1.6) in the four configurations; further, more detailed traverses in and out-of-core have also been obtained for some sensors. Nuclear emulsion measurements of the proton-recoil rates (n-p scattering) are available for the 1/4 T positions for the 8/7 and 4/12 configurations, and for the TSB, 1/4 T, 1/2 T, 3/4 T, and VB positions for the 12/13 configuration. Silicon damage rate measurements are available for the 8/7 and 4/12 SSC configurations (Mc81).

To obtain the highest possible accuracy, all measurements [fission chambers, solid state track recorder (SSTR), radiometric (RM), and nuclear research emulsions (NRE)] have been experimentally referenced to standard fission fields at NBS and CEN/SCK. Active neutron and gamma spectroscopy and passive gamma-ray dose measurements have also been performed [see (Mc81) and Sections 3 and 4, respectively].

S.2.2 General Conclusions

As stated in ASTM Standards E853 [E706(IA)], E482 [E706(IID)] and E1006 [E706(II)] (Figure S.1), an accurate transport calculation of the neutron flux-spectrum at several locations is essential for the analysis of integral dosimetry measurements and for predicting irradiation damage exposure parameters in the PV and in the support structures of operating LWR nuclear power plants. Further, values of exposure parameters may be obtained directly from calculations or indirectly from calculations that are adjusted with dosimetry measurements using the procedures recommended in ASTM Standard E944 [E706(IIA)].

The PCA and PCA Replica Experiments and Blind Test provide benchmarked experimental and theoretical data and information that are necessary for the assessment of the limiting accuracy and subsequent validation of physics and dosimetry analytical tools and procedures used in 1) making plant specific FSAR projections and 2) the analysis and interpretation of nuclear reactor surveillance program results. Consequently, this and two other NUREG documents (Mc81 and Bu84) are believed to provide sufficient information for any regulatory body, reactor vendor, service laboratory, or utility to optimally use the PCA Benchmarks, for 1) and 2) above, in their respective areas of responsibility.

The past PCA (Mc81), the present PCA (Section 5), and the PCA Replica (Bu84) computational results support the statement (Fa79) that under idealized environmental conditions (benchmark), modern computational techniques are currently capable of predicting absolute in-vessel neutron reaction rates per unit reactor core power to within $\pm 15\%$ (1σ) (but generally not to within $\pm 5\%$); this is a great improvement compared with the situation prevailing a few years ago, before the PCA experiments were undertaken (Mc79,Mc81a,Fa79), where factors of two or more differences between FSAR predictions and surveillance capsule measurements were not uncommon (see Figure S.2). The achievable accuracy will be markedly less, however, in applications to actual power plants because of new low-leakage neutron core fuel management schemes, geometrical complexities and other factors; all of which will continue to require careful study and evaluation for specific PWR and BWR plants.

For routine LWR power plant calculations using transport methods, the PCA results validate the statement (Se80) "that results can be obtained as accurate as $\pm 15\%$ (1σ) for flux and fluence greater than $E > 1.0$ MeV, if the calculations are properly modeled and subjected to benchmark neutron field verification. Otherwise, errors can be a factor of two or more." For the dpa exposure parameter, the PCA results would support a similar statement.

A new area of concern for LWR surveillance programs and safety, licensing and regulatory issues related to pressurized thermal shock (PTS) (Di82) is the possible contribution of thermal neutrons and helium production from boron and steel to the embrittlement process (Gu84a,Mc84,Mc84e). If it is shown that thermal neutrons and helium are contributing significantly to the

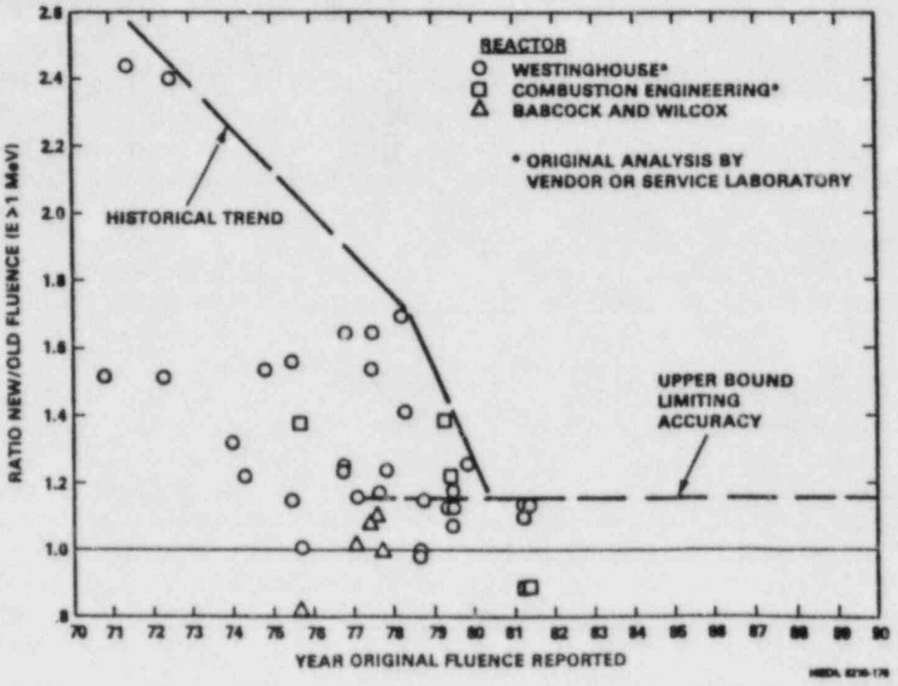

FIGURE S.2. Ratio of New Fluence to Old Fluence as a Function of Reported Old Fluence Data (revision of Si81 data).

RT_{NDT} shift at the PV steel inner and outer surfaces, it will be necessary to better define the thermal component of the neutron flux-fluence-spectrum through the PV wall and within surveillance capsules. No effort has been made to define this component of the neutron field for the present PCA experiments.

S.2.3 Specific Conclusions and Recommendations

1) Compared with the measurements and with reference to the previous Blind Test results (Mc81, Section 7), most calculations showed a trend towards underestimating the fluxes (E > 0.1 and 1.0 MeV) by 5% to 25%, and even more at higher neutron energies and deeper steel penetrations. This raises several relevant questions:

   - How does this tendency imply a general nonconservatism in the safety analysis of LWR-PV integrity in regulatory and economic terms? The general answer is that a bias on the order of 10% to 15% is likely to affect any current in-vessel damage exposure projection; such a bias appears consistent with known uncertainties in the iron cross-section data. This is a small bias compared to all other neutronic, mechanical, chemistry, temperature, stress,...

uncertainties that plague in-vessel embrittlement and crack propagation assessments. Nevertheless, because the bias is nonconservative in a safety sense, it must be factored into the upper bound estimates for in-vessel quarter thickness damage correlation studies.

- To what extent does a specific PCA "validated" calculation justify the applied method and data for their transposition to power reactor analysis? There is no general answer to this question, partly because, in many respects, the PCA benchmark is not prototypic of a generic LWR concept. Consequently, in-depth examination of every submitted calculation (unless it is grossly faulty) is necessary before any statement can be made as to whether calculated-to-experimental (C/E) agreement in PCA or C/E bias in PCA means the same in an actual LWR analysis.

2) Detailed comparisons in terms of the C/E ratios for the $^{58}Ni(n,p)$ and other reactions at different locations are provided in Section 7 and in (Mc81). They show that not only are the calculations generally lower than the experimental values, but that the C/E ratios decrease with increasing distance from the core.* The absolute C/E traverses (Mc81, Section 7.2) clearly establish that discrepancies between integral measurements and transport theory in PCA:

   - Are not a problem of flux normalization.
   - Are $\leq$10% for the damage exposure parameters dpa** and fluence >1 MeV.
   - Are significant (>10%) only at energies >2 MeV and thus involve a spectral shape, but are not a flux scale problem.
   - Are most likely due to inadequacies in the iron nonelastic scattering cross-section data above ~4 to 5 MeV. This is pin-pointed by the results of the sensitivity study in (Mc81), Section 6.1.

3) There is evidence from dosimetry experiments in LWR-PV environments that corrections of up to about 35% for photofission in ^{238}U are necessary to explain experimental results (Si79). If photofission contributions

---

*Here it should be pointed out that NRE sensors bracket the flux above ~0.4 MeV in about 0.1 MeV steps up to 0.7 MeV; $^{237}Np(n,f)$, $^{103}Rh(n,n')$ and $^{115}In(n,n')$ sensors bracket the flux >1.0 MeV; the $^{238}U(n,f)$ and $^{58}Ni(n,p)$ responses are significantly higher in the 1.5- to 2.5-MeV range; while, the $^{27}Al(n,\alpha)$ sensor responds above ~6.0 MeV. Further, the ^{237}Np's response is nearly proportional to dpa in steel (Fa80a).

**Confirmed by silicon damage results in the PCA 4/12 SSC configuration.

are as large as these findings indicate, corrections for this effect would become mandatory for routine LWR-PV neutron dosimetry. As discussed in Section 4.5 and in Mc81, Section 5.0, photo-fission corrections for the PCA measurements have been made, as appropriate, for the fission and (n,n') reactions. Next to ^{232}Th, the largest photofission corrections are required for ^{238}U fission, and they appear to be less than 7% for all PCA configurations and locations. Corrections for fission in ^{237}Np are only about one third as large, and those for the other sensors are negligibly small.

4) Results of the comparisons and consistency checks between calculated and measured integral reaction rate and flux-spectral data are presented in Section 7.0 and in Mc81, Sections 4.0 and 7.0. Included are discussions of the uncertainties in derived values of flux-spectra and exposure parameters (total fluence, fluence > 0.1 MeV and 1.0 MeV, and dpa) based on least-squares analysis using HEDL, ORNL, and RR&A adjustment codes. It is concluded that, in general, values of these exposure parameters can be derived with accuracies in the range of $\pm$5% to $\pm$15% (1σ) for the PCA and similarily benchmarked neutron fields. The accuracy, however, will be generally less in applications to actual power plants due to greater uncertainty in defining core boundary source distributions (particularly for new low-leakage neutron cores), greater complexity of geometric modeling, and a reduced degree of benchmark referencing of both dosimetry and neutron transport calculations.

1.0 DESCRIPTION OF EXPERIMENTAL FACILITY

F. B. K. Kam (ORNL)

SUMMARY

As described in a previous document,* the Pool Critical Assembly (PCA) at the Oak Ridge National Laboratory (ORNL) was the site of an extensive experimental and calculational program to qualify this facility as a reference benchmark field. This report is concerned primarily with the x/y configurations of 4/12, and 4/12 SSC which were performed in support of the metallurgical experiments at the Oak Ridge Research Reactor (ORR) Poolside Facility (PSF). Here the x/y refers to the water gaps (in cm) from the reactor window simulator to the thermal shield/thermal shield to the pressure vessel simulator as shown in Fig. 1.1.1. Current as-built information for the two configurations is provided in Section 1.1 and run-to-run monitoring measurements and absolute normalizations in Section 1.2. The PCA physical parameters and the core power and buckling measurements described in (Mc81) are applicable to this report. This report described the ORR-PSF physics-dosimetry support experiments performed in the PCA and updates any data, recommendations, and conclusions from previous 8/7 and 12/13 configurations.

*(Mc81).

1.1 PHYSICAL DESCRIPTION OF PCA 4/12 and 4/12 SSC CONFIGURATIONS

F. B. K. Kam (ORNL)

The PCA Benchmark Facility established at ORNL consists of the PCA reactor core and the ex-core components that are used to mock up pressure vessel surveillance configurations for LWRs. These ex-core components are the thermal shield (TS), the simulated surveillance capsule (SSC), the pressure vessel simulator (PVS), and the simulated reactor cavity [void box (VB) in PCA]. Because high-power metallurgical irradiations were carried on concurrently at the ORR-PSF for a selected TS, SSC, PVS and VB configuration, an aluminum window that is a permanent part of the ORR was added to the PCA Benchmark Facility. Thus, the PCA Benchmark Facility serves three purposes:

1) To determine how well reactor physics computations predict measurements for several TS, PVS and VB configurations for a representative power reactor pressure vessel wall thickness

2) To assess and improve current in- and ex-vessel state-of-the-art dosimetry techniques

3) To provide technical support for the final TS, SSC, PVS, and VB configuration for the ORR Metallurgical Benchmark Facility.

The PCA core is a light water moderated, enriched uranium fueled, Material Test Reactor (MTR) plate-type elements critical assembly that provides the source of leakage neutrons for the TS-SSC-PVS-VB. The Benchmark Facility components are located in a large pool of water maintained at approximately 37.7°C that provides experimental access to locations in or adjacent to the TS, SSC, PVS, and VB so measurements related to physics, dosimetry, and damage analysis can be made in conditions similar to those existing in a LWR power reactor.

An overall view is given in Fig. 1.1.1, which shows the facility in its water pool. The pool water serves as reactor coolant, moderator, and personnel shielding. The dosimetry measurements were performed in locations A1 through A7 for the 4/12 and 4/12 SSC configurations shown in plan views in Figs. 1.1.2 and 1.1.3. The elevation view is given in Fig. 1.1.4 and a vertical section of the void box is shown in Fig. 1.1.5. Figure 1.1.6 shows the PCA simulated surveillance capsule (SSC) used in Fig. 1.1.3. The SSC centerline is located 5.08 cm below the reactor horizontal midplane and centered relative to the vertical midplane.

The PCA core consists of 25 elements as shown in Fig. 1.1.7. This loading pattern was established after several other loadings were tested and rejected. The criteria for the selection specified: 1) that fuel elements contain essentially no fission products; 2) that fuel elements on the first row facing the experiment should be the same type and should have the same ^{235}U loadings; 3) quarter core symmetry (if practical); 4) that the core be critical with the control rods withdrawn more than 18 inches; and 5) that a fuel element be inserted at core

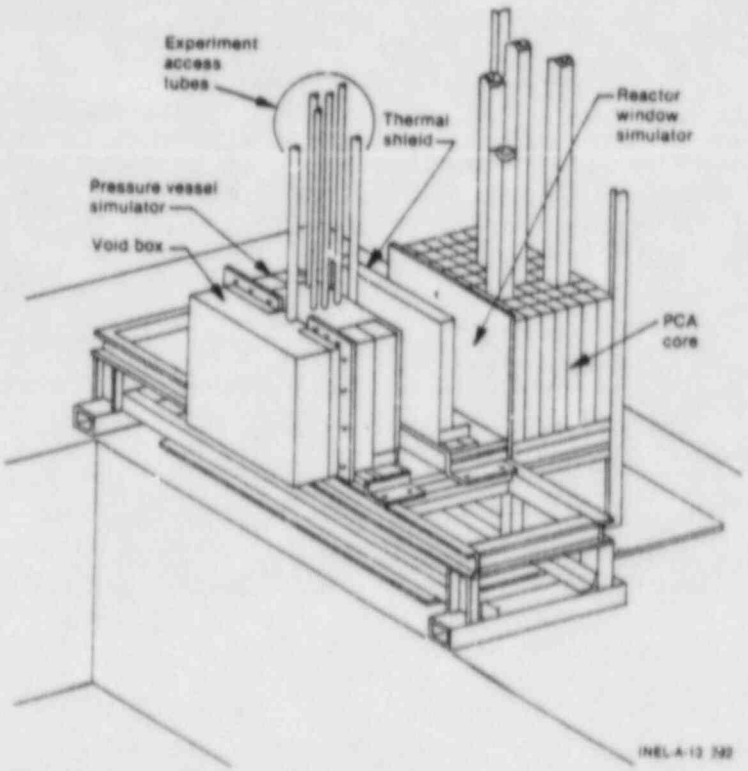

FIGURE 1.1.1. PCA Pressure Vessel Wall Benchmark Facility.

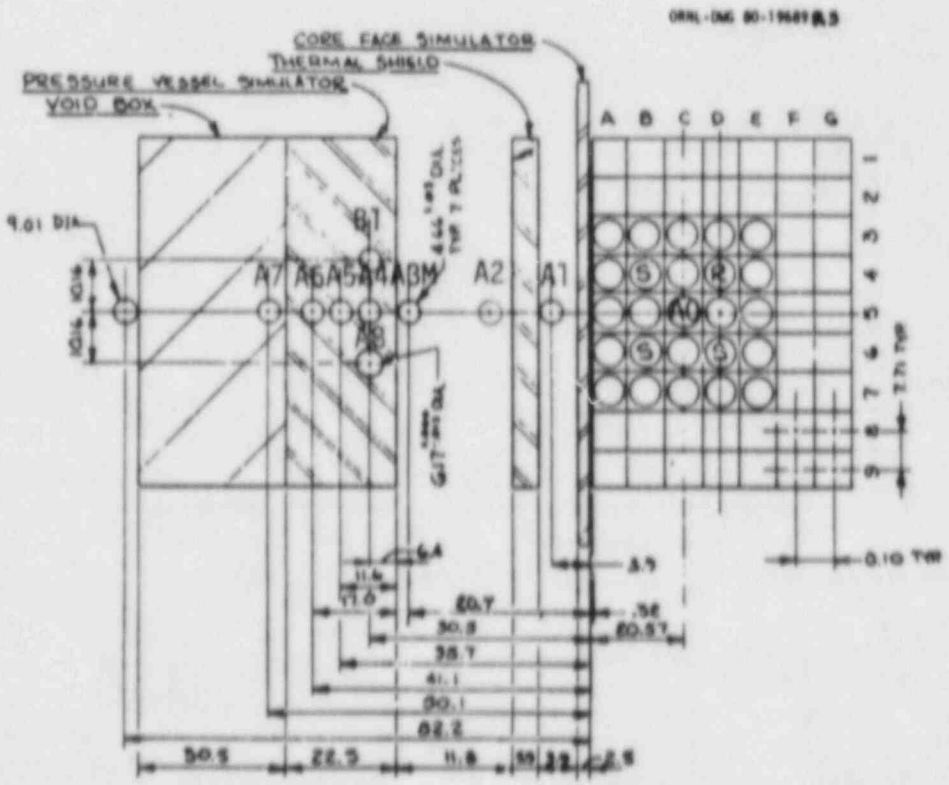

FIGURE 1.1.2. PCA-PV Benchmark Facility - Plan View: 4/12 Configuration. (All dimensions are in cm.)

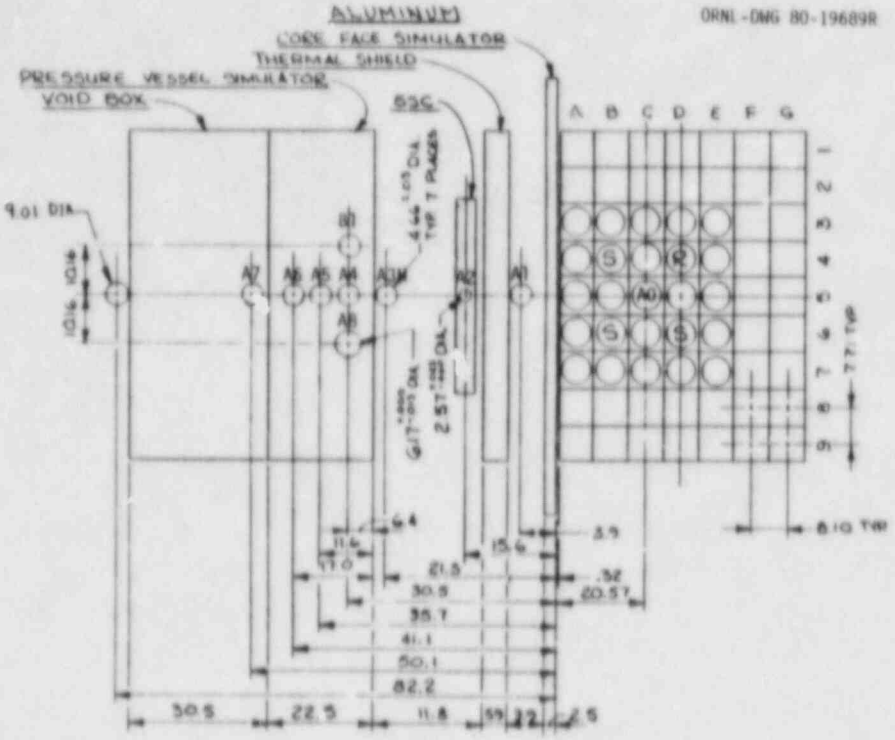

FIGURE 1.1.3. PCA-PV Benchmark Facility - Plan View: 4/12 Configuration with SSC. (All dimensions are in cm.)

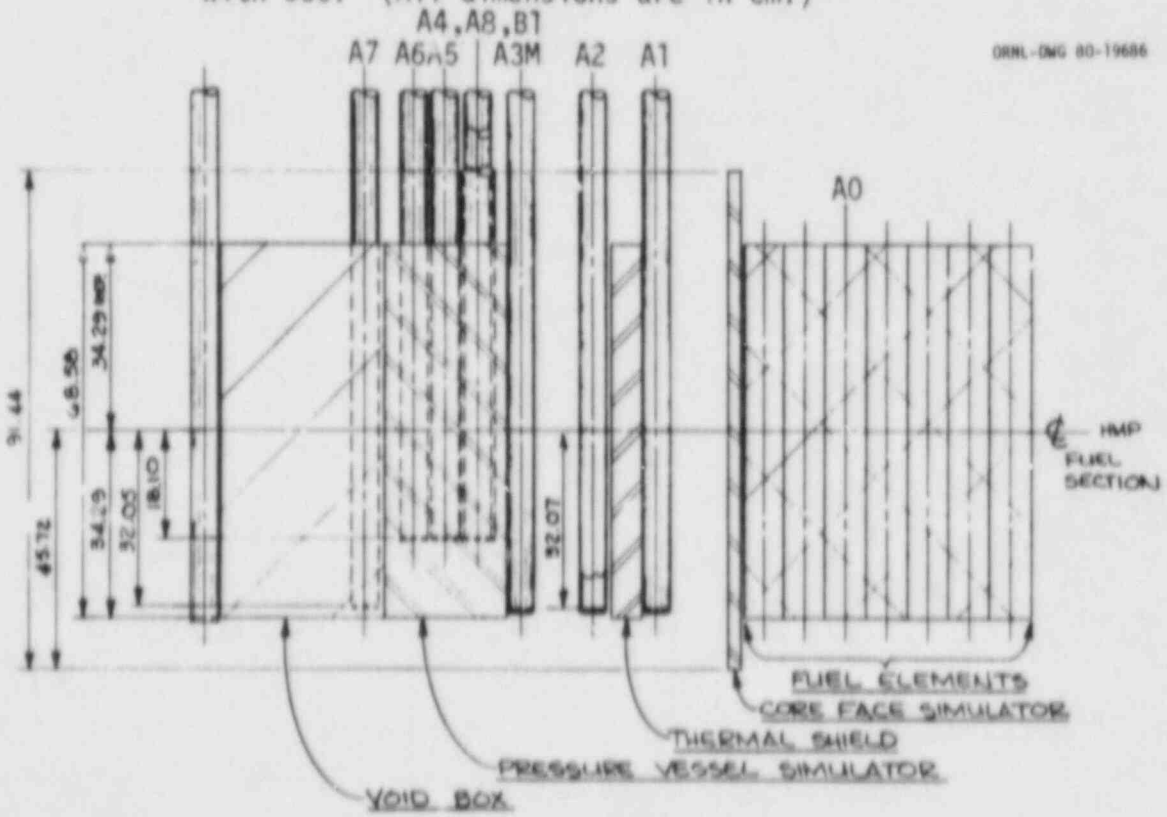

FIGURE 1.1.4. PCA-PV Benchmark Facility - Elevation View. (All dimensions are in cm.)

ORNL-DWG 80-19690

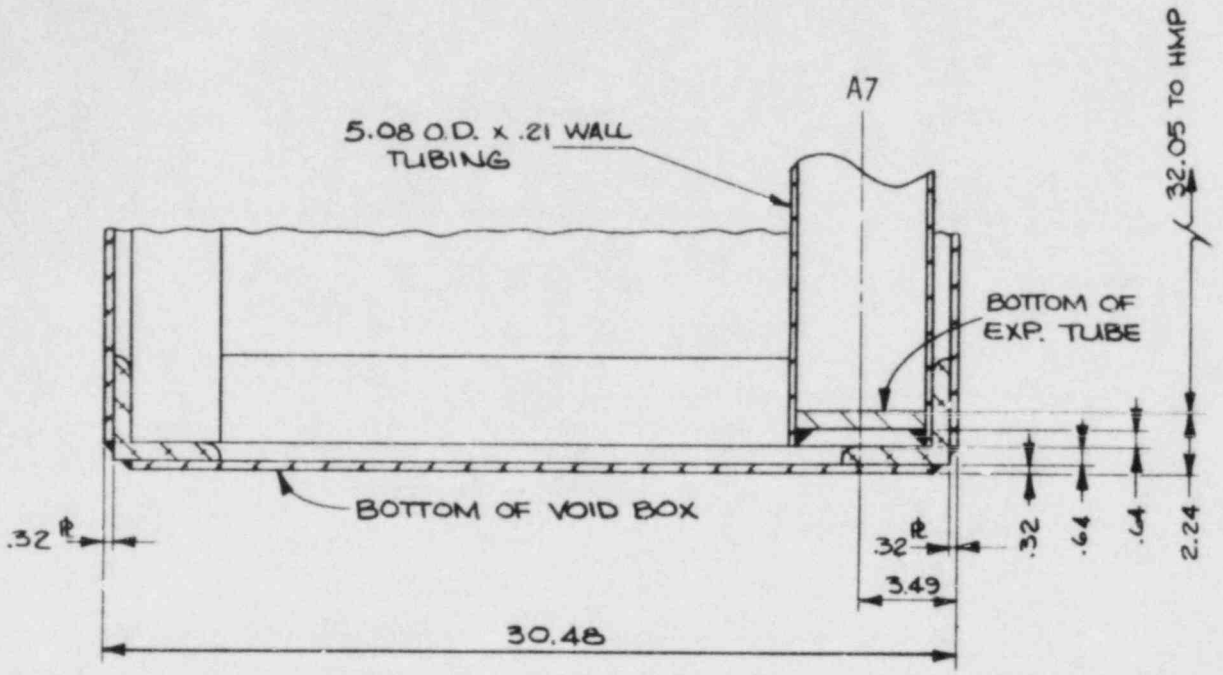

FIGURE 1.1.5. PCA-PV Benchmark Facility Void Box - Section View. (All dimensions are in cm.)

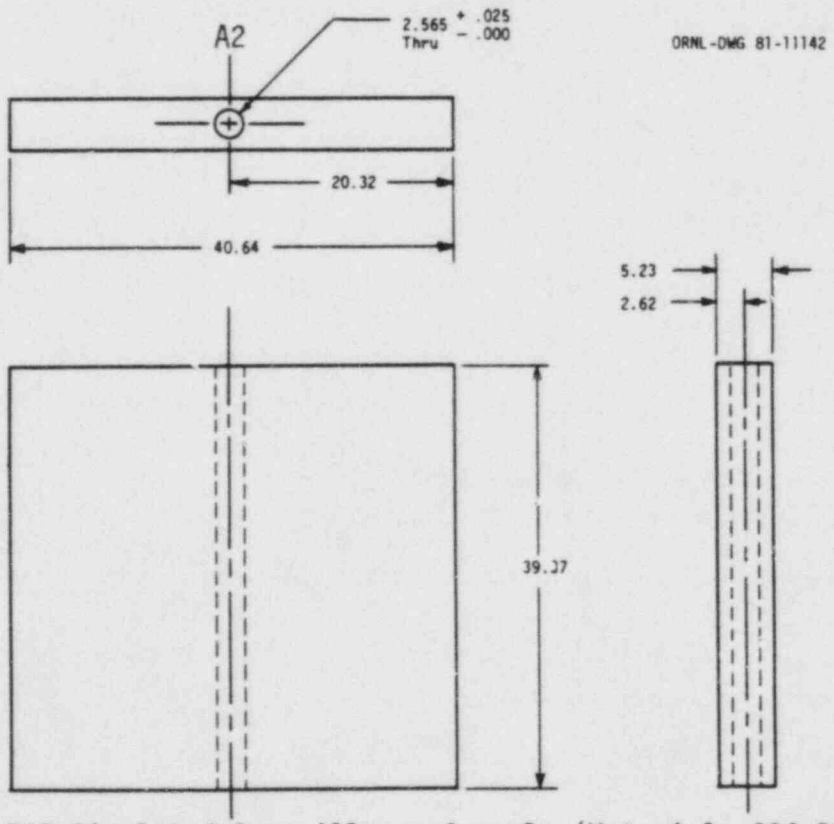

FIGURE 1.1.6. PCA Simulated Surveillance Capsule (Material: 304 SS). (All dimensions are in cm.)

	1	2	3	4	5	6	7	8	9
A		AUX FC	140 A-80	140 A-177	140 I-116	140 B-182	140 A-77		
B			140 A-55	S-1 70 B-114	140 B-180	S-3 70 B-127	140 A-64		
C			140 B-168	200 M-49-H	133 B-149-P	200 M-48-H	140 I-113		
D			140 I-115	S-2 70 B-147	140 S-17	RR 70 B-197	140 B-188		
E		PRI FC	140 A-81	140 A-61	140 A-75	140 A-60	140 I-117		
F									
G									

Critical Rod Positions: No. 1 Safety - 19. inches
No. 2 Safety - 19. inches
No. 3 Safety - 19. inches
Regulating Rod - 15.13 inches

Critical mass: 3336.01 grams ^{235}U

The numbers in the core locations are the fuel element identifications and the approximate ^{235}U loadings, within 1%, for each fuel element. Safety rods 1-3 are denoted by S-1, S-2, and S-3. The regulating rod is denoted by PR, and the auxiliary and primary fission chambers are denoted by AUX FC and PRI FC. Note that the fuel elements are not precisely square and that there is a water gap between each element; Tables 1.1.2 and 1.1.3 give details on the fuel element geometry. The pitch between rows is 3.189 inches, and the pitch between columns is 3.035 inches.

FIGURE 1.1.7. Fuel Loading Pattern for the PCA-PV Experiment.

center with a missing fuel plate to permit run-to-run normalization.* It was assumed that the critical rod positions listed in Fig. 1.1.7 satisfy criteria 4 since the regulating rod is worth a small fraction of the three safety rods. The fully withdrawn position of the safety rods is 24 inches, and the fully withdrawn position of the regulating rod is 22.2 inches.

The dimensions of the ex-core components are given in Table 1.1.1. The TS and SSC are fabricated from type 304L stainless steel, containing not more than 0.03% C, 2.00% Mn, 1.00% Si, 18.00 to 20.00% Cr, and 8.00 to 11.00% Ni. The nominal density of this material is 8.0 g/cm^3. The PVS is composed of type SA-36 carbon steel, containing not more than 0.25% C, 0.04% P, and 0.05% S. Its nominal density is 7.85 g/cm^3. The aluminum window is made from aluminum 6061-T6, which has a nominal density of 2.7 g/cm^3.

Table 1.1.1
DIMENSIONS OF PCA CONFIGURATION

Component	Thickness (cm)	Width (cm)	Height (cm)
Aluminum window	2.5	91.44	89.535
Thermal shield (TS)	5.9	68.58	68.58
Simulated surveillance capsule (SSC)	5.23	40.64	39.37
Pressure vessel simulator (PVS)	22.5	68.58	68.58
Void box (VB)	30.48†	68.58	68.58

†Void box dimensions include 0.3175-cm aluminum wall thickness on all sides.

The measuring accuracy and reproducibility of the dimensions in Figs. 1.1.2 and 1.1.3 are estimated to be ±0.1 cm (2σ) based on field measurements. The deviations from the exact geometry as a result of surface imperfections and tilts are ±0.2 cm maximum. The contribution of these uncertainties to the calculations of the reaction rates of the surveillance position and 1/4 T position is reported in (Ma80a).

The origin of the coordinate system for locating all positions is placed at the intersection of the aluminum window surface facing the core and the extension of the core centerline. This coordinate system is also used for reporting the relative power distributions and reactor core axial bucklings in Section 1.2.

The temperature of the water in the pool is approximately 37.7°C. However, there is a 5°C fluctuation of water temperature from summer to winter.

*The missing plate was restored during the fission chamber measurements so that the core power distribution in Section 1.2 is based on a full 140-g element in position C5. The effect on the out-of-core fluxes should be negligible.

1.2 RUN-TO-RUN MONITORING AND ABSOLUTE NORMALIZATIONS OF EXPERIMENTS

E. D. McGarry, A. Fabry, Raymond Gold, L. Kellogg and F. H. Ruddy

1.2.1 Summary

Although satisfactory from the safety and general user's viewpoints, the accuracy, precision and linearity of the PCA reactor control instrumentation in the nominal core power range of 1 watt to 10 kilowatts (maximum permissible power) are not sufficient for an adequate normalization, on a permanent basis, of the high-accuracy LWR-PVS benchmark-referenced experiments. Consequently, a long-term, run-to-run power-level monitoring and absolute normalization capability was provided.

NUREG/CR-1861, which dealt with the 8/7 and 12/13 configurations of the PCA Reactor Pressure Vessel Mockup experiment and which covered measurements in those configurations in the period September 1978 to January 1981, inferred that the precision of power normalization for any given PCA exposure was in the 0.5% to 1.0% range. Data, herein, for the 4/12 SSC in the period September 1979 to November 1981 also support this conclusion.

The run-to-run monitor data in both periods tend to substantiate that the accuracy of the reactor instrumentation at powers exceeding 10 watts is consistent and on the average with the accuracy of measurements discussed herein. This is significant because it has not been possible to have a permanently positioned run-to-run monitor. In particular, it has been removed every time the fuel grid is changed, which has been at least twice each year.

1.2.2 Rationale

The run-to-run monitoring method is conceptually simple. The response of a double fission chamber monitor, containing a "light" and "heavy" mass ^{238}U deposit, which is placed in a particular position at the lateral edge of the PCA core, is calibrated with respect to the core-center response of a miniature ^{235}U fission chamber. The latter is used to establish total core power. NBS provided the run-to-run monitor chamber; CEN/SCK provided the calibration tie with the core power.

1.2.3 Experimental Details and Results

The relative CEN/SCK calibration factor was 0.01204 ± 0.00015. NBS re-verified this calibration in June 1981 as 0.0119 ± 0.0002. NBS also made additional re-calibration measurements of the run-to-run monitor in October and November 1981. These are reported in Tables 1.2.2 and 1.2.3. Normalization measurements relative to specific dosimetry in 8/7, 12/13 and 4/12 configurations of the PCA are discussed throughout the text of this report.

TABLE 1.2.1

SUMMARY OF RUN-TO-RUN MONITOR CALIBRATIONS
FOR VARIOUS PERIODS FROM JUNE 1979* TO THE PRESENT

Period in Program History	Run-to-Run Monitor Calibration Factors** in Watts/cps of Monitor Heavier Deposit
June 1979 - January 1980	1.656 ± 0.5%***
November 1980	0.775 ± 0.8%
January 1981	0.738 ± 0.9%
October 1981	0.774 ± 0.9%
November 1981	0.759 ± 0.8%****

*There are no reliable run-to-run monitor data prior to June 1979.

**Calibrations between June 1979 and January 1981 were done by A. Fabry, CEN/SCK. Subsequent to this, calibrations were done by E. D. McGarry, NBS.

***Not the same deposits as used for subsequent operations. Note June 1979 thru January 1981 data were reported in (Mc81). October and November 1981 calibrations are reported herein. See Tables 1.2.2 and 1.2.3.

****The above quoted uncertainties refer to reproducibility. There is one additional factor to consider relative to the November 1981 measurements. The plexiglass piece used to guarantee repositioning of the Mol fission chamber was broken off of the center PCA fuel element sometime in late October or early November. Therefore, there are greater uncertainties about positioning even though greater time and effort were taken to reposition. Furthermore, some measurements taken by L. Kellogg and A. Fabry on about 10/23/81 suggest that a factor of 0.77 was still applicable at that time.

TABLE 1.2.2

PCA RUN-TO-RUN MONITOR CALIBRATION FOR OCTOBER 1981 MEASUREMENTS

Nominal PCA Power (W)	Mol Chamber* Data			NBS Chamber Data**		Ratio $\frac{\text{watts}}{\text{NBS cps}}$
	Raw Data (cps)	Resolving Time Corrected Data	Power (watts)	Raw Data (cps)	Resolving Time Corrected Data	
	Tuesday 29 Sept.					
100	8216 ± 46	8486 ± 68	101.4 ± 1.9%	130.9 ± 0.8	130.9 ± 1.0	0.775 ± 2.0%
50	4088 ± 15	4155 ± 30	49.65 ± 1.8%	64.50 ± 1.1	64.50 ± 1.2	0.770 ± 2.6%
	Wednesday 30 Sept.					
100	8216 ± 86	8486 ± 107	101.4 ± 2.1%	130.2 ± 1.7	130.2 ± 1.8	0.779 ± 2.5%
50	4087 ± 11	4154 ± 27	49.64 ± 1.8%	64.70 ± 0.7	64.70 ± 0.8	0.767 ± 2.2%
25	2135 ± 23	2153 ± 28	25.73 ± 2.1%	33.26 ± 0.61	33.26 ± 0.63	0.774 ± 2.8%
10	841.4 ± 7.2	844.2 ± 9	10.10 ± 2.0%	13.15 ± 0.51	13.15 ± 0.54	0.768 ± 4.6%
	Thursday 1 Oct.					
100	8237 ± 48	8508 ± 73	101.7 ± 1.9%	129.1 ± 1.6	129.1 ± 1.7	0.788 ± 2.3%
5	415.7 ± 3.5	416.4 ± 3.7	4.976 ± 1.9%	6.45 ± 0.23	6.45 ± 0.24	0.771 ± 4.2%

Weighted Average = 0.774 ± 0.9%

* All data refer to a vertical position of 12.5 on the new positioning tool for the Mol chamber. Dead time (DT) corrections thenfor Mol chamber are based upon 4×10^{-6} seconds resolving time. The true power is based upon NBS and Mol measurements of central core power chamber 0.01195 ± 0.0002 watts/cps.

**Heavy deposit only because operation was restricted to low power levels. Dead time (DT) corrections are based upon 2.5×10^{-6} seconds resolving time.

TABLE 1.2.3

PCA RUN-TO-RUN MONITOR CALIBRATION FOR NOVEMBER 1981 HEDL RADIOMETRIC AND SSTR MEASUREMENTS

Nominal PCA Power (W)	Mol Chamber Data			NBS Chamber Data*		Ratio $\frac{\text{watts}}{\text{NBS cps}}$
	Raw Data (cps)	Resolving Time Corrected Data	Power (watts)	Raw Data (cps)	Resolving Time Corrected Data	
10	833.1 ± 1.4	835.9 ± 1.7	9.99 ± 0.17	13.27 ± 0.11	13.27 ± 0.11	0.753 ± 1.8%
25	2140 ± 6.3	2158 ± 7.6	25.8 ± 0.44	34.18 ± 0.26	34.18 ± 0.26	0.755 ± 1.8%
50	4127 ± 2.0	4195 ± 2.4	50.1 ± 0.83	66.82 ± 0.39	66.83 ± 0.34	0.750 ± 1.7%
10	833.4 ± 1.4	836.2 ± 1.7	9.99 ± 0.17	13.32 ± 0.07	13.32 ± 0.07	0.750 ± 1.7%
5	416.4 ± 0.62	417.1 ± 0.74	4.98 ± 0.08	6.55 ± 0.05	6.55 ± 0.06	0.760 ± 2.6%
25	2165 ± 23	2184 ± 27	26.1 ± 0.54	34.36 ± 0.18	34.36 ± 0.18	0.759 ± 2.4%
100	8157 ± 17	8423 ± 20	100.7 ± 0.29	132.5 ± 0.48	132.6 ± 0.49	0.760 ± 0.8%

*Heavy deposit only because operation restricted to low power levels.
Dead time (DT) corrections based upon 2.5×10^{-6} seconds resolving time.

Weighted Average = 0.759 ± 0.8%

1.2.4 PCA Reactor Power Unit Conversions

F. H. Ruddy (HEDL)

Reaction rates measured at PCA have been variously reported in units of reactions per atom per kilowatt-hour, reactions per hour per second at 10 kilowatts, and reactions per atom per second per core neutron. Similarly, equivalent fission fluxes have been reported both as fission equivalent fluxes per square centimeter per second at 10 kilowatts and as fission equivalent fluxes per square centimeter per core neutron. Table 1.2.4 contains a compilation of factors for conversions between these various units.

Reaction rates and equivalent fission fluxes should be reported in terms of the true PCA power. When PCA is operated at a instrument power of 10.0 kilowatts, the true power is 9.75 kilowatts (Mc81b).

After June 1979 mechanical modifications were made to the PCA support structures in order to accommodate the PCA 4/12 configuration. As a result, the dimensions of the water gaps between the core, thermal shield, and pressure vessel simulator changed slightly. Reaction rates and fission equivalent fluxes should be reported consistent with the post-June 1979 specifications. A compilation of factors for converting pre-June 1979 measurements is contained in Table 7.2.1 of Fa81d.

TABLE 1.2.4

CONVERSIONS AND CONVERSION FACTORS

The average number of neutrons produced per fission is 2.420.
The average energy released per fission is 3.204×10^{-11} watts.

To Convert	To,	Multiply By
Reactions per atom per second at 10 kilowatts	Reactions per atom per kilowatt-hour	360
Reactions per atom per kilowatt-hour	Reactions per atom per second per core neutron	3.679×10^{-18}
Reactions per atom per second at 10 kilowatts	Reactions per atom per second per core neutron	1.324×10^{-15}
Fission equivalent flux	Reaction rate	Fission spectrum-averaged cross section in cm^{-2}

2.0 EXPERIMENTAL PROGRAM: INTEGRAL MEASUREMENTS

E. G. McGarry (NBS), Raymond Gold, L. S. Kellogg and
F. H. Ruddy (HEDL)

SUMMARY

The physics dosimetry information in this NUREG report is derived from extensive neutron and gamma-ray fluence and spectrum measurements made to provide a detailed understanding of the spatial and energy behavior of radiation in light water reactor pressure vessel environments. From an overall point of view, this information is used to test the validity of neutron and gamma transport theory calculations for commercial nuclear reactors. From a more focused point of view, the information defines the radiation environment of a particular pressure vessel simulator with sufficient power (or fluence) to simultaneously carry out metallurgy and dosimetry experiments. For example, the 4/12 SSC configuration at the PCA is a zero-power mockup of the SDMF (Standard Dosimetry Measurement Facility). The SDMF is a high-flux (30 MW) pressure vessel simulator at the Pool Side Facility (PSF) of the Oak Ridge Research Reactor (ORR). The information reported herein addresses the PCA 4/12 SSC configuration for the first time, whereas supplementary and updated information is provided for two pressure vessel mockups studied earlier: the 8/7 and 12/13 configurations (Mc81).

2.1 TEST MATRIX SELECTION AND RATIONALE

E. G. McGarry (NBS), Raymond Gold, L. S. Kellogg and F. H. Ruddy (HEDL)

Dosimetry techniques in the PCA are necessarily limited by small fluences available from the 10-keV maximum reactor power. Neutron measurements primarily address neutrons whose energies exceed 0.1 MeV. These are made with two different types of fission chambers, with radiometric foil techniques, and with solid state track recorders (SSTRs). The measurements are made in terms of absolute core power (±4%), which is based upon extensive traverse buckling measurements throughout the plates of the fuel elements using a miniature ^{235}U fission chamber whose mass (±2%) was independently calibrated (Mc81b). Absolute accuracies, inclusive of the power uncertainty, are presently at the 10% to 12% level (see primarily discussion in Section 2.6). Further, investigation may reduce the overall uncertainty to a ±6% level. Even with a benchmark referencing effort at the ±2.5% accuracy level, this would appear, however, to be the presently achievable limit of accuracy for the PCA neutron measurements.

Gamma measurements address photons with energies less than 6 MeV, but two of the three methods (ion chambers and TLDs) are primarily sensitive to significantly lesser energies (<3 MeV). The third method, for both spectrum and intensity measurements, is Compton recoil spectrometry with a silicon semiconductor detector known as the Janus probe (Go70a,Go70b,Go71b). The absolute accuracy of the gamma intensity measurements is more difficult to define precisely but, from agreement among measurement methods, is estimated at 10% to 15%. This is adequate for low-energy gamma measurements since the main interest is to verify calculations of gamma heating. Higher energy uncertainties are more speculative because considerable emphasis has been placed on reaching as high in energy as possible to better understand effects of photofission. The degree to which this has been successful is discussed in Section 4.0.

2.2 BENCHMARK FIELD REFERENCING

E. D. McGarry and J. A. Grundl (NBS) and A. Fabry (CEN/SCK)

2.2.1 Principles of Benchmark Referencing to a Standard Neutron Field

Controlled irradiations in a standard neutron field provide known fluences of neutrons with a well-known energy distribution. Such irradiations, therefore, provide a means of benchmark referencing neutron measuring techniques. Reference (Mc81) provided an extensive discussion of the principles and techniques. Only the main issues of benchmark referencing will be reviewed here.

2.2.1.2 Flux Transfer from Benchmark Fields

To obtain the neutron flux in an applied field relative to that in the standard field, a neutron sensor is used as a transfer instrument whose response is calibrated in terms of the absolute flux in the benchmark field. The driving source of neutrons for LWRs is fission in ^{235}U. Therefore, this fission spectrum is the appropriate benchmark for neutron fields found in and around pressure vessels. However, ^{235}U neutron fields of sufficient intensity for calibration of many types of detectors can only be produced in reactors. This presents a problem: How can the source strengths of variable-power reactor fields be accurately established? In the US, ^{252}Cf sources with a well-known fission spectrum are used to produce the primary standard neutron fields. Their neutron source strengths are accurately determined relative to an international standard, Ra-Ba source NBS-1, by measurements in a manganous sulphate bath (No63). However, most ^{252}Cf sources have too little source strength for materials dosimetry calibrations Therefore, flux transfers from ^{252}Cf must be made to establish the absolute flux scales of appropriate ^{235}U fission sources.

2.2.1.3 Standard ^{235}U Fission Neutron Field Irradiation

The calibration irradiations necessary for benchmark referencing PCA-RPV dosimetry were carried out in the fast fission flux from a ^{235}U converter. Such a converter may be found in a spherical cavity within the thermal columns of the research reactors either at NBS (Gaithersburg, MD) or at CEN/SCK (Mol, Belgium). During irradiations in the ^{235}U converter, dosimetry foils are held within cadmium thermal-neutron shields by light-weight pieces of aluminum. At NBS, for example, indium foils are irradiated simultaneously with other dosimetry foils of interest. The relative indium activity provides information necessary to correct for spatial variations in the fast flux between two fissioning ^{235}U disks. The absolute indium activity provides the flux transfer from the ^{252}Cf. The electronics for counting the 4.5-hour $^{115}In(n,n')^{115m}In$ activity is previously calibrated by counting indium from a known-fluence irradiation in a ^{252}Cf neutron field.

2.2.1.4 Measurements of Fission Equivalent Fluxes in PCA

A principal purpose of the PCA-RPV simulator is to provide experimentally characterized neutron fields representative of a pressure vessel environment

so that transport theory calculations may be validated. The primary quantities for confrontation of measurement and calculation are ratios of calculated quantities to experimental quantities derived from threshold neutron sensors that have been calibrated in the ^{235}U fission spectrum. The quantities chosen are benchmark-referenced neutron fluxes. A fundamental point here is that neutron flux is the quantity that is certified for all standard neutron field calibrations. The benchmark-referenced fluxes measured in PCA are called "equivalent fission fluxes." They are defined by

$$\phi_{fi} = \int_0^\infty \sigma_i(E) \quad \phi(E) \quad dE \Big/ \int_0^\infty \chi_{25}(E) \quad \sigma_i(E) \quad dE \qquad (1)$$

where:

$\sigma_i(E)$ = the appropriate reaction cross-section.

$\phi(E)$ = neutron energy spectrum of interest at various PCA-RPV locations.

χ_{25} = ^{235}U fission spectrum normalized to an integral of unity.

The numerator is a reaction (or fission) probability rate per target nucleus, R/N, in the PCA-RPV. The denominator is the ^{235}U spectrum-average cross section. Therefore, the equivalent fission flux ϕ_{fi} is detector-dependent.

To relate the symbolism of Eq. (1) to operational measurements, observe that in terms of the mentioned reaction probability rates, R/N, the fission equivalent flux ϕ_{fi} is given directly by

$$\phi_{fi} = \frac{(R/N)_{PCA}}{(R/N)_{25}} \cdot \phi_{25} \qquad (2)$$

where ϕ_{25} is flux of the ^{235}U spectrum. Furthermore, since $(R/N)_{25}/\phi_{25}$ in Eq. (2) is a ^{252}Cf spectrum-averaged cross section, the product of that cross section and the associated ϕ_{fi} equals a reaction probability rate in PCA.

The equivalent fission flux has the advantage that many uncertainties such as those associated with absolute cross sections, detector efficiencies and branching ratios will disappear from the measured relative response ratios by physical compensation rather than by calculational corrections.

Throughout Section 2 it is important to understand that "detector response" can mean the counting rate of a fission chamber, the track density of fission tracks in a SSTR, or the radioactivity in activation foils or fission foils. Furthermore, "response" refers not only to the response of the neutron-sensing element but also to the associated counting system used to measure the results of the interaction of the detector with the neutron field.

2.2.1.5 Measurements of Spectral Indices in PCA

A spectral index, $S_{\alpha/\beta}$, for two isotopes α and β, is equivalent to the ratio of their responses per target atom, or in turn, their spectrum-averaged cross sections. See Eq. (3).

$$S_{\alpha/\beta} = \frac{(R/N)_\alpha}{(R/N)_\beta} = \frac{\bar{\sigma}_\alpha}{\bar{\sigma}_\beta} \tag{3}$$

The benchmark-referenced spectral index for iostopes α and β is a double ratio; the spectral index in a neutron field under study divided by that in the ^{235}U fission spectrum. For the PCA-RPV simulator:

$$\frac{S^{PCA}_{\alpha/\beta}}{S^{25}_{\alpha/\beta}} = \frac{(R/N)^{PCA}_\alpha (R/N)^{25}_\beta}{(R/N)^{25}_\alpha (R/N)^{PCA}_\beta} \tag{4}$$

The uncertainties in the masses of the sensors are cancelled by this calibration technique. As shown by Eq. (5), this double ratio is also equal to the ratios of the equilvalent fission fluxes obtained from measurements with isotopes α and β.

$$\frac{S^{PCA}_{\alpha/\beta}}{S^{25}_{\alpha/\beta}} = \phi_{f\alpha}/\phi_{f\beta} \tag{5}$$

2.2.1.6 Benchmark Referencing Measurements

The remainder of Section 2 deals with specific measurements made to benchmark the physics dosimetry in PCA. Also extensive benchmarking measurements are reported in Section 2 of Reference (Mc81).

2.2.2 Validation and Benchmark Referencing of PCA Dosimetry Measurements

2.2.2.1 Introduction

The purpose of this section is to identify and summarize results from activities undertaken to provide accurate physics dosimetry for development of the PCA-RPV Benchmark. A similar section in Reference (Mc81) addressed many of these same subjects and its contents are, first, briefly reviewed. The benchmark referencing subjects were:

(1) Measurements in the NBS ^{252}Cf Standard Neutron Field to provide calibration data for spectral index measurements of ^{237}Np and ^{238}U with the NBS dual fission chamber.

(2) Calibration measurements in the ^{235}U Standard Neutron Fields at NBS and CEN/SCK to provide the bases for measurements of fission equivalent fluxes with fission chambers and with CEN/SCK radiometric sensors.

(3) Measurements in the ^{235}U Standard Neutron Field at NBS to validate radiometric sensor measurements made by both HEDL and CEN/SCK.

(4) Measurements in the ^{252}Cf spectrum to validate HEDL nuclear emulsion spectroscopy.

(5) Measurements in the ^{252}Cf spectrum to validate HEDL SSTR dosimetry.

(6) Thermal neutron flux calibration of the effective mass of ^{235}U in the CEN/SCK miniature fission chamber used to measure absolute power profiles in the PCA reactor core.

In this report there is additional information on measurements relative to items (3) and (5) as well as:

(7) Revision of benchmark calibration factors for the dual NBS fission chambers because of a re-evaluation of the masses of NBS deposits and new cross-section information (Gr83). The revised ^{235}U spectrum-averaged cross sections for fission in ^{237}Np and ^{238}U are 1.344 barns ± 4.0% and 0.308 barns ± 2.7%, respectively.

(8) Measurements in the ^{235}U Standard Neutron Field at NBS to calibrate radiometric counting equipment at ORNL which was used by HEDL to make measurements at PCA in 1981.

(9) Information about recent, additional comparisons between NBS ^{252}Cf and ^{235}U standard neutron fields and the European Standard ^{235}U Fission Spectrum at the CEN/SCK Laboratories, Mol, Belgium.

2.2.2.2 Use of ^{252}Cf Neutrons to Benchmark Reference NBS Spectral Index Measurements in the PCA-PV Simulator

Even though the ^{235}U fission spectrum is designated as the reference neutron field for benchmarking the PCA-RPV measurements, the ^{252}Cf fission spectrum has been of necessity used on several occasions. In particular, it was used to calibrate the dual NBS fission chambers for the 1979-1981 PCA measurements and it was used to calibrate SSTRs and nuclear emulsions. To make these ^{252}Cf calibrations applicable to reactor (e.g., PCA) dosimetry and to the ^{235}U fission spectrum, it is necessary to multiply the ^{252}Cf results by the ratio of spectrum-averaged cross sections in the two neutron fields. For ^{237}Np and ^{238}U these values, as derived from (Gr83), are 1.017 and 1.049, respectively. The fission response per unit flux, R_f/ϕ, for the α-th deposit in the ^{235}U spectrum is

$$R_f/\phi\Big]^{\alpha}_{^{235}U} = R_f/\phi\Big]^{\alpha}_{^{252}Cf} \left(\frac{\bar{\sigma}_{235}}{\bar{\sigma}_{252}}\right)^{\alpha} \qquad (6)$$

Tables 2.2.1, 2.2.2, and 2.2.3 summarize the relative responses of pairs of specific NBS fissionable deposits in the ^{252}Cf field. The ^{252}Cf irradiations are conducted in the immediate vicinity (4- to 12-cm source-to-deposit distances) of an isolated, single, steel-encapsulated, point source of californium of approximately 3×10^9 neutrons/s source strength. The irradiations are carried out in compensated-beam geometry where the two pairs of deposits are irradiated on opposite sides of the source so that the critical distance is that between the foil sets. The chambers' responses are observed for two orientations: the fronts toward the source and then the backs toward the source. The source is pulled into position several times to observe effects of rotation, which will arise if the californium oxide bead is not at the exact center of the source.

Table 2.2.1 gives details of the benchmark referenced calibration factors for measuring spectral indices in the PCA. Tables 2.2.2 and 2.2.3 provide information about the benchmark calibrations necessary to derive fission equivalent fluxes from NBS fission chamber measurements. These latter two tables also show the effect of the re-evaluation of the masses of the NBS deposits. In particular, Tables 2.2.2 and 2.2.3 compare R_f/ϕ values derived from calibrations made by different people, using different neutron sources, fission chambers and electronics. For ^{237}Np the ratio of the R_f/ϕ value in Table 2.2.2 to the new value in Table 2.2.3 is 1.001, while for ^{238}U, the corresponding ratio is 0.996. Both indicate excellent agreement. Furthermore, the new R_f/ϕ values from Table 2.2.3 must also yield the cross section ratio of $^{237}Np/^{238}U$ in the ^{252}Cf spectrum, 4.19 ± 1.5%, as given in Table 2.2.1. The following calculation which takes into account the masses of the two foils also indicates very good agreement.

$$\frac{9.051 \times 10^{-7} \times 691.0}{5.698 \times 10^{-7} \times 260.8} = 4.21 \ (\pm \sim 2.2\%) \qquad (7)$$

TABLE 2.2.1

CALIBRATION FACTORS FOR MEASURING SPECTRAL INDEXES IN THE LWR-PV SIMULATOR AS OBTAINED FROM CALIFORNIUM-252 NEUTRON IRRADIATIONS OF NBS FISSION DEPOSITS

Foil Pairs Used for Spectral Index Measurements	Observed ETZ & D.T. Corrected Fission Rate Ratios	Corrections for Fissions in Impurities in the Cf-252 Field	Adjustments* for Scattering in the Cf-252 Field	$\left[R_\alpha / R_\beta\right]$	$\left(\bar{\sigma}_\alpha / \bar{\sigma}_\beta\right)$ **	Calibration Factor $\frac{\left(\bar{\sigma}_\alpha / \bar{\sigma}_\beta\right)}{\left[R_\alpha / R_\beta\right]}$
$\frac{37S\text{-}2\text{-}2}{28HD\text{-}5\text{-}2}$	1.656 ±0.12%	$\frac{0.99973 \pm .00007}{1.000 \pm .001}$	$\frac{1.0035 \pm .0015}{1.007 \pm .0035}$	1.650 ±0.41%	4.19 ±1.5%	2.540 ±1.56%
$\frac{25K\text{-}1\text{-}1}{28S\text{-}4\text{-}4}$	1.143 ±0.10%	$\frac{0.99961 \pm .00007}{0.9976 \pm .0008}$	$\frac{0.9922 \pm .0030}{1.007 \pm .0035}$	1.128 ±0.48%	3.73 ±1.2%	3.305 ±1.29%

*These corrections are for scattering in the Cf-252 encapsulation. No corrections for scattering or removal in the fission chamber housing or fission deposit backing. See text for discussion of this.

**See Reference (Gr83).

TABLE 2.2.2

SUMMARY OF ^{252}Cf BENCHMARK REFERENCED CALIBRATION FACTORS* FOR NBS ^{237}Np AND ^{238}U FISSION CHAMBERS AS MEASURED** FOR PCA/RPV PROGRAM

Fissionable Deposit	^{252}Cf** Flux	ETZ & DT*** Corrected $\langle S_u \rangle$	Correction for Fissionable Impurities	Observed R_f/ϕ
37S-2-2	1.875×10^7 ± 2.0%	16.70 ± 1.4%	0.99973	8.90×10^{-7} ± 2.5%
28HD-5-2	(same)	10.08 ± 1.6%	1.00000	5.38×10^{-7} ± 2.6%

Ratio of the Observed ^{237}Np and ^{238}U Calibration Factors*

$$\frac{(R_f/\phi)^{37}}{(R_f/\phi)^{28}} = 1.656 \pm 2.1\%$$

* Fission counting rate per unit fluence: R_f/ϕ.
** Fission source was NS-100 on 11 May 1979.
***ETZ = Extrapolation-to-Zero Correction [See Ref. (Gr77)]; DT = Deadtime or resolving time loss correction which was for the most part negligible because of low counting rates; $\langle S_u \rangle$ = counts of fission response above one of two (the upper level) discriminators.

TABLE 2.2.3

SUMMARY OF ^{252}Cf BENCHMARK REFERENCED CALIBRATION FACTORS* FOR NBS ^{237}Np AND ^{238}U FISSION CHAMBERS AS DEDUCED FROM RAW DATA FOR CROSS SECTION MEASUREMENTS**

Fissionable Deposit	R_f/ϕ Adjusted for Fission Fragment Absorption and Scattering in the ^{252}Cf Source Capsule***		
	With New Masses and Revised Cross Sections****	Used Previously;***** Prior to Mass/Cross Section Revision	New/Old Ratio of R_f/ϕ Factors
37S-2-2	$\frac{9.051 \times 10^{-7}}{(1.0145)(1.0035)} = 8.891 \times 10^{-7} \pm 2.4\%$	8.81×10^{-7}	1.0091
28HD-5-2	$\frac{5.698 \times 10^{-7}}{(1.0381)(1.0070)} = 5.451 \times 10^{-7} \pm 2.4\%$	5.40×10^{-7}	1.0094

Ratio of the Derived ^{237}Np and ^{238}U Calibration Factors*

$$\frac{(R_f/\phi)^{37}}{(R_f/\phi)^{28}} = 1.631 \pm 1.9\%$$

* Fission counting rate per unit fluence: R_f/ϕ.
** See Reference (Gr77b).
*** See text Section 2.2 for explanation.
**** See Reference (Gr83). The first factor in denominator is for fragment absorption; the second, scattering.
*****See Reference (Mc81).

It should be noted that three quantities, fission equivalent fluxes, fission rates and spectral indices, are derived from the NBS fission chamber measurements. These are obviously not independent quantities, and within the quoted precisions the latter two may be derived from the fission equivalent fluxes, which are the primary measurements. However, fission equivalent fluxes and spectral indices are, in principle, different measurements because they are related to two separate calibrations. Furthermore, the ^{237}Np to ^{238}U spectral index when measured with back-to-back deposits in a dual fission chamber is independent of absolute reactor power. On the other hand, all fission equivalent flux measurements must be adjusted to a reactor power of 10 kW. Consequently, the ratio of fission equivalent fluxes (or fission rates) do not necessarily yield the exact same values of spectral indices as the "measured" indices, again, the preferred values. Fission rates, incidentally, are only derived from NBS chamber measurements for comparisons with those from SSTRs, which are not yet completely benchmarked in terms of fission equivalent fluxes. Derivation of fission rates from NBS chamber measurements requires explicit knowledge of deposit masses, which are, in general, 1.5 to 2% (see Table 2.2.4).

The benchmark calibrations of the miniature, Mol fission chambers, not discussed herein, have not changed and are reported in (Mc81).

TABLE 2.2.4

UPDATED CHARACTERISTICS OF NBS FISSIONABLE DEPOSITS USED FOR PCA MEASUREMENTS BETWEEN SEPTEMBER 1979 AND NOVEMBER 1981

Deposit Type and Identification	Mass of Deposit (micrograms)	Principal Isotope (atom percent)	Principal Fissionable Impurities (atom percent)
^{237}Np: 37S-2-2	260.8 ± 1.4%	99.98 ± 0.01	^{239}Pu: 0.02 ± 0.01
^{238}U: 28HD-5-2*	691 ± 1.3%	99.999 ± 0.002	^{235}U: 0.0002 ± 0.0002
^{235}U: 25K-1-1	129 ± 1.3%	99.89 ± 0.01	^{238}U: 0.053 ± 0.002 ^{234}U: 0.035 ± 0.001 ^{236}U: 0.025 ± 0.001
^{238}U: 28S-4-4**	453 ± 1.9%	99.94 ± 0.01	^{235}U: 0.061 ± 0.002 ^{234}U: <0.001 ^{236}U: <0.005
^{238}U: 28HD-8-1***	858 ± 1.5%	99.999 ± 0.002	^{235}U: 0.0002 ± 0.0002

*Always measured in the chamber with 37S-2-2 until September 1981.

**Always measured in the chamber with 25K-1-1.

***Only used in the chamber with 37S-2-2 in period September 1981 to November 1981.

2.3 FISSION CHAMBER MEASUREMENTS

E. D. McGarry (NBS) and A. Fabry (CEN/SCK)

2.3.1 NBS Fission Chamber Measurements

Table 2.3.1 is a summary of the ratios of NBS fission chamber response for ^{237}Np and ^{238}U deposits. Because the fissionable deposits are separated by only 0.025 cm during irradiation (each deposit is on a 0.013-cm thick backing whose unplated sides are in contact), the two deposits see essentially the same flux and the ratio measurements are independent of reactor power level. Inspection of Table 2.3.1 shows the ratio measurements are very reproducible. The averages and standard deviations are given on the table. The ratio data are used to derive the $^{237}Np/^{238}U$ spectral indices given in Table 2.3.2. Further discussion of the spectral indices is delayed until Sect. 2.3.1.3.

In addition to the ratio measurements, the NBS fission chamber provides data directly proportional to absolute fission rates, with close to 100% efficiency. Such measurements are, however, power level dependent. Table 2.3.3 indicates the extent (several percent) to which this is a reproducibility problem. Table 2.3.4 shows how use is made of the run-to-run power monitoring information, given in Sect. 1.2, to adjust the ^{237}Np and ^{238}U data of Table 2.3.3 for power level differences. Then, Table 2.3.5 shows the reproducibility of the adjusted data. A nominal factor-of-three improvement is evident. Finally, the adjusted averages of Table 2.3.5 are used to derive NBS values of ^{237}Np and ^{238}U fission equivalent fluxes for the PCA 4/12 SSC configuration. These data, including error propagation in quadrature, are given in Table 2.3.7. Table 2.3.6 gives similar, updated information for the 8/7 and 12/13 configurations. The original 8/7 and 12/13 fission equivalent fluxes were reported in (Mc81).

2.3.1.1 Fission Equivalent Fluxes

As mentioned, Table 2.3.6 contains revised NBS data for the 8/7 and 12/13 configurations. Changes to the data, which are in general less than 2%, come about because of recent re-evaluations of deposit masses and more recent re-evaluations of best integral cross-section values for standard neutron fields (Gr83). The associated adjustments to the benchmark calibration constants for NBS chamber measurements are discussed in Sect. 2.2.

The significance of the ratios of fission rates to fission equivalent fluxes (see column seven of Table 2.3.6), is that the ratios should equal the ^{235}U spectrum-averaged cross sections for ^{237}Np and ^{238}U. Nominally, these values are 1344 for ^{237}Np and 308 for ^{238}U. Observed differences result from two factors: (1) a nearly constant difference of about 0.5% when masses are used to derive fission rates as opposed to using benchmarked constants (K-factors) to derive fission equivalent

TABLE 2.3.1

SUMMARY OF $^{237}Np/^{238}U$ SPECTRAL INDEX MEASUREMENTS MADE IN THE PCA 4/12 SSC PV CONFIGURATION

Data	Measured Fission Counter Response Ratio	Averaged Data
	PCA 1/4 T Data	
Sept. 79	3.402 ± 0.025	
Nov. 80	3.374 ± 0.028	3.381 ± 0.33%
Jan. 81	3.365 ± 0.023	
Oct. 81	3.383 ± 0.033	
	PCA 1/2 T Data	
Sept. 79	4.336 ± 0.042	
Nov. 80	4.330 ± 0.031	4.315 ± 0.42%
Jan. 81	4.279 ± 0.030	
	PCA 3/4 T Data	
Sept. 79	5.457 ± 0.048	
Nov. 80	5.463 ± 0.045	5.447 ± 0.52%
Jan. 81	5.422 ± 0.042	
	Void Box Data	
Jan. 81	6.17 ± 0.11	6.17 ± 1.8%

TABLE 2.3.2

$^{237}Np/^{238}U$ SPECTRAL INDEXES IN THE PCA 4/12 SSC CONFIGURATION

PCA Pos	Observed Fission Rate Ratios ETZ- and DT-Corrected	Corrections for Fissions in Impurity Isotopes	^{252}Cf Benchmark Calibration Factors	Spectral Index in PCA not Corr. for Photofission	Photofission Correction	Spectral** Indexes in PCA
1/4 T	3.381±0.33%	$\frac{0.9978\pm.0015}{0.9995\pm.0003}$		8.573±1.59%	1.0169±1.7%	8.72±2.3%
1/2 T	4.315±0.42%	$\frac{0.9976\pm.0015}{0.9996\pm.0003}$	2.540±1.56% or* $\frac{(\sigma\alpha/\sigma\beta)}{[R\alpha/R\beta]}$	10.93 ±1.61%	1.0109±1.0%	11.1 ±2.1%
3/4 T	5.447±0.22%	$\frac{0.9976\pm.0015}{0.9996\pm.0003}$		13.81 ±1.58%	1.0246±2.0%	14.2 ±3.2%
VB	6.17 ±1.80%	$\frac{0.9972\pm.0020}{0.9993\pm.0004}$		15.64 ±2.38%	1.0752±4.3%	16.8 ±6.5%

*See last column of Table 2.2.1.

**Uncertainties dependent substantially upon the photofission corrections.

TABLE 2.3.3

EXAMINATION OF THE REPRODUCIBILITY OF NBS DUAL FISSION CHAMBER 4/12 SSC DATA FROM MEASUREMENTS ON FOUR DIFFERENT DATES
(Data* have not been normalized for PCA power level differences)

Date	Observed Counting Rates ^{237}Np	^{238}U	Counting Rates Relative to Averages** ^{237}Np	^{238}U
	PCA Position = 1/4 T			
Sept. 79	335.2 ± 1.4 %	98.52 ± 1.8%	0.974	0.968
Nov. 80	353.9 ± 0.81%	104.9 ± 1.9%	1.028	1.030
Jan. 81	342.9 ± 0.62%	101.9 ± 1.8%	0.996	1.001
1/4 T Averages**	344.3 ± 2.7 %	101.8 ± 3.1%		
	Additional 1/4 T Data			
Oct. 81	344.0 ± 1.6 %			
	PCA Position = 1/2 T			
Sept. 79	183.8 ± 1.7 %	42.39 ±2.0%	0.970	0.966
Nov. 80	194.4 ± 1.0 %	44.90 ±2.0%	1.027	1.023
Jan. 81	189.8 ± 1.0 %	44.36 ±1.5%	1.003	1.011
1/2 T Averages**	189.3 ± 2.9 %	43.88 ±3.0%		
	PCA Position = 3/4 T			
Sept. 79	97.63 ± 1.9 %	17.89± 2.2%	0.983	0.982
Nov. 80	100.91 ± 1.1 %	18.47± 2.5%	1.016	1.013
Jan. 81	99.34 ± 0.8 %	18.32± 1.7%	1.001	1.005
3/4 T Averages**	99.29 ± 1.7 %	18.23± 2.5%		

* The data recorded are DT- and ETZ-corrected counting rates for ^{237}Np and ^{238}U deposits back-to-back in the NBS fission chamber. DT implies dead time (or resolving-time loss) corrected; ETZ implies an extrapolation-to-zero correction.

**Linear averages of the three values.

TABLE 2.3.4

NORMALIZATION OF NBS FISSION CHAMBER MEASUREMENTS TO ACCOUNT FOR PCA POWER LEVEL DIFFERENCES

PCA Position	Fission Chamber <Su> Counting Rates (cps) Corrected for Deadtimes and Extrapolation to Zero		NBS Run-To-Run Monitor <Su> Counting Rate (cps) (Dead Time Corrected Only)	Run-To-Run Monitor Calibration Factor* (watt/cps) and PCA Power	Fission Chamber <Su> Counting Rates (cps) Normalized to 10kw PCA Reactor Power Level	
	^{237}Np Data	^{238}U Data			^{237}Np Data	^{238}U Data
	September 1979 Data			1.656 ± 0.5%		
1/4T	335.2 ±4.7	98.52±1.77	6011		338.9 ±1.7%	99.62±2.0%
1/2T	183.8 ±3.1	42.39±0.84	5940		185.8 ±2.2%	42.86±2.2%
3/4T	97.63±1.9	17.89±0.39	5978	9.89kW± 0.95%**	98.72±2.4%	18.09±2.4%
			AVE = 5977±0.8%			
	November 1980 Data			0.776 ± 0.8%		
1/4T	353.9 ±2.9	104.9 ±1.99	13482		336.7 ±1.4%	99.81±2.2%
1/2T	194.4 ±1.9	44.90±0.90	13650		185.0 ±1.5%	42.72±2.3%
3/4T	100.9 ±1.1	18.47±0.46	13497	10.51kW± 1.1%	96.00±1.6%	17.57±2.7%
			AVE = 13543±0.7%			
	January 1981 Data			0.738 ± 0.9%		
1/4T	342.9 ±2.1	101.9 ±1.83	13864		338.8 ±1.4%	100.7 ±2.2%
1/2T	189.8 ±1.9	44.36±0.67	13700		187.5 ±1.6%	43.83±2.0%
3/4T	99.34±0.81	18.32±0.31	13596	10.12kW± 1.3%	98.16±1.5%	18.10±2.1%
VB	27.14±0.31	4.39±0.12	AVE = 13720±1.0%		26.82±1.8%	4.34±2.1%
	October 1981 Data			0.774 ± 0.9%		
1/4T	351.1 ±3.0	103.8 ±3.8	AVE = 13280±0.8%	10.48kW± 1 %	335.0 ±1.9%	99.0 ±3.6%

*As derived by A. Fabry in Ref. (1) for 1979 to January 1981; as derived by NBS after that. See Section 1.2 of this report.

**±0.5% is the precision of this determination; ±4% is the actual uncertainty on the absolute power level.

TABLE 2.3.5

EXAMINATION OF THE REPRODUCIBILITY OF NORMALIZED NBS DUAL FISSION CHAMBER 4/12 SSC DATA FROM MEASUREMENTS ON FOUR DIFFERENT DATES
(Data* have been normalized to 10.00 kW PCA power level)

	Observed Counting Rates		Counting Rates Relative to Averages**	
Date	^{237}Np	^{238}U	^{237}Np	^{238}U
	PCA Position = 1/4 T			
Sept. 79	338.9 ± 1.7 %	99.62 ± 2.0 %	1.004	0.998
Nov. 80	336.7 ± 1.4 %	99.81 ± 2.2 %	0.998	1.000
Jan. 81	338.8 ± 1.4 %	100.7 ± 2.2 %	1.004	1.009
Oct. 81	335.0 ± 1.9 %	99.0 ± 3.6 %	0.998	0.992
1/4 T Averages**	337.4 ± 0.81%	99.78 ± 0.85%		
	PCA Position = 1/2 T			
Sept. 79	185.8 ± 2.2 %	42.86 ± 2.2 %	0.998	0.994
Nov. 80	185.0 ± 1.5 %	42.72 ± 2.3 %	0.994	0.990
Jan. 81	187.5 ± 1.6 %	43.83 ± 2.0 %	1.008	1.016
1/2 T Averages	186.1 ± 1.0 %	43.14 ± 1.6 %		
	PCA Position = 3/4 T			
Sept. 79	98.72 ± 2.4 %	18.09 ± 2.4 %	1.011	1.009
Nov. 80	96.00 ± 1.5 %	17.57 ± 2.7 %	0.983	0.980
Jan. 81	98.16 ± 1.5 %	18.10 ± 2.1 %	1.005	1.010
3/4 T Averages	97.63 ± 1.1 %	17.92 ± 2.0 %		

*The data recorded are DT- and ETZ-Corrected counting rates rates normalized to 10 kW power for ^{237}Np and ^{238}U deposits back-to-back in the NBS fission chamber.

Linear averages of three or four values.*

***Normalized void box data are still: ^{237}Np = 26.82 ± 1.8%
^{238}U = 4.34 ± 2.1%
The 4.1% absolute power uncertainty has not yet been included.

TABLE 2.3.6

UPDATED* FISSION EQUIVALENT FLUENCE RATES AND FISSION RATES
AS DEDUCED FROM NBS FISSION CHAMBER MEASUREMENTS IN PCA 8/7 AND 12/13 CONFIGURATIONS

Conf.		PCA Pos.	Observed** ETZ and DT Corrected Fission Response	Foil I.D.	Fission Equiv. Flux per Nucleus per Neutron (x 10^{8})	Fission/s per Nucleus per Neutron (x 10^{33})	Ratio*** of Fission Rate to Fission Equiv. Flux (Barns)	Photo-fission Correct.	Corrected Results	
									Fiss Rate per Nucleus per Neutron (x 10^{33})	Fiss Equiv. Flux**** per Nucleus per Neutron (x 10^{8})
8/7	^{237}Np	1/4 T	375. ±2.2%	37S-2-2	58.1	779.	1.341	0.994	774.	57.9 ±5.5%
		1/2 T	208. ±2.2%		32.3	432.	1.337	0.997	431.	32.2 ±5.5%
		3/4 T	110. ±2.2%		17.0	228.	1.341	0.992	226.	16.9 ±5.6%
	^{238}U	1/4 T	130. ±2.2%	28HD-5-2	34.2	105.	0.307	0.977	103.	33.4 ±6.7%
		1/2 T	56.7 ±2.5%		14.9	45.8	0.307	0.985	45.1	14.7 ±6.7%
		3/4 T	23.5 ±2.5%		6.19	19.0	0.307	0.949	18.0	5.87 ±7.2%
12/13	^{237}Np	1/4 T	60.5 ±2.3%	37S-2-2	9.38	126.	1.343	0.990	125.	9.29 ±5.5%
		1/2 T	34.0 ±2.5%		5.26	70.4	1.338	0.996	70.1	5.24 ±5.7%
		3/4 T	17.8 ±2.5%		2.76	36.9	1.337	0.993	36.6	2.74 ±5.8%
	^{238}U	1/4 T	24.1 ±2.5%	28HD-5-2	6.33	19.4	0.306	0.964	18.7	6.11 ±6.9%
		1/2 T	10.6 ±2.6%		2.78	8.54	0.307	0.981	8.38	2.73 ±6.8%
		3/4 T	4.40±2.7%		1.16	3.55	0.306	0.962	3.41	1.12 ±7.1%

*Values published in (Mc81) are hereby revised to reflect new masses and cross sections (see text, Sec. 2.2.2).

**As given in Table 2.3.2 (Mc81).

***Algebraic check to show internal consistency with new experimental cross sections since they are not involved in the derivation of fission rates.

****Uncertainties do reflect ±4.2% uncertainty on absolute power level determination. The do not, however, reflect any uncertainty associated with the possible bias between fission chamber and SSTR results.

fluxes, and (2) use of slightly different averaged raw data in deriving the two quantities. The preferred final values are the fission equivalent fluxes, which are the benchmark referenced quantities. However, in view of the nominal 2.5% precision of the data and the 4.2% uncertainty on the power level adjustment, it is immaterial to any comparison with calculation as to which are used. Furthermore, Sect. 2.6 identifies a presently undefined but nearly constant, 10% difference between fission chamber and SSTR measurements in steel. This difference exists for all three PCA configurations, that is the 8/7, the 12/13 and the 4/12 SSC configurations. Investigations to resolve the discrepancies are in progress.

2.3.1.2 Flux Distributions in the 4/12 SSC Configurations

Table 2.3.7 and 2.3.8 present fission equivalent fluxes and fission rates, respectively, for the 4/12 SSC configuration. As opposed to the abbreviated update format for Table 2.3.6, these tables give a detailed account of the correction factors and multiplicative constants, and their respective uncertainties, used to derive final results. The calculated uncertainties, in the vicinity of 5.5%, are due in most part to the 4.2% absolute power level uncertainty and relatively large corrections for photofission in ^{238}U beyond the 1/2T positions in the PV simulator block. More about photofission is discussed in Sect. 2.3.1.3.

The fission equivalent fluxes in the 4/12 SSC configuration are 14.5% less for ^{237}Np and 33% less for ^{238}U than those in the 8/7 configuration. The larger difference in the ^{238}U fluxes is a result of the introduction of additional inelastic scattering by the steel SSC in place of water. However, as compared to the 12/13 PCA configuration where there is almost a factor of two difference in the water thickness between the core and the simulator block, the 4/12 SSC fission equivalent fluxes are factors of 5.4 and 4.1 larger for ^{237}Np and ^{238}U, respectively.

As with the former PCA measurements (Mc81), the larger volume NBS fission chambers could not be used to measure in the water locations because of flux perturbations introduced by voids when the NBS chambers are surrounded by plexiglass for in-water measurements. Also no ^{235}U fission rate measurements were made with the NBS chamber in the 4/12 SSC configuration.*

2.3.1.3 Long-Term Reproducibility of Measurements

Up to this point, the fission chamber data have been used to derive absolute fluence rate and fission rate information and Table 2.3.1 demonstrated the reproducibility of this kind of data between September 1979 and January 1981. Even more impressive, however, are the data of

*A number of bare and cadmium-covered ^{235}U fission rate measurements are reported in Sect. 4.5.4 for the miniature volume CEN/SCK fission chambers.

TABLE 2.3.7

FISSION EQUIVALENT FLUXES FOR 4/12 SSC PCA CONFIGURATION BASED UPON REVISED MASSES AND NEW CROSS-SECTION VALUES

Conf.	PCA Pos	Observed ETZ and DT Corrected Fiss. Rate	Corr. for Fission in Other Isotopes	Multiplier Constants: Calibration Const. (Benchmark)	Multiplier Constants: $\frac{252_{Cf}}{235_U}$	Multiplier Constants: 10 kW to per Core Neutron	Net** Multiplier	$\phi_{eq}^{235_U}$	Photofission Corrections	Corrected ϕ_{eq} Flux per Nucleus per Neutron
4/12 SSC ^{237}Np	1/4 T	337.4±0.81%	0.9978	1.125×10^6 ± 2.6%	$\frac{1366}{1344} = 1.0164$ ± 0.23%	$(7.55 \times 10^{10} \times 10^4$ watts) $\frac{1}{7.55 \times 10^{14}} = 1.3245 \times 10^{-15}$ ± 4.3%	1.511×10^{-9} ± 5.0%	5.098×10^{-7}	0.9960±0.2%	5.08×10^{-7} ±5.1%
	1/2 T	186.1±1.0%	0.9976					2.812×10^{-7}	0.9980±0.1%	2.81×10^{-7} ±5.2%
	3/4 T	97.63±1.1%	0.9976					1.475×10^{-7}	0.9980±0.1%	1.47×10^{-7} ±5.2%
	VB	26.82±1.8%	0.9972					0.405×10^{-7}	0.9900±0.5%	4.01×10^{-8} ±5.8%
			0.9976 ± 0.0008							
^{238}U	1/4 T	99.78±0.85%	0.9995	1.835×10^6 ± 2.6%	$\frac{326}{309} = 1.055$ ± 1.65%		2.563×10^{-9} ± 5.0%	2.557×10^{-7}	0.9794±1.2%	2.50×10^{-7} ±5.1%
	1/2 T	43.14±1.6%	0.9996					1.106×10^{-7}	0.9872±1.0%	1.09×10^{-7} ±5.2%
	3/4 T	17.92±2.0%	0.9996					0.459×10^{-7}	0.9740±2.0%	4.47×10^{-8} ±5.4%
	VB	4.34±2.1%	0.9993					0.111×10^{-7}	0.9208±4.3%	1.02×10^{-8} ±5.8%
			0.9995 ± 0.0003							

*See Reference 10.

**FOR EXAMPLE:

$0.9976 \times 1.125 \times 10^6 \times 1.0164 \times 1.3245 \times 10^{-15} = 1.511 \times 10^{-9}$.

***^{235}U fission equivalent flux.

TABLE 2.3.8

FISSION REACTION RATES FROM OBSERVED FISSIONS AND CONCENSUS MASSES
BASED UPON REVISED MASS SCALE AND NEW CROSS-SECTION VALUES*

Conf		PCA Pos	Observed ETZ and DT Corrected Fiss. Rate	Corr. for Fission in Other Isotopes		Foil ID Mass (μg) and Nuclei	Frag Abs Corr.	Neutrons per 10.0 kW	Multi. Fact.**	Fiss/s per Nucleus per Neutron	Photofission Corrections	Corrected Fiss/s per Nucleus per Neutron***
4/12 SSC	^{237}Np	1/4T	337.4±0.81%	0.9978	0.9976	37S-2-2 260.8±1.4% 6.625×10^{17}	1.0145±0.0015	$7.55 \times 10^{10} \times 10^{4} = 7.55 \times 10^{14}$ (±4.3%)	2.023×10^{-33} ±1.5%	6.826×10^{-31} ±1.7%	0.9960±0.2%	67.99×10^{-32} ±4.4%
		1/2T	186.1±1.0%	0.9976						3.765×10^{-31} ±1.8%	0.9980±0.1%	37.57×10^{-32} ±4.5%
		3/4T	97.63±1.1%	0.9976						1.975×10^{-31} ±1.9%	0.9980±0.1%	19.71×10^{-32} ±4.5%
		VB	26.82±1.8%	0.9972						5.426×10^{-32} ±2.3%	0.9900±0.5%	5.37×10^{-32} ±4.7%
	^{238}U	1/4T	99.78±0.85%	0.9995	0.9995	25HD-5-2 691.0±1.4% 1.748×10^{18}	1.0381±0.0039		7.862×10^{-34} ±1.6%	7.845×10^{-32} ±1.8%	0.9794±1.2%	7.683×10^{-32} ±4.6%
		1/2T	43.14±1.6%	0.9996						3.392×10^{-32} ±2.3%	0.9872±1.0%	3.349×10^{-32} ±4.8%
		3/4T	17.92±2.0%	0.9996						1.409×10^{-32} ±2.6%	0.9852±0.8%	1.388×10^{-32} ±4.9%
		VB	4.34±2.1%	0.9993						3.412×10^{-33} ±2.6%	0.9208±4.3%	0.314×10^{-32} ±6.5%

*See Reference 10.

**FOR EXAMPLE:

$$\frac{0.9976 \times 1.0145}{6.625 \times 10^{17} \times 7.55 \times 10^{14}} = 2.023 \times 10^{-33}.$$

***It appears that the values in this table should be increased by 1.0035 for ^{237}Np and 1.0070 for ^{238}U to account for scattering effects.

Table 2.3.9 which provide an additional measure of reproducibility of data for the ratios of spectral index measurements among all of the configurations studied (i.e., 8/7, 12/13, 4/9, 4/12 and 4/12 SSC). Note, maximum-to-minimum ratios in all cases are less than 1.2%. It should also be noted that the data in Table 2.3.9 have not been corrected for photofission. When this correction is made, there is at least a factor of two greater spread in the data. This may be due to the fact that the photofission corrections,which are calculated, are only significant towards the back of the PV simulator block, i.e., at the 3/4T position. The calculations are, however, very sensitive to modeling of the void box and relatively small calculational errors can effect the spectral index ratios.

Table 2.3.10 also shows highly reproducible, relative measurements among the 1/4T, 1/2T and 3/4T in-steel locations for all of the various PCA PV simulator configurations. Since the simulator block remained the same for the different water thicknesses, the relative flux gradient through the block is independent of the water gap thicknesses and this is clearly seen from the data in Table 2.3.10. The attenuation is seen to follow a straight exponential rule with attenuation rates for $^{238}U(n,f)$ of 0.160/cm and $^{237}Np(n,f)$ 0.116/cm.

TABLE 2.3.9

COMPARISON OF DOUBLE RATIOS* OF $^{237}Np/^{238}U$ SPECTRAL INDEX RESPONSE AMONG THE VARIOUS PCA CONFIGURATIONS

4/12 SSC ÷ 8/7

1/4 T $\frac{3.381}{2.895} = 1.168$

1/2 T $\frac{4.315}{3.689} = 1.170$

3/4 T $\frac{5.447}{4.638} = 1.174$

Avg = 1.171 ± 0.002
Max/Min = 1.005

4/12 SSC ÷ 12/13

1/4 T $\frac{3.381}{2.526} = 1.338$

1/2 T $\frac{4.315}{3.210} = 1.344$

3/4 T $\frac{5.447}{4.057} = 1.343$

Avg = 1.342 ± 0.002
Max/Min = 1.004

4/12 SSC ÷ 4/9

1/4 T $\frac{3.381}{2.840} = 1.191$

1/2 T $\frac{4.315}{3.645} = 1.184$

3/4 T $\frac{5.447}{4.590} = 1.187$

Avg = 1.187 ± 0.002
Max/Min = 1.006

8/7 ÷ 12/13

1/4 T $\frac{2.895}{2.526} = 1.146$

1/2 T $\frac{3.689}{3.210} = 1.149$

3/4 T $\frac{4.638}{4.057} = 1.143$

Avg = 1.146 ± 0.002
Max/Min = 1.005

8/7 ÷ 4/9

1/4 T $\frac{2.895}{2.840} = 1.019$

1/2 T $\frac{3.689}{3.645} = 1.012$

3/4 T $\frac{4.638}{4.590} = 1.011$

Avg = 1.014 ± 0.003
Max/Min = 1.008

4/9 ÷ 12/13

1/4 T $\frac{2.840}{2.526} = 1.124$

1/2 T $\frac{3.645}{3.210} = 1.136$

3/4 T $\frac{4.590}{4.057} = 1.131$

Avg = 1.130 ± 0.003
Max/Min = 1.011

---

*Data are the ratios of DT- and ETZ-corrected observed fission count rates for $^{237}Np/^{238}U$. These are essential raw data and, in particular, have not been corrected for photofission.

TABLE 2.3.10

COMPARISON OF RELATIVE FAST FLUX GRADIENTS WITHIN THE PVS
FOR VARIOUS CONFIGURATIONS OF THE PCA-PRV FACILITY

PCA-RPV Configuration	Normalized* Results for: ^{237}Np Fission 1/4 T	^{237}Np Fission 1/2 T	^{237}Np Fission 3/4 T	^{238}U Fission 1/4 T	^{238}U Fission 1/2 T	^{238}U Fission 3/4 T
12/13	1.617	0.908	0.475	1.851	0.813	0.336
8/7	1.622	0.902	0.475	1.856	0.808	0.337
8/12	1.636	0.896	0.467	1.862	0.811	0.332
4/9	1.628	0.913	0.481	1.845	0.807	0.338
9/79 4/12 SSC	1.631	0.894	0.475	1.861	0.801	0.338
11/80 4/12 SSC	1.635	0.898	0.466	1.870	0.800	0.329
1/81 4/12 SSC	1.628	0.901	0.472	1.857	0.809	0.334
Average:	1.628	0.902	0.473	1.857	0.807	0.335
$\left[\frac{(Xi - \bar{X})^2}{N}\right]^{1/2}$	±0.007	±0.007	±0.005	±0.008	±0.005	±0.003
Deviation in Percent:	±0.43%	±0.78%	±1.08%	±0.43%	±0.62%	±1.027%

*Normalization achieved by dividing fission equivalent fluxes measured with the NBS chamber by the average fission flux for all three positions (i.e., the 1/4 T, 1/2 T, and 3/4 T positions).

2.4 RADIOMETRIC MEASUREMENTS

L. S. Kellogg (HEDL) and A. Fabry (CEN/SCK)

2.4.1 Introduction and Summary

The previous report in this series (Fa81a) contained the results of radiometric measurements performed in the PCA 8/7 and 12/13 configurations up to Spring 1980. Additional radiometric measurements made or reported subsequent to the last report for the 8/7, 12/13, and 4/12 SSC configurations are reported here, along with the previously reported data.

The reactions and experimental techniques used have been reported previously (Fa81a). The PCA specifications are those reported by Kam (Ka81a). Individual runs were normalized using run-to-run monitoring as detailed in Section 1.2. The comments relative to the continuity in reporting PCA experimental data and uncertainties that were made in Fa81a may also be applied to these measurements.

2.4.2 Experimental Methods

The experimental methods employed in the present measurements are identical to those reported in Fa81a with the exception of the radiometric counting equipment. HEDL radiometric foils were counted using the new ORNL counting equipment. This equipment is identical in design to the CEN/SCK transportable NaI(Tl) spectrometers described in Fa81a.

2.4.3 Experimental Results, Uncertainties, and Discussion

The experimental results listed in Tables 2.4.1 to 2.4.4 are given in units of equivalent fission flux at a measured PCA core power of 9.75 kW for the PCA geometrical specifications valid after June 1979 (Ka81a). Included for comparison are the previously reported PCA 8/7 and 12/13 configuration results (Fa81a). The In, Al, and Ni foils used in the present measurements have been benchmark referenced. The Rh has been benchmarked in a secondary manner by counting the same foil on both the CEN/SCK and ORNL systems. In all cases, the agreement between present measurements and the previously reported measurements is consistent with the reported uncertainties. The means of replicate radiometric measurements and the standard deviations of these means are reported in Table 2.4.1 through 2.4.4. With few exceptions, the standard deviation of the mean (expressed as percent) is in the range of 1% to 3%.

2.4.4 Recommended Radiometric Equivalent Fission Flux per PCA Core Neutron

Individual fission flux values at power, as listed in Table 2.4.1 through 2.4.4, have been averaged, converted to equivalent fission flux per unit core neutron source, using the relationship ϕf source = (ϕf at power X/X) x 1.314 E-14, and tabulated in Table 2.4.5. The 1978 data, which included an additional position gradient correction (Mc81, Section 7.2), was weighted. All other measurements were averaged directly. The conversion of the HEDL reaction rate measurements during 1978, 1979 and 1980 to equivalent fission flux values, with associated uncertainties; and the comparison to the directly measured Mol and subsequent 1981 HEDL-measured equivalent fission flux values has been discussed thoroughly in Fa81a.

2.4.5 Interconfiguration Consistency

Confirmation that attenuation in the PVS block appears to be independent of the configuration, first noted in Mc81b, is further substantiated by the data in Table 2.4.6. At the same time and in a secondary manner, this also tends to confirm the experimental and RM analytical consistency.

TABLE 2.4.1

$^{103}Rh(n,n')^{103m}Rh$ EQUIVALENT FISSION FLUXES ($cm^{-2}s^{-1}$)
IN THE PCA BLIND TEST CONFIGURATIONS[a]

Midplane Location	Y[b] (mm)	HEDL 1981	Mol 1978[d]	Mol 1979	Mol 1981
4/12 SSC Configuration					
SSC	156	No measurements	--	3.994 E+9	--
1/4 T	305	taken for this	--	3.319 E+8	--
1/2 T	357	configuration	--	1.825 E+8	--
8/7 Configuration					
TSF (A1)	79.1	(f)	(e)	--	--
PVF (A3M)	197.0	(f)	(e)	--	--
1/4 T (A4)	295.0	3.513 E+8	3.500 E+8	3.481 E+8	--
1/2 T (A5)	346.6	1.907 E+8	1.910 E+8 (±1.5%)	1.881 E+8	--
3/4 T (A6)	401.2	9.721 E+7	9.57 E+7 (±1.8%)	9.75 E+7	--
VB[f] (A7)	491.2	2.81 E+7 (±3%)	2.68 E+7 (±2%)	2.79 E+7 (±1.4%)[c]	--
12/13 Configuration					
TSF (A1)	119.8	4.139 E+9	(e)	4.078 E+9	--
TSB (A2)	238	--	--	--	4.55 E+8 (±1.1%)
PVF (A3M)	297.1	1.495 E+8	(e)	1.510 E+8	1.474 E+8 (±1.1%)
1/4 T (A4)	395.1	5.629 E+7	5.791 E+7	5.613 E+7	--
1/2 T (A5)	446.7	3.31 E+7 (±4.3%)	3.25 E+7 (±5%)	--	--
3/4 T (A6)	501.3		1.64 E+7 (±5%)	--	--
VB[f] (A7)	591.3	4.899 E+6 (±5.3%)	--	--	--

(a) At peak vertical flux on the centerline of experimental channels and for a core power of 9.75-kW, geometry of configurations after June 1979 (Mc81, Section 8.1).
(b) Distance to the inner face of core aluminum window.
(c) Experimental precision indicated within parentheses when >1%.
(d) Original data multiplied by corrections gathered in Mc81, Table 7.2.1.
(e) Measurements affected by instrumental neutron field perturbations.
(f) Data highly questionable due to rod drops and to reduced power operation during irradiation.
(g) Uncertainties on the order of ±3% can be induced by vertical positioning difficulties.

TABLE 2.4.2

$^{115}In(n,n')^{115m}In$ EQUIVALENT FISSION FLUXES ($cm^{-2}s^{-1}$)
IN THE PCA BLIND TEST CONFIGURATIONS[a]

Midplane Location	Y[b] (mm)	HEDL 1978[d]	HEDL 1979	HEDL 1981	Mol 1978[d]	Mol 1979	Mol 1981
4/12 SSC Configuration							
SSC	156	No measurements taken for this configuration			--	2.887 E+9	--
1/4 T	305				--	2.239 E+8	--
1/2 T	357				--	1.070 E+8	--
8/7 Configuration							
TSF (A1)	79.1	(e)	--	--	(e)	--	9.249 E+9 (±2.5%)
PVF (A3M)	197.0	(e)	--	7.622 E+8	(e)	--	--
1/4 T (A4)	295.0	2.527 E+8	2.515 E+8	--	2.490 E+8 (±1.7%)	2.531 E+8	--
1/2 T (A5)	346.6	1.179 E+8	1.192 E+8	--	1.167 E+8 (±1.8%)	1.207 E+8 (±2.5%)[c]	--
3/4 T (A6)	401.2	5.205 E+7	5.271 E+7	5.387 E+7	5.1 E+7 (±7%)	5.457 E+7	--
VB[f] (A7)	491.2	1.336 E+7	1.392 E+7	--	1.325 E+7 (±1.6%)	--	--
12/13 Configuration							
TSF (A1)	119.8	(e)	4.084 E+9[g]	4.078 E+9	(e)	4.129 E+9	4.131 E+9 (±1.8%)
TSB (A2)	238	--	--	--	--	--	4.463 E+8 (±1.1%)
PF (A3M)	297.1	(e)	1.439 E+8[g]	1.412 E+8	(e)	1.466 E+8	1.465 E+8 (±1.1%)
1/4 T (A4)	395.1	--	4.350 E+7	4.388 E+7	4.293 E+7 (1.54%)	4.359 E+7	--
1/2 T (A5)	446.7	--	2.071 E+7	2.060 E+7	1.994 E+7 (±2%)	--	--
3/4 T (A6)	501.3	--	--	8.90 E+6 (±3.4%)	8.62 E+6 (±3%)	--	--
VB[f] (A7)	591.3	--	--	2.526 E+6 (±4%)	--	--	--

(a) At peak vertical flux on the centerline of experimental channels and for a core power of 9.75-kW, geometry of configurations after June 1979 (Mc81, Section 8.1).
(b) Distance to the inner face of core aluminum window.
(c) Experimental precision indicated within parentheses when >1%.
(d) Original data multiplied by corrections gathered in Mc81, Table 7.2.1.
(e) Measurements affected by instrumental neutron field perturbations.
(f) Uncertainties on the order of ±3% can be induced by vertical positioning difficulties.
(g) Run-to-run normalization monitor results are somewhat questionable for this particular irradiation.

TABLE 2.4.3

$^{58}Ni(n,p)^{58}Co$ EQUIVALENT FISSION FLUXES ($cm^{-2}s^{-1}$)
IN THE PCA BLIND TEST CONFIGURATIONS[a]

Midplane Location	Y[b] (mm)	HEDL		Mol		
		1978[d]	1979	1978[d]	1979	1981
4/12 SSC Configuration						
SSC	156	No measurements taken		--	1.942 E+9	--
1/4 T	305	for this configuration		--	1.286 E+8	--
1/2 T	357			--	5.172 E+7	--
8/7 Configuration						
TSF (A1)	79.1	(e)	--	(e)	--	9.279 E+9
PVF (A3M)	197.0	(e)	--	(e)	--	--
1/4 T (A4)	295.0	1.825 E+8	1.828 E+8	1.790 E+8	1.764 E+8	--
1/2 T (A5)	346.6	7.170 E+7	--	6.977 E+7	--	--
3/4 T (A6)	401.2	2.622 E+7	--	2.536 E+7	--	--
VB[f] (A7)	491.2	6.35 E+6[g]	--	--	--	--
12/13 Configuration						
TSF (A1)	119.8	(e)	--	(e)	4.246 E+9	4.293 E+9
TSB (A2)	238	--	--	--	--	4.551 E+8
PVF (A3M)	297.1	(e)	--	(e)	1.684 E+8	1.701 E+8
1/4 T (A4)	395.1	3.910 E+7	--	3.851 E+7 (±1.5%)[c]	3.841 E+7	--
1/2 T (A5)	446.7	--	--	1.526 E+7 (±1.5%)	--	--
3/4 T (A6)	501.3	--	--	5.414 E+6 (±2%)	--	--
VB[f] (A7)	591.3	--	--	--	--	--

(a) At peak vertical flux on the centerline of experimental channels and for a core power of 9.75-kW geometry of configurations after June 1979 (Mc81, Sec. 8.1).
(b) Distance to the inner face of core aluminum window.
(c) Experimental precision indicated within parentheses when >1%.
(d) Original data multiplied by corrections gathered in Mc81, Table 7.2.1.
(e) Measurements affected by instrumental neutron field perturbations.
(f) Uncertainties on the order of ±3% can be induced by vertical positioning difficulties.
(g) Derived from traverse data in unmonitored run in 1978.

TABLE 2.4.4

$^{27}Al(n,\alpha)^{24}Na$ EQUIVALENT FISSION FLUXES ($cm^{-2}s^{-1}$)
IN THE PCA BLIND TEST CONFIGURATIONS[a]

Midplane Location	Y[b] (mm)	HEDL 1978[d]	HEDL 1979	HEDL 1981	Mol 1978[d]	Mol 1979	Mol 1981
4/12 SSC Configuration							
SSC	156	No measurements taken for this			--	2.129 E+9	--
1/4 T	305	configuration			--	1.798 E+8	--
1/2 T	357				--	1.613 E+8	--
8/7 Configuration							
TSF (A1)	79.1	(e)	--	--	(e)	--	1.096 E+10 (±2.1%)
PVF (A3M)	197.0	(e)	--	1.210 E+9 (±2.4)	(e)	--	--
1/4 T (A4)	295.0	2.626 E+8	2.564 E+8	--	2.638 E+8	2.620 E+8	--
1/2 T (A5)	346.6	1.018 E+8	1.026 E+8	--	1.052 E+8	--	--
3/4 T (A6)	401.2	3.865 E+7	3.838 E+7	--	3.840 E+7	--	--
VB[f] (A7)	491.2	--	1.132 E+7	--	1.016 E+7 (±10%)	1.134 E+7 (±9%)[c]	--
12/13 Configuration							
TSF (A1)	119.8	--	--	5.72 E+9 (±3%)	(e)	5.796 E+9	5.788 E+1 (±1.1%)
TSB (A2)	238	--	--	--	--	--	7.541 E+1 (±1.1%)
PVF (A3M)	297.1	--	--	--	(e)	3.302 E+8	3.247 E+1 (±1.1%)
1/4 T (A4)	395.1	--	--	7.461 E+7	7.702 E+7 (±2%)	7.383 E+7 (±2%)	--
1/2 T (A5)	446.7	--	--	--	3.078 E+7 (±2%)	--	--
3/4 T (A6)	501.3	--	--	1.193 E+7 (±3%)	1.154 E+7 (±2%)	--	--
VB[f] (A7)	591.3	--	--	4.52 E+6 (±5.6%)	--	--	--

(a) At peak vertical flux on the centerline of experimental channels and for a core power of 9.75 kW, geometry of configurations after June 1979 (Mc81, Section 8.1).
(b) Distance to the inner face of core aluminum window.
(c) Experimental precision indicated within parentheses when >1%.
(d) Original data multiplied by corrections gathered in Mc81, Table 7.2.1.
(e) Measurements affected by instrumental neutron field perturbations.
(f) Uncertainties on the order of ±3% can be induced by vertical positioning difficulties.

TABLE 2.4.5

INTERLABORATORY RECOMMENDED RESULTS FOR RADIOMETRIC MEASUREMENTS OF EQUIVALENT FISSION FLUXES[a]

Midplane Location	Y[b] (mm)	Equivalent Fission Fluxes [per unit PCA Core Neutron Source (cm^{-2})][c] $^{103}Rh(n,n')$	$^{115}In(n,n')$	$^{58}Ni(n,p)$	$^{27}Al(n,\alpha)$
Core Center Configuration					
CC (A0)	-205.7	(d)	(d)	2.21 E-4 (±0.5%)	2.14 E-4 (±1%)
4/12 SSC Configuration					
SSC (A2)	156	5.42 E-6 (±1.4%)	3.89 E-6 (1.3%)	2.64 E-6 (±1.2%)	2.87 E-6 (±0.8%)
1/4 T (A4)	305	4.51 E-7 (±0.7%)	3.02 E-7 (1.2%)	1.75 E-7 (±1.7%)	2.42 E-7 (±0.8%)
1/2 T (A5)	357	2.48 E-7 (±1.0%)	1.44 E-7 (1.3%)	7.04 E-8 (±2.2%)	9.62 E-8 (±1.3%)
8/7 Configuration					
TSF (A1)	79.1	(d)	1.25 E-5 (±2.5%)	1.26 E-5 (±1.3%)	1.48 E-5 (±2.0%)
PVF (A3M)	197.0	---	1.03 E-6 (±3%)	---	---
1/4 T (A4)	295.0	4.71 E-7 (±0.5%)	3.39 E-7 (±0.7%)	2.44 E-7 (±1.2%)	3.52 E-7 (±1.2%)
1/2 T (A5)	346.6	2.56 E-7 (±0.8%)	1.60 E-7 (±1.8%)	9.58 E-8 (±1.9%)	1.39 E-7 (±1.7%)
3/4 T (A6)	401.2	1.30 E-7 (±1.2%)	7.12 E-8 (±2.6%)	3.49 E-8 (±2.4%)	5.19 E-8 (±0.8%)
VB (A7)	491.2	3.72 E-8 (±2.6%)	1.82 E-8 (±2.7%)	8.56 E-9 (±3.0%)	1.47 E-8 (±0.7%)
12/13 Configuration					
TSF (A1)	119.8	5.54 E-6 (±1.0%)	5.53 E-6 (±1.3%)	5.81 E-6 (±0.8%)	7.77 E-6 (±0.8%)
TSB (A2)	238	6.13 E-7 (±1.5%)	6.01 E-7 (±2.0%)	6.19 E-7 (±2.0%)	1.01 E-6 (±0.6%)
PVF (A3M)	297.1	2.02 E-7 (±1.5%)	1.95 E-7 (±1.7%)	2.30 E-7 (±0.8%)	4.45 E-7 (±2.1%)
1/4 T (A4)	395.1	7.66 E-8 (±1.6%)	5.86 E-8 (±0.9%)	5.25 E-8 (±1.0%)	1.01 E-7 (±2.2%)
1/2 T (A5)	446.7	4.42 E-8 (±1.4%)	2.75 E-8 (±2.0%)	2.08 E-8 (±1.6%)	1.58 E-8 (±2.3%)
3/4 T (A6)	501.3	2.21 E-8 (±5.0%)	1.18 E-8 (±2.3%)	7.37 E-9 (±2.1%)	6.06 E-9 (±5.6%)
VB (A7)	591.3	6.60 E-9 (±5.3%)	3.40 E-9 (±4.0%)	---	---

(a) Uncertainties estimates are based on experimental precision only, as defined in Mc81, Section 2.4.4; overall combined uncertainties are ±6% for a precision of ±1% (see Mc81, Tables 2.4.8 and 2.4.9).
(b) Distance to inner face of core aluminum simulator (or window).
(c) All Mol nickel data were increased by 1.0% when deriving weighted best values by combination with HEDL data or whenever HEDL data were not available; this introduces a 1% difference when compared to all the nickel tabulations of Mc81, Section 7.2.
(d) Measurements are available, but analyses or evaluations are still in progress.
(e) Interpolated values.

TABLE 2.4.6

INTERCONFIGURATION EQUIVALENT FISSION FLUX RATIOS

Location	Rh	In	Ni	Al
	(4/12 Configuration)/(8/7 Configuration)			
1/4 T	0.9575 (±0.9%)*	0.8909 (±1.4%)	0.7119 (±2.1%)	0.6875 (±1.4%)
1/2 T	0.9687 (+1.3%)	0.9000 (+1.7%)	0.7314 (+2.4%)	0.6921 (+2.1%)
Average	0.9631 (±0.8%)**	0.8955 (±0.7%)	0.7216 (±1.9%)	0.6898 (±0.5%)
	(8/7 Configuration)/(12/13 Configuration)			
1/4 T	6.1488 (±1.7%)	5.7850 (±1.7%)	4.6641 (±2.1%)	3.8851 (±2.8%)
1/2 T	5.7918 (±1.6%)	5.8182 (±1.1%)	4.6262 (±2.8%)	3.3902 (±2.4%)
3/4 T	5.8824 (+5.1%)	6.0339 (+3.5%)	4.7671 (+3.7%)	3.2848 (+5.6%)
Average	5.9410 (±2.2%)	5.8790 (±1.6%)	4.6858 (±1.1%)	3.3867 (±2.1%)

*The uncertainty of the fission flux ratios was obtained by combining the uncertainties of the reaction rates in quadrature.

**The uncertainty of the average is the standard deviation of the mean of the ratios averaged.

2.5 SOLID STATE TRACK RECORDER MEASUREMENTS

F. H. Ruddy, J. H. Roberts, Raymond Gold and C. C. Preston (HEDL)

Initial fission rate measurements using Solid State Track Recorders (SSTRs) were reported for the PCA 8/7 and 12/13 configurations in the preceding document in this series (Mc81). Additional measurements, which have been carried out in the 8/7, 12/13, and 4/12 SSC configurations, are summarized in Table 2.5.1. The experimental details of these measurements are identical to those in (Ru81). Subsequent to the reporting of the initial SSTR fission rate measurements, the optical efficiency for fission tracks in mica has been remeasured. The newer value (0.9875 ± 0.0085) tracks/fission has been used for the more recent measurements. All previous measurements must be corrected to correspond to the newer optical efficiency values when comparisons are made with the more recent data.

2.5.1 PCA 12/13 Configuration

In November 1981, fission rates were measured for all seven radial locations simultaneously in separate runs for ^{237}Np and ^{238}U. These data represent the only PCA radial traverses where relative fission rates can be obtained without power normalization uncertainties for the seven radial locations. The SSTR fission rates measured in the PCA for ^{237}Np and ^{238}U are listed as a function of radial position for the 12/13 configuration in Table 2.5.2. These data are plotted in Figure 2.5.1 for ^{237}Np and Figure 2.5.2 for ^{238}U. These fission rates display the pseudologarithmic decrease as a function of distance within the PVS block that is characteristic of threshold reactions. The departure of the ^{237}Np fission rates in Figure 2.5.1 from linearity in the water locations is due to contributions to the fission rate from subthreshold fission. The cross section for neutron-induced ^{237}Np fission shows resonances in the epithermal energy range, and the relative number of epithermal neutrons increases as the core is approached.

In the case of the ^{238}U data plotted in Figure 2.5.2, a straight line with a slope slightly less than the slope in the PVS is obtained in the water positions. These lines intersect at the PVS-H_2O boundary. The contribution to the measured fission rate from ^{235}U in the ^{238}U foils is appreciable in the water positions. A 14.6% correction was required in the PVF position, and a 30% correction was required at the TSB location. The thermal fission correction resulted in an overall uncertainty of 15% for the TSB ^{238}U fission rate. Although this point has been plotted in Figure 2.5.2, it has been omitted from Table 2.5.2 because of its large uncertainty.

In the TSF position, the ^{238}U fission rate could not be accurately measured even with ^{238}U deposits containing as little as 6 ppm ^{235}U due to the extremely high thermal-to-fast-neutron ratio at this location. The relative uncertainties (1σ) have been obtained by combining the sources of error tabulated in (Ru81) in quadrature. Uncertainties in power normalization do

TABLE 2.5.1

SCHEDULE OF PCA SOLID STATE TRACK RECORDER MEASUREMENTS

Run Number	Date	Configuration	Isotope	Positions*
PCA37	01/14/81	4/12 SSC	^{237}Np	SSC (+75 mm, MP, -75 mm), 1/4 T (+150 mm, MP, -130 mm), 1/2 T (MP)
PCA38	01/14/81	4/12 SSC	^{238}U	SSC (+75 mm, MP, -75 mm), 1/4 T (+75 mm, MP, -75 mm), 1/2 T (MP), 3/4 T (MP)
PCA39	10/15/81	8/7	^{238}U	1/4 T, 1/2 T, 3/4 T, VB (all MP)
PCA40	10/15/81	8/7	^{237}Np	1/4 T, 1/2 T, 3/4 T, VB (all MP)
PCA42	10/16/81	12/13	^{238}U	1/4 T, 1/2 T, 3/4 T, VB (all MP)
PCA43	10/16/81	12/13	^{237}Np	1/4 T, 1/2 T, 3/4 T, VB (all MP)
PCA51	11/18/81	12/13	^{238}U	TSF, TSB, PVF, 1/4 T, 1/2 T, 3/4 T, VB (all MP)
PCA52	11/18/81	12/13	^{237}Np	TSF, TSB, PVF, 1/4 T, 1/2 T, 3/4 T, VB (all MP)
PCA53	11/19/81	12/13	^{235}U	TSF, TSB, PVF, 1/4 T, 1/2 T, 3/4 T, VB (all MP)
PCA54	11/19/81	12/13	^{238}U	TSF, TSB, PVF (all +75 mm, MP, -75 mm)

*1/4 T, 1/2 T and 3/4 T refer to depths in a PVS of total thickness T. The other acronyms are defined as follows: Simulated Surveillance Capsule (SSC), Thermal Shield Front (TSF), Thermal Shield Back (TSB), Pressure Vessel Front (PVF), Void Box (VB), and Mid-Plane (MP).

TABLE 2.5.2

SSTR FISSION RATES MEASURED IN THE PCA 12/13 CONFIGURATION

Location	Distance from Core (cm)*	Fission Rate** (fissions per atom per core neutron) ^{237}Np	^{238}U
TSF	12.0	7.90×10^{-30} (±3.3%)	---
TSB	23.8	7.47×10^{-31} (±3.3%)	---
PVF	29.7	3.19×10^{-31} (±3.3%)	6.48×10^{-32} (±4.1%)
1/4 T	39.5	1.18×10^{-31} (±3.6%)	1.75×10^{-32} (±2.7%)
1/2 T	44.7	6.19×10^{-32} (±5.4%)	7.50×10^{-33} (±2.7%)
3/4 T	50.1	3.32×10^{-32} (±3.3%)	3.23×10^{-33} (±2.7%)
VB	59.1	9.70×10^{-33} (±3.4%)	9.70×10^{-34} (±2.7%)

*Distance from inner face of core aluminum simulator (or window).
**All SSTR fission rates were calculated using the newly measured value for the mica optical efficiency (0.9875 ± 0.0085) tracks/fission.

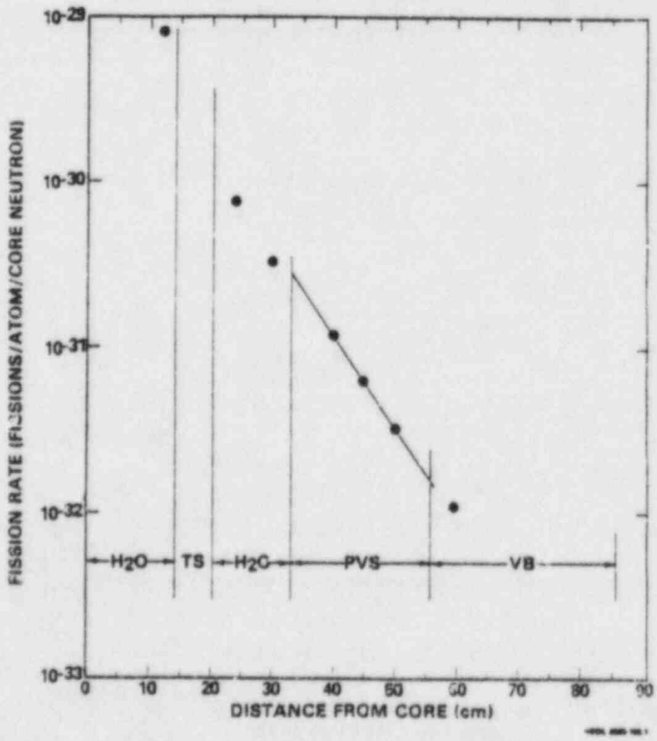

FIGURE 2.5.1. Radial Fission Rate Distribution for ^{237}Np in the PCA 12/13 Configuration.

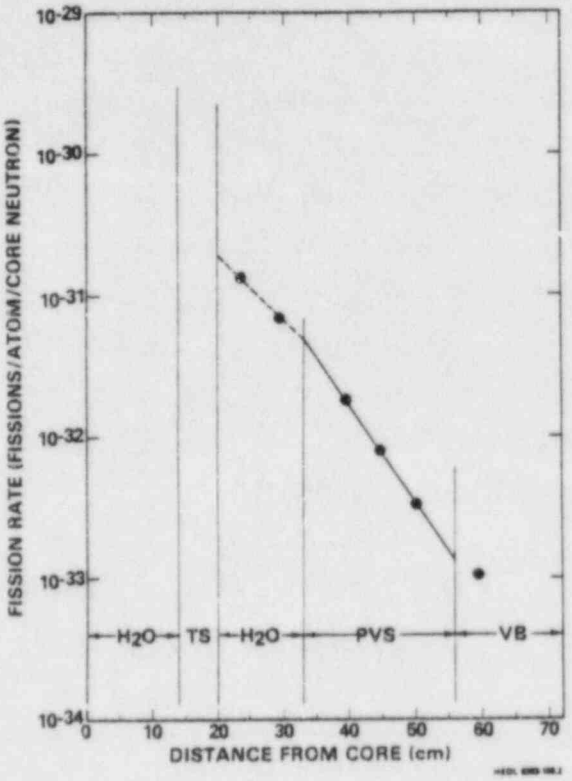

FIGURE 2.5.2. Radial Fission Rate Distribution for ^{238}U in the PCA 12/13 Configuration.

not enter into the calculation of the relative uncertainties, since a single run was used for ^{238}U or ^{237}Np. To obtain the absolute uncertainties from the relative uncertainties of Table 2.5.2, the 4.1% uncertainty in the absolute power normalization must be combined in quadrature with the tabulated values. The absolute uncertainties in these data are generally 5% (1 σ) or less.

Note that the November 1981 SSTR fission rates for ^{237}Np were 15% lower than the SSTR fission rates measured in October 1978, which are tabulated in (Ru81). This difference must be due to a mispositioning of the PCA 12/13 configuration during the earlier measurements, as a 15% error is far too large to be accounted for by any other experimental error. Additional ^{237}Np and ^{238}U 12/13 fission rates are available from the October 1981 runs, and these data are contained in Table 2.5.3. The fission rates measured in November 1981 and the ratios of the fission rates are shown for comparison. In general, the agreement between the two sets of data is excellent, indicating that the measurements are reproducible within the quoted experimental uncertainties.

TABLE 2.5.3

RATIOS OF DUPLICATE PCA 12/13 SSTR FISSION RATE MEASUREMENTS

Isotope	Location	Fission Rate [(fissions per atom per core neutron) x 10^{33}] October 1981	November 1981	Oct 1981/Nov 1981
^{238}U	1/4 T	17.4 (±2.7%)	17.5 (±2.7%)	0.992 (±3.6%)
	1/2 T	7.44 (±2.7%)	7.50 (±2.7%)	0.992 (±3.6%)
	3/4 T	3.24 (±2.7%)	3.23 (±2.7%)	1.01 (±3.6%)
	VB	0.970 (±2.7%)	0.970 (±2.7%)	1.00 (±3.6%)
^{237}Np	1/4 T	116.0 (±3.3%)	118.0 (±3.6%)	0.983 (±4.7%)
	3/4 T	32.3 (±3.3%)	33.2 (±3.3%)	0.970 (±4.5%)
	VB	9.79 (±3.3%)	9.70 (±3.4%)	1.01 (±4.6%)
			Average	0.994 (±1.45%)

2.5.2 PCA 8/7 Configuration

Additional ^{237}Np and ^{238}U fission rates were measured during October 1981. Unfortunately, malfunctioning electronic equipment associated with the run-to-run monitor resulted in loss of the PCA power information. New absolute fission rates are, therefore, not available; however, the relative fission rates are useful and are referred to in Section 2.5.4.

2.5.3 PCA 4/12 SSC Configuration

^{237}Np and ^{238}U fission rates were measured in the SSC, 1/4 T, 1/2 T and 3/4 T locations in the PCA 4/12 SSC configuration during January 1981. These data are summarized in Tables 2.5.4 and 2.5.5. The relative fission rates are plotted as a function of axial location in Figure 2.5.3. All data were normalized to the midplane location. The solid line plotted for comparison is the result of Mol fission chamber traverses (Mc81b). The agreement of the relative SSTR fission rates with the shape of the axial distribution indicated by the fission chamber is consistent with the experimental uncertainties of the data. Fission rates as a function of radial location are plotted for ^{237}Np in Figure 2.5.4 and for ^{238}U in Figure 2.5.5. Data from the 8/7 and 12/13 configurations are also plotted for comparison. Relative

TABLE 2.5.4

PCA ^{237}Np FISSION RATES

PCA Configuration	Axial Location (mm)	Fission Rate (fissions per atom per core neutron) SSC Position	1/4 T Position	1/2 T Position
4/12 SSC	+150	---	5.078 E-31 (±2.6%)	---
	+75	8.162 E-30 (±2.6%)	---	---
	0	8.479 E-30 (±2.6%)	6.254 E-31 (±2.6%)	3.435 E-31 (±2.6%)
	-75	8.416 E-30 (±2.6%)	---	---
	-130	---	5.520 E-31 (±2.6%)	---

TABLE 2.5.5

PCA ^{238}U FISSION RATES

PCA Configuration	Axial Location (mm)	Fission Rate (fissions per atom per core neutron) SSC Position	1/4 T Position	1/2 T Position	3/4 T Position
4/12 SSC	+75	1.037 E-30 (±2.6%)	5.826 E-32 (±2.4%)	---	---
	0	1.147 E-30 (±2.6%)	6.596 E-32 (±2.4%)	2.993 E-32 (±2.4%)	1.292 E-32 (±2.4%)
	-75	1.115 E-30 (±2.6%)	6.507 E-32 (±2.4%)	---	---

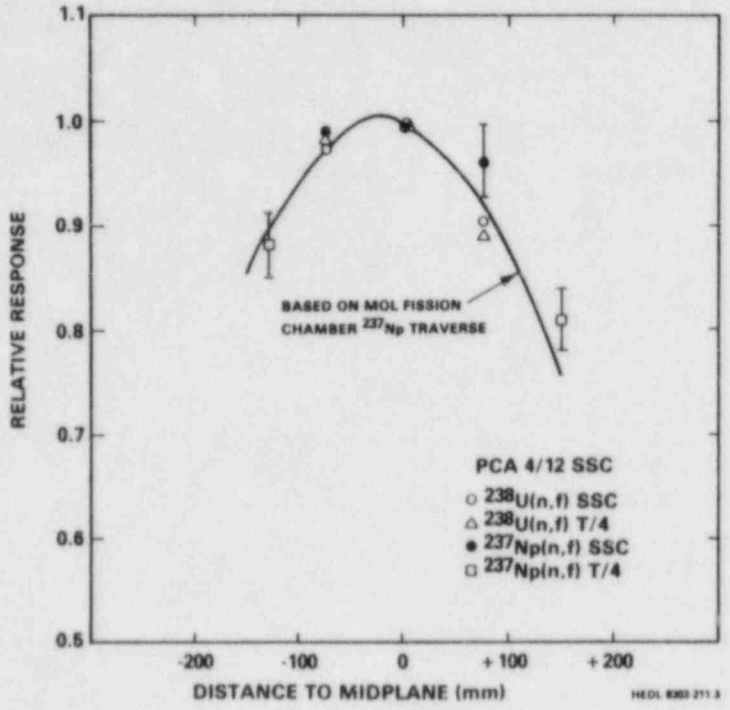

FIGURE 2.5.3. Axial Distributions of the ^{237}Np and ^{238}U Fission Rates in the PCA 4/12 SSC Configuration.

uncertainties are indicated for the data in Tables 2.5.4 and 2.5.5. To obtain the absolute uncertainties from these relative uncertainties, the 4.1% uncertainty in the absolute power normalization must be combined in quadrature with the tabulated values. The absolute uncertainties in these data are generally <5% (1σ).

2.5.4 General Data Trends

The data plotted in Figures 2.5.4 and 2.5.5 show that the slopes of the attenuation in the PVS block appear to be independent of configuration. This fact, which was first noted in (Mc81b), is further substantiated by the data in Table 2.5.6. Here all fission rates have been normalized to one at the 1/4 T location, and the 1/2 T and 3/4 T relative fission rate values are seen to be independent of configuration. The small standard deviations of the means of the relative reaction rates for each location indicate that the precision of the SSTR results is within the quoted uncertainties.

As a further check on the consistency of the SSTR reaction rates, ratios were taken for equivalent locations in the different configurations. These data are contained in Table 2.5.7. For the PVS block, the reaction rate ratios are independent of location. Again, the standard deviations of the means are consistent with the experimental uncertainties of the data.

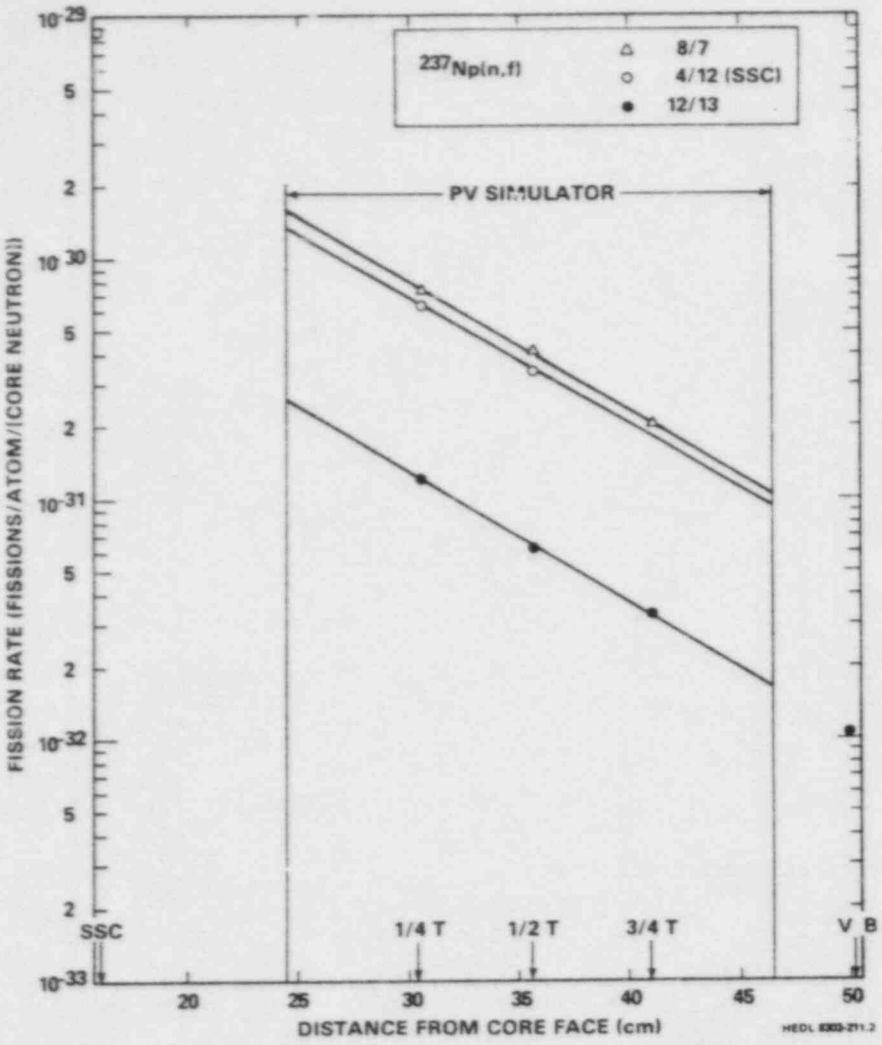

FIGURE 2.5.4. Radial Fission Rate Distributions for ^{237}Np in the PCA 8/7, 4/12 SSC, and 12/13 Configurations. The distances from core face apply to the 4/12 SSC data only.

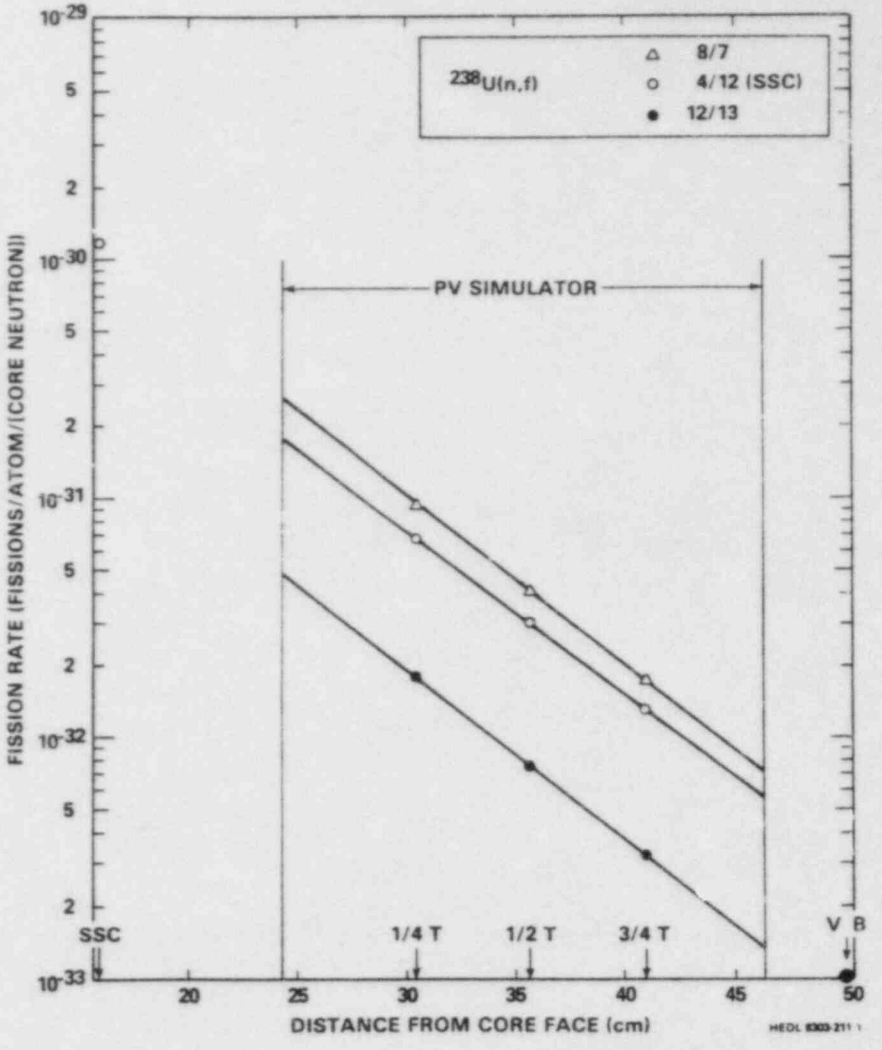

FIGURE 2.5.5. Radial Fission Rate Distributions for ^{238}U in the PCA 8/7, 4/12 SSC and 12/13 Configurations. The distances from core face apply to the 4/12 SSC data only.

TABLE 2.5.6

RELATIVE REACTION RATES IN THE PCA PRESSURE VESSEL SIMULATOR

Isotope	Configuration	Location 1/4 T*	1/2 T	3/4 T
^{238}U	8/7 (Oct 1981)	1.00	0.442 (±3.7%)	0.193 (±3.7%)
	8/7 (Oct 1978)	1.00	0.443 (±3.8%)	0.187 (±3.6%)
	4/12 SSC	1.00	0.454 (±3.2%)	0.196 (±3.2%)
	12/13 (Oct 1981)	1.00	0.427 (±3.7%)	0.187 (±3.7%)
	12/13 (Nov 1981)	1.00	0.429 (±3.7%)	0.185 (±3.7%)
	Average	--	0.439 (±2.5%)	0.190 (±2.5%)
^{237}Np	8/7 (Oct 1981)	1.00	0.593 (±3.7%)	0.275 (±3.7%)
	8/7 (Oct 1978)	1.00	0.564 (±3.5%)	0.275 (±5.1%)
	4/12 SSC	1.00	0.549 (±3.5%)	---
	12/13 (Oct 1981)	1.00	---	0.278 (±3.7%)
	12/13 (Nov 1981)	1.00	0.524 (±6.4%)	0.281 (±4.7%)
	Average	--	0.558 (±5.2%)	0.277 (±1.0%)

*Reaction rates normalized to the 1/4 T position. Uncertainties in relative reaction rates were obtained by combining the uncertainties of reaction rates in quadrature. The uncertainty of the average is the standard deviation of the mean of the values averaged.

TABLE 2.5.7

INTER-CONFIGURATION REACTION RATE RATIOS

Isotope	Ratio	Location 1/4 T	1/2 T	3/4 T	Average
^{238}U	(8/7)/(4/12 SSC)	1.38 (±3.4%)*	1.35 (±3.6%)*	1.32 (±3.4%)*	1.35 (±2.2%)*
	(4/12 SSC)/(12/13)	3.78 (±3.5%)	3.99 (±3.5%)	4.01 (±3.5%)	3.93 (±3.2%)
	(8/7)/(12/13)	5.22 (±3.6%)	5.39 (±3.8%)	5.30 (±3.6%)	5.30 (±1.6%)
^{237}Np	(8/7)/(4/12 SSC)	1.14 (±5.3%)	1.17 (±5.9%)	---	1.16 (±1.8%)
	(4/12 SSC)/(12/13)	5.30 (±4.3%)	5.55 (±6.0%)	---	5.42 (±3.3%)
	(8/7)/(12/13)	6.06 (±5.8%)	6.51 (±7.6%)	5.92 (±5.5%)	6.16 (±5.0%)

*Uncertainties on the reaction rate ratios were obtained by combining the uncertainties of the reaction rates in quadrature. The uncertainty of the average is the standard deviation of the mean of the ratios averaged.

The relative reaction rate data of Tables 2.5.6 and 2.5.7, as well as the data of Table 2.5.3 indicate that all the PCA SSTR reaction rate measurements are self-consistent on a relative basis and that the measurements are reproducible within the stated experimental uncertainties on an absolute basis.

Discrepancies have been found with the results of fission chamber measurements, however, and these discrepancies are explored in Section 2.6.

2.5.5 Photofission-Corrected SSTR Fission Rates

The SSTR measured fission rates have been corrected for assumed photofission contributions using the calculated correction factors of Section 4.5. The corrected values are contained in Tables 2.5.8 - 10. Also included for comparison are the updated ^{232}Th and ^{235}U fission rates, which were measured in 1978. In addition to using the new optical efficiency value, the ^{232}Th and ^{235}U measurements for the 12/13 configuration have been corrected for a probable mispositioning of the PCA during the 1978 runs by using the ratio of the 1981 ^{237}Np fission rates in the 12/13 configuration to the 1978 values.

Cadmium ratios derived from the SSTR ^{235}U fission rates are contained in Table 2.5.11.

2.5.6 Conclusions

Final SSTR fission rates are presented for the PCA 8/7, 12/13, and 4/12 SSC configurations. These measurements are found to be reproducible and self-consistent both on an intra- and inter-configuraion basis. Absolute discrepancies with NBS fission chamber fission rates and recommendations appear in Section 2.6.

TABLE 2.5.8

SSTR NEUTRON-INDUCED FISSION RATES MEASURED IN THE PCA 8/7 CONFIGURATION

Location	Distance from Core (cm)*	Fission Rate** (fissions per atom per core neutron)				
		^{237}Np	^{238}U	^{232}Th	^{235}U	^{235}U-Cd
1/4 T	29.5	7.11 E-31 (±6.2%)	8.92 E-32 (±4.8%)	2.15 E-32 (±4.8%)	2.44 E-29 (±5.1%)	1.32 E-29 (±4.9%)
1/2 T	34.7	4.02 E-31 (±6.7%)	3.98 E-32 (±5.0%)	9.24 E-33 (±4.8%)	7.08 E-30 (±4.7%)	6.33 E-30 (±5.1%)
3/4 T	40.1	1.95 E-31 (±6.1%)	1.62 E-32 (±4.8%)	3.46 E-33 (±4.8%)	3.53 E-30 (±4.9%)	2.95 E-30 (±4.7%)
VB	49.1	---	---	7.82 E-34 (±5.0%)	---	1.03 E-30 (±4.8%)

*Distance from the inner face of core aluminum simulator (or window).

**All fission rates were corrected to a true core power of 9.75 kW at 10 kW. The ^{235}U and ^{232}Th fission rates were measured in November 1978. Corrections to these fission rates (due to slight mechanical modifications of the PCA support in June 1979) were made using the factors from Table 7.2.1 in Mc81. In the case of ^{235}U-bare and ^{232}Th, the factors for ^{235}U-Cd and ^{238}U were used, respectively. The 3/4 T factors were used to correct the VB fission rates. The ^{238}U and ^{237}Np fission rates were measured after June 1979. All SSTR fission rates were calculated using the newly measured value for the mica optical efficiency (0.9875 ± 0.0085) in units of tracks/fission. Photofission corrections were made using the data from Table 4.5.6.

TABLE 2.5.9

SSTR NEUTRON-INDUCED FISSION RATES MEASURED IN THE PCA 12/13 CONFIGURATION

Location	Distance from Core (cm)*	Fission Rate** (fissions per atom per core neutron)				
		^{237}Np	^{238}U	^{232}Th	^{235}U	^{235}U-Cd
TSF	12.0	7.85 E-30 (±5.3%)	---	---	---	---
TSB	23.8	7.35 E-31 (±5.3%)	---	---	---	---
PVF	29.7	3.10 E-31 (±5.3%)	6.07 E-32 (±5.8%)	---	---	---
1/4 T	39.5	1.17 E-31 (±5.5%)	1.69 E-32 (±4.9%)	3.56 E-33 (±4.9%)	---	1.26 E-30 (±5.0%)
1/2 T	44.7	6.17 E-32 (±6.8%)	7.36 E-33 (±4.9%)	1.55 E-33 (±5.1%)	8.03 E-31 (±4.9%)	6.43 E-31 (±4.9%)
3/4 T	50.1	3.30 E-32 (±5.3%)	3.11 E-33 (±4.9%)	5.95 E-34 (±4.9%)	4.01 E-31 (±5.0%)	3.66 E-31 (±4.7%)
VB	59.1	9.56 E-33 (±5.3%)	8.67 E-34 (±4.9%)	1.32 E-34 (±4.7%)	1.61 E-31 (±5.1%)	1.20 E-31 (±5.0%)

*Distance from the inner face of core aluminum simulator (or window).

**All fission rates were corrected to a true core power of 9.75 kW at 10 kW. The ^{235}U and ^{232}Th fission rates were measured in November 1978. Corrections to these fission rates (due to slight mechanical modifications of the PCA support in June 1979) were made using the factors from Table 7.2.1 in Mc81. In the case of ^{235}U-bare and ^{232}Th, the factors for ^{235}U-Cd and ^{238}U were used, respectively. The 3/4 T factors were used to correct the VB fission rates. The ^{238}U and ^{237}Np fission rates were measured after June 1979. All SSTR fission rates were calculated using the newly measured value for the mica optical efficiency (0.9875 + 0.0085) in units of tracks/fission. Photofission corrections were made using the data from Table 4.5.6. The ^{232}Th, ^{235}U, and ^{235}U-Cd fission rates have been adjusted by a factor of 1.149 to account for a probable mispositioning of the PCA in the 1978 runs.

TABLE 2.5.10

SSTR NEUTRON-INDUCED FISSION RATES MEASURED IN THE PCA 4/12 SSC CONFIGURATION

Location	Distance from Core (cm)*	Fission Rate** (fissions per atom per core neutron) ^{237}Np	^{238}U
SSC	15.6	8.42 E-30 (±4.8%)	1.12 E-30 (±4.8%)
1/4 T	30.5	6.23 E-31 (±4.8%)	6.46 E-32 (±4.8%)
1/2 T	35.7	3.43 E-31 (±4.8%)	2.96 E-32 (±4.8%)
3/4 T	41.1	---	1.26 E-32 (±4.8%)

*Distance from the inner face of core aluminum simulator (or window).
**All fission rates were corrected to a true core power of 9.75 kW at 10 kW. The ^{238}U and ^{237}Np fission rates were measured after June 1979. All SSTR-fission rates were calculated using the newly measured value for the mica optical efficiency (0.9875 ± 0.0085) in units of tracks/fission. Photofission corrections were made using the data from Table 4.5.6.

TABLE 2.5.11

PCA ^{235}U FISSION RATE CADMIUM RATIOS

Configuration	Position 1/4 T	Position 1/2 T	Position 3/4 T	Void Box
8/7	1.857 ± 0.074	1.121 ± 0.042	1.201 ± 0.042	---
12/13	---	1.248 ± 0.048	1.096 ± 0.040	1.339 ± 0.056

2.6 COMPARISON OF SSTR AND FISSION CHAMBER RESULTS

F. H. Ruddy (HEDL), E. D. McGarry (NBS), Raymond Gold (HEDL), J. H. Roberts (HEDL), C. C. Preston (HEDL) and A. Fabry (CEN/SCK)

At present, pending the result of benchmark irradiations of the SSTR fissionable deposits, the SSTR results are reported as absolute fission rates. The fission chamber results, on the other hand, have been benchmark referenced, and the fission chamber results are reported as fission equivalent fluxes. In order to make direct comparisons between the SSTR and fission chamber results, the fission chamber data from Section 2.3 of this report were converted into the coresponding reaction rates. These comparisons are contained in Tables 2.6.1 through 2.6.4.

For the PCA 12/13 configuration, the data of Tables 2.6.1 and 2.6.2 indicate that the SSTR results are lower than the fission chamber results by ~10%. The overall mean of the fission rate ratios from Table 2.6.1 is 0.902 ± 0.023 and from Table 2.6.2 is 0.896 ± 0.023. The mean of the eleven fission rate ratio values from both tables is 0.899 ± 0.022. The magnitude of the standard deviation of this mean (2.4%) is consistent with the experimental uncertainties, indicating good relative precision of the SSTR and fission chamber data but an absolute discrepancy (10%) that is not consistent with the quoted experimental uncertainties on the absolute fission rates.

The data for the PCA 8/7 configuration are contained in Table 2.6.2. The overall mean of these six fission rate ratios is 0.902 ± 0.023. Again, the relative precision is good, but an absolute 10% discrepancy exists between the SSTR and fission chamber data.

The data for the PCA 4/12 SSC configuration are contained in Table 2.6.4. The overall mean of these five fission rate ratios is 0.896 ± 0.034. Once again, the relative precision is consistent with the experimental uncertainties, but a 10% discrepancy in magnitude exists.

The similarity of the discrepancy for all three configurations suggests that the discrepancy is configuration-independent. The mean of all the fission rate ratios tabulated in Tables 2.6.1 through 2.6.4 is 0.897 ± 0.025.

Therefore, although both the SSTR and fission chamber data sets are internally consistent and have good relative precision, an ~10% absolute bias exists between the two sets of data. A possible explanation for this bias is the fact that the void introduced by the NBS fission chamber causes a perturbation.

2.6.1 Facts in Conflict with the Perturbation Hypothesis

In previous measurements there was good agreement between NBS and CEN/SCK fission rates in ^{237}Np. Prior to 1981, but not afterwards, there was a valid, absolute calibration for the smaller CEN/SCK neptunium chamber. Its volume is about 1/15th that of the NBS chamber. However, neptunium fission

TABLE 2.6.1

COMPARISON OF SSTR AND FISSION CHAMBER MEASURED FISSION RATES
FOR THE PCA 12/13 CONFIGURATION - NOVEMBER 1981 SSTR RESULTS

Isotope	Location	Fission Rate [(fissions per atom per core neutron) x 10^{32}] Fission Chamber		SSTR		SSTR/ Fission Chamber Ratio*
^{237}Np	1/4 T	12.55	(±2.9%)	11.8	(±3.6%)	0.940 ± 0.043
	1/2 T	7.045	(±3.1%)	6.19	(±5.4%)	0.879 ± 0.055
	3/4 T	3.690	(±3.1%)	3.32	(±3.3%)	0.900 ± 0.041
					Average	0.906 ± 0.031
^{238}U	1/4 T	1.943	(±3.0%)	1.75	(±2.7%)	0.901 ± 0.036
	1/2 T	0.8536	(±3.1%)	0.750	(±2.7%)	0.879 ± 0.036
	3/4 T	0.3546	(±3.1%)	0.323	(±2.7%)	0.911 ± 0.037
					Average	0.897 ± 0.016

*The uncertainties on individual ratios were obtained by combining the uncertainties on the SSTR and fission chamber measurements in quadrature. The uncertainty on the average is the standard deviation of the mean of the three ratios.

TABLE 2.6.2

COMPARISON OF SSTR AND FISSION CHAMBER MEASURED FISSION RATES
FOR THE PCA 12/13 CONFIGURATION - OCTOBER 1981 RESULTS

Isotope	Location	Fission Rate [(fissions per atom per core neutron) x 10^{32}] Fission Chamber		SSTR		SSTR/ Fission Chamber Ratio*
^{237}Np	1/4 T	12.55	(±2.9%)	11.6	(±3.3%)	0.924 ± 0.037
	3/4 T	3.690	(±3.1%)	3.23	(±3.3%)	0.875 ± 0.040
					Average	0.899 ± 0.035
^{238}U	1/4 T	1.943	(±3.0%)	1.74	(±2.7%)	0.896 ± 0.037
	1/2 T	0.8536	(±3.1%)	0.744	(±2.7%)	0.872 ± 0.036
	3/4 T	0.3546	(±3.1%)	0.324	(±2.7%)	0.914 ± 0.021
					Average	0.894 ± 0.021

*See footnote for Table 2.6.1.

TABLE 2.6.3

COMPARISON OF SSTR AND FISSION CHAMBER MEASURED FISSION RATES FOR THE PCA 8/7 CONFIGURATION

Isotope	Location	Fission Rate [(fissions per atom per core neutron) x 10^{31}] Fission Chamber	SSTR	SSTR/ Fission Chamber Ratio*
^{237}Np	1/4 T	7.789 (±2.9%)	7.15 (±4.6%)	0.918 ± 0.050
	1/2 T	4.321 (±2.9%)	4.03 (±5.4%)	0.933 ± 0.057
	3/4 T	2.282 (±2.9%)	1.97 (±4.4%)	0.863 ± 0.045
			Average	0.905 ± 0.037
^{238}U	1/4 T	1.050 (±2.8%)	0.913 (±2.6%)	0.870 ± 0.033
	1/2 T	0.4575 (±3.0%)	0.404 (±2.9%)	0.883 ± 0.037
	3/4 T	0.1899 (±3.0%)	0.171 (±2.7%)	0.900 ± 0.036
			Average	0.884 ± 0.016

*See footnote for Table 2.6.1.

TABLE 2.6.4

COMPARISON OF SSTR AND FISSION CHAMBER MEASURED FISSION RATES FOR THE PCA 4/12 SSC CONFIGURATION

Isotope	Location	Fission Rate [(fissions per atom per core neutron) x 10^{31}] Fission Chamber	SSTR	SSTR/ Fission Chamber Ratio*
^{237}Np	1/4 T	6.826 (±1.7%)	6.25 (±2.6%)	0.916 ± 0.031
	1/2 T	3.765 (±1.9%)	3.44 (±2.6%)	0.914 ± 0.029
			Average	0.915 ± 0.002
^{238}U	1/4 T	0.7845 (±1.8%)	0.660 (±2.4%)	0.841 ± 0.025
	1/2 T	0.3392 (±2.3%)	0.299 (±2.4%)	0.882 ± 0.029
	3/4 T	0.1409 (±2.6%)	0.130 (±2.4%)	0.923 ± 0.033
			Average	0.882 ± 0.041

*See footnote for Table 2.6.1.

rates in the two chambers disagreed by no more than 3.5%, with the tiny CEN/SCK chamber giving the slightly higher results. This fact is inconsistent with the 10% perturbation being caused by the NBS chamber void.

Direct comparisons between the SSTRs and CEN/SCK chamber can be made only at two locations in the 12/13 configuration. As can be seen from the data in Table 2.6.5, no detectable bias exists between the SSTR and CEN/SCK chamber measurements at these two locations, which are both external to the PVS block.

TABLE 2.6.5

COMPARISON OF SSTR AND CEN/SCK FISSION CHAMBER ^{237}Np FISSION RATES IN THE PCA 12/13 CONFIGURATION

Location	Equivalent Fission Fluxes (x 10^8) CEN/SCK	SSTR	Fission Chamber/SSTR Ratio
PVF	22.7 (±6.3%)	23.1 (±3.3%)	0.983 ± 0.071
VB	0.73 (±9.2%)	0.711 (±3.4%)	1.027 + 0.101
		Average	1.005 ± 0.031

The effects of possible void perturbations were considered previously (Mc81). Measurements showed that in the PCA water locations, such as the TSF, TSB and PVF locations, a perturbation of 10% to 12% was observed when passing the miniature, needle-like, CEN/SCK fission chamber through an empty NBS chamber housing, which was in position for measurements in the PCA. See Figures 2.6.1 through 2.6.4. However, when these measurements were repeated in the PV simulator block, no perturbation greater than 1% was observed. It should be noted that these measurements were made with only one orientation of the cavity and whether that orientation was 0° or 180° is not known.

2.6.2 Facts That Support the Perturbation Hypothesis

There are NBS fission chamber data that suggest perturbations take place in a void in the steel. See Tables 2.6.6 and 2.6.7.

The NBS chamber contains two deposits, and fission rates are an average of measurements taken with the ^{237}Np deposit facing the PCA reactor core and then measurements taken with the ^{237}Np facing away from the core. That is, one orientation is rotated 180° from the other. The chamber holder is designed to have the center point between the two deposits not shift during this rotation. This means that a deposit face moves about 0.25 mm (twice the thickness of the stainless backing on a deposit, which is 0.005 inches thick). This movement is negligible for the problem at hand since gradients are on the order of 1.0 to 1.5% per millimeter in the steel block. What

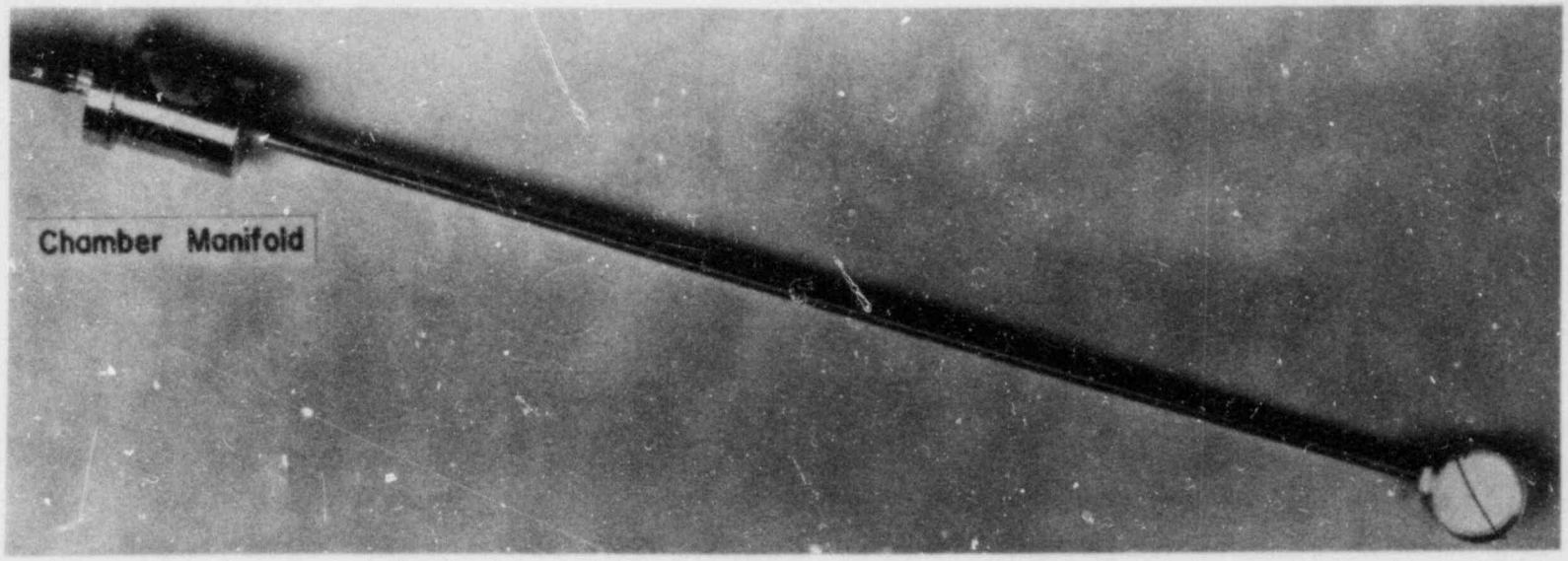

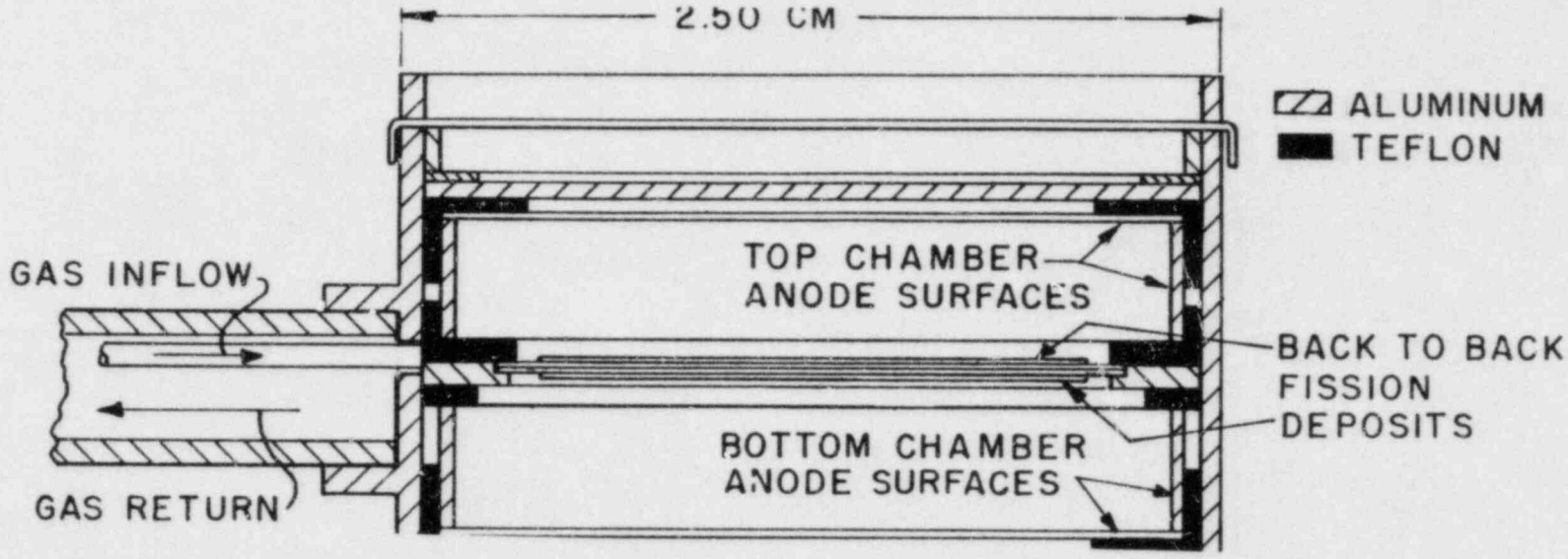

FIGURE 2.6.1. NBS Double Fission Chamber.

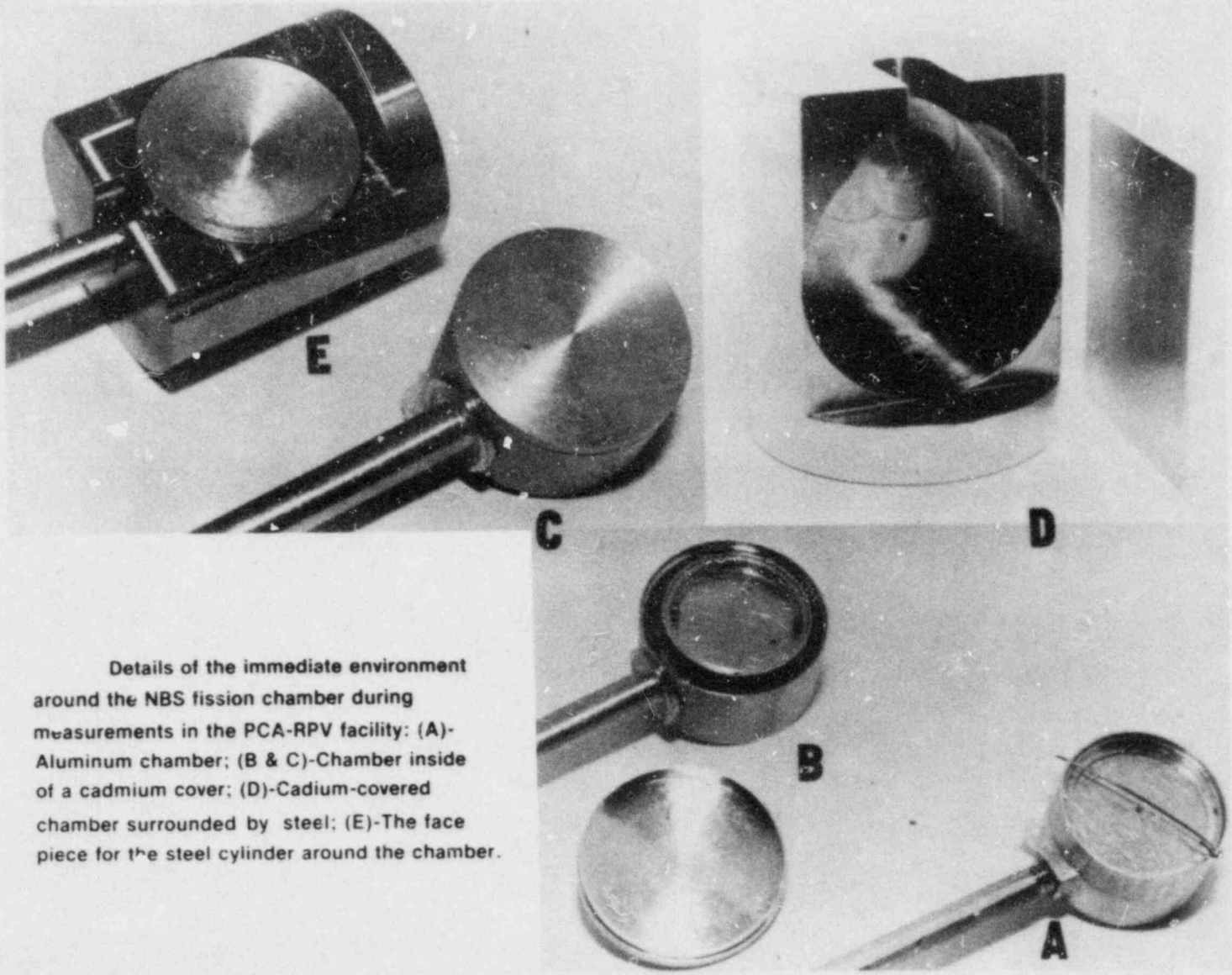

Details of the immediate environment around the NBS fission chamber during measurements in the PCA-RPV facility: (A)-Aluminum chamber; (B & C)-Chamber inside of a cadmium cover; (D)-Cadium-covered chamber surrounded by steel; (E)-The face piece for the steel cylinder around the chamber.

FIGURE 2.6.2. Details of the Immediate Environment Around the NBS Fission Chamber.

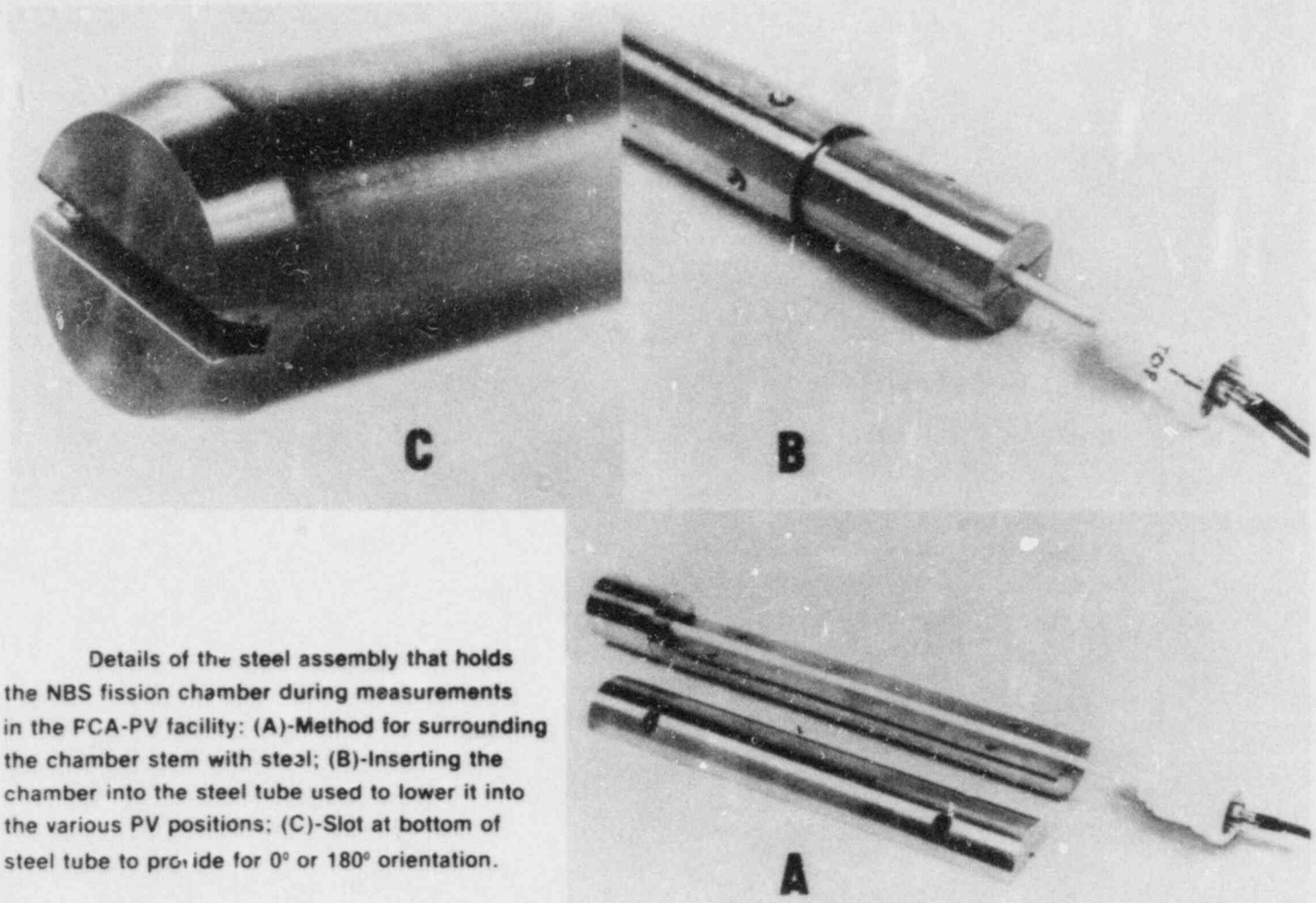

Details of the steel assembly that holds the NBS fission chamber during measurements in the FCA-PV facility: (A)-Method for surrounding the chamber stem with steel; (B)-Inserting the chamber into the steel tube used to lower it into the various PV positions; (C)-Slot at bottom of steel tube to provide for 0° or 180° orientation.

FIGURE 2.6.3. Details of the Steel Assembly That Holds the NBS Fission Chamber.

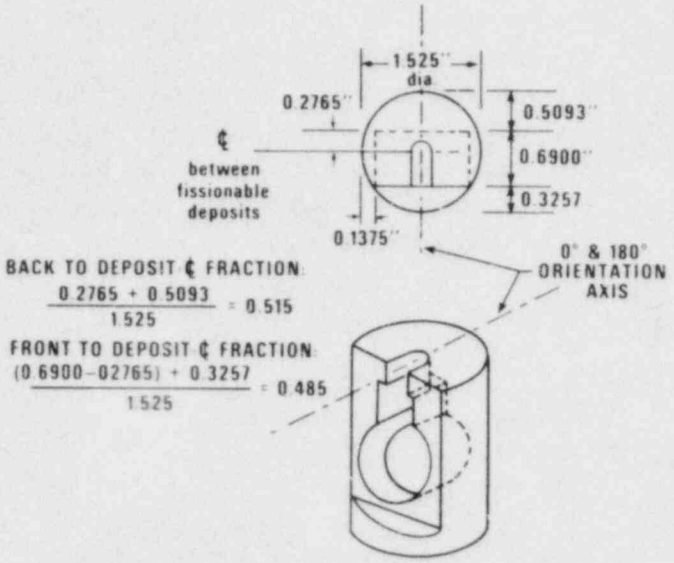

A

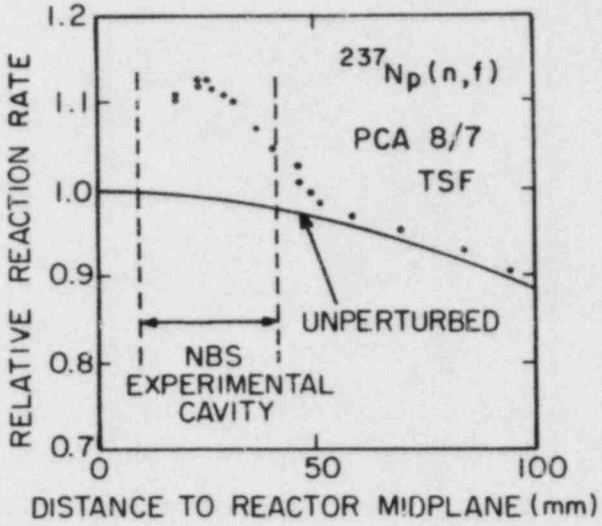

B

FIGURE 2.6.4. Measurement of Perturbation by NBS Fission Chamber in Water.

TABLE 2.6.6

EXAMINATION OF 0°/180° RATIOS FOR THE NBS ^{237}Np AND ^{238}U FISSION CHAMBER RESPONSES IN THE 4/12 SSC* CONFIGURATION OF THE PCA

PCA Position	Orientation	^{237}Np	^{238}U	Ratio Np/U	^{237}Np (0°/180°)	^{238}U (0°/180°)	Ratio Np/U (0°/180°)
1/4 T	0°	341.3	101.2	3.374	1.037	1.055	1.018
	180°	329.1	95.82	3.433			
1/2 T	0°	188.2	43.54	4.323	1.050	1.056	1.027
	180°	179.3	41.25	4.347			
3/4 T	0°	100.5	18.46	5.444	1.061	1.066	1.006
	180°	94.77	17.31	5.475			
1/4 T off center	0°	303.8	90.21	3.378	1.052	1.067	1.011
	180°	288.7	84.51	3.416			
				Average	1.050 ±0.010	1.061 ±0.006	1.015 ±0.009

*September 1979 data; adjusted for dead time and extrapolation to zero but not for absolute power normalization.

TABLE 2.6.7

EXAMINATION OF 0°/180° RATIOS FOR THE NBS ^{237}Np AND ^{238}U FISSION CHAMBER RESPONSES IN THE 4/9 CONFIGURATION OF THE PCA

PCA Position	Orientation	^{237}Np	^{238}U	Ratio Np/U	^{237}Np (0°/180°)	^{238}U (0°/180°)	Ratio Np/U (0°/180°)
1/4 T	0°	506.2	173.3	2.921	1.036	1.048	1.012
	180°	488.5	165.3	2.955			
1/2 T	0°	286.5	77.52	3.696	1.028	1.045	1.016
	180°	278.7	74.20	3.757			
3/4 T	0°	151.1	31.79	4.753	1.031	1.030	0.999
	180°	146.5	30.85	4.749			
				Average	1.032 ±0.004	1.041 ±0.010	1.009 ±0.009

does matter, however, is that the amount of steel, between deposit and core, in the small insert that holds the chamber inside a steel sleeve (see Figures 2.6.2 and 2.6.3) is different for the two orientations. The difference in thickness is 4.67 mm. The differences in attenuation upon rotation result in differences in the 0° and 180° absolute fission rate measurements as shown in Tables 2.6.6 and 2.6.7.

2.6.3 Fission Rate Intercomparisons

Recently, NBS and HEDL intercompared measurements of absolute fission rates with chambers and SSTRs in a ^{252}Cf standard fission spectrum. The measurements were made using both NBS and HEDL fissionable deposits, and all results show agreement to within a combined uncertainty of several percent (<2%). The NBS and HEDL deposits used at PCA are not the same as those intercompared. However, it is important to be aware that this experiment did not intercompare the masses of the HEDL or NBS fissionable deposits.

It is also significant to know that no large discrepancy, say greater than a few percent, is expected between the mass calibration of the NBS and HEDL fissionable deposits as indirect intercomparisons between NBS and HEDL deposits have been made in the past. For example, both laboratories have had deposits made by the Geel Laboratory, Mol, Belgium; and QA overchecks by both laboratories agree to within a few percent with the masses assigned by Geel.

2.6.4 Recommended Actions

In order to directly compare the SSTR and the fission chamber measurements, a series of experiments have been planned. SSTRs and ILRR radiometric foils will be irradiated both in the standard configurations when all voids are filled and inside NBS fission chambers. Hopefully, these measurements will ascertain whether the fission rate measured inside the fission chamber is different from that measured in a void-free environment and will identify the source of the 10% discrepancy between the SSTR and the fission chamber measurements.

Pending the outcome of these measurements, the discrepancy between the SSTR and the fission chamber measurements remains unresolved. The recommended fission rates in Section 6.1 are, therefore, a linear average of the SSTR and fission chamber results. The averaging of these two sets of measurements unavoidably contributes an additional 5% uncertainty, resulting from the 10% bias between the two sets.

3.0 EXPERIMENTAL PROGRAM: NEUTRON SPECTROMETRY

Raymond Gold (HEDL)

SUMMARY

In the LWR-PV Surveillance Dosimetry Improvement Program (SDIP), fast neutron spectrum measurements were carried out to provide the neutron spectral definition required to appropriately analyze and intrepret neutron dosimetry measurements related to fast neutron damage in LWR-PV steels. Spectral measurements also provide data for comparison with calculations. Three different fast neutron spectrometry methods have been applied, namely:

- Proton-recoil spectrometry with proportional counters
- Triton- and alpha-particle coincidence spectrometry based on the $^{6}Li(N,\alpha)^{3}H$ reaction
- Proton-recoil spectrometry with nuclear research emulsions

Proton-recoil proportional counter methods using hydrogen and methane gas-filled detectors were applied to obtain the proton spectra from which the neutron spectra were derived. Cylindrical and spherical geometry detectors were used to cover the neutron energy range between ~50 keV and 2 MeV. ^{6}Li spectrometry was used to cover the energy region between ~100 keV and 6 MeV. Both the triton spectrum and the sum spectrum (triton + alpha particle) were used to derive the neutron spectrum. Passive spectrometry between ~500 keV and 8 MeV was obtained by irradiating Ilford L-4 emulsions.

Proton-recoil proportional counter measurements were conducted primarily at midplane in the 1/4 T, 1/2 T, 3/4 T, and VE locations of the 8/7, 12/13, and 4/12 SSC configurations of the LWR pressure vessel simulator. Proportional counter results have already been reported for the 8/7 and 12/13 configurations in the first of this series of reports (Ro81). This chapter will present proportional counter results for the 4/12 SSC configuration from PCA experiments carried out in the fall of 1981.

Additional neutron spectrometry was conducted in the fall of 1981 at the PCA with nuclear research emulsions (NRE). Earlier NRE measurements of PCA spectra have been reported (Mc81), including a detailed exposition of integral-mode NRE scanning (Go81d,Go81e). Integral mode scanning of these 1981 irradiated NRE has now been completed, and these results are presented in Section 3.2, which follows.

The proportional counter and NRE results show that the neutron spectrum softens, i.e., shifts toward lower energy, as one proceeds from the front to the back of the PV. The relative neutron flux densities increase in the lower energy range with increasing steel thickness. Neutron spectrum fine structure shapes and changes are observed. These results aid in the generation of more accurate, effective cross sections and fluences for use in LWR-PV fast neutron dosimetry and materials damage analyses. As a consequence, a more accurate evaluation of the condition of LWR-PV is possible especially for PVs in LWR plants using low-leakage fuel management schemes.

3.1 TEST MATRIX SELECTION AND RATIONALE

Raymond Gold (HEDL)

The energy dependence of damage produced by neutrons in LWR-PV steel has been recognized for some time (Ro63,Ro65,Mc69). In LWR-PV environments, neutron-induced radiation damage in steel is significant in the 0.1 to 1.0 MeV energy region. Moreover, the damage in steel possesses non-negligible variation with neutron energy. However, differential measurement of neutron energy spectra in LWR-PV environments has not been possible heretofore. Inherent limitations prevent differential techniques from being applied in power reactor environments (Go77c). Passive techniques that are applicable in power reactor environments, such as radiometric (RM), Solid State Track Recorder (SSTR) or Helium Accumulation Fluence Monitor (HAFM), are inherently limited by their integral nature and hence possess severely restricted energy resolution. Moreover, these high-power techniques offer little coverage in the 0.1 to 1.0 MeV energy region. Hence, the establishment of a low-power LWR-PV benchmark at the PCA has offered a unique opportunity for progress in the LWR-PV Surveillance Dosimetry Improvement Program (SDIP).

In operating LWR, neutron-induced damage in the PV arises predominantly in the energy range from 0.02 to 6.0 MeV. Fortunately, a number of differential neutron spectrometry techniques already existed and were applied in consort to this energy region. In particular, the use of gas-filled proton-recoil spectroscopy, proton-recoil nuclear research emulsions, and $^{6}Li(n,\alpha)$ fast neutron spectroscopy to cover this energy region in earlier experiments has already been described in the first of this series of reports.

Table 3.1.1 summarizes the test matrix of neutron spectral measurements carried out in the fall of 1981. It can be compared with the test matrix for earlier PCA neutron spectrometry by consulting Chapter 3 of the first NUREG report on PCA experiments (Go81f).

By conducting neutron spectrometry at different locations, one obtains the variation of the differential neutron spectrum through the PV, which can be used to validate calculations. This spatial variation is an especially powerful probe for examining trends between theory and experiment, thereby furnishing greater insight into any observed differences.

Section 3.2 presents integral mode scanning results for NRE irradiated in the 1981 PCA experiments. Analysis and interpretation of these absolute proton-recoil integral NRE data are presented in comparison with two commonly used LWR-PV-SDIP dosimetry reactions, namely $^{237}Np(n,f)$ and $^{238}U(n,f)$. Proportional counter results for the 1981 experiments in the 4/12 SSC configuration are presented in Section 3.3.

TABLE 3.1.1

TEST MATRIX OF 1981 LWR-PV NEUTRON SPECTROMETRY IN THE PCA*

In-Situ Location**	LWR-PV Configuration 8/7	12/13	4/12 SSC
SSC	---	---	---
PVF	E	E	---
1/4 T	E	E	P
1/2 T	E	E	P
3/4 T	E	E	P
VB	E	E	P

*E = Emulsions; P = Gas Proportional Counter.
**Observations were restricted to reactor midplane.

3.2 NEUTRON DOSIMETRY WITH NUCLEAR RESEARCH EMULSIONS

J. H. Roberts, Raymond Gold, C. C. Preston, J. P. McNeece and F. H. Ruddy (HEDL)

3.2.1 Introduction

If Nuclear Research Emulsions (NRE) are exposed in a given reactor environment, proton recoil tracks result from the neutron-proton (n-p) scattering of fast neutrons in the emulsion (Ro53,Ro57,Ro68). Two integral reaction rates have been defined based on the proton recoil data (Go81d,Go81e). The first of these, $I(E_0)$, is the number of proton tracks of energy E_0 per MeV per hydrogen atom produced per watt-second (W-s) of reactor operation. These proton tracks of energy E_0 will be produced by the n-p scattering of neutrons of energy $E \geq E_0$. The second, $J(E_0)$, is the number of proton tracks of all energies $E \geq E_0$ per hydrogen atom produced per W-s of reactor operation.

For reactor-type spectra, $I(E_0)$ is more sensitive to neutrons having energies at and slightly above E_0, whereas $J(E_0)$ is more sensitive to neutrons of somewhat higher energy. The two reaction rates thus compliment each other. (See Figures 3.2.7 and 3.2.8 for details.) The reaction rates are defined in Eqs. 10 and 11, respectively.

The importance of using these reaction rates is that the cross section for elastic scattering of fast neutrons by protons is known at the 1% level. There are, however, experimental errors in determining the proton track data. Unfortunately, these errors are most difficult to evaluate in the region of neutron energy E_n below 0.8 MeV, where reaction rate data are most needed to fill gaps in data obtained by other methods. These difficulties result from coulomb scattering of the low-energy protons in the emulsion, from the finite size of the silver bromide grains, from the intrinsic range straggling, and from difficulties in measuring depth differences for points along short tracks. The principal uncertainties thus do not result from cross-section data, but from the experimental problems mentioned above. Estimates of the various uncertainties have been reported (Go81e) and are discussed further in Section 3.2.4. These and other possible uncertainties are still under investigation. In spite of these difficulties, the use of an independent technique to obtain additional reaction rates in the region from ~0.4 to 0.8 MeV is of great value.

Data and results obtained for six NRE from the 1981 exposures in the PCA are given in this report. Exposure data for these six NRE are given in Table 3.2.1. The runs were monitored with the Mo and NBS fission chambers.

NRE exposed in the 12/13 and 8/7 configurations were placed in Cd boxes in such a way that the only void present was that of the Cd box itself. The volume of the box was 1.08 cm^3. Previous exposures (Go81e) were made in dummy proportional counters that created a much larger void. This change was made so that a more direct comparison of the emulsion data could be made with data from SSTR and radiometric sensor sets when perturbation effects were minimized.

TABLE 3.2.1

IRRADIATION DATA FOR SIX NRE EXPOSED DURING 1981 IN THE LWR-PVS
(Ilford L4 Emulsions, 200- and 400-μm Thick on Glass Backing,
and Covered with 0.02-in. Cd were Exposed in Each Position)

Exposure Date	Rem No.	Emulsion No.	Config-uration	Loca-tion	Reactor Power (W)	Exposure (W-s)
10/12/81	1	K4A	12/13	1/4 T	20	2.656×10^4
10/13/81	3	K5A	12/13	1/2 T	50	4.798×10^4
10/13/81	4	K6A	12/13	3/4 T	100	8.393×10^4
10/14/81	8	K7A	12/13	VB	200	1.556×10^4
11/16/81	2	W9	12/13	TSB	1802.8	1.8028×10^3
10/15/81	13	K4B	8/7	1/4 T	20	3.914×10^3

3.2.2 Thermal Neutron-Induced $^{14}N(n,p)^{14}C$ Reaction Data

As a check of the range-energy relationship for proton tracks in NRE, exposures were made in the thermal neutron facility at NBS. Thermal neutrons react with nitrogen in the emulsion to produce a proton-^{14}C pair of tracks from a $^{14}N(n,p)^{14}C$ reaction. 158 track pairs were measured. The combined mean range of the protons and ^{14}C recoil was 6.91 ± 0.67 μm, as shown in Figure 3.2.1. The estimated range of the ^{14}C is 0.3 μm (Ba73), giving a mean proton range of 6.61 μm. From the proton range-energy curve for "standard" emulsions (Ba63), this gives a proton energy of 0.595 MeV. If the Q of the $^{14}N(n,p)^{14}C$ reaction is taken as 0.6263 MeV, the proton energy is 0.5845 MeV. The difference between the observed and calculated values is 1.8%. As shown in Figure 3.2.1, the distribution is approximately Gaussian; and the standard deviation is consistent with the 0.5-μm spread (Go83) in range measurements made with the Emulsion Scanning Processor, if the effect of range straggling is also included. This measurement confirmed the use of the proton range-energy curve (Ba63) for "standard" emulsion as a satisfactory approximation.

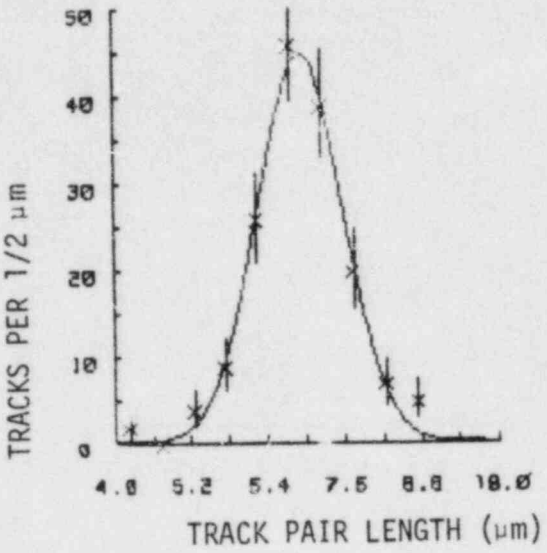

FIGURE 3.2.1. Distribution of the Lengths of ^{14}C-^{1}H Pairs in Ilford L4 Emulsions Exposed to Thermal Neutrons. (The track pairs result from the capture of the thermal neutrons in the nitrogen contained in the emulsion, giving the reaction $^{14}N(n,p)^{14}C$. The smooth curve is a Gaussian, $G(r) = 44.74 \exp[-1.125(x - 6.194)^2]$, fit to the data consisting of 158 track pairs.)

3.2.3 Integral Mode Track Data

Six emulsions exposed in the PCA (Table 3.2.1) were scanned with the Emulsion Scanning Processor (ESP) (Go81e,Go83) to obtain the data. Tracks within the range interval from ~3 to ~16 µm were measured, whereas tracks >16 µm in length were counted but not measured. Track data down to 4.0 µm were accepted as valid. Table 3.2.2 gives the results of the scan, and Figure 3.2.2 gives plots of the tracks per micron as a function of track length in microns.

Of particular interest are the plots for emulsions W9 and K7A. W9 was in the water behind the thermal shield, and K7A was in the void box behind the block. The smooth curves in these plots are from a nonlinear regression code in which it is assumed that the distribution is the result of a superposition of a straight line and a Gaussian curve. For W9 the equation obtained is

$$M(r) = 172.996 - 13.297\ r + 64.537\ e^{-1.366(r-7.356)^2} \qquad (1)$$

TABLE 3.2.2

INTEGRAL MODE TRACK DATA

Emulsion No.	Configuration	Position	Emulsion Thickness (μm)	Volume Scanned (cm^3)	Tracks Tallied >4.0 μm	Tracks/μm* Range Interval (μm) 4.01-5.00	5.01-6.00	6.01-7.00	7.01-8.00	8.01-9.00	9.01-10.00	10.01-11.00	11.01-12.00
K7A	12/13	VB	232.5	7.267×10^{-5}	1003 (820)	167 (167)	144 (143.1)	156 (121.6)	202 (89.0)	91 (57.4)	54 (33.1)	29 (29)	13 (13)
K4B	8/7	1/4 T	240.5	6.633×10^{-5}	1026	188	135	107	92	73	47	42	24
K5A	12/13	1/2 T	233.0	5.549×10^{-5}	1032	213	156	108	83	53	53	35	25
K4A	12/13	1/4 T	232.5	5.649×10^{-5}	1026	167	155	96	90	73	33	35	34
W9	12/13	TSB	218.1	1.442×10^{-4}	1080 (982)	112 (112)	103 (102.4)	116 (92.0)	133 (70.4)	67 (56.4)	46 (45.9)	44 (44)	35 (35)
K6A	12/13	3/4 T	232.5	5.679×10^{-5}	1005	243	149	138	94	56	46	34	31

*Data in parenthesis for K7A and W9 give the number of tracks per micron after subtracting the contribution due to the capture of slow neutrons in ^{14}N (see test).

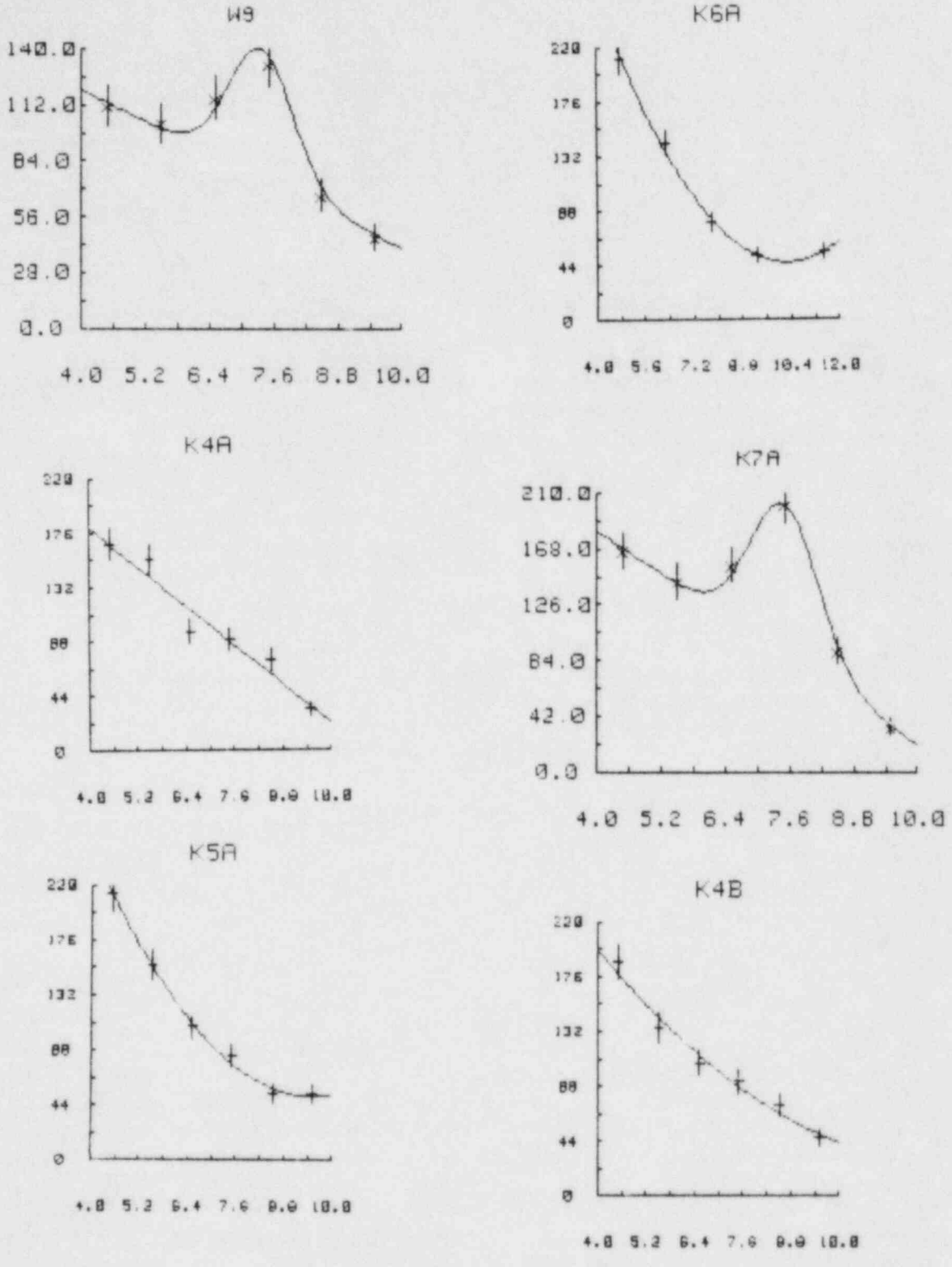

FIGURE 3.2.2. Track Distribution for the Emulsions Scanned. (The abscissas are the track lengths in μm, and the ordinates are the number of tracks per μm.)

where:

M(r) = number of tracks/micron
r = track length (μm)

The corresponding equation for K7A is

$$M(r) = 293.945 - 27.648\ r + 115.518\ e^{-1.165(r-7.485)^2} \qquad (2)$$

The choice of these functions is based on the assumption that the Gaussian distribution is due to track-pairs from the $^{14}N(n,p)^{14}C$ reaction produced by the capture of epithermal neutrons in the nitrogen contained in the emulsions (Ba73). These curves peak at 7.356 and 7.485 μm, respectively. These results are to be compared with 6.91 μm for the peak of the thermal neutron exposure discussed in Section 3.2.2 (Figure 3.2.1). Even ignoring uncertainties introduced in the fitting routine, the results are consistent within error limits. The linear portion of the data is attributed to the n-p scattering of the fast neutrons in the emulsion.

For the emulsions in the block, the data for K4A are fit to a linear equation, and for K5A, K6A, and K4B to a second-degree equation. These plots effectively smooth the data and make it possible to calculate a variance-covariance matrix to give a statistical estimate of M(r), the tracks per μm as calculated from the curves in Figure 3.2.2.

3.2.4 Integral Mode Results and Treatment of Experimental Error

If we let M(r) represent the number of tracks per μm of range r, we assume that

$$M(r) = a + br + cr^2 + \ldots \qquad (3)$$

where a, b, and c are constants. We shall use primed quantities, such as $M'(r)$, to represent the actual data points. Using a least-squares code with statistical weights for the data points, the constants and their statistical accuracies are determined. It was found that either a linear or quadratic function gave the best fit to the data; the statistical accuracy of the data did not justify higher terms. The standard deviation of $M'(r)$ for each data point is taken as $\sqrt{M'(r)}$, except for emulsions W9 and K7A, where the track distribution N(r) is represented by the superposition of a linear function M(r) and a Gaussian G(r):

$$N(r) = M(r) + G(r). \qquad (4)$$

We are interested here in M(r) and its standard deviation. Solving for M(r), we have

$$M(r) = N(r) - G(r). \tag{5}$$

From Eqs. (1) and (2) we can calculate the number of tracks G'(r) associated with the n-p reaction ^{14}N. Then,

$$M'(r) = N'(r) - G'(r) \pm N'(r) + G'(r) \tag{6}$$

This statistical accuracy is used to obtain the statistical weights for M(r) in obtaining a and b from the least-squares fit code for

$$M(r) = a + br \tag{7}$$

Another code, which calculates an error matrix for each fit is used to give the statistical estimates of M(r) for Eqs. (3) and (7). The quoted statistical uncertainties given in Table 3.2.3 are obtained from the variance-covariance error matrices. Other sources of uncertainty have been previously discussed. These are proton range straggling (2%), proton energy based on range-energy relation (2%), volume of emulsion scanned with ESP system (2%), hydrogen directly in the emulsion (3%), elastic scattering cross section, $\sigma_{np}(E)$ (1%). All of these in quadrature give an uncertainty of 4.7%. The 4.7% is put in quadrature with the statistical uncertainties obtained from the error matrices, to give the total uncertainties given in Table 3.2.3. This does not include an estimated uncertainty of 6% due to power normalization.

Having obtained M(r) we must then determine M(E), the number of tracks per MeV.

The standard range-energy relationship for Ilford emulsion (Ba63) can be represented by

$$\log_e E = B_0 + B_1 \log r + B_2(\log r)^2 + B_3(\log r)^3 + B_4(\log r)^4 \tag{8}$$

where B_0, B_1, B_2, B_3 and B_4 are constants. For the region $3 \leq r \leq 40$ μm, the following table gives the values of these constants:

Constant	Value	Constant	Value
B_0	-2.20842	B_3	0.04118
B_1	1.16519	B_4	-0.00331
B_2	-0.20952		

TABLE 3.2.3

I AND J-INTEGRAL REACTION RATE RESULTS FOR THE 1981 NRE EXPOSURES IN THE PCA

Emul No./ Config-uration	Location/ Distance from Core Center (cm)	I-Integral [protons/(MeV)(at.)(W-s)]				J-Integral [protons/(at.)(W-s)]			
		Energy (MeV)	Integral	Statistical Uncertainty (%)	Total* Uncertainty (%)	Energy (MeV)	Integral	Statistical Uncertainty (%)	Total* Uncertainty (%)
W9	TSB	0.4467	1.81×10^{-19}	6.61	8.10	0.4073	1.18×10^{-19}	3.19	5.67
		0.5198	1.73×10^{-19}	5.82	7.48	0.4837	1.05×10^{-19}	3.40	5.79
12/13	23.8	0.5877	1.59×10^{-19}	5.19	7.00	0.5540	9.37×10^{-20}	3.58	5.90
		0.6515	1.42×10^{-19}	5.36	7.12	0.6197	8.52×10^{-20}	3.76	6.01
		0.7119	1.21×10^{-19}	7.42	8.78	0.6197			
K4A	1/4 T	0.4467	4.58×10^{-20}	6.79	8.25	0.4073	2.15×10^{-20}	3.11	5.63
		0.5198	4.18×10^{-20}	4.55	6.53	0.4837	1.78×10^{-20}	3.41	5.80
12/13	39.5	0.5877	3.63×10^{-20}	5.17	6.98	0.5540	1.47×10^{-20}	3.77	6.02
		0.6515	2.96×10^{-20}	6.72	8.19	0.6197	1.27×10^{-20}	4.06	6.20
		0.7119	2.19×10^{-20}	7.47	8.82				
K5A	1/2 T	0.4467	3.31×10^{-20}	5.80	7.46	0.4073	1.21×10^{-20}	3.11	5.63
		0.5198	2.61×10^{-20}	4.42	6.44	0.4837	9.64×10^{-20}	3.50	5.85
12/13	44.7	0.5877	1.96×10^{-20}	5.39	7.14	0.5540	7.81×10^{-21}	3.88	6.09
		0.6515	1.47×10^{-20}	7.42	8.78	0.6197	6.53×10^{-21}	4.25	6.33
		0.7119	1.15×10^{-20}	7.94	9.22				
K6A	3/4 T	0.4467	1.99×10^{-20}	4.99	6.85	0.4073	6.61×10^{-21}	3.15	5.65
		0.5198	1.61×10^{-20}	4.00	6.17	0.4837	5.08×10^{-21}	3.59	5.91
12/13	50.1	0.5877	1.25×10^{-20}	5.50	7.23	0.5540	3.96×10^{-21}	4.07	6.21
		0.6511	9.40×10^{-21}	5.51	7.23	0.6197	3.14×10^{-21}	4.58	6.55
		0.7119	7.08×10^{-21}	7.00	8.43				
K7A	VB	0.4467	6.18×10^{-21}	5.23	7.02	0.4073	2.28×10^{-21}	4.21	6.30
		0.5198	5.62×10^{-21}	4.89	6.78	0.4837	1.81×10^{-21}	4.88	6.77
12/13	59.1	0.5877	4.87×10^{-21}	4.63	6.59	0.5540	1.41×10^{-21}	5.80	7.46
		0.6511	3.93×10^{-21}	4.62	6.58	0.6197	1.08×10^{-21}	6.74	8.21
		0.7119	2.84×10^{-21}	4.86	6.75				
K4B	1/4 T	0.4467	2.82×10^{-19}	6.60	8.10	0.4073	1.24×10^{-19}	3.11	5.63
		0.5198	2.47×10^{-19}	4.55	6.53	0.4837	1.01×10^{-19}	3.45	5.82
8/7	39.5	0.5877	2.09×10^{-19}	5.31	7.08	0.5540	8.48×10^{-20}	3.77	6.02
		0.6511	1.72×10^{-19}	6.86	8.31	0.6197	7.19×10^{-20}	4.10	6.23
		0.7119	1.36×10^{-19}	7.26	8.64				

*Does not include an estimated 6% for power normalization.

The number of tracks per MeV, M(E), at range r is then calculated from

$$M(E) = M(r) \frac{dE}{dr} \tag{9}$$

where dE/dr is the slope of the range-energy curve, obtained by taking the first derivative of Eq. (8). The I-integral for each energy is then obtained as

$$I(E_o) = \frac{M(E_o)}{n_p \, wt} \tag{10}$$

where:

$n_p = 3.192 \times 10^{22}$ at/cm^3, the hydrogen density in the emulsion
wt = number of W-s used in the exposure to obtain $m(E_o)$
$I(E_o)$ is given for various E_o energies in Table 3.2.3

It should be noted that the emulsion technique provides a "variable threshold" for I-integral reaction rates. The J-integral reaction rate is

$$J(E_o) = \frac{\mu(E_o)}{n_p \, wt} \tag{11}$$

where $\mu(E_o)$ is the total number of proton tracks produced in a unit volume of emulsion for neutrons of energy $E_n \geq E_o$. These are also tabulated for various energies and, thus, can also be measured for various thresholds. The values of $\mu(E_o)$ above the cut-off range $r_c = 4.0$ μm ($E_n = 0.4073$ MeV) are obtained by subtracting the tracks in an interval Δr with lower boundary at r_o to give the number of tracks above $r_o + \Delta r$. $J(E_o)$ for various values of E_o are given in Table 3.2.3.

The spatial dependence of the values of the I-integrals and of the J-integrals, from the back of the thermal shield through the block and into the void box, are shown in Figures 3.2.3 and 3.2.4. The J-integrals all drop off exponentially with the distance from the center of the reactor core. The I-integrals are consistent with an exponential drop through the block, but only for $E_o = 0.6515$ and 0.7119 MeV are they consistent with an exponential throughout the entire region investigated.

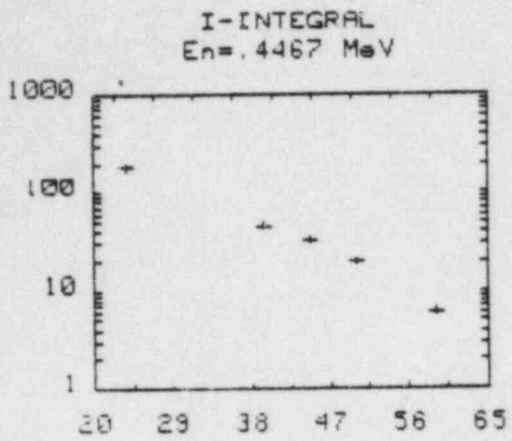

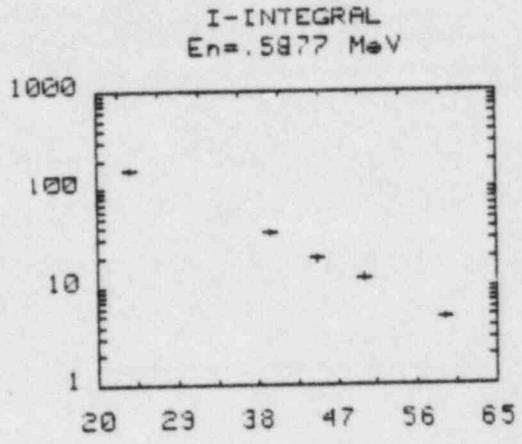

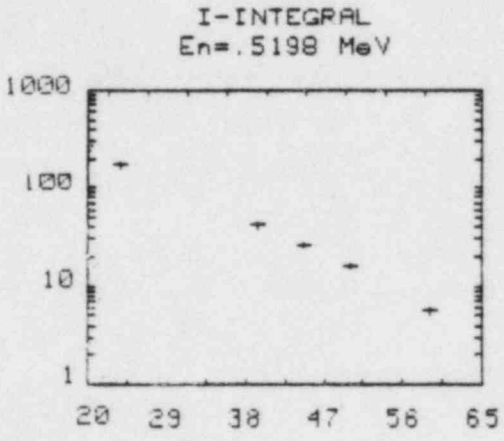

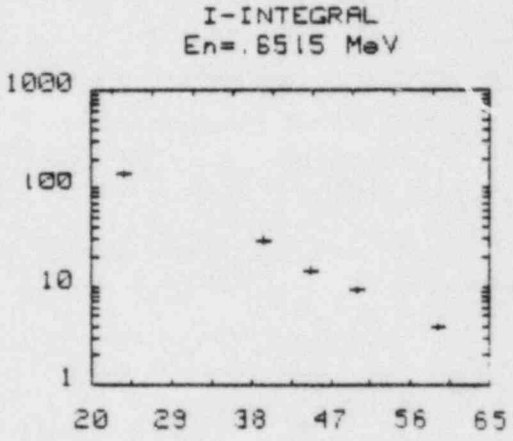

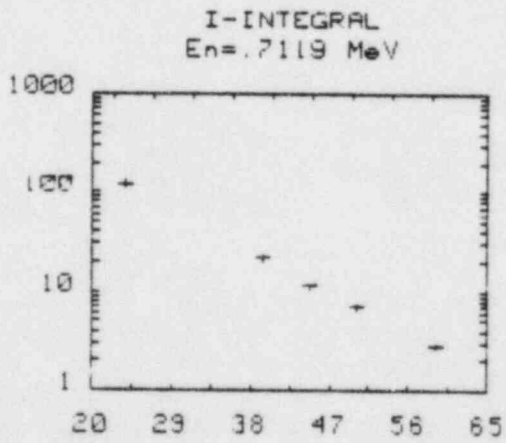

FIGURE 3.2.3. I-Integral Results for Various Thresholds. (The abscissas are the distrances from the core center in cm. The ordinates are the I-integrals in [protons/(MeV)(at.)(W-s) x 10^{21}].)

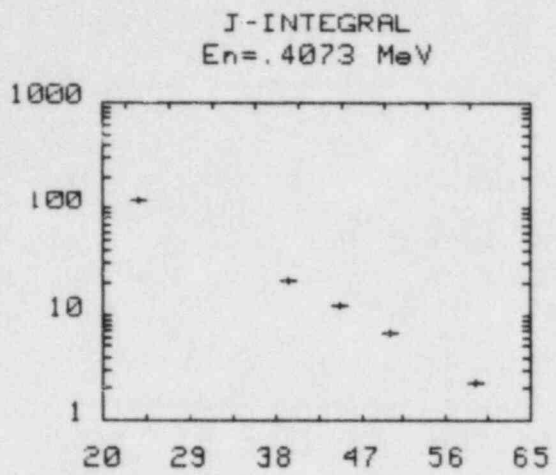

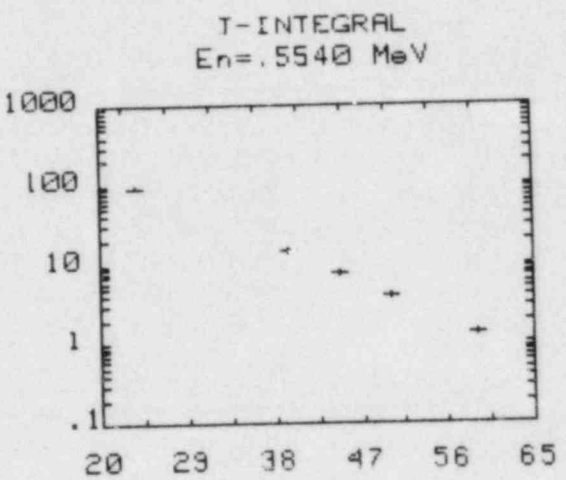

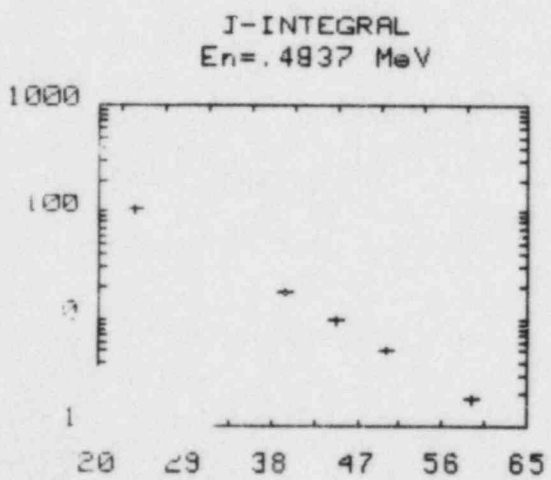

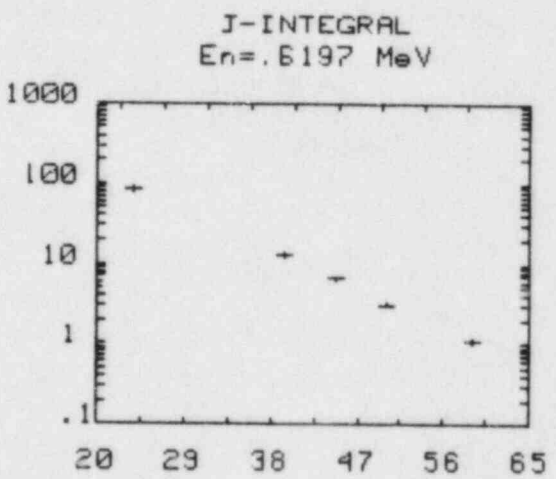

FIGURE 3.2.4. J-Integral Results for Various Thresholds. (The abscissas are the distances from the core center in cm. The ordinates are the J-integrals in [proton/(at.)(W-s) x 10^{21}].)

In order to investigate the behavior of the I and J reaction rates relative to the reaction rates of ^{237}Np and ^{238}U, the ratios given in Tables 3.2.4 and 3.2.5 have been calculated. The ^{237}Np and ^{238}U reaction rates, expressed as fissions per atom per core neutron, were measured with mica SSTR. These ratios, expressed as functions of distance from the core center and as functions of E_0, are plotted in Figures 3.2.5 and 3.2.6. Clearly the behavior of these ratios is complicated, and only qualitative interpretations of some of them will be attempted here.

To interpret the behavior of the I and J reaction rates relative to the ^{237}Np reaction rates, a plot of the I and J response functions are given in Figures 3.2.7 and 3.2.8. The I-response functions has the form $\sigma(E)/E$, (Go81d,Go81e), where $\sigma(E)$ is the n-p scattering cross section and E is the neutron energy. Clearly it is expressed in barns/MeV. The J-response function, on the other hand, has the form $\sigma(E)(1 - E_0/E)$, where E_0 is the chosen threshold energy (Go81d,Go81e). It is expressed in barns.

There is only one curve for the I response function, and the effect of different threshold energies is seen by choosing different minimum energies on this curve. On the other hand, there is a unique J-response function curve for each minimum energy selected.

For qualitative interpretation of the behavior of the I- and J- integrals relative to the ^{237}Np reaction rates for different positions and I- and J-threshold energies, the ^{237}Np fission cross section is plotted pointwise on the curves for the I- and J-response functions (Figures 3.2.7 and 3.2.8).

The I-integral response function is seen to have the highest sensitivity to neutrons at the threshold; its behavior is thus quite in contrast to the response function (cross section) of most detectors. The J-integral response function, on the other hand, behaves more like the cross section for a threshold detector. However, from the plots shown in Figure 3.2.8 it can be seen that the J-integral response function at E_0 rises more rapidly than the fission cross section of ^{237}Np just above threshold. Thus, the two integrals both supply significantly different kinds of information than is obtained from the fissioning of ^{237}Np.

Consider the family of curves in Figure 3.2.5. In all positions the ratios increase with increasing J-integral thresholds. For E_0 = 0.407 MeV, the emulsion "sees" neutrons over most of the energy range for which ^{237}Np has a significant response, but at E_0 = 0.620 MeV, the emulsion does not "see" neutrons below this energy, thus missing many that the ^{237}Np "sees", and its response is less than for E_0 = 0.407 MeV, even above E_0 = 0.620 MeV. Thus the observed rise with increasing E_0 is expected. It is also observed that the ratio increases faster at the 3/4 T than at the 1/4 T position. This suggests a softening of the neutron spectrum as one proceeds through the block.

TABLE 3.2.4a

RATIO OF ^{237}Np REACTION RATES TO I-INTEGRALS

Distance from Core Center (cm)	Location	^{237}Np Reaction Rate	Ratio* of ^{237}Np Reaction Rates to I-Integrals				
			R_{1I}	R_{2I}	R_{3I}	R_{4I}	R_{5I}
39.5	1/4 T	122 ± 2.93	2.66 ± 0.24	2.92 ± 0.21	3.36 ± 0.26	4.11 ± 0.36	5.57 ± 0.52
50.1	3/4 T	34.1 ± 0.78	1.71 ± 0.13	2.12 ± 0.15	2.73 ± 0.22	3.63 ± 0.29	4.82 ± 0.43
59.1	VB	10.15 ± 0.23	1.64 ± 0.13	1.81 ± 0.14	2.08 ± 0.15	2.58 ± 0.19	3.57 ± 0.27

*R_{1I}, R_{2I}, R_{3I}, R_{4I} and R_{5I} are the ratios for E_o = 0.447, 0.520, 0.588, 0.652 and 0.712 MeV, respectively. The ratios have been multiplied by 10^{12}.

TABLE 3.2.4b

RATIO OF ^{237}Np REACTION RATES TO J-INTEGRALS

Distance from Core Center (cm)	Location	^{237}Np Reaction Rate	Ratio* of ^{237}Np Reaction Rates to J-Integrals			
			R_{1J}	R_{2J}	R_{3J}	R_{4J}
39.5	1/4 T	122 ± 2.93	5.67 ± 0.37	6.85 ± 0.45	8.30 ± 0.57	9.61 ± 0.67
50.1	3/4 T	34.1 ± 0.78	5.16 ± 0.33	6.70 ± 0.45	8.61 ± 0.60	10.86 ± 0.79
59.1	VB	10.15 ± 0.23	4.45 ± 0.31	5.61 ± 0.42	7.20 ± 0.58	9.40 ± 0.83

*R_{1J}, R_{2J}, R_{3J} and R_{4J} are the ratios for E_o = 0.407, 0.484, 0.554 and 0.620 MeV, respectively. The ratios have been multiplied by 10^{12}.

TABLE 3.2.5a

RATIO OF ^{238}U REACTION RATES TO I-INTEGRALS

Distance from Core Center (cm)	Location	^{238}U Reaction Rate	Ratio* of ^{238}U Reaction Rates to I-Integrals				
			R_{1I}	R_{2I}	R_{3I}	R_{4I}	R_{5I}
39.5	1/4 T	18.15 ± 0.33	3.96 ± 0.34	4.34 ± 0.31	5.00 ± 0.37	6.13 ± 0.53	8.29 ± 0.74
44.7	1/2 T	7.78 ± 0.14	2.35 ± 0.19	2.98 ± 0.21	3.97 ± 0.30	5.29 ± 0.48	6.77 ± 0.65
50.1	3/4 T	3.37 ± 0.06	1.69 ± 0.12	2.09 ± 0.14	2.70 ± 0.21	3.59 ± 0.28	4.76 ± 0.42
59.1	VB	1.01 ± 0.02	1.63 ± 0.12	1.80 ± 0.13	2.07 ± 0.15	2.57 ± 0.18	3.56 ± 0.26

*R_{1I}, R_{2I}, R_{3I}, R_{4I} and R_{5I} are the ratios for E_o = 0.447, 0.520, 0.588, 0.652 and 0.712 MeV, respectively. The ratios have been multiplied by 10^{13}.

TABLE 3.2.5b

RATIO OF ^{238}U REACTION RATES TO J-INTEGRALS

Distance from Core Center (cm)	Location	^{238}U Reaction Rate	Ratio* of ^{238}U Reaction Rates to I-Integrals			
			R_{1J}	R_{2J}	R_{3J}	R_{4J}
39.5	1/4 T	18.15 ± 0.33	8.44 ± 0.52	10.2 ± 0.65	12.4 ± 0.81	14.3 ± 0.96
44.7	1/2 T	7.78 ± 0.14	6.43 ± 0.40	8.07 ± 0.52	9.96 ± 0.66	11.9 ± 0.81
50.1	3/4 T	3.37 ± 0.06	5.10 ± 0.32	6.62 ± 0.43	8.51 ± 0.57	10.7 ± 0.76
59.1	VB	1.01 ± 0.02	4.43 ± 0.30	5.58 ± 0.40	7.16 ± 0.57	9.35 ± 0.90

*R_{1J}, R_{2J}, R_{3J} and R_{4J} are the ratios for E_o = 0.407, 0.484, 0.554 and 0.620 MeV, respectively. The ratios have been multiplied by 10^{13}.

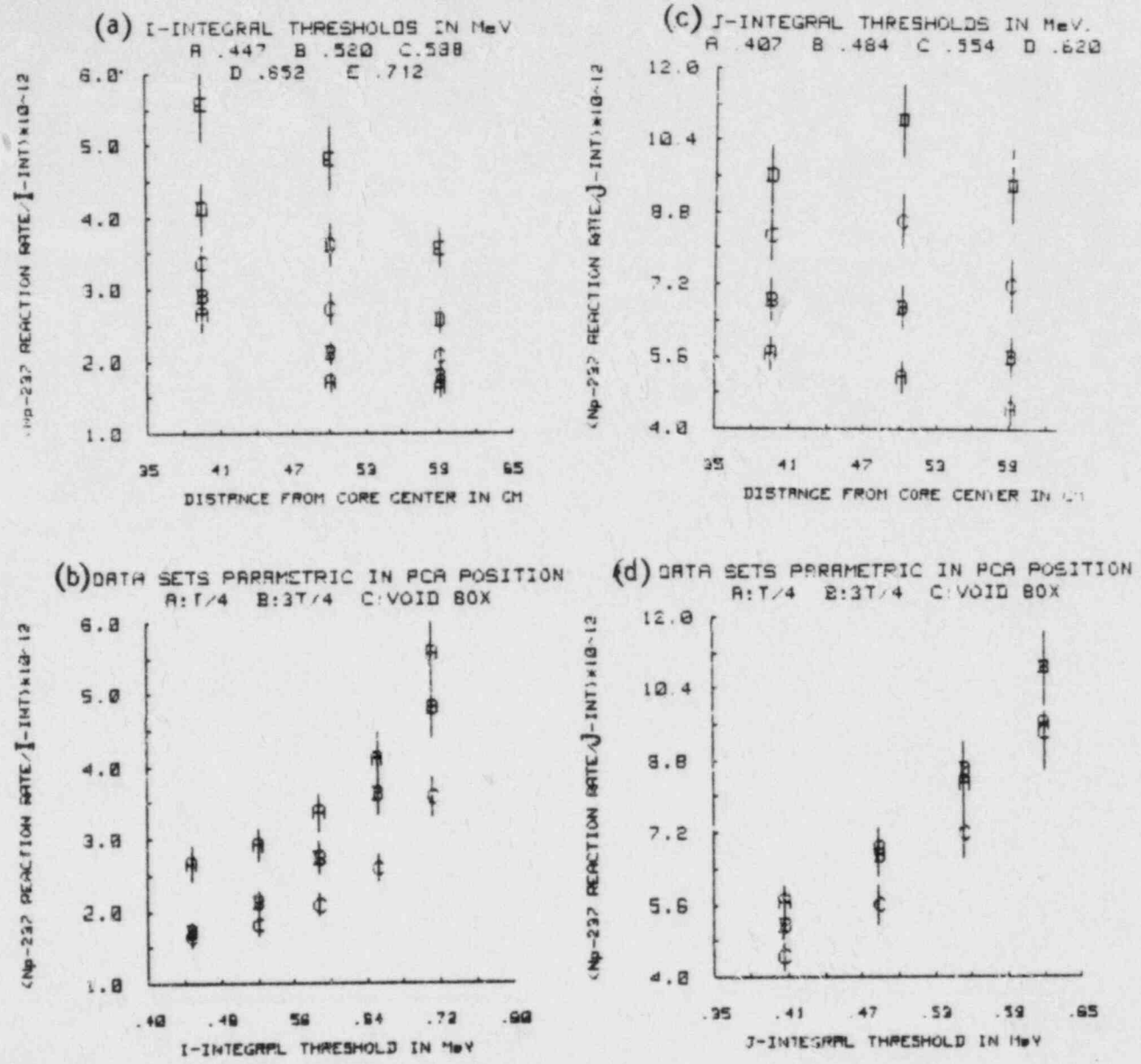

FIGURE 3.2.5. Ratios of ^{237}Np Reaction Rates to I-Integrals [Curves (a) and (b)] as Functions of Position in the PCA (a) and as Functions of I-Integral Thresholds (b). [The corresponding ratios of ^{237}Np reaction rates to J-integral are given in curves (c) and (d).]

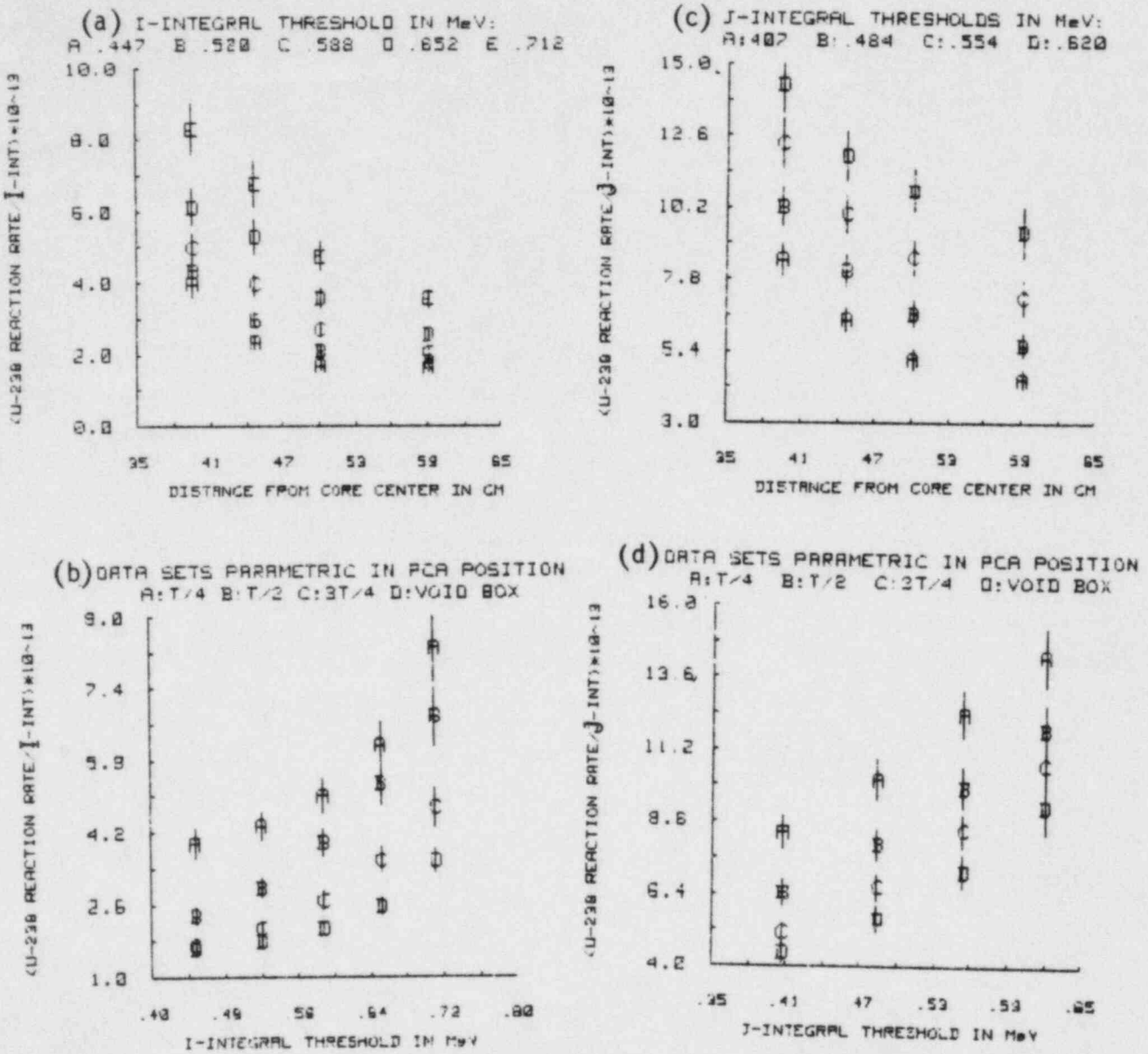

FIGURE 3.2.6. Ratios of ^{238}U Reaction Rates to I-Integrals [Curves (a) and (b)] as Functions of Position in the PCA (a) and as Functions of I-Integral Thresholds (b). [The corresponding ratios of ^{238}U reaction rates to J-integrals are given in Curves (c) and (d).]

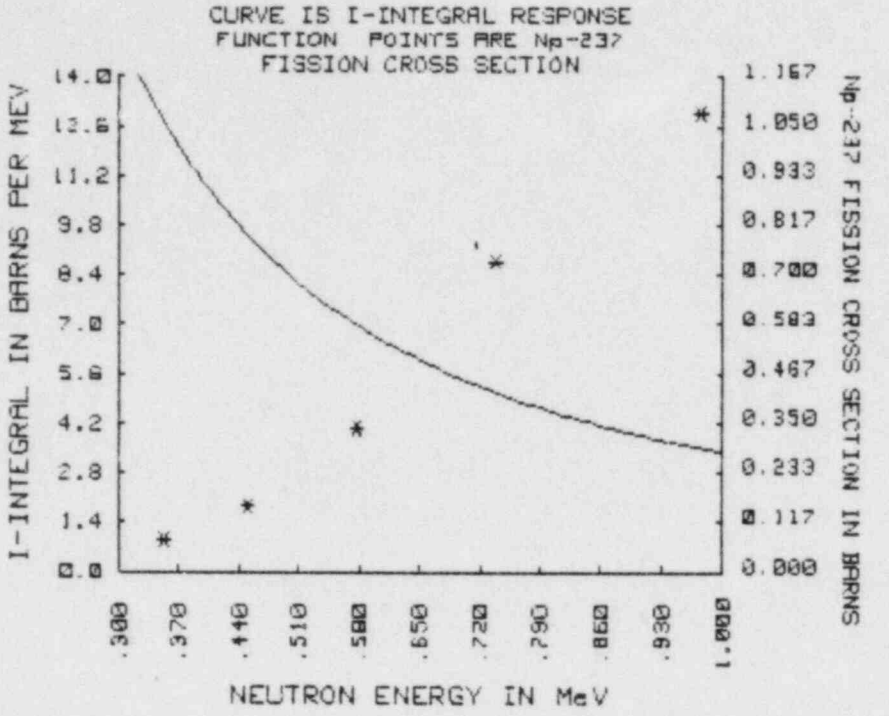

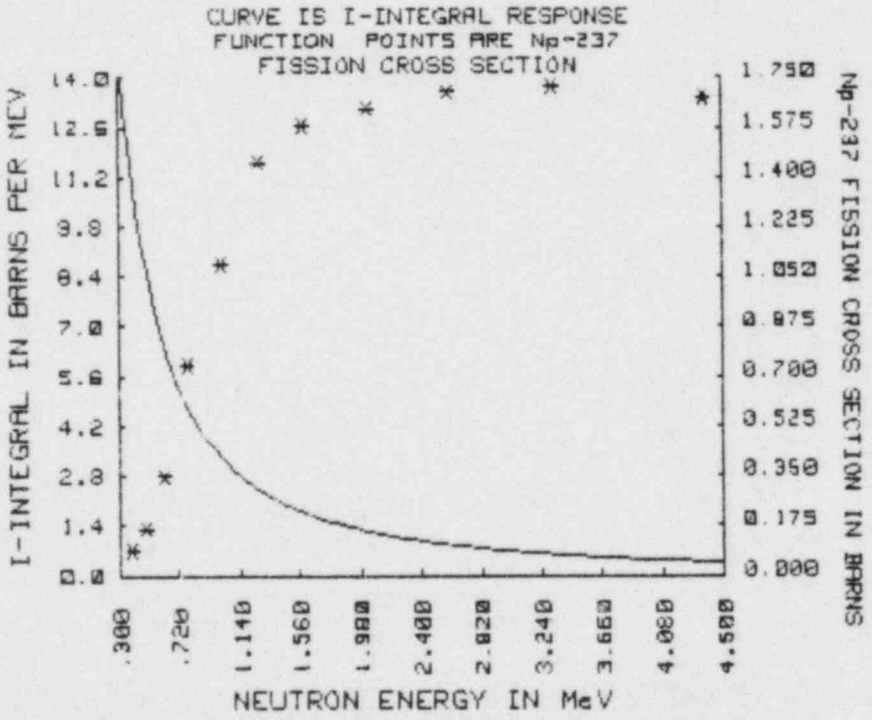

FIGURE 3.2.7. I-Integral Response Functions and ^{237}Np Fission Cross Sections as a Function of Neutron Energy. [Curve (a) shows the behavior of these quantities in the region from 0.300 to 1.000 MeV, whereas in (b) the quantities are plotted from 0.30 to 4.50 MeV.]

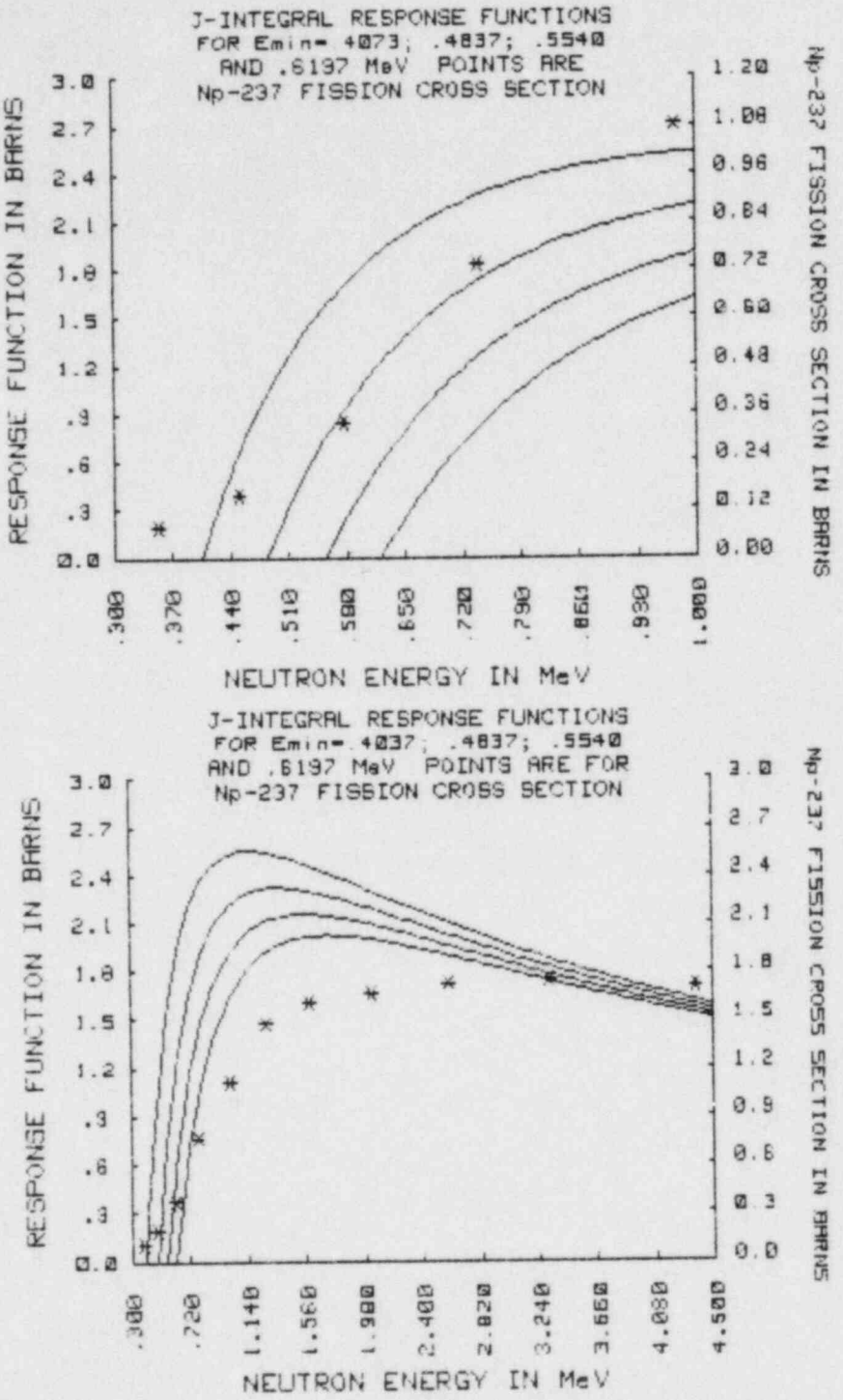

FIGURE 3.2.8. J-Integral Response Functions and ^{237}Np Fission Cross Section as a Function of Neutron Energy. [The curves are parametric in the J-integral thresholds. Curves (a) show the behavior from 0.30 to 1.00 MeV, whereas in (b) the quantities are plotted from 0.30 to 4.50 MeV.]

It is interesting to compare the J-integral response ratios for ^{237}Np and ^{238}U. (i.e., Figure 3.2.5c with Figure 3.2.6c and Figure 3.2.5d with Figure 3.2.6c). The ratio of the ^{238}U fission rate to the J-integral reaction rate behaves very systematically both as a function of location and as a function of threshold. For all the thresholds used here, the J-integrals clearly possess a lower energy response than the ^{238}U fission cross section. Hence, one can qualitatively conclude from Figure 3.2.6c that the spectrum softens with increasing distance from the core.

In contrast, the ratio of the ^{237}Np fission rate to the J-integral reaction rate is not as simple. In Figure 3.2.5c, one finds that the behavior of this ratio as a function of location changes dramatically with threshold. Also in Figure 3.2.5d there is a crossover between the A and B curves as a function of threshold for the highest threshold; curve D first rises and then falls. An examination of the plots in Figure 3.2.8, however, make it clear why a complicated behavior might be expected, since the relative response of the ^{237}Np fission cross section and the J-integral are changing rapidly for the different J-integral thresholds. Only a quantitative analysis based on spectral changes in the energy region can lead to a meaningful interpretation of these results.

3.3 GAS PROTON-RECOIL SPECTROMETRY

J. W. Rogers (EG&G)

This section is in preparation and will be added during a future revision of this document.

4.0 GAMMA-RAY DATA

Raymond Gold (HEDL)

SUMMARY

To meet the needs of the LWR-PV Surveillance Dosimetry Improvement Program, in-situ gamma-ray dosimetry has been carried out over the past four years in the LWR-PVS at the PCA. These observations provide gamma-ray data that are needed to:

1) Benchmark industry-wide reactor physics computational tools; e.g., independently, the gamma-ray spectrometry measurements provide absolute data for comparison with calculations;

2) Assess the radial, azimuthal, and axial contributions of gamma-ray heating to the temperature attained within the PV wall and other components of commercial LWR power reactors;

3) Design and analyze high-power LWR irradiation tests, such as the PSF metallurgical test; and

4) Assess photofission background in LWR-PV passive neutron fission dosimetry.

Continuous gamma-ray spectrometry was carried out using Compton recoil gamma-ray spectroscopy. Measurements were conducted primarily at midplane in the 1/4 T, 1/2 T, 3/4 T, and VB locations of the 8/7, 12/13, and 4/12 SSC configurations of the LWR-PVS. Observed gamma-ray continua have already been reported for these configurations in the first of this series of reports (Mc81). This chapter will focus on the most recent gamma-ray efforts undertaken at the PCA in the fall of 1981.

In order to complement these gamma spectrometry efforts, integral gamma-ray dosimetry was carried out in the 4/12 SSC configuration using thermoluminescent dosimetry (TLD). Results of the integral TLD dosimetry measurements are reported and are also compared to the most recent dosimetry results based on absolute gamma-ray spectrometry. Both of these experimental techniques are, in turn, compared with calculation.

4.1 TEST MATRIX SELECTION AND RATIONALE

Raymond Gold (HEDL)

In the LWR-PV Surveillance Dosimetry Improvement Program, there is need for gamma-ray data to:

1) Benchmark industry-wide reactor physics computational tools; e.g., independently, the gamma-ray spectrometry measurements provide absolute data for comparison with calculations.

2) Assess the radial, azimuthal, and axial contributions of gamma heating to the temperature attained within surveillance capsules, the PV wall, and other components of commercial LWR power reactors (Ra82a).

3) Design, control, and analyze high-power metallurgical irradiation tests.

4) Interpret fission neutron dosimetry in LWR-PV environments, where non-negligible photofission contributions can arise (Bo77,Si79, Go79d,Ve80).

Consequently, the establishment of a low-power LWR-PV benchmark at the PCA has provided a unique opportunity to obtain gamma-ray data heretofore unavailable. Indeed, this has been attested to by the inclusion of an entire chapter of new gamma-ray data (Go81b) in the first of this series of reports.

Existing techniques for gamma-ray spectrometry and dosimetry were applied directly in the PCA. Compton recoil gamma-ray spectroscopy was used for both continuous gamma-ray spectrometry as well as absolute gamma-ray dosimetry. Gamma-ray dose measurements were also carried out at the PCA with thermoluminescent dosimetry (TLD). The results of these efforts through 1980 are fully described in Chapter 5 of the first NUREG report on PCA experiments (Go81b). As a consequence, only the follow-on experiments performed in 1981 are considered here. Moreover, in these more recent experiments, the very latest developments in experimental techniques were applied and recognized systematic effects were taken into account.

The test matrix for the 1981 gamma-ray measurements is given in Table 4.1.1. It can be compared with the test matrix for earlier PCA gamma-ray work by consulting Chapter 5 of the first NUREG report on PCA experiments (Go81b). Table 4.1.1 reveals that the 1981 efforts were confined solely to continuous gamma-ray spectrometry. Additional ionization chamber and TLD measurements were conducted, but only to determine perturbation factors introduced by the Janus gamma-ray spectrometry probe.

TABLE 4.1.1

TEST MATRIX FOR THE 1981 GAMMA-RAY SPECTROMETRY EFFORTS AT THE PCA

In-Situ Location	LWR-PV Configuration		
	T2/13	4/12	4/12 SSC
1/4 T	X	X	X
1/2 T	X		X
3/4 T	X		X
VB	X		X

Section 4.2 presents the experimental Si(Li) spectrometry efforts and results, including comparisons with available calculations. Si(Li) gamma-ray dosimetry results are presented in Section 4.3 and are compared to TLD measurements as well as to calculations. Measurement of the Janus probe perturbation factors is described in Section 4.4.

4.2 GAMMA-RAY SPECTROMETRY

J. P. McNeece, Raymond Gold, and B. J. Kai

4.2.1 Introduction

The radiation field found in nuclear reactors is comprised of two components rather than just a single component, i.e, gamma rays as well as neutrons. The interdependence of these two neutral particle components in reactor radiation fields has been recognized for some time (Go70a) and has been stressed in reviews (Go75,Go78a), which provide the general motivation for gamma-ray characterization efforts in reactor environments.

Just as in reactor neutron metrology, gamma-ray spectrometry and gamma-ray dosimetry are techniques that complement each other at low power. Gamma-ray spectrometry provides absolute differential data, whereas gamma-ray dosimetry furnishes absolute integral data. Both differential and integral gamma-ray data can be used for comparison with reactor calculations.

Gamma-ray efforts in the LWR-PV mockup at the PCA represent an effective collaboration between groups at two major laboratories; namely, the Center for the Study of Nuclear Energy, Mol, Belgium (CEN/SCK) and the Hanford Engineering Development Laboratory (HEDL). The HEDL group carried out continuous gamma-ray spectrometry and dosimetry with Si(Li) detectors, as well as ionization chamber measurements. The CEN/SCK group carried out TLD measurements and coupled neutron-gamma transport calculations. These earlier efforts, through 1980, are described in Chapter 5 of the first of this series of NUREG reports (Go81b). More recent analyses and comparisons of these earlier data were presented at the Fourth ASTM-EURATOM Symposium on Reactor Dosimetry (Go82b).

In the last few years, progress in defining the gamma-ray component of the radiation field in the LWR-PVS environment has been exceptional. This progress can be attributed, in the main, to the synergistic collaboration between the CEN/SCK and HEDL groups. At the outset, absolute gamma-ray spectral calculations performed by the CEN/SCK group for the 12/13 configuration were roughly an order of magnitude higher than continuous gamma-ray spectrometry carried out by the HEDL group in this (12/13) LWR-PVS configuration at the PCA.

This initial comparison provided the impetus for more detailed calculations as well as complementary TLD measurements by the CEN/SCK group. Subsequent comparisons in the 4/12 SSC configuration revealed that the absolute spectrometry measurements of the HEDL group were now a factor of two or so higher than these new calculations. Furthermore, Si(Li) gamma-ray dosimetry was roughly 35% higher than TLD measurements within the PV block. The CEN/SCK group pointed out that the Si(Li) measurements could be high due to voids created upon insertion of the Janus probe into the PV block. The HEDL group concurred, noting that the gamma-ray intensity gradient in the PV block, together with voids arising by introduction of the Janus probe, could produce the higher absolute results observed in the Si(Li) measurements.

As a consequence, miniature ionization chambers were developed to actually measure the perturbation that arises through introduction of the Janus probe into the PV block. These measurements are described in Section 4.4. In addition, the Janus probe was redesigned to minimize voids for the 1981 PCA measurements. This new design, together with the latest developments in experimental technique, are described in Section 4.2.2, which follows. Gamma-ray continua observed in the 1981 PCA experiments are presented in Section 4.2.3. Comparisons of the observed gamma-ray spectra with theory are presented whenever appropriate reactor calculations are available.

4.2.2 Experimental Technique

The basic principles underlying Compton recoil gamma-ray spectroscopy have been adequately documented (Go68a,Go70a,Go70b,Ko75,Ji78,Si68,Si69). Since its inception, however, this method has undergone continuous improvement. Advances in this technique were reviewed at the last two international ASTM-EURATOM Symposia on reactor dosimetry (Go80d,Go82b). Further developments as well as applications in breeder reactor (BR) environments have also been reported (Go79b,Go80b). This method continues to evolve so that even the most recently reported efforts (Go82b) require updating. Consequently, improvements incorporated into the Janus spectrometer for the 1981 PCA experiments are explained below.

Janus Spectrometer -- The basic elements that comprise the Si(Li) gamma spectrometer Janus probe system are displayed in Figure 4.2.1a. This optimized system differs from that previously reported in four important ways:

1) Two separate, but identical, cooled 1-cm^3 Si(Li) detectors are placed face-to-face as shown in Figure 4.2.1a.

2) Each detector output is fed into a reconfigured version of the ORTEC 142A preamplifier, in which the front end FET stage is cooled.

3) The pulse processing instrumentation has been altered somewhat from the original Janus probe electronics. Coincident counting between Si(Li) detectors is still possible, but no pulse shape discrimination is used.

4) The detector vacuum enclosure has also been modified, as shown in Figure 4.2.1b, to reduce the probe perturbation on the LWR-PVS gamma field. Specifically, the detectors now are separated from the electronics below by a 0.254-cm steel plate. Steel plates have been used as well to reduce the vacuum voids beside and above the detector to 0.254 cm.

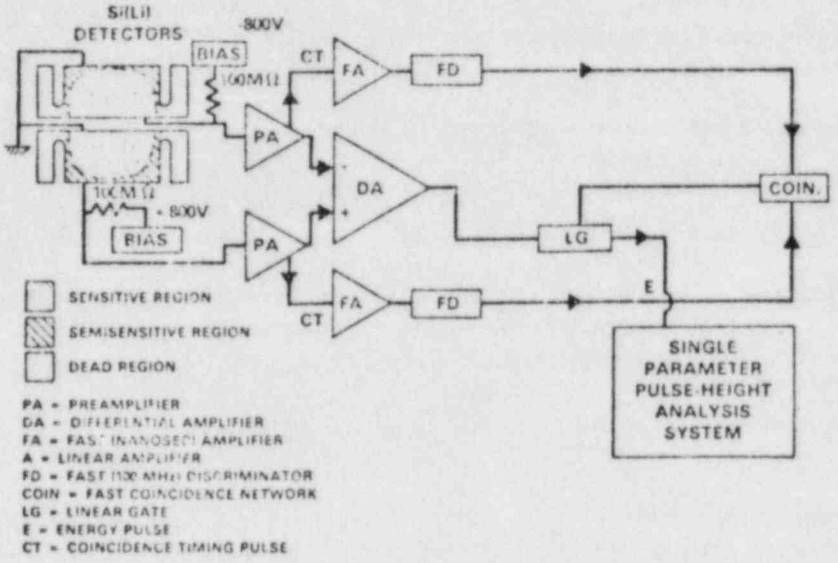

FIGURE 4.2.1a. Cross-Sectional View of the Janus Detector Configuration and Block Diagram of the Pulse Processing Instrumentation.

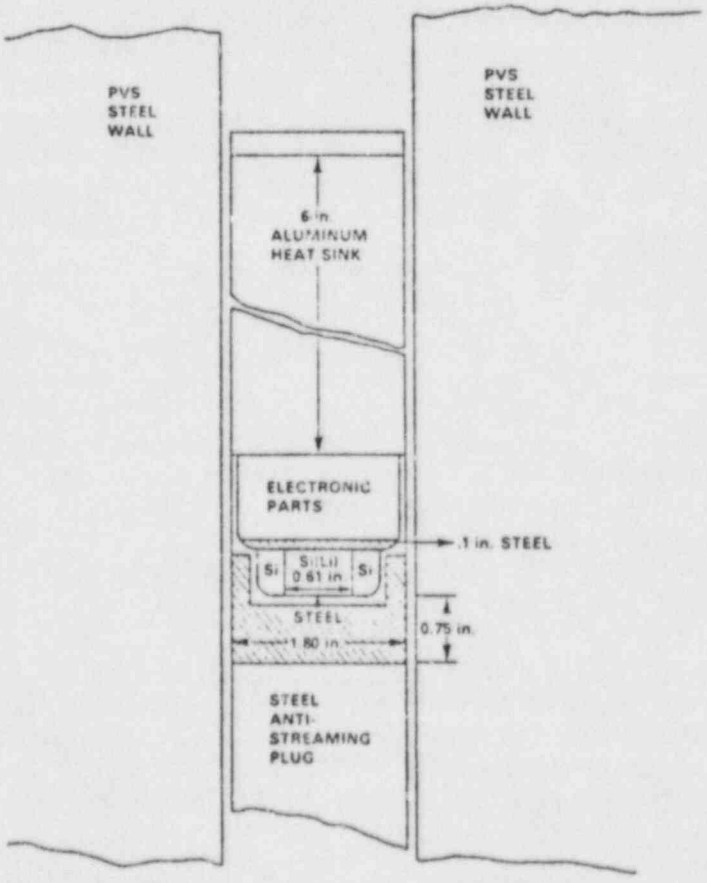

FIGURE 4.2.1b. In-Situ Irradiation Environment of the Si(Li) Janus Probe in the LWR-PVS.

These modifications provide the following capabilities:

1) Two complementary modes of operation:

   - The noncoincidence mode for low energy spectrometry ($\lesssim$3 MeV).
   - The coincidence mode for high energy spectrometry ($\gtrsim$3 MeV).

2) Improved discrimination against neutron-induced events, since neutron interactions produce short-range events that are excluded in the coincidence-mode operation.

3) Improved high energy coincidence-mode response for unfolding analyses.

4) Lower common mode noise and better resolution by utilizing a differential shaping amplifier, in place of the cascaded differential and linear amplifiers previously used.

5) Single-parameter, rather than dual-parameter analysis, reduces the complexity of the pulse processing instrumentation as well as the procedures necessary for data collection and unfolding.

The recent change from dual- to single-parameter pulse analysis was based upon a careful study of Si(Li) energy and rise-time spectra as a function of gamma-ray energy, using monoenergetic gamma-ray sources in the 0.1 to 7.0 MeV energy region. The two most significant observations generated in this study were:

1) Rise-time spectra were found to be electron (hence gamma-ray) energy-dependent.

2) The variation of observed electron energy spectra was not adequately described by theory (Klein-Nishina formula). [These energy spectra were obtained from monoenergetic gamma-ray sources in the 0.1 to 7.0 MeV energy region using rise-time discrimination to reject electron escape from the Si(Li) detectors.]

As a result of this study, the use of theory as the basis for response matrix construction, as practiced in earlier continuous gamma-ray spectrometry efforts (Go70), was not appropriate for the Janus probe. Under these conditions, empirical response matrix construction affords greater accuracy, since systematic effects are automatically included in the observed monoenergetic responses that are used, in turn, to construct the response matrix. Moreover, the experimental technique is simplified considerably by use of single-parameter as opposed to dual-parameter pulse analysis. The success of this single-parameter, empirical response matrix approach has

already been demonstrated through the satisfactory comparison of Janus probe results with a Ge(Li) spectrometer observation of a line spectrum from a ^{226}Ra source (Go81c,Go82b).

Data Analysis -- Empirical response matrix construction to date has only been performed in the low-energy (noncoincidence) region. Hence, results reported here are necessarily confined to the energy region $\lesssim$3 MeV.

The empirical response matrix was constructed from the measured responses of eight monoenergetic gamma-ray sources. Monoenergetic gamma-ray energies ranged from 0.3208 to 2.754 MeV. Table 4.2.1 lists the sources used. The following sections describe data preparation and response matrix construction in detail.

TABLE 4.2.1

MONOENERGETIC SOURCES USED IN THE RESPONSE MATRIX CONSTRUCTION

Radioisotope	Photon Energy (MeV)	Compton Edge Energy (MeV)
^{52}Cr	0.3208	0.1779
^{198}Au	0.4118	0.2541
^{64}Cu	0.511	0.3407
^{137}Cs	0.5616	0.4773
^{54}Mn	0.8348	0.6394
^{65}Zn	1.115	0.9071
^{22}Na	1.275	1.0618
^{24}Na	2.754	2.5201

Initial Data Preparation -- The first step in preparing the eight measured monoenergetic responses is to normalize each response to a fixed fluence at the center of the detector. Using absolute source strength together with geometric correction factors, each monoenergetic Compton recoil spectrum is normalized to 10^6 γ/cm^2 at the detector center. In addition the ^{22}Na and ^{24}Na spectra are corrected to remove secondary gammas (0.511 MeV for ^{22}Na and 1.3686 MeV for ^{24}Na).

Response Matrix Generation -- An empirical response matrix (256 x 256) is constructed for the Janus probe. Each column, j, of the matrix represents the response of the detector for a gamma-ray fluence of 10^6 γ/cm^2 at the detector center. The gamma-ray energy of each column is that energy having its Compton edge at row i=j. Rows of the matrix possess a 10-keV electron energy width.

Construction of the matrix is accomplished by the use of an analytical expression having parameters computed from the eight measured monoenergetic gamma-ray responses. The analytical expression contains terms to account for the basic Gaussian broadened theoretical Compton recoil spectrum, low-energy tails due to escape and electronic noise, photopeaks, pair production peaks, and multiple-scattering effects. To more clearly explain how these parameters are computed, the analysis of the ^{137}Cs will be shown in detail.

The measured response (electron spectrum) for ^{137}Cs is shown in Figure 4.2.2. The first step in the analysis is to define the Gaussian broadened theoretical Compton spectrum portion of the measured response. Figure 4.2.3 shows the theoretical Compton recoil spectrum for a 0.662-MeV gamma ray. A trial-and-error method is used to define a broadening term that, when applied to the theoretical spectrum, will produce a spectrum having a shape at the Compton edge comparable to the measured response. The Gaussian broadened spectrum is then normalized to the measured response magnitude at the Compton edge. Figure 4.2.4 shows the normalized, Gaussian broadened spectrum. The broadening factor and the magnitude of the response at the Compton edge are two terms used in the final expression.

Parameters for the other components of the spectrum are determined from the result of subtracting the broadened, theoretical spectrum from the measured response. This result is shown in Figure 4.2.5. Three of the four possible components are shown: the low-energy tail, the multiple-scattering peak, and the photopeak. The pair production peak is not a part of the ^{137}Cs response since the gamma-ray energy is below the threshold for pair production ($\sim$1.02 MeV).

The low-energy tail is fit to a sum of two decaying exponentials using a nonlinear least-squares fitting routine. Four parameters are generated from this fitting process. The multiple-scattering peak is represented by the coupling of two Gaussians, both having the same height but different widths. Figure 4.2.6 shows the result for the ^{137}Cs spectrum. Three parameters are generated from this fit. The photopeak is treated as a single Gaussian. A least-squares fit is made to calculate the height and width parameters. Pair production peaks are treated in the same manner as photopeaks.

The result of the analysis is a set of eleven (thirteen, if there is a pair production peak) parameters for each of the monoenergetic gamma-ray sources. Each of these parameters is, in turn, fit to a smooth curve in gamma-ray energy space. Thirty values are tabulated between 0.32 MeV and 2.75 MeV for each parameter.

The response matrix is generated column by column. The gamma energy is chosen such that its Compton edge lies in row i=j, and the parameters for this gamma-ray energy are determined by interpolation in the parameter

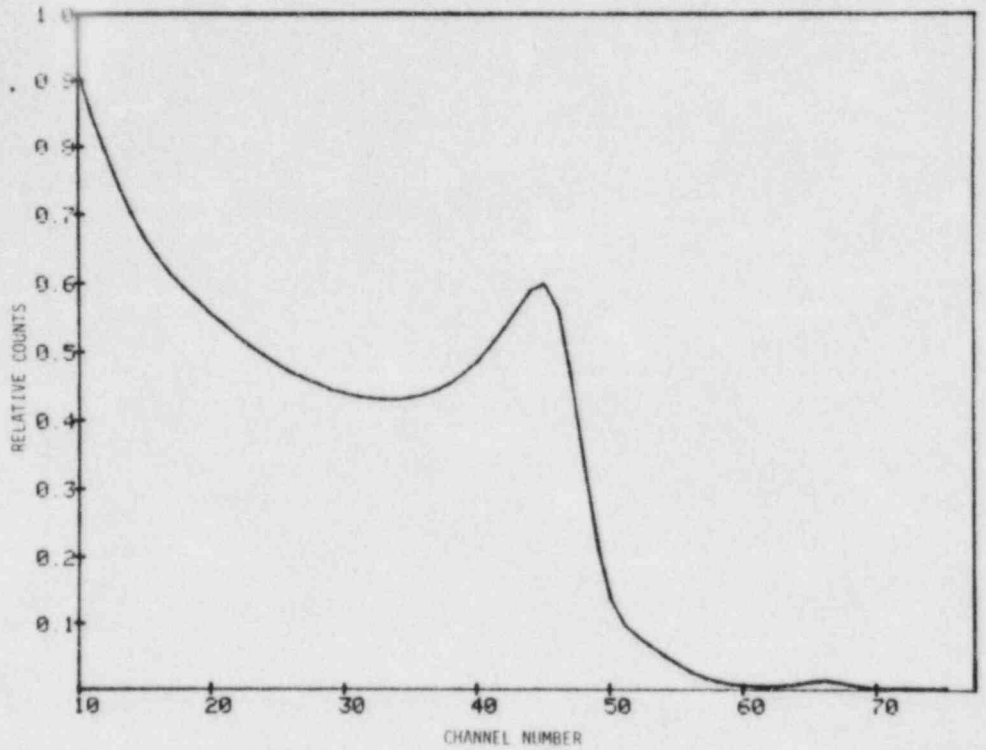

FIGURE 4.2.2. Measured Electron Spectrum for ^{137}Cs.

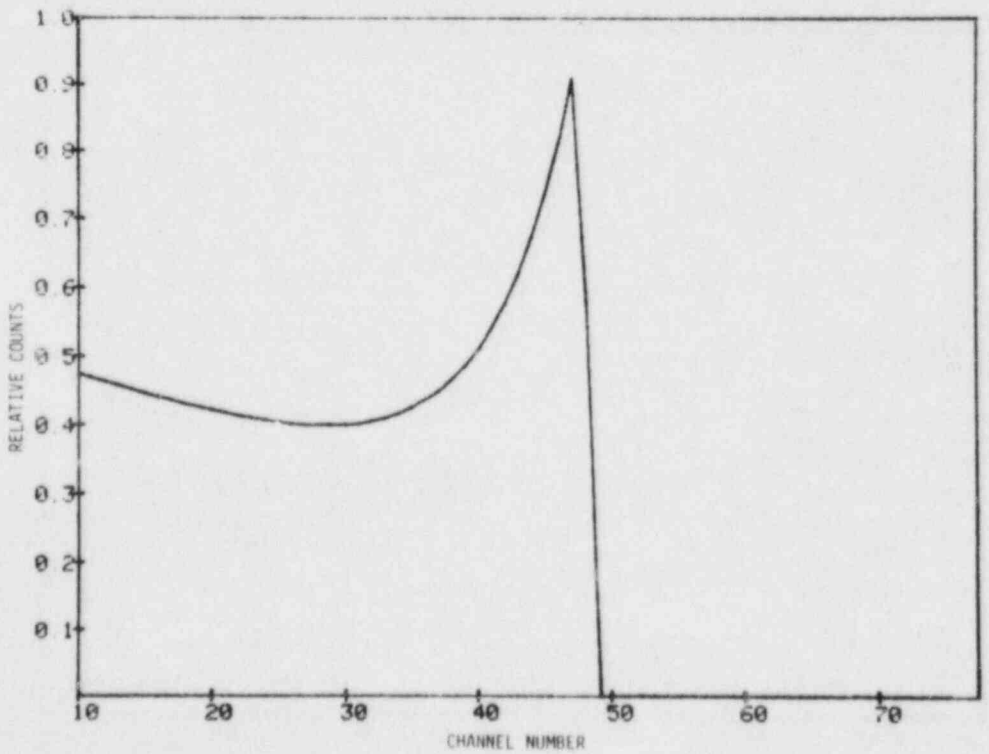

FIGURE 4.2.3. Theoretical Compton Recoil Spectrum for the 0.662-MeV Gamma Ray of ^{137}Cs.

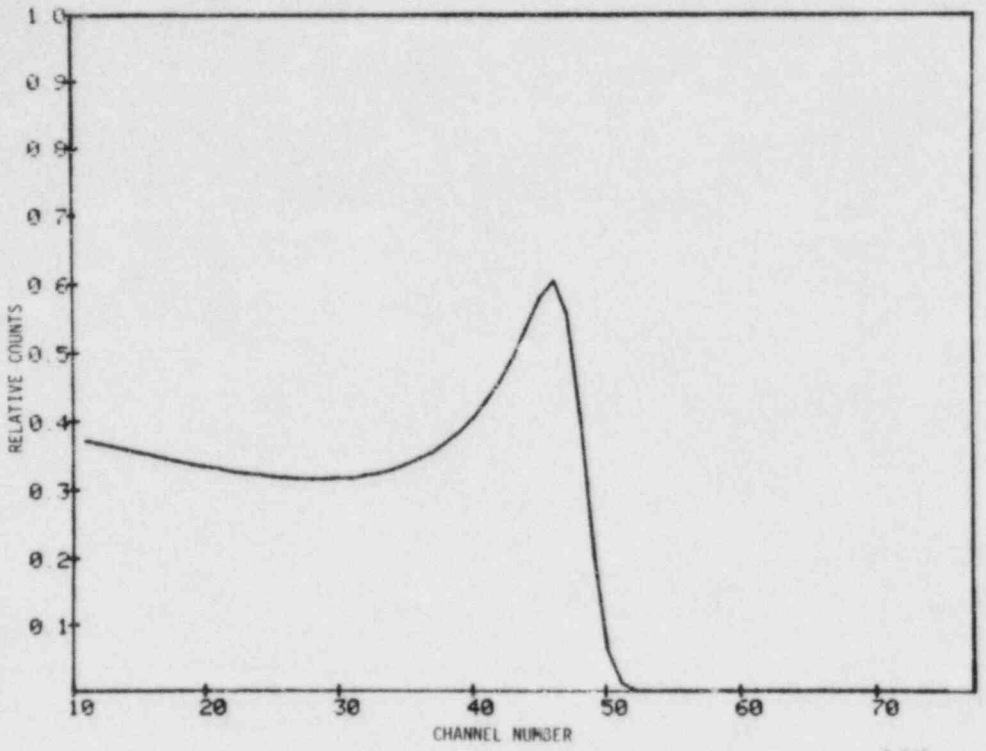

FIGURE 4.2.4. The Normalized Gaussian Broadened Spectrum for ^{137}Cs.

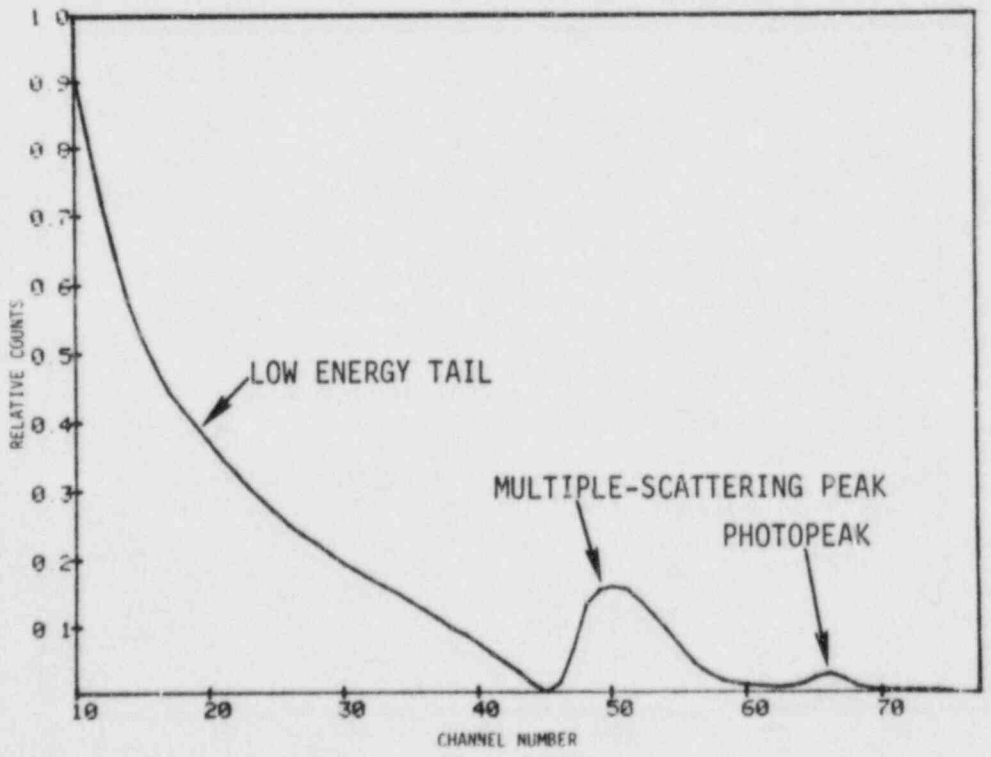

FIGURE 4.2.5. Results of Subtracting the Broadened Theoretical Spectrum from the Measured Spectrum for ^{137}Cs.

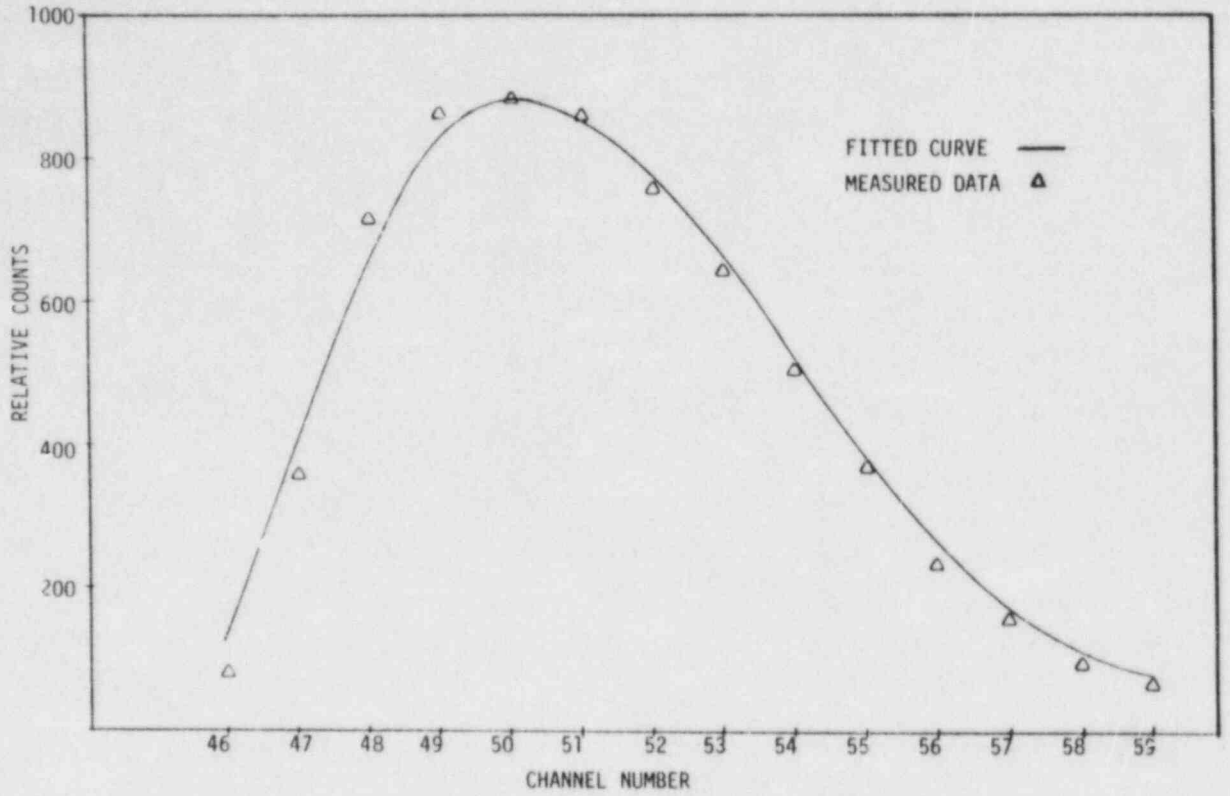

FIGURE 4.2.6. Result of Nonlinear Least-Squares Fit of the Multiple-Scatter Peak for the ^{137}Cs Spectrum.

tables. Figure 4.2.7 shows the calculated response for ^{137}Cs, and Table 4.2.2 presents a comparison between the calculated and measured ^{137}Cs responses. The deviation between parametric and observed responses can exceed 10%. However, these larger deviations arise in regions where the response is relatively small. In regions where the response is substantial, the deviation between parametric and observed responses is generally less than 5%.

Unfolding -- Gamma continua are obtained with iterative unfolding (Go70c). The arresting criterion for the iteration process was modified to account for not only the statistical fluctuation in the data, but also for the error, σ_E, in energy calibration. Hence, the standard deviation at each channel σ_i was computed as:

$$\sigma_i^2 = N_i + \left(\frac{\partial W}{\partial E}\right)_i^2 (\sigma_E)_i^2 \qquad (1)$$

TABLE 4.2.2

COMPARISON BETWEEN CALCULATED AND MEASURED
COMPTON RECOIL SPECTRA FOR ^{137}Cs

Channel No.	Calc/ Meas	Channel No.	Calc/ Meas	Channel No.	Calc/ Meas
10	0.987	32	0.947	54	1.060
11	0.956	33	0.947	55	1.087
12	0.947	34	0.948	56	1.102
13	0.948	35	0.950	57	1.140
14	0.954	36	0.950	58	1.022
15	0.958	37	0.951	59	1.136
16	0.960	38	0.953	60	1.131
17	0.959	39	0.955	61	1.128
18	0.956	40	0.957	62	1.128
19	0.953	41	0.960	63	1.125
20	0.951	42	0.965	64	1.116
21	0.951	43	0.973	65	1.093
22	0.951	44	0.988	66	1.026
23	0.951	45	1.019	67	1.091
24	0.950	46	1.080	68	1.128
25	0.950	47	0.970	69	1.118
26	0.949	48	0.921	70	1.116
27	0.948	49	0.900	71	1.096
28	0.948	50	0.932	72	1.110
29	0.948	51	0.990	73	1.130
30	0.948	52	1.047	74	1.146
31	0.947	53	1.063	75	1.138

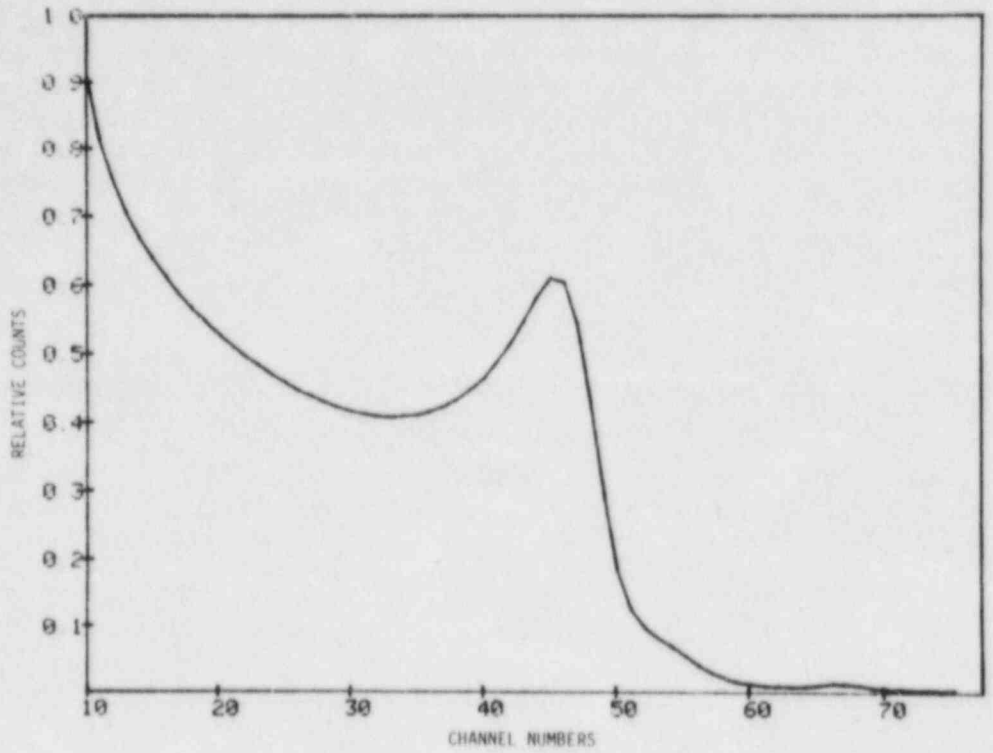

FIGURE 4.2.7. The ^{137}Cs Response Calculated from the Empirical Response Matrix.

where:

N_i = Number of counts in channel i

$\left(\frac{\partial W}{\partial E}\right)_i$ = Slope of the spectrum at channel i

$(\sigma \quad)_i$ = Error in electron energy at channel i

Iterative unfolding is arrested when the sum of the residuals decreases below a prescribed bound A. The initial estimate for A is taken as:

$$A = \sum \sigma_i^2 \qquad (2)$$

The arresting criterion is empirically refined by observing the results of unfolding a known gamma-ray line spectrum, such as ^{226}Ra.

The adequacy of using single-parameter data acquisition together with empirical response matrix unfolding has already been demonstrated through comparison with a Ge(Li) spectrometer using the line spectrum from a ^{226}Ra source (Go81b,Go82b). Obviously, unfolding a line spectrum, such as ^{226}Ra, is a very rigorous test for a continuum spectrometry method. Nonetheless, the unfolded gamma-ray continuum is indeed a line spectrum, and the energy of the unfolded peaks agrees with known ^{226}R energy peaks to an uncertainty of less than 1%. Of equal significance was the fact that the absolute peak intensities of the Janus and Ge(Li) spectrometers agreed to within ~10% over the low-energy region, i.e., <3 MeV.

4.2.3 LWR-PV Gamma-Ray Spectrometry Results from 1981 PCA Experiments

Different power-time histories were used to collect gamma-ray spectrometrty data in the 1981 PCA experiments. These power-time histories are summarized in Table 4.2.3.

TABLE 4.2.3

POWER-TIME HISTORY FOR 1981 PCA GAMMA-RAY SPECTROMETRY

	LWR-PV Configuration								
	12/13			4/12			4/12 SSC		
Location	Date	Power*	Time**	Date	Power*	Time**	Date	Power*	Time**
1/4 T	10/8/81	1.19	68.1	10/7/81	0.30	86.6	10/9/81	1.1	71.1
1/2 T	10/8/81	5.04	68.0	---	--	--	10/9/81	3.9	69.8
3/4 T	10/8/81	20.0	67.6	---	--	--	10/9/81	11.9	68.7
VB	10/8/81	41.0	31.5	---	--	--	10/9/81	23.5	66.0

*PCA power in watts.
**Irradiation time interval in minutes.

Electron and gamma spectra from the 1981 Janus probe measurements at the PCA have been grouped by location and configuration. At each location the following spectra are presented:

a. High-energy electron spectrum.

b. Low-energy background electron spectrum.

c. Low-energy foreground minus background electron spectrum.

d. Low-energy gamma spectrum.

A single figure, which is actually a composite of these four spectra, is used for each location. For example, Figures 4.2.8a, 4.2.8b, 4.2.8c, and 4.2.8d show the high-energy electron spectrum, the low-energy background electron spectrum, the low-energy foreground minus background electron spectrum, and the low-energy gamma spectrum, respectively, for the 4/12 configuration (without SSC). Figures 4.2.9, 4.2.10, 4.2.11 and 4.2.12 present results for the 1/4 T, 1/2 T, 3/4 T, and VB locations of the 4/12 SSC configuration, respectively. Similarly, Figures 4.2.13, 4.2.14, 4.2.15, and 4.2.16 present results for the 1/4 T, 1/2 T, 3/4 T, and VB locations of the 12/13 configuration, respectively.

Data from the high-energy electron spectrum are used to form the infinite medium dose rate, as explained in Section 4.3 below. The low-energy foreground minus background electron spectrum is used to obtain the low-energy gamma spectrum. Consequently, all low-energy gamma spectra have been corrected for background and possess absolute units of gamma rays/(cm^2•MeV•s) at 1 watt of PCA power. In addition, all gamma spectra have been corrected for the perturbation created by the introduction of the Janus probe. A detailed treatment of Janus probe perturbation factors can be found in Section 4.4.

For the low-energy gamma spectra, calculational results are also presented. For the 12/13 configuration, calculations have been performed by ORNL (Ma83) and CEN/SCK (Mi81) for the 1/4 T, 1/2 T and 3/4 T locations. For the 4/12 SSC configuration, calculations have been performed by Mol (Mi81) for the 1/4 T, 1/2 T, and 3/4 T locations.

For the 12/13 configuration, ORNL calculations are roughly a factor of two lower than experimental gamma-ray spectra, whereas CEN/SCK calculations occupy an intermediate position. Similar behavior can be observed in the comparisons between theory and experiment shown for the 4/12 SSC configuration. It is surprising to see that comparisons between theory and experiment generally improve with increasing penetration into the PV. However, calculations generally decrease more rapidly than experimental results with increasing gamma-ray energy.

Satisfactory progress has been made in extending the Janus probe response matrix to higher energy. Measurements have been completed with the gamma-rays from $^{12}C^*$ (~4.4 MeV) and ^{16}O (~6.1 MeV). Analyses of these data are underway with the goal of providing PCA experimental gamma-ray spectra in the energy range above 3.0 MeV. These higher-energy gamma-ray spectra will be reported in subsequent LWR-PV-SDIP quarterly progress reports.

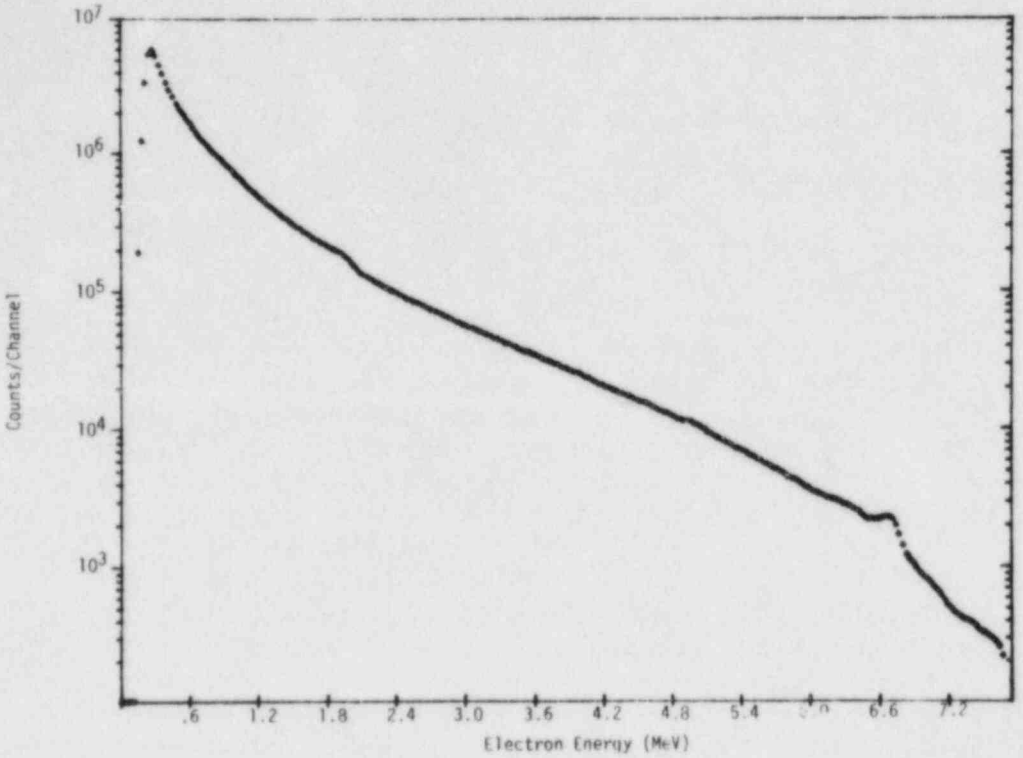

FIGURE 4.2.8a. High-Energy Electron Spectrum for the 1/4 T Location of the 4/12 Configuration (Without SSC).

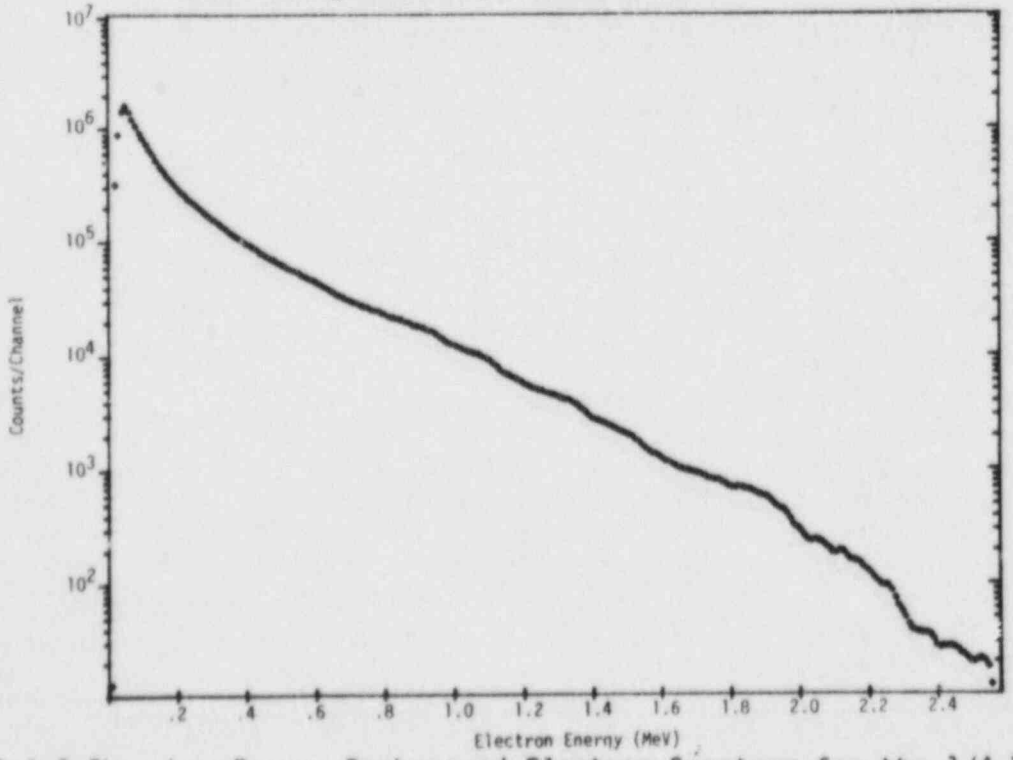

FIGURE 4.2.8b. Low-Energy Background Electron Spectrum for the 1/4 T Location of the 4/12 Configuration (Without SSC).

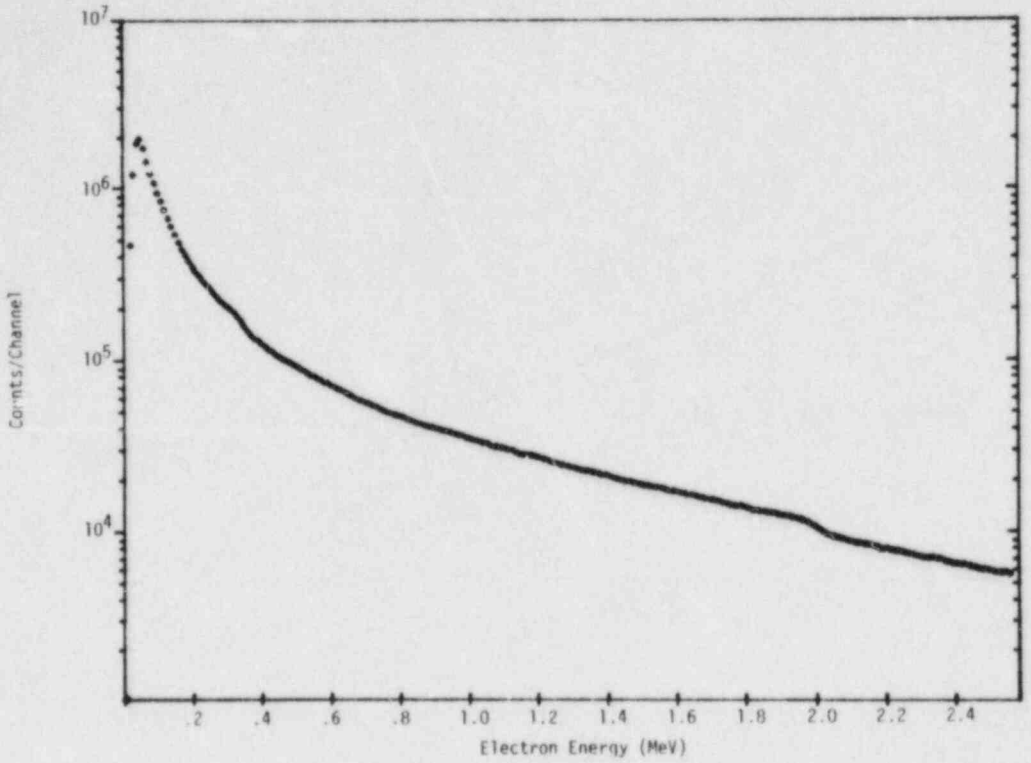

FIGURE 4.2.8c. Low-Energy Foreground Minus Background Electron Spectrum of the 1/4 T Location of the 4/12 Configuration (Without SSC).

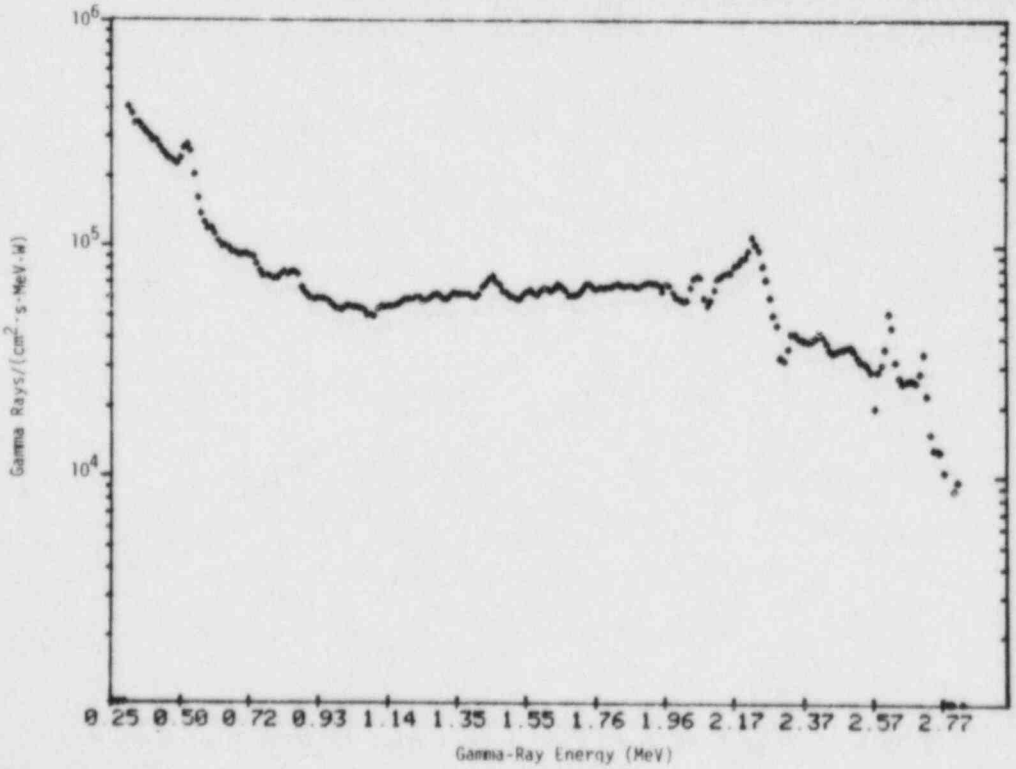

FIGURE 4.2.8d. Low-Energy Gamma-Ray Continuum for the 1/4 T Location of the 4/12 Configuration (Without SSC).

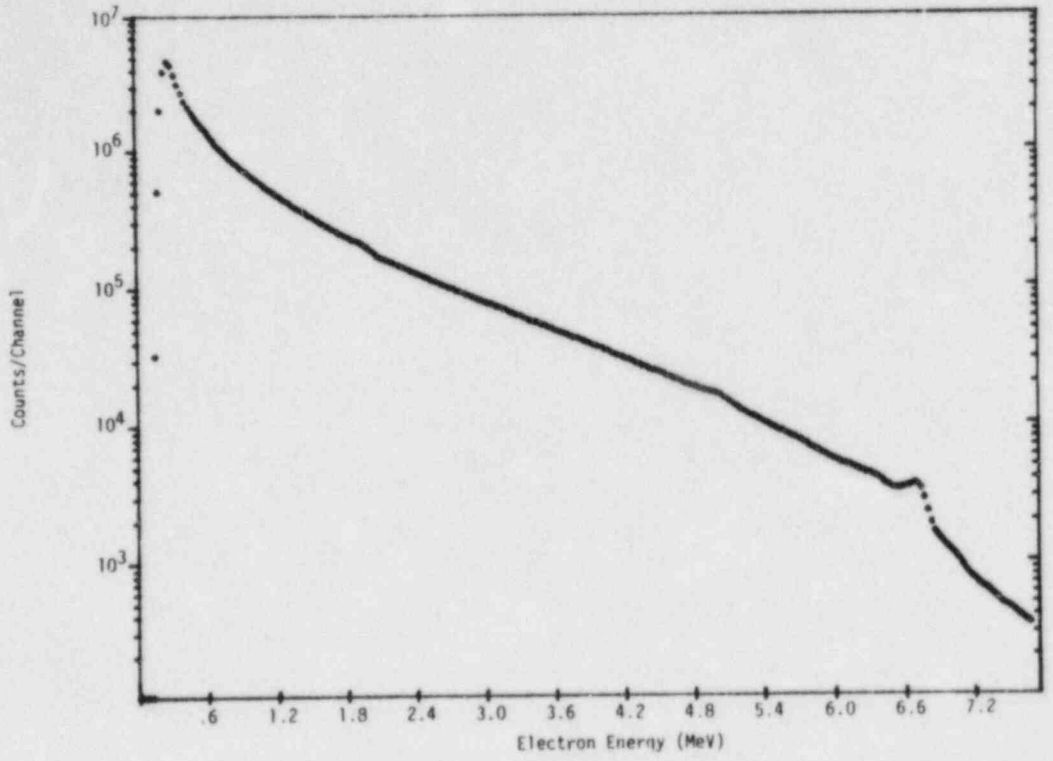

FIGURE 4.2.9a. High-Energy Electron Spectrum for the 1/4 T Location of the 4/12 SSC Configuration.

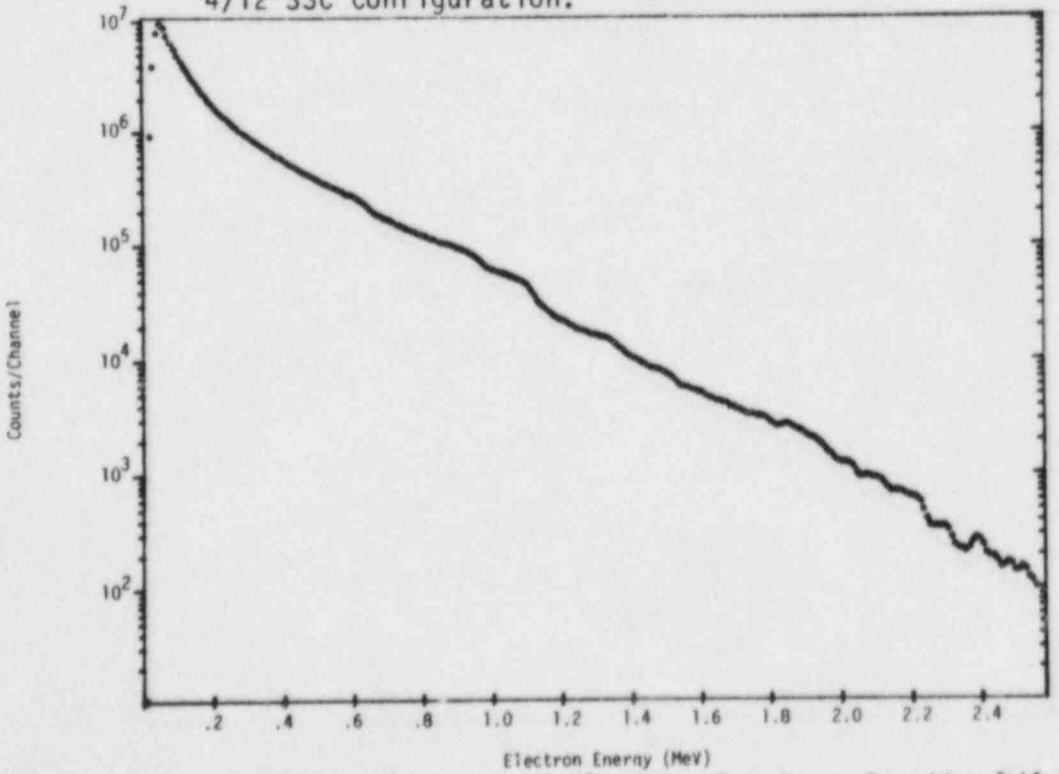

FIGURE 4.2.9b. Low-Energy Background Electron Spectrum for the 1/4 T Location of the 4/12 SSC Configuration.

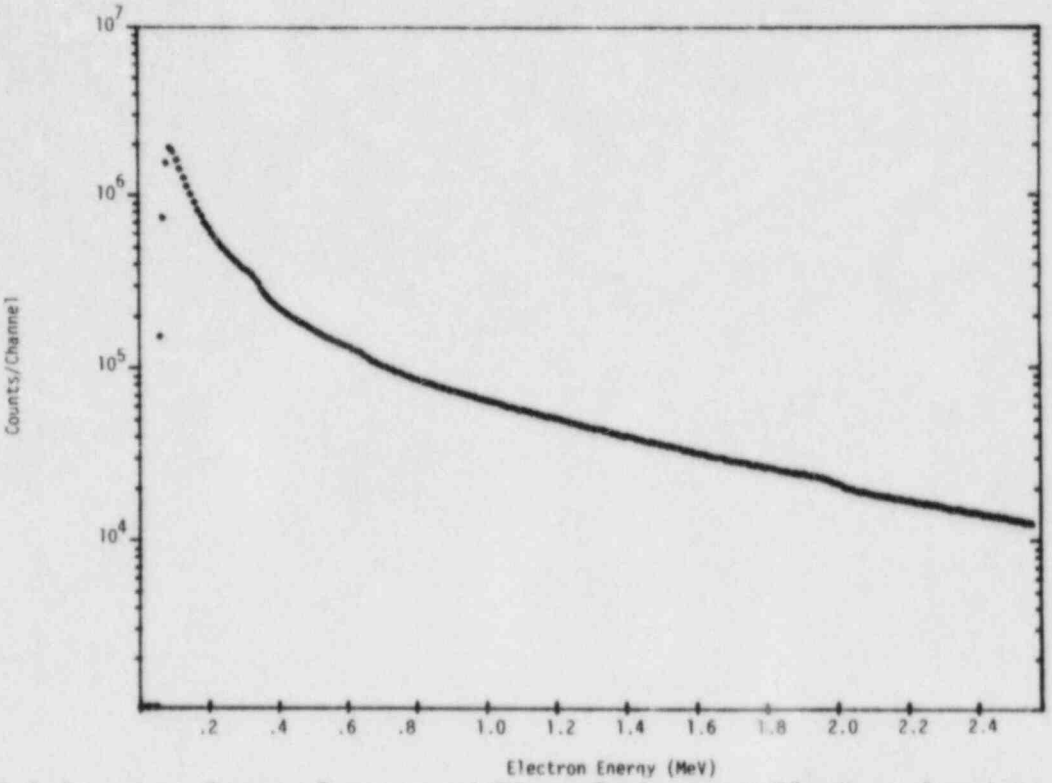

FIGURE 4.2.9c. Low-Energy Foreground Minus Background Electron Spectrum for the 1/4 T Location of the 4/12 SSC Configuration.

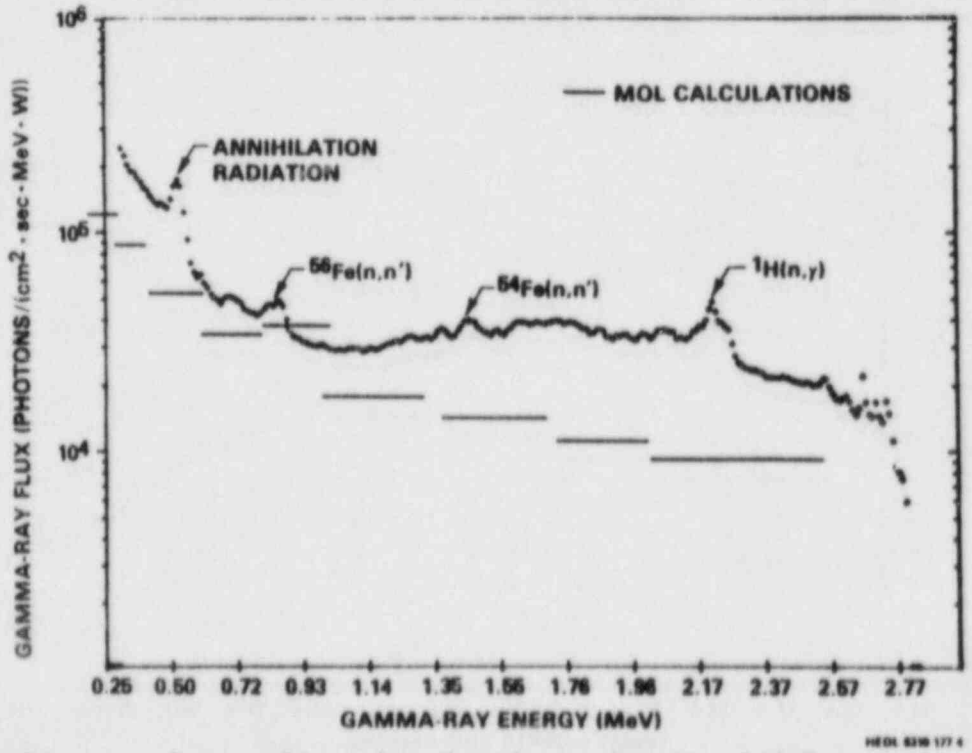

FIGURE 4.2.9d. Low-Energy Gamma-Ray Continuum for the 1/4 T Location of the 4/12 SSC Configuration as Compared with CEN/SCK Calculational Results.

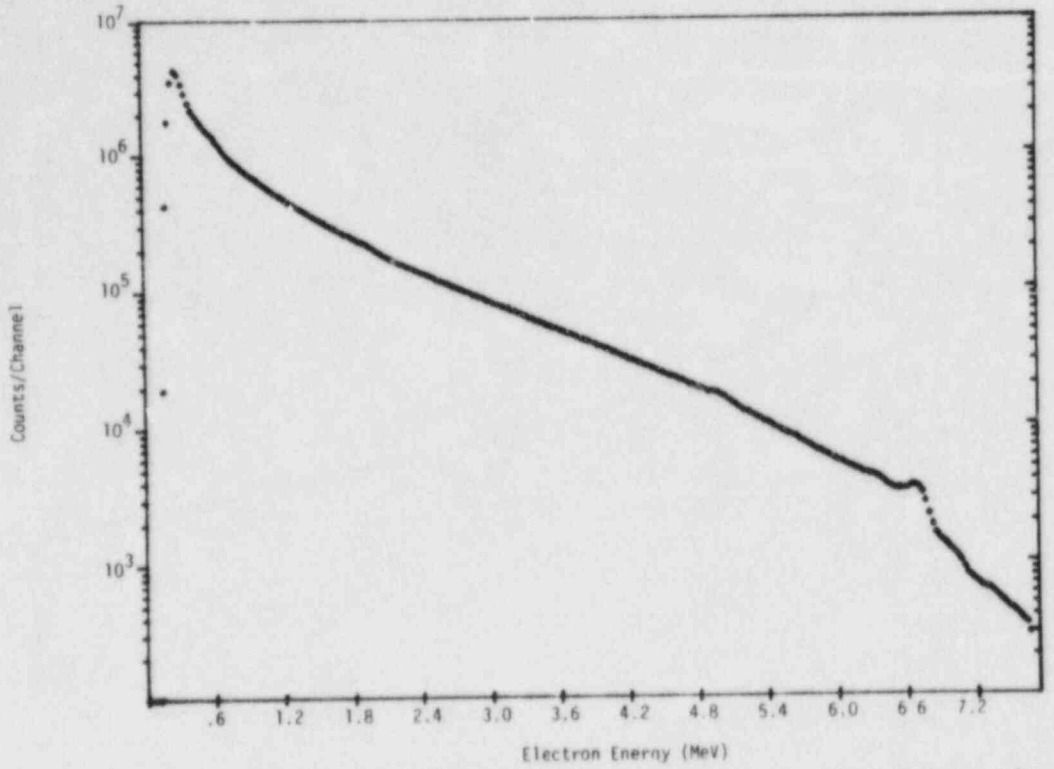

FIGURE 4.2.10a. High-Energy Electron Spectrum for the 1/2 T Location of the 4/12 SSC Configuration.

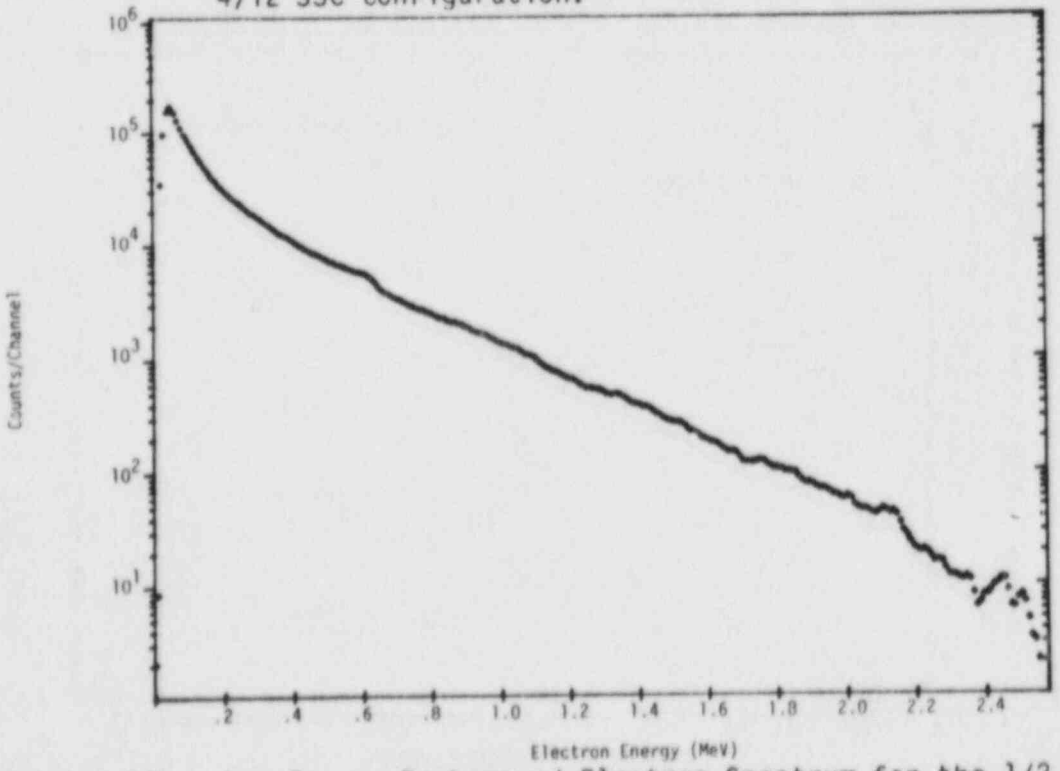

FIGURE 4.2.10b. Low-Energy Background Electron Spectrum for the 1/2 T Location of the 4/12 SSC Configuration.

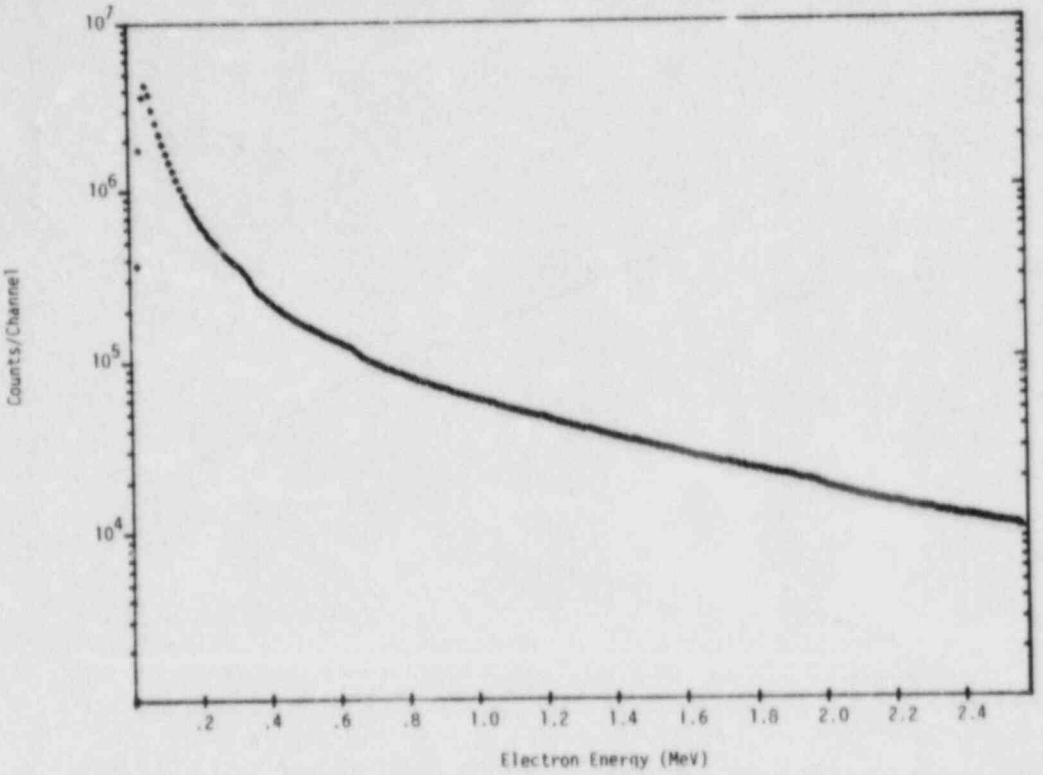

FIGURE 4.2.10c. Low-Energy Foreground Minus Background Electron Spectrum for the 1/2 T Location of the 4/12 SSC Configuration.

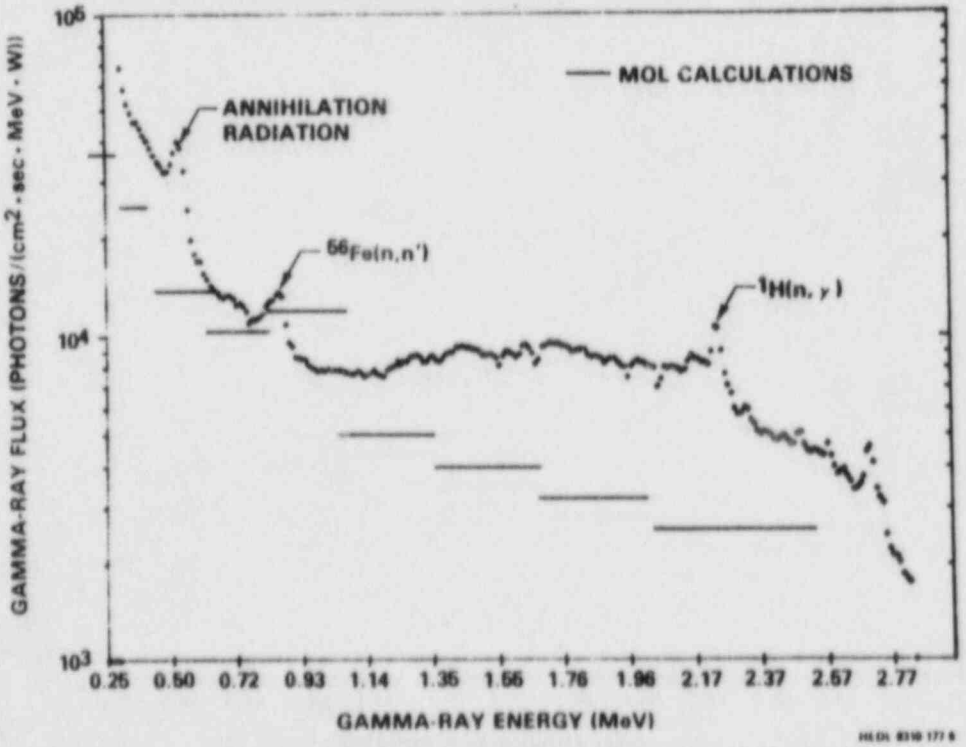

FIGURE 4.2.10d. Low-Energy Gamma-Ray Continuum for the 1/2 T Location of the 4/12 SSC Configuration as Compared with CEN/SCK Calculational Results.

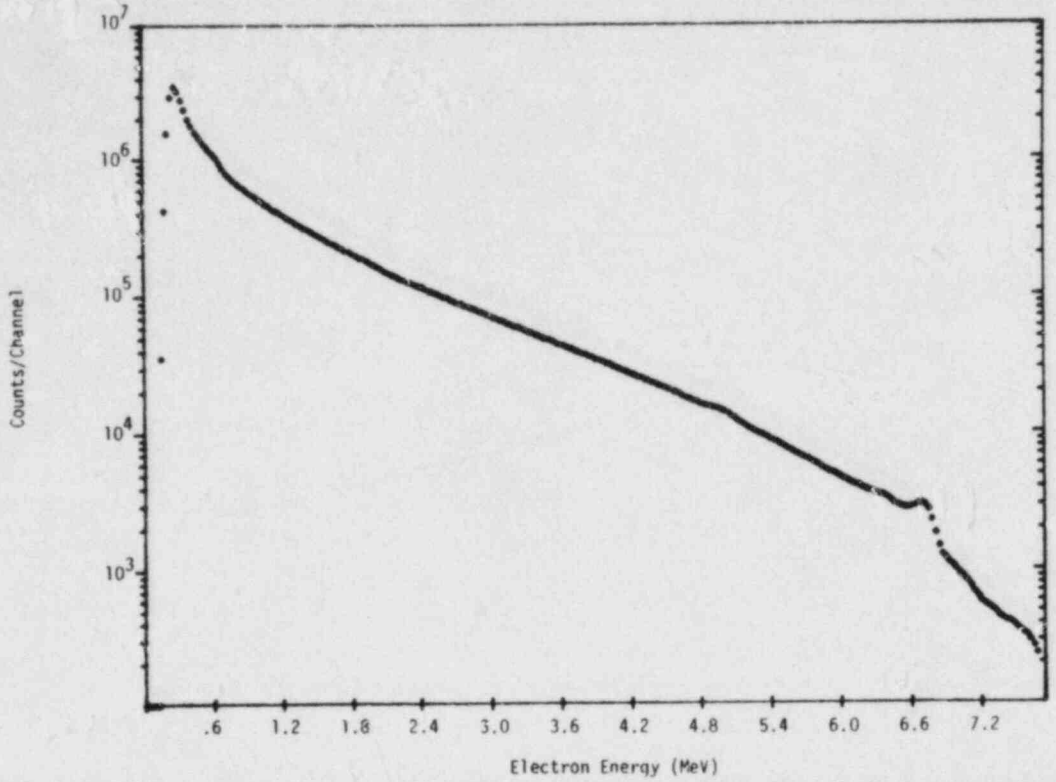

FIGURE 4.2.11a. High-Energy Electron Spectrum for the 3/4 T Location of the 4/12 SSC Configuration.

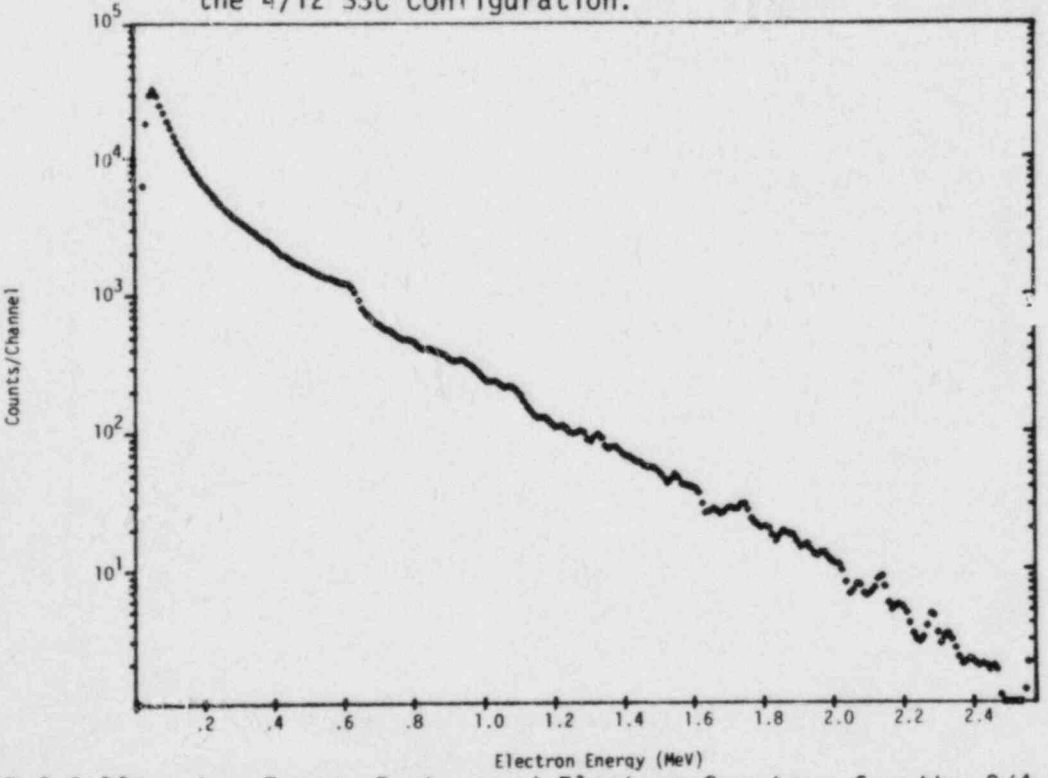

FIGURE 4.2.11b. Low-Energy Background Electron Spectrum for the 3/4 T Location of the 4/12 SSC Configuration.

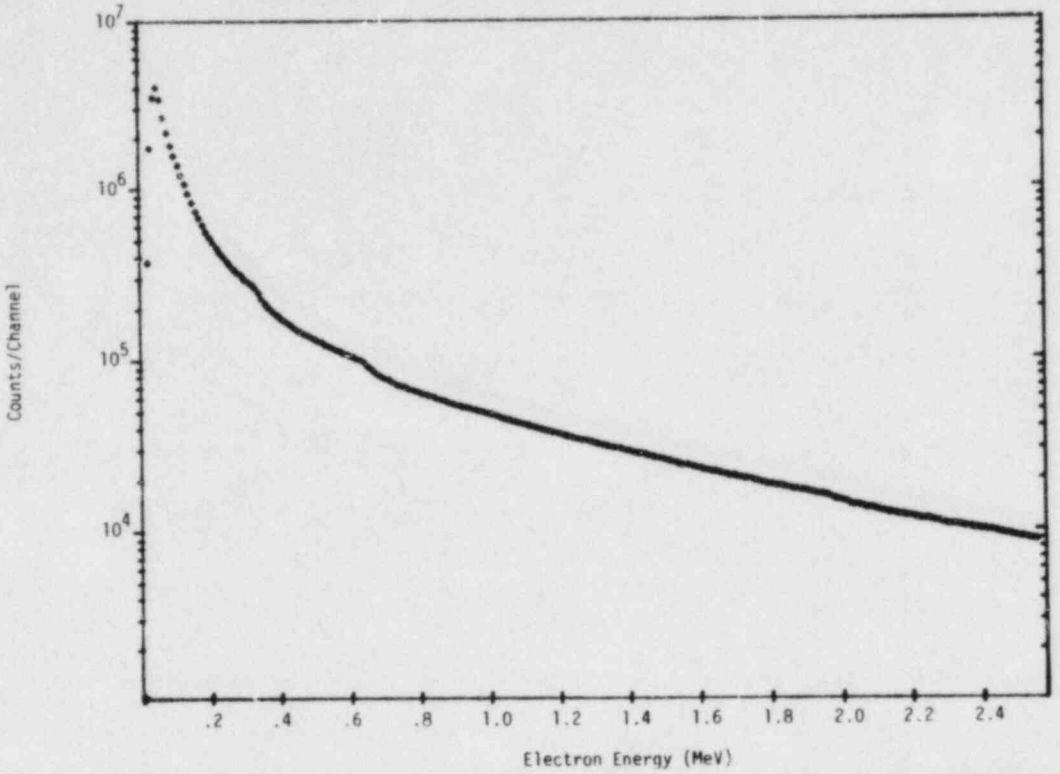

FIGURE 4.2.11c. Low-Energy Foreground Minus Background Electron Spectrum for the 3/4 T Location of the 4/12 SSC Configuration.

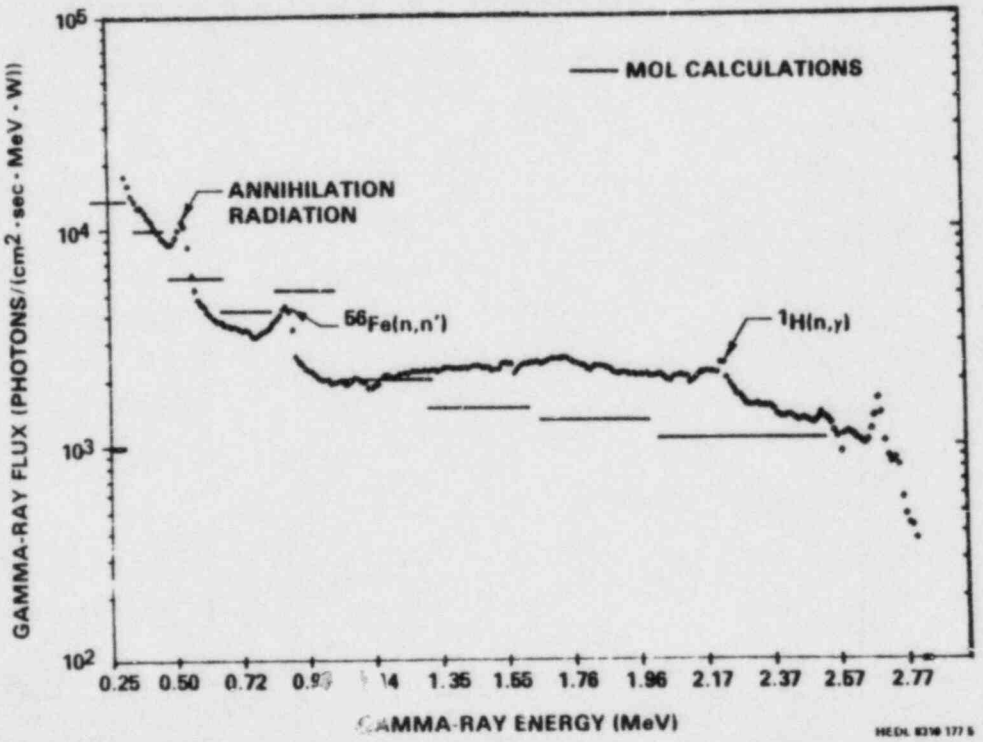

FIGURE 4.2.11d. Low-Energy Gamma-Ray Continuum for the 3/4 T Location of the 4/12 SSC Configuration as Compared with CEN/SCK Calculational Results.

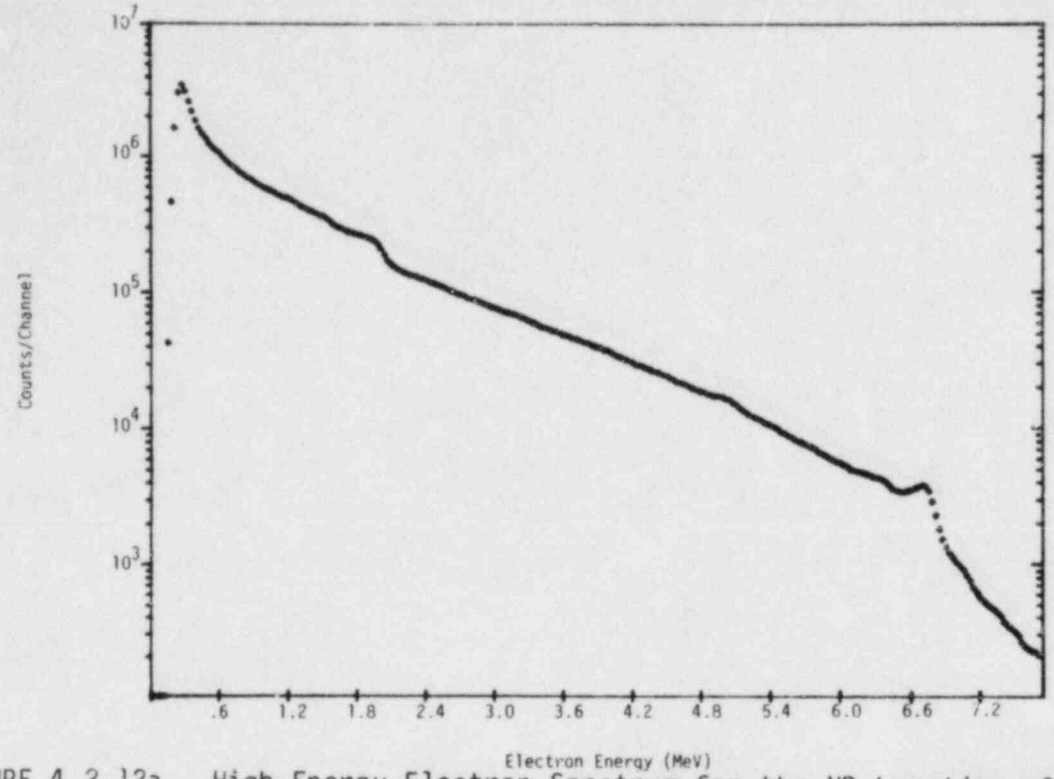

FIGURE 4.2.12a. High-Energy Electron Spectrum for the VB Location of the 4/12 SSC Configuration.

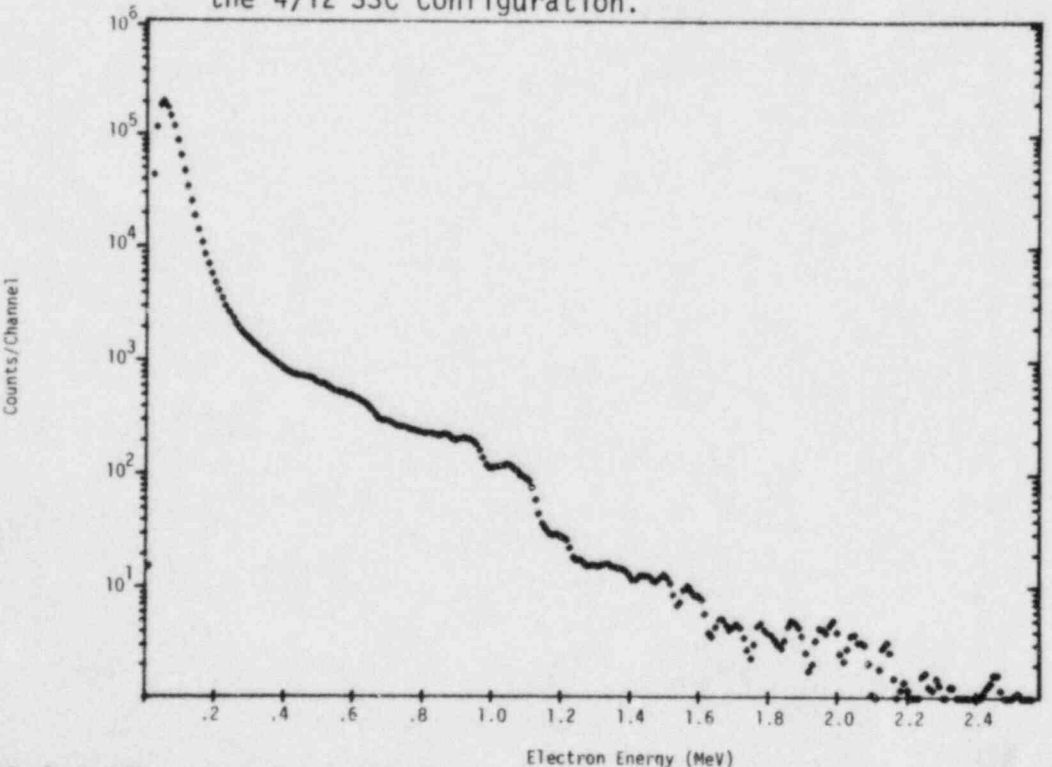

FIGURE 4.2.12b. Low-Energy Background Electron Spectrum for the VB Location of the 4/12 SSC Configuration.

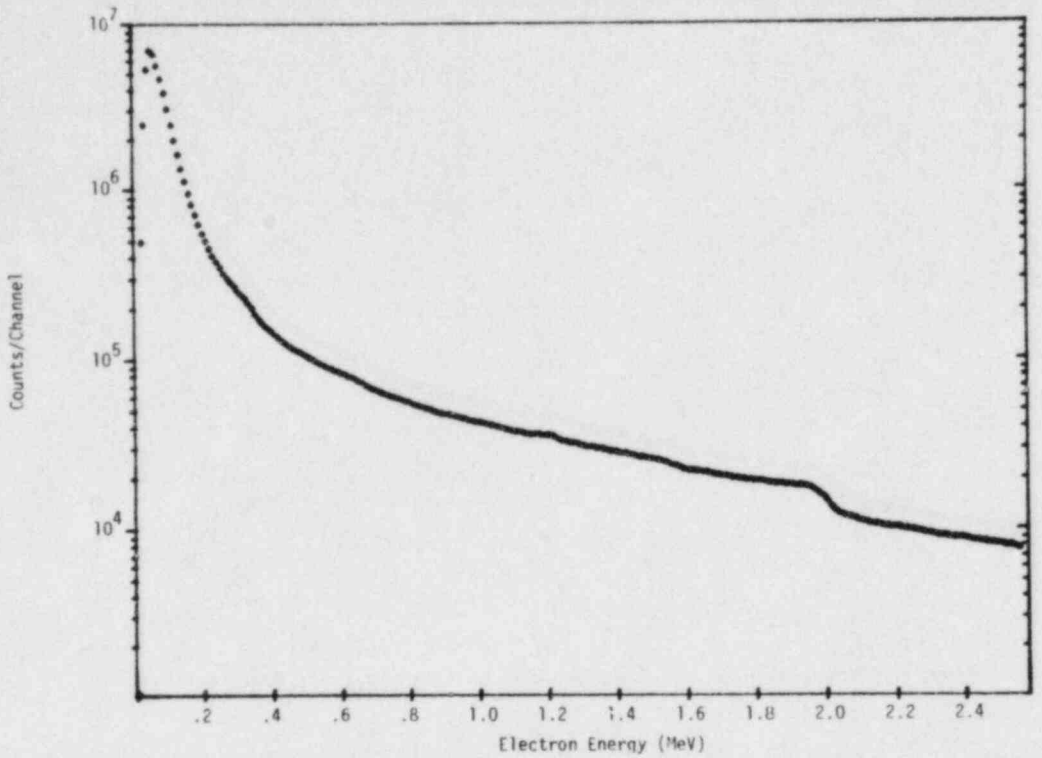

FIGURE 4.2.12c. Low-Energy Foreground Minus Background Electron Spectrum for the VB Location of the 4/12 SSC Configuration.

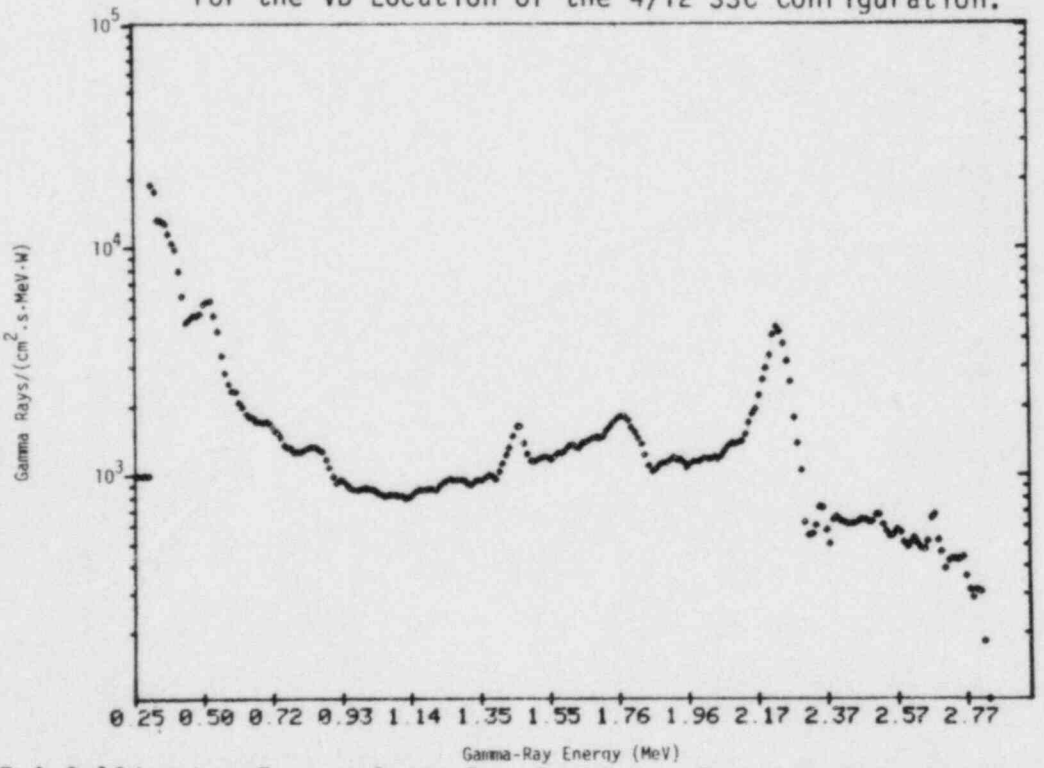

FIGURE 4.2.12d. Low-Energy Gamma-Ray Continuum for the VB Location of the 4/12 SSC Configuration.

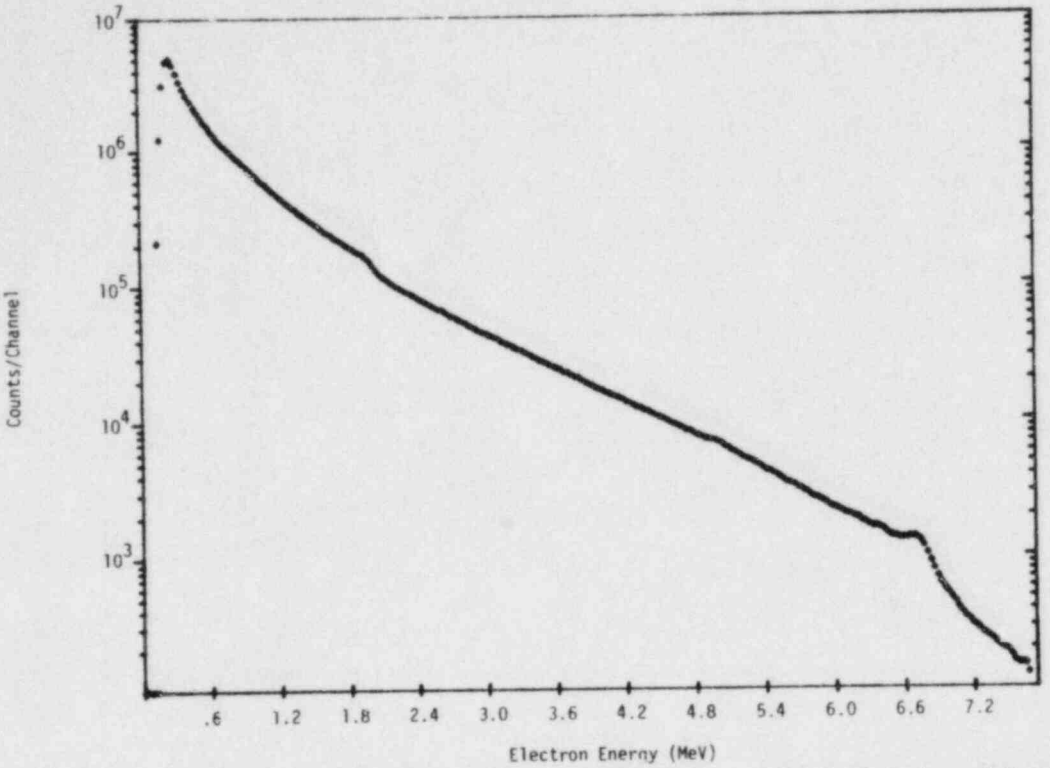

FIGURE 4.2.13a. High-Energy Electron Spectrum for the 1/4 T Location of the 12/13 Configuration.

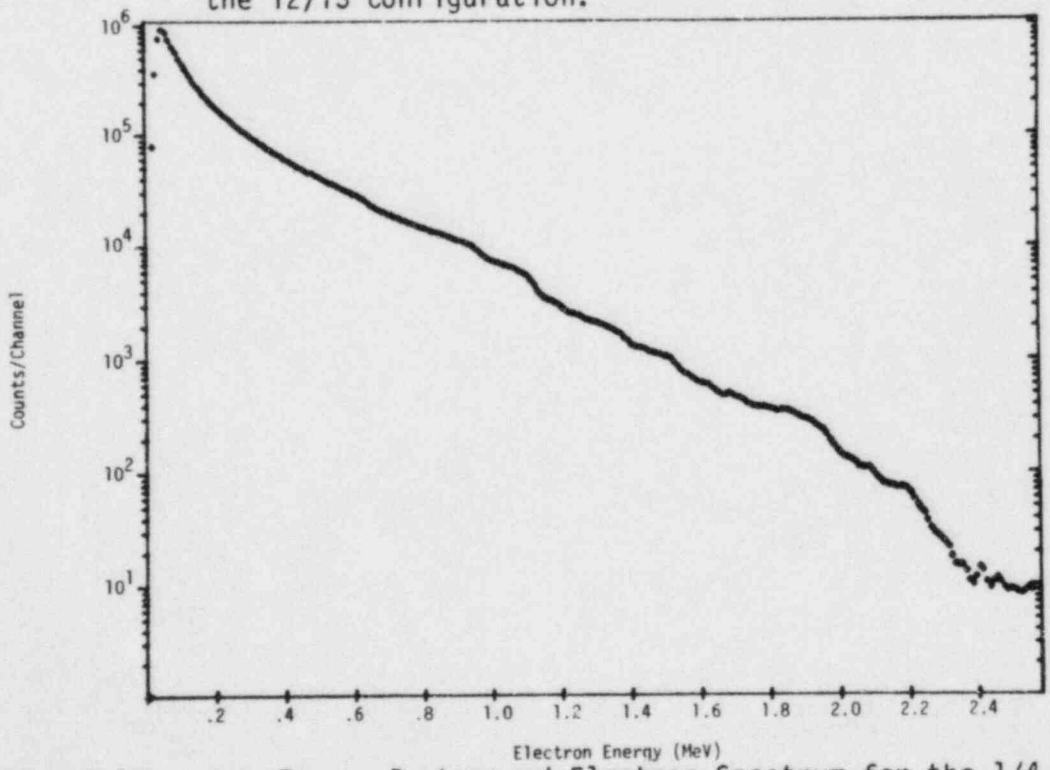

FIGURE 4.2.13b. Low-Energy Background Electron Spectrum for the 1/4 T Location of the 12/13 Configuration.

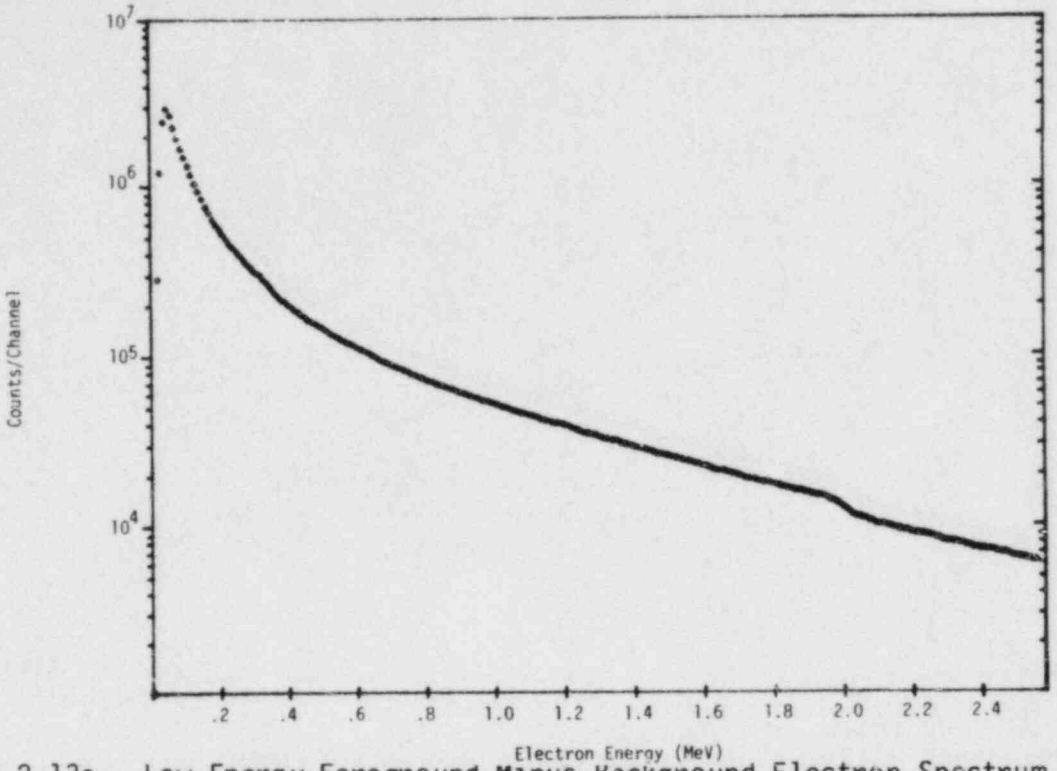

FIGURE 4.2.13c. Low-Energy Foreground Minus Background Electron Spectrum for the 1/4 T Location of the 12/13 Configuration.

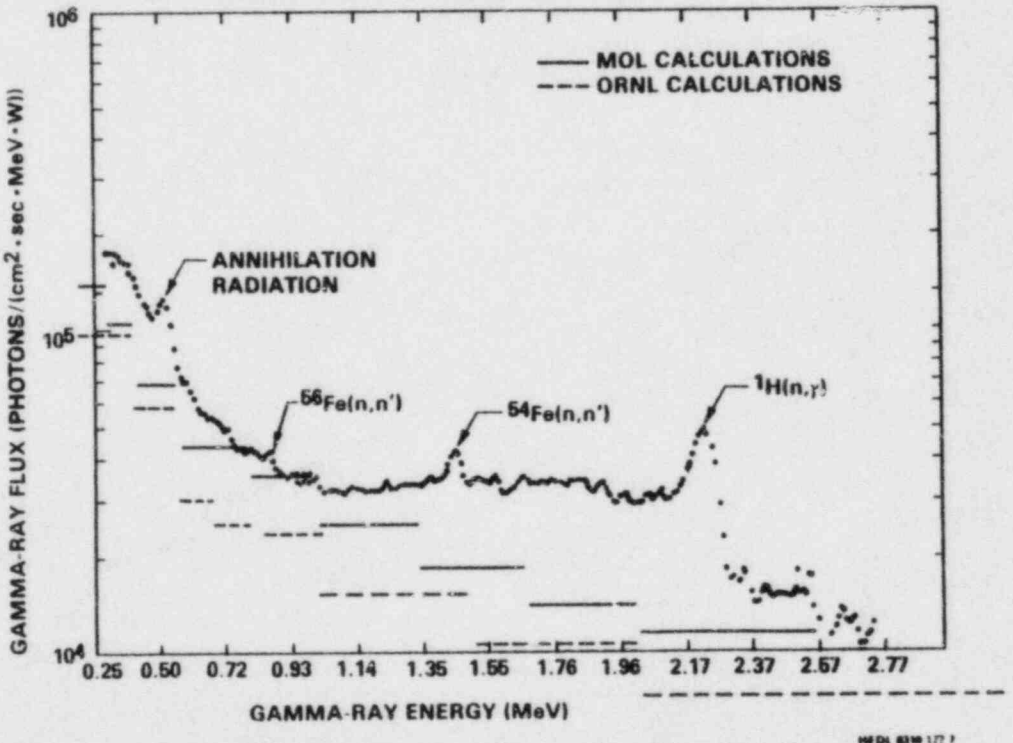

FIGURE 4.2.13d. Low-Energy Gamma-Ray Continuum for the 1/4 T Location of the 12/13 Configuration as Compared with CEN/SCK and ORNL Calculational Results.

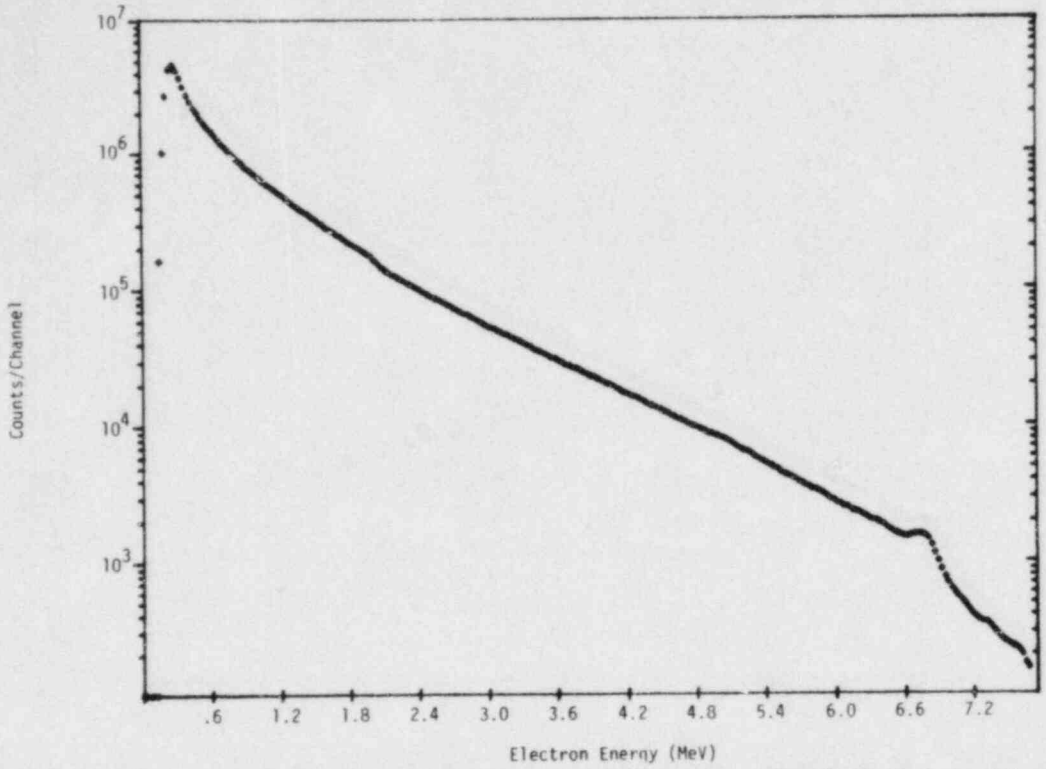

FIGURE 4.2.14a. High-Energy Electron Spectrum for the 1/2 T Location of the 12/13 Configuration.

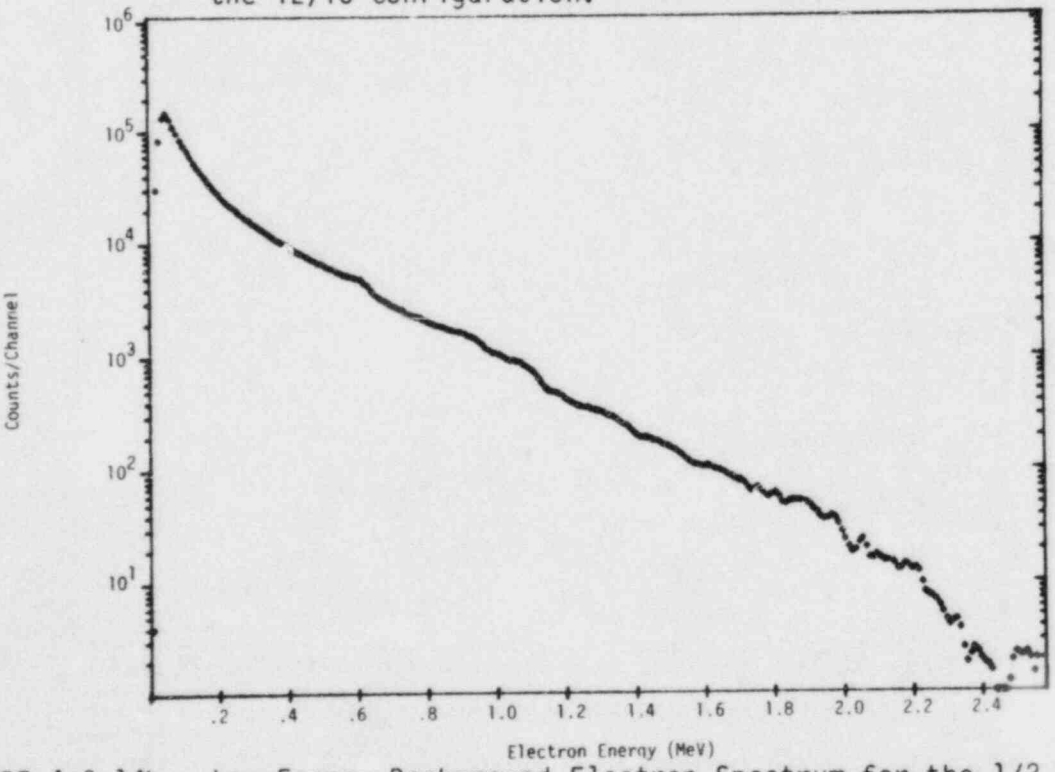

FIGURE 4.2.14b. Low-Energy Background Electron Spectrum for the 1/2 T Location of the 12/13 Configuration.

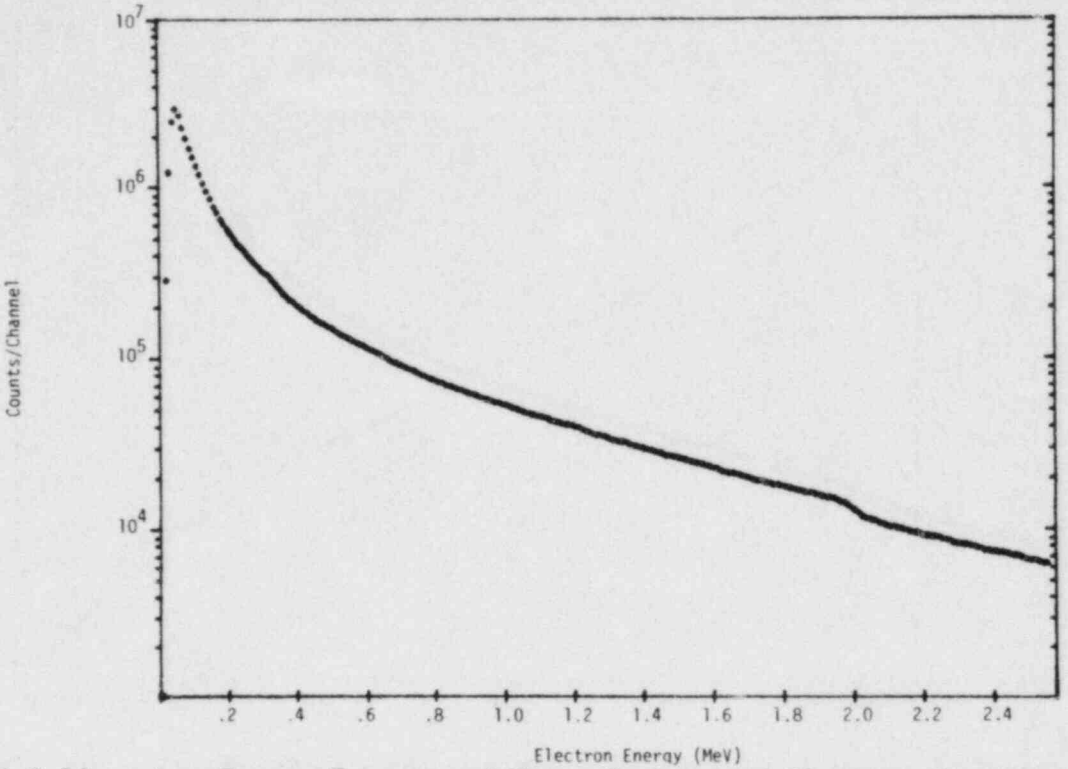

FIGURE 4.2.14c. Low-Energy Foreground Minus Background Electron Spectrum for the 1/2 T Location of the 12/13 Configuration.

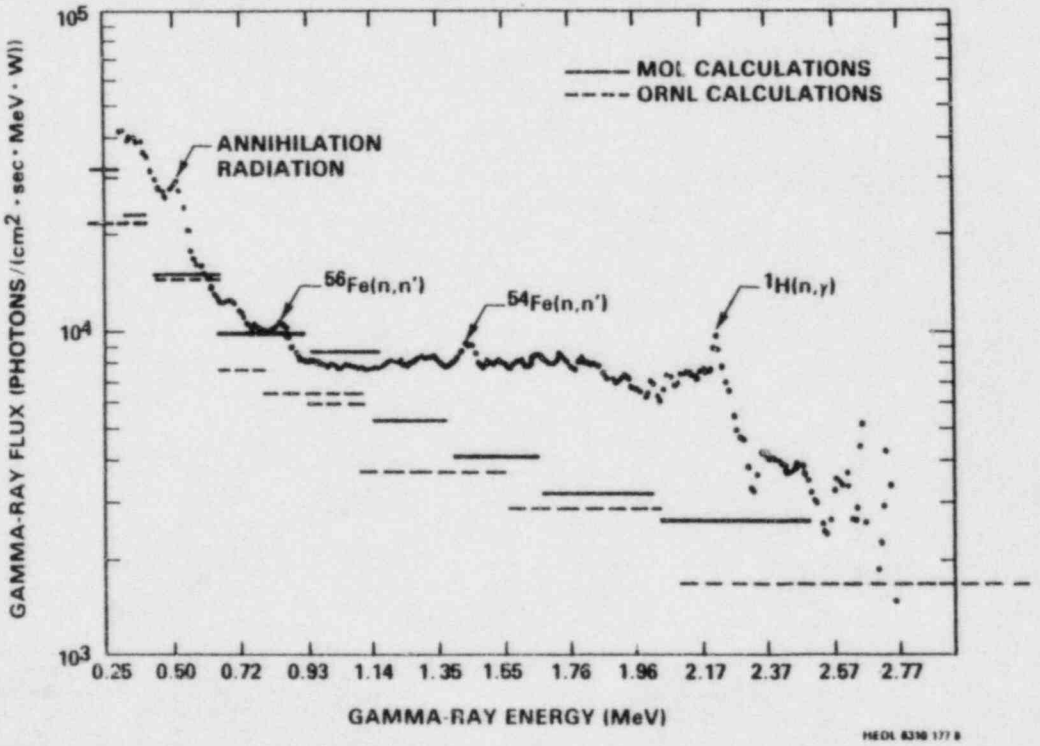

FIGURE 4.2.14d. Low-Energy Gamma-Ray Continuum for the 1/2 T Location of the 12/13 Configuration as Compared with CEN/SCK and ORNL Calculational Results.

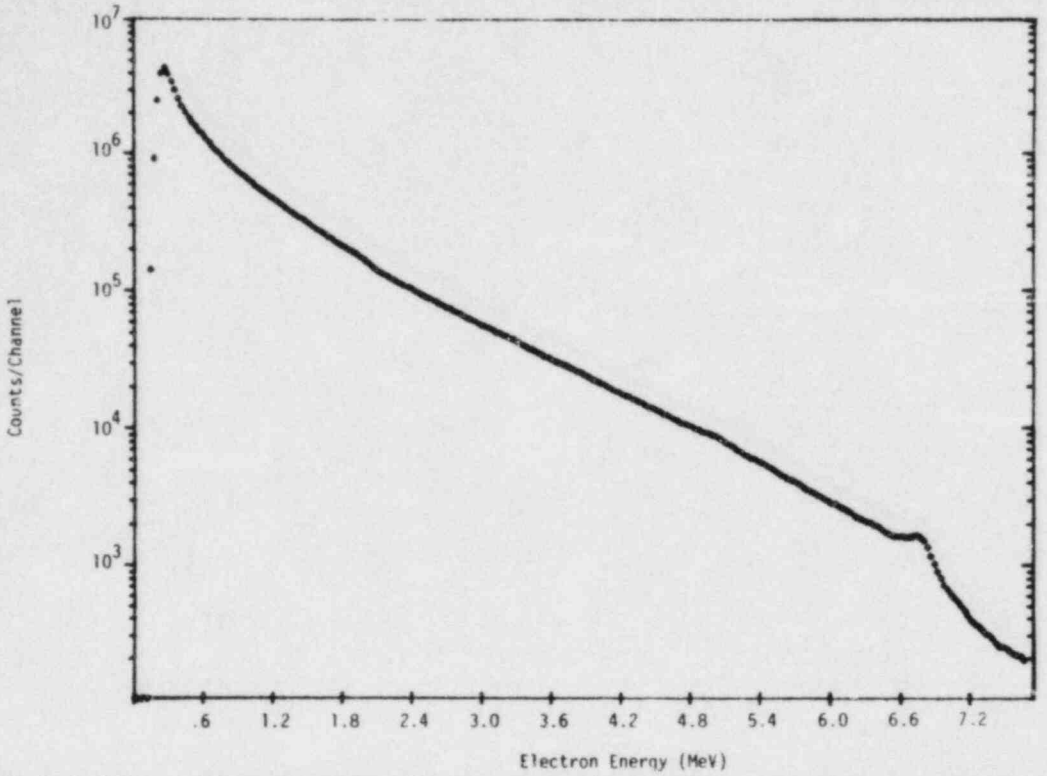

FIGURE 4.2.15a. High-Energy Electron Spectrum for the 3/4 T Location of the 12/13 Configuration.

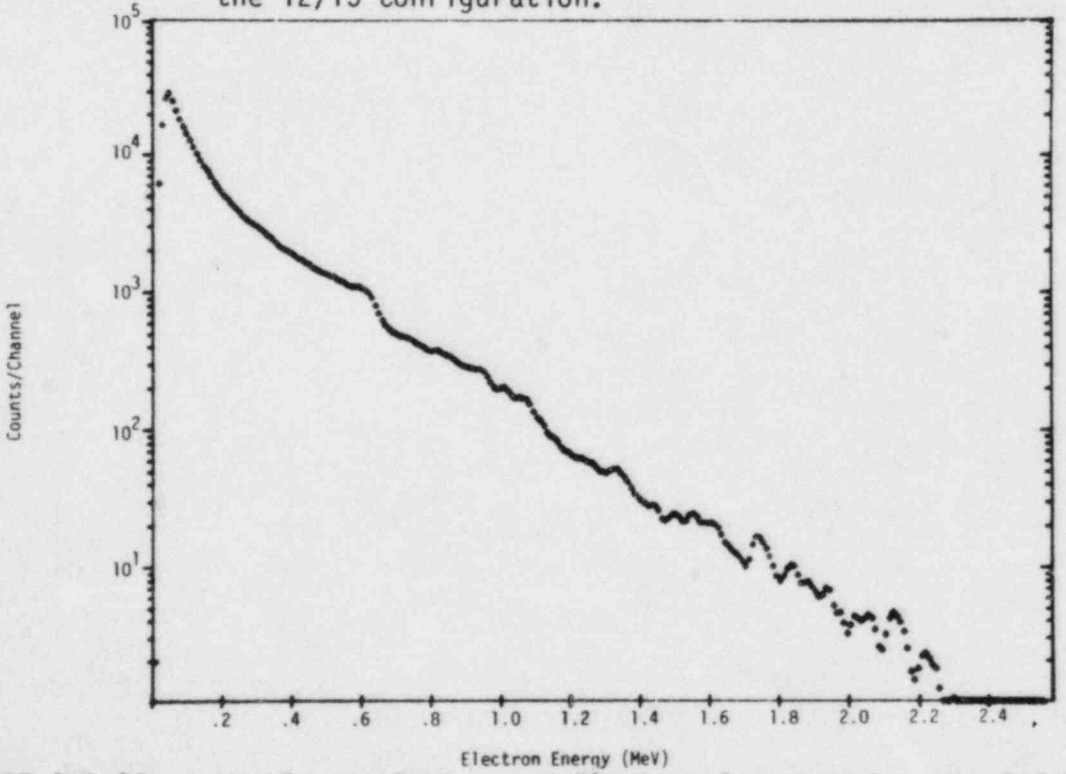

FIGURE 4.2.15b. Low-Energy Background Electron Spectrum for the 3/4 T Location of the 12/13 Configuration.

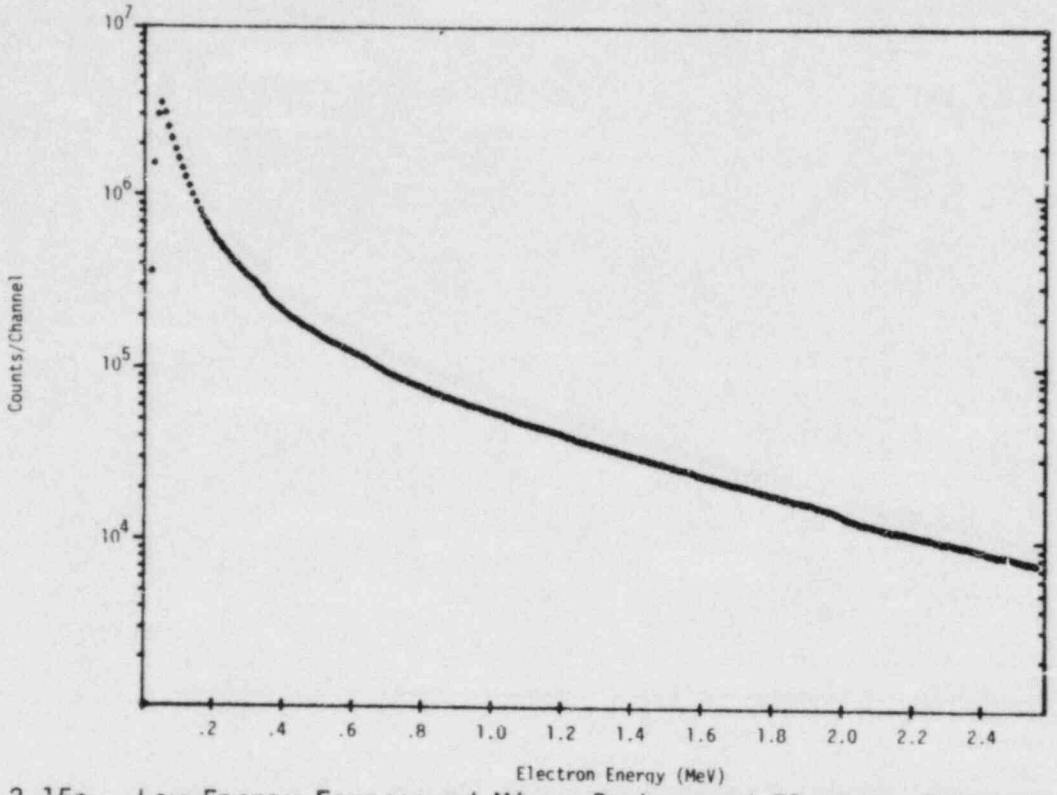

FIGURE 4.2.15c. Low-Energy Foreground Minus Background Electron Spectrum for the 3/4 T Location of the 12/13 Configuration.

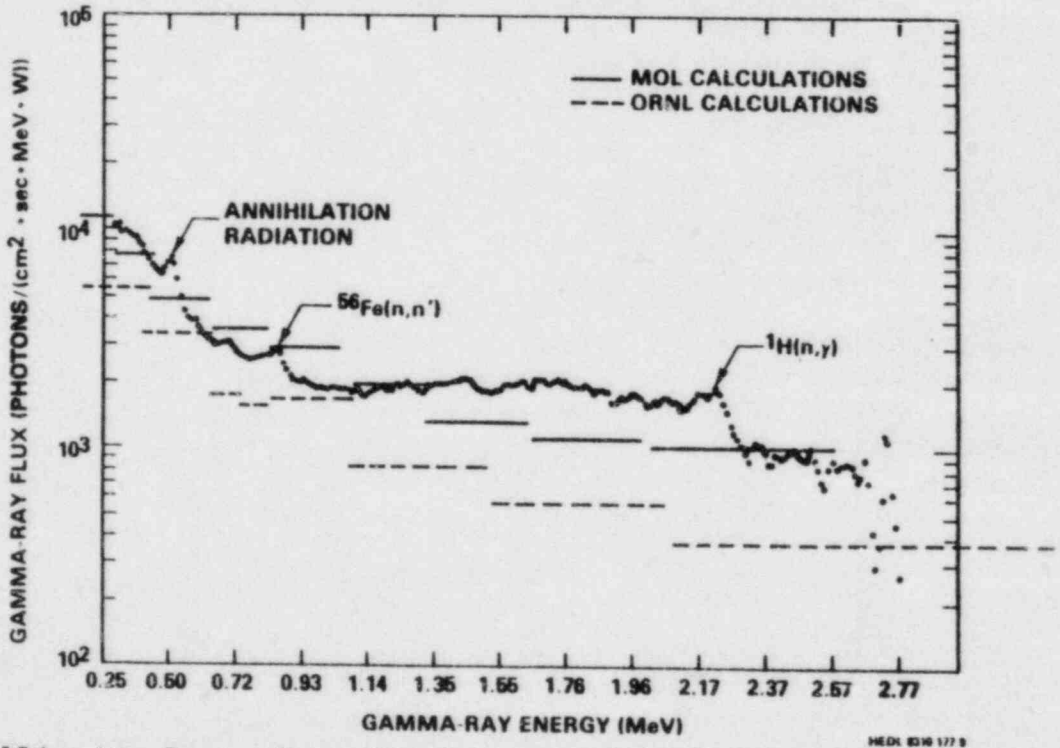

FIGURE 4.2.15d. Low-Energy Gamma-Ray Continuum for the 3/4 T Location of the 12/13 Configuration as Compared with CEN/SCK and ORNL Calculational Results.

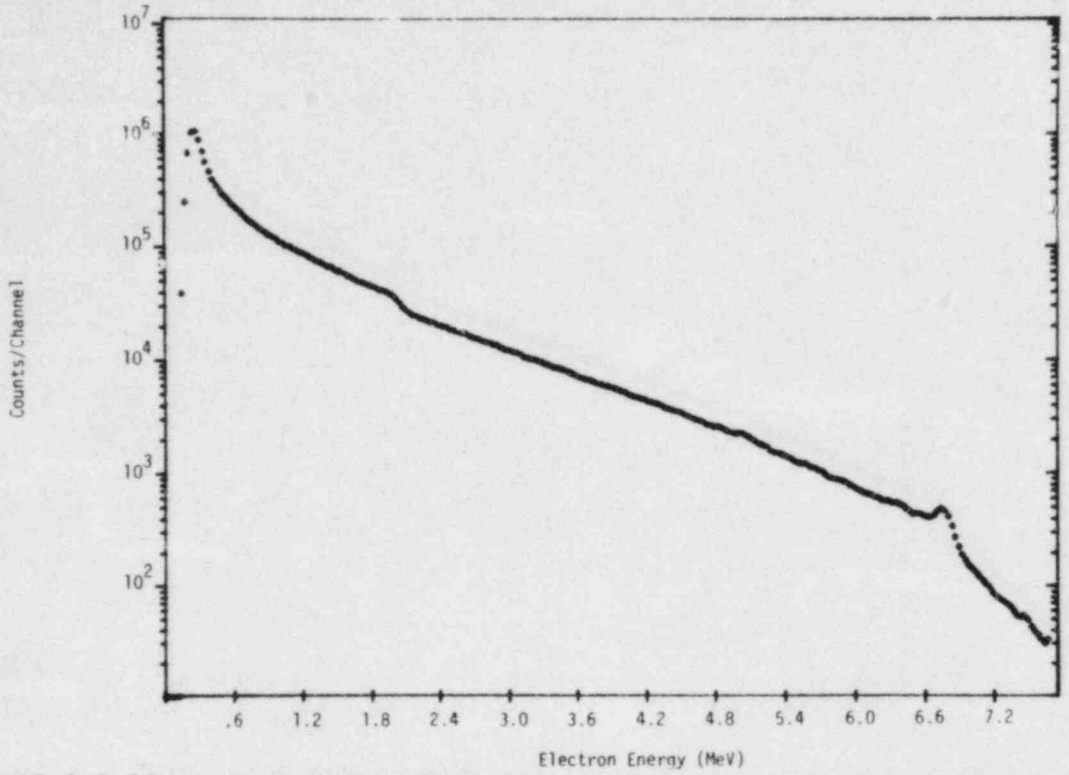

FIGURE 4.2.16a. High-Energy Electron Spectrum for the VB Location of the 12/13 Configuration.

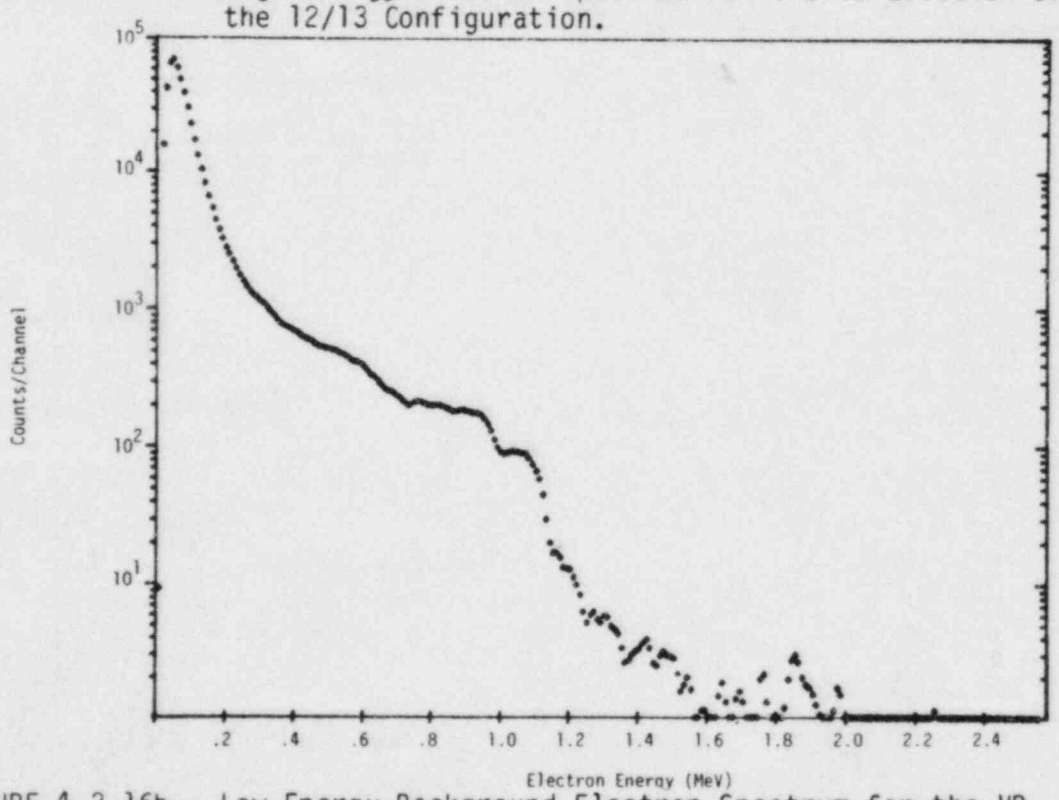

FIGURE 4.2.16b. Low-Energy Background Electron Spectrum for the VB Location of the 12/13 Configuration.

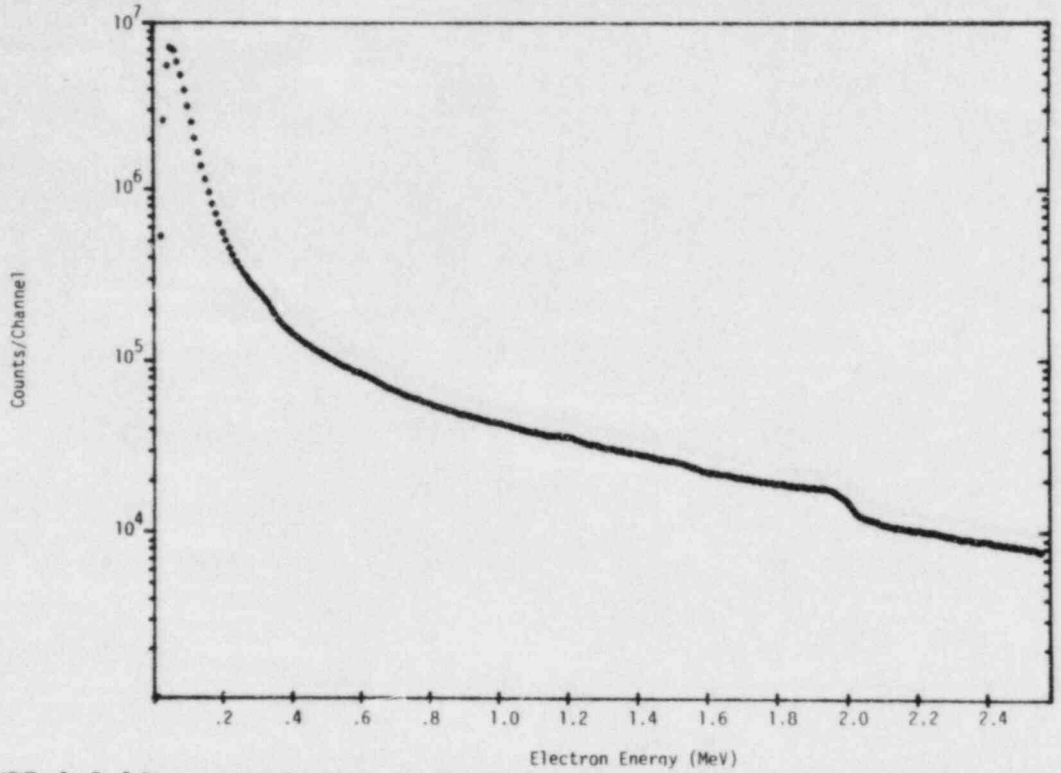

FIGURE 4.2.16c. Low-Energy Foreground Minus Background Electron Spectrum for the VB Location of the 12/13 Configuration.

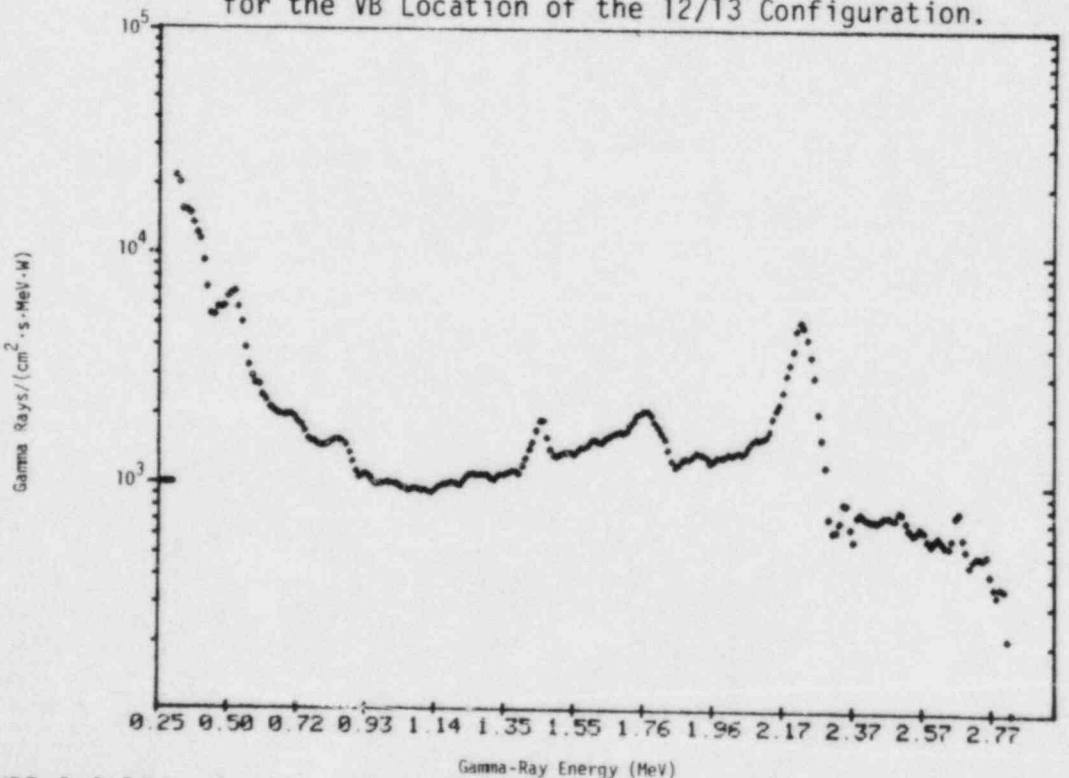

FIGURE 4.2.16d. Low-Energy Gamma-Ray Continuum for the VB Location of the 12/13 Configuration.

4.3 Si(Li) GAMMA-RAY DOSIMETRY

B. J. Kaiser, Raymomd Gold, and J. P. McNeece (HEDL)

4.3.1 Introduction

General motivations for gamma-ray dosimetry in reactor environments have been adequately reviewed (Go75,Go78,Go78a). More specific needs for gamma-ray dosimetry in LWR-PV environments were addressed in Go81b, Section 5. In LWR-PV mockups, three different gamma-ray dosimetry methods have been used to date. These are:

1) Lithium-drifted silicon solid-state detectors, Si(Li), which are simultaneously used for continuum gamma-ray spectrometry, as described in Section 4.2 above.

2) Thermoluminescent dosimetry (TLD).

3) Ionization chambers.

The ionization chambers were only used for relative measurements in order to determine Janus probe perturbation factors. Consequently, further information on these ionization chambers has been included in Section 4.4. The CEN/SCK group carried out the TLD work through 1980 using ^{7}LiF. The results of these efforts were reported at the Fourth ASTM-EURATOM Symposium on Reactor Dosimetry (Ma82), as well as in Section 5.4 of the first NUREG report on the PCA experiments (Fa81b).

Si(Li) dosimetry by the HEDL group through 1980 has also been reported at the Fourth ASTM-EURATOM Symposium on Reactor Dosimetry (Go82), as well as in Section 5.3 of the first NUREG report on the PCA experiments (Ka81). Consequently, only the most recent advances in Si(Li) gamma-ray dosimetry need be considered here. However, since Si(Li) dosimetry is not widely practiced, a rudementary description of the method is repeated below with special emphasis given to important changes in experimental technique that have been introduced by use of the Janus probe for the 1981 PCA experiments.

4.3.2 Experimental Method of Si(Li) Gamma-Ray Dosimetry

The method of Si(Li) gamma-ray dosimetry is not new, but has its conception in the original work done with these detectors for continuous gamma-ray spectroscopy (Go70,Go71a,St71). Two different dose rates have been used in Si(Li) gamma-ray dosimetry. The finite-size dose rate $\dot{D}_{FS}$, arising in the Si(Li) detector, is given by:

$$\dot{D}_{FS} = \frac{F}{PTm} \sum_{i=n}^{k} C_i E_i \qquad (1)$$

where:

E_i = Mid-bin electron energy of channel i (MeV)
C_i = Number of counts observed in the channel i bin
m = Mass of the sensitive volume of the Si(Li) detector (g)
T = Live time of the measurement (h)
P = Reactor power level maintained during the measurement (W)
F = 1.602×10^{-8} rad-g/MeV

The constant F is a conversion factor that provides the finite-size dose rate $\dot{D}_{FS}$ in units of rad/(h·W). Note, according to Eq. (1), that the finite-size dose is defined in a specified electron energy range, namely $[E_n, E_k]$.

Unfolded absolute gamma-ray continua obtained from Si(Li) detectors, as described in Section 4.2, can also be used to obtain gamma-ray dose rates. In this case, finite-size effects have been properly treated in the empirical response matrix. Consequently, electron escape or entry into the sensitive volume of the Si(Li) detector has been properly accounted for in the absolute gamma continuum unfolded with this empirical response matrix. Hence, dose rate calculated with this absolute continuum has been called the infinite medium dose rate $\dot{D}_{IM}$.

The infinite medium dose rate in material M, $\dot{D}_{IM}$, is given by

$$\dot{D}_{IM} = \frac{F}{PT} \sum_{i=n}^{k} (\epsilon_o)_i \cdot \phi_i \cdot \left[{}^{M}\left(\mu_{en}/\rho\right) \right]_i \qquad (2)$$

where:

$(\epsilon_o)_i$ = Mid-bin gamma-ray energy of channel i (MeV)

ϕ_i = Gamma-ray flux in the channel i bin $[\gamma/(cm^2\text{-}s)]$

${}^{M}(\mu_{en}/\rho)_i$ = Mass energy absorption coefficient for material M at gamma-ray energy $(\epsilon_o)_i$ (cm^2/g)

The factors P, T, and F can be taken as defined earlier, so that $\dot{D}_{IM}$ possesses units of rad/(h·W). Note, according to Eq. (2), that the infinite medium dose is defined in a specified gamma-ray energy range, namely $[(\epsilon_o)_n, (\epsilon_o)_k]$, which corresponds to the measurement domain of the absolute gamma continuum.

These definitions of $\dot{D}_{FS}$ and $\dot{D}_{IM}$ correspond to the use of Si(Li) detectors as originally practiced in earlier gamma-ray work (Go70c,Go71,St71). It is instructive at this point to provide a better understanding of each of these two different dose rates as well as to clearly define distinctions that existed between them in these earlier efforts. The finite-size dose rate $\dot{D}_{FS}$ is calculable directly from the observed electron continuum, whereas the infinite medium dose rate $\dot{D}_{IM}$ is obtained from the absolute gamma continuum. Higher accuracy can generally be attained for finite-size dose rates, since unfolding is not necessary in the calculation of $\dot{D}_{FS}$. For $\dot{D}_{FS}$ calculations, integration can be carried out over any electron energy interval $[E_n, E_k]$ that lies within the range of the electron measurements. However, from a rigorous viewpoint, $\dot{D}_{FS}$ corresponds to energy deposition in silicon and effects of finite size can still exist in the data.

On the other hand, effects of finite detector size have been properly accounted for in the infinite medium dose $\dot{D}_{IM}$. In $\dot{D}_{IM}$ calculations, integration can be carried out over any interval $[(\varepsilon_o)_n, (\varepsilon_o)_k]$ within the range of definition of the unfolded gamma continuum. In contrast to $\dot{D}_{FS}$, the infinite medium dose can be calculated for any medium from the observed gamma continuum. In fact, for theoretical dose calculations, the relation used is precisely Eq. (2) except that ϕ_i is now the calculated gamma spectrum. From this viewpoint, the infinite medium dose provides a more direct comparison between theory and experiment.

Introduction of the Janus probe configuration as well as associated changes in experimental technique have significantly altered the meaning of observed Si(Li) gamma-ray dose rates. In earlier work, pulse-shape discrimination was used together with fully depleted Si(Li) detectors. Hence, formation of the dose according to Eq. (1) did indeed include effects of finite size. However, formation of the observed Janus probe dose rate, $\dot{D}_J$, according to this prescription, i.e.,

$$\dot{D}_J = \frac{F}{PTm} \sum_{i=n}^{k} C_i E_i \qquad (3)$$

does not include finite-size effects. According to the configuration shown in Figure 4.2.1a, the sensitive region of the Janus probe Si(Li) detectors is completely surrounded by a combination of the semi-sensitive and dead Si regions. Of equal significance is the elimination of dual-parameter pulse analysis for the Janus probe configuration so that electron spectra are observed without pulse-shape discrimination.

Because of these two factors, electron spectra observed with the Janus probe possess negligible finite-size effects. Since electron spectra observed with the Janus probe in this manner are essentially equilibrium spectra, dose rates derived from these electron spectra must be infinite medium dose rates (in silicon). Hence, Eq. (3) generalizes to

$$\dot{D}_{IM} = \dot{D}_J = \frac{F}{PTm} \sum_{i=n}^{k} C_i E_i \qquad (4)$$

For work prior to 1981, the sensitive volume of the Si(Li) detectors was measured with collimated gamma-ray sources as described in Section 5.3 of the first NUREG report on the PCA experiments (Ka81). A simpler method has now been devised. It is based on the photopeak response of a fully depleted Si(Li) detector. A fully depleted Si(Li) detector possesses no semi-sensitive or dead regions, so that the sensitive volume is identical to the physical (or spatial) volume. Since the physical volume of the fully depleted Si(Li) detector can be accurately obtained from spatial measurements, the sensitive volume of the Janus Si(Li) detectors can be determined from a comparison of photopeak areas observed with these detectors relative to those observed with fully depleted detectors.

A fully depleted Si(Li) detector of the same nominal size as the Janus Si(Li) detectors was used with monoenergetic gamma-ray sources of different energies, namely, ^{137}Cs (0.6616 MeV), ^{54}Mn (0.835 MeV), and Zn (1.116 MeV). The photopeak areas from these two types of detectors were equal, within experimental uncertainty, for all three gamma-ray energies. On this basis, the mass of the Janus Si(Li) detectors was found to be 4.53 $\pm$ 0.3 g for the 1981 PCA experiments. Since this mass uncertainty dominates the overall uncertainty in Janus probe dose rate measurements, the relative (1σ) uncertainty in $\dot{D}_J$, or equivalently in $\dot{D}_{IM}$, is ~7%.

4.3.3 Si(Li) Gamma-Ray Dosimetry Results

Infinite medium dose rates $\dot{D}_{IM}$ observed with the Janus probe in the 1981 PCA experiments are enumerated in Table 4.3.1. These results have been corrected for Janus probe field perturbation, which varies with both configuration and location (see Section 4.4). These dose rates can be taken as infinite medium dose rates in steel. It has already been shown that the difference between infinite medium dose rates for silicon and iron is negligible (Ka81).

Table 4.3.2 presents a comparison of experimental and calculated gamma-ray dose rates for the 4/12 SSC configuration. In addition to the D_{IM} results from the 1981 Janus probe experiments, this table presents results obtained by the CEN/SCK group (Fa81,Ma82) who performed both TLD measurements and calculations.

Using the results from all four locations of the 4/12 SSC configuration given in Table 4.3.2, one finds a $\dot{D}_{IM}$/TLD average ratio of 0.92. Consequently, the Si(Li) and TLD methods agree within experimental uncertainty. Comparison of these experimental results with calculations does not show consistent agreement. The extremely low calculational result at the VB location might be due to inadequate modeling of the actual geometric configuration used in the PCA.

TABLE 4.3.1

INFINITE MEDIUM DOSE RATES* OBSERVED IN THE 1981 PCA EXPERIMENTS

Midplane Location	Configuration		
	4/12 SSC	12/13	4/12
1/4 T	220	152	490***
1/2 T	65.4	35.6	---
3/4 T	19.1	9.24	---
VB	11.0**	2.56	---

*Dose rates in mrad/h at 1-W PCA power were corrected for Janus probe field perturbation.

**A perturbation factor of 0.9 has been applied corresponding to that obtained at the VB location in the 12/13 configuration (see Table 4.4.1).

***A perturbation factor of 1.16 has been applied corresponding to that obtained at the 1/4 T location in the 4/12 SSC configuration (see Table 4.4.1).

TABLE 4.3.2

GAMMA-RAY DOSE RATES* FOR THE 4/12 SSC CONFIGURATION

Midplane Location	Experiment		Calculation		
	TLD	$\dot{D}_{IM}$	CEN/SCK	$\dot{D}_{IM}$/TLD	$\dot{D}_{IM}$/CAL
1/4 T	255	220	210	0.86	1.05
1/2 T	68	65.4	52	0.96	1.26
3/4 T	21.5	19.1	19.1	0.89	1.00
VB	11.5	11.0	2.2	0.96	5.05

*Dose rates in mrad/h at 1-W PCA power.

Extension of continuous gamma-ray spectrometry into the energy region above 3.0 MeV will provide a more comprehensive basis for further comparisons between experimental and theoretical gamma-ray dose rates. Consequently, forthcoming LWR-PV-SDIP quarterly reports will feature these PCA comparisons.

4.4 JANUS PROBE PERTURBATION FACTORS

Raymond Gold, J. P. McNeece, and B. J. Kaiser (HEDL); T. A. Lewis and P. J. H. Heffer (BNL-UK); and M. D. Carter (AEEW-UK)

4.4.1 Introduction

A significant outgrowth of the collaborative efforts of the CEN/SCK and HEDL working groups was the recognition and subsequent quantification of the perturbation factor (PF) created by the Janus probe. It was conjectured that the PF arises from the void or semi-voided regions introduced by the Janus probe into the gamma-ray intensity gradient that exists in the PV block. Initial analysis of the 1981 work performed in the 4/12 SSC configuration has already been presented (Go82b) that confirms the existence of such PF.

Since the significance of this PF is now clearly established, further elaboration on PF measurement and interpretation is warranted. To this end, Section 4.4.2 below contains a description of the experimental methods used to measure PF. Analysis and interpretation of the observed PF are then considered in Section 4.4.3.

4.4.2 Experimental Method

Two different gamma-ray dosimetry methods were used to measure Janus probe perturbation factors, namely, ionization chambers (IC) and TLD. Both techniques were implemented using a "dummy" Janus probe. Measurements are first carried out at a given location by incorporating the miniature IC or TLD in the "dummy" Janus probe. Measurements are then repeated at this location with the channel completely back-filled with appropriate material so as to eliminate voids. The perturbation factor (PF) is defined by the ratio

$$PF = \dot{D}_p / \dot{D}_u \qquad (1)$$

where $\dot{D}_p$ is the perturbed dose rate observed in the presence of the "dummy" Janus probe and $\dot{D}_u$ is the unperturbed dose rate observed in the back-filled channel.

Special miniature ICs were developed at HEDL specifically for PF measurements in the PV block. The design of these air-filled ICs is shown in Figure 4.4.1. There are actually two such chambers, which differ only in the E dimension, so that a broader response range of gamma dose can be covered. The shorter chamber, with E = 0.191 in., possesses a full-scale sensitivity of 2.5 rad, whereas the longer chamber, with E = 0.469 in., possesses a full-scale sensitivity of 25.0 rad. Absolute measurements with these ICs are not necessary to determine PF, since, as defined in Eq. (1), only the ratio of observations in the perturbed and unperturbed environments is needed. Use of relative IC measurements eliminated an otherwise large effort that would have been entailed for absolute calibration of these chambers.

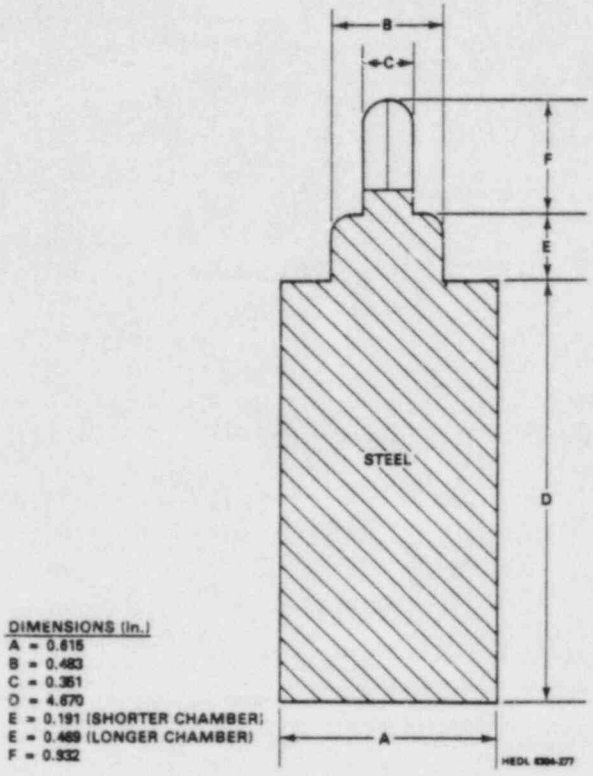

FIGURE 4.4.1. Miniature Ionization Chamber Design for the Janus Perturbation Factor Measurements in the PV Block.

Janus probe PFs have been determined with these miniature ICs in the 4/12 SSC configuration during the 1981 PCA experiments. These results have already been reported (Go82b) and can be found in Table 4.4.1.

Recent work in the LWR-PV mockup in the Nestor reactor at the Atomic Energy Establishment, Winfrith (AEEW), UK, provided an opportunity to measure PF for the 12/13 configuration. These measurements were carried out, in part, under the auspices of the Nestor Dosimetry Improvement Programme (NESDIP). While data from gamma spectrometry efforts at NESDIP have not as yet been analyzed and are to be issued in a later NUREG report, the relevance of these recent PF results for the 1981 PCA work warrants inclusion of these NESDIP-PF measurements in this report. PF measurements at NESDIP were carried out in the 12/13 configuration with beryllium oxide TLDs.

The use of beryllium oxide TLDs has been developed for measuring gamma exposures in the presence of thermal neutrons in gas-cooled reactors. Although chosen primarily for low thermal neutron sensitivity, the BeO TLDs have an advantage over other low thermal neutron sensitive materials of being dosimetrically well matched to the graphite medium in which they are normally used. They are less well matched to steel, and future work is planned to evaluate the degree of correction necessary. This work should not affect

TABLE 4.4.1

JANUS PROBE PERTURBATION FACTORS

Location	PCA - 4/12 SSC	NESDIP - 12/13	
	IC	TLD	IC
A2	--	1.12	--
1/4 T	1.16	1.30	1.27
1/2 T	1.14	1.24*	--
3/4 T	1.11	1.18	--
VB	--	0.90	--

*Since the 1/2 T location is not readily available at NESDIP, this value was obtained by linear interpolation of the 1/4 T and 3/4 T results.

perturbation factor measurements. Dosimetry values for BeO TLDs are usually quoted in roentgens of ^{60}Co, which describe the amount of thermoluminescence measured relative to that measured by the same TLD exposed to 1 R of ^{60}Co build-up in graphite.

Considerable effort has gone into establishing the use of BeO for in-reactor measurements. The material used has two glow peaks in the range of most TLD readers: one at ∿180°C and one at ∿300°C. The higher temperature peak was found to be reproducible and linear up to at least 100 R. Pure beryllium oxide was found to be unsuitable. Material with a higher temperature glow peak at least as large as the less predictable lower temperature peak has been chosen. The material is sintered into discs 6 mm in diameter and 0.5 mm thick.

In this form the TLDs have been shown to measure less than 0.005 R per 10^{10} thermal neutrons above the equilibrium mixed field that exists in a pure graphite thermal column. The fast neutron response has not yet been measured definitively, but all indications are that the value will be ∿20% less than LiF TLD chips.

4.4.3 Analysis and Interpretation of PF Results

PF results obtained for the 12/13 configuration at NESDIP are presented in Table 4.4.1, where earlier 4/12 SSC results obtained at the PCA are included for comparison. Due to the limitations of the miniature IC design as well as NESTOR power operation, IC measurements could be carried out only for the 1/4 T location of the 12/13 configuration at NESDIP. The gamma-ray intensity levels that could be attained at the 3/4 T and VB locations were too low to provide reliable readings. Moreover, it is well to note that the

design of these miniature ICs, shown in Figure 4.4.1, restricts applicability for PF measurements to the PV block. In view of the restricted nature of the IC results for the 12/13 configuration, the BeO TLD results, which represent a consistent set of PF for the 12/13 configuration, are recommended for use at this time. Nevertheless, it is important to stress that the IC and TLD results agree within experimental uncertainty at the 1/4 T location of the 12/13 configuration.

PF results shown in Table 4.4.1 vary with both configuration and location. In order to understand this behavior, it is instructive to examine the spatial dependence of dose rates within the PV block. Figure 4.4.2 compares (uncorrected) finite-size dose rates for the 4/12 SSC and 12/13 configurations. It is clear from Figure 4.4.2 that the 12/13 configuration gamma data possesses a larger gradient. In light of the results in Table 4.4.1, one finds that, when the Janus probe is used in a field possessing a larger gradient, the PFs are, in turn, larger.

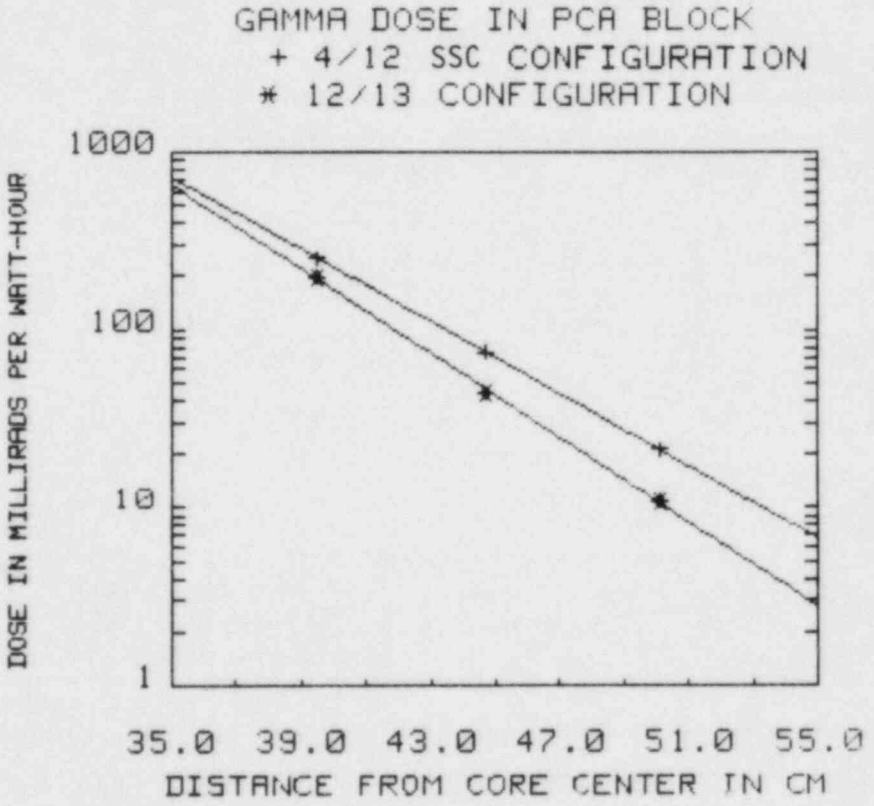

FIGURE 4.4.2. Comparison of the Spatial Behavior of the Finite-Size Dose Rate, $\dot{D}_{FS}$, for the 4/12 SSC and 12/13 Configurations. (The smooth lines are linear least-squares fits of the logarithm of the experimental data.)

This conclusion is also supported by the PF result for the A2 water position of the 12/13 configuration. This PF result, namely 1.12, is essentially as low as any result obtained within the PV block for either the 12/13 or 4/12 SSC configuration. However, it is well known that water is a rather poor attenuator of gamma radiation compared with the iron medium of the PV. Hence gamma-ray intensity gradients at water locations are generally less than those in the PV block, and the corresponding Janus probe PF is indeed lower. Consequently these overall PF results confirm the original conjecture that Janus probe PF stem from the introduction of voids or semi-voided regions into a gamma field possessing an intensity gradient.

The existence of a PF less than unity for the VB location of the 12/13 location can also be qualitatively explained. Comparison of the Janus probe with a point detector for measurements in a void reveals that the probe must produce some attenuation of gamma radiation in the solid angle that the probe subtends at the Si(Li) sensitive volume. Consequently in a void, one must expect that the perturbed dose rate $\dot{D}_p$ would be less than the unperturbed dose rate $\dot{D}_u$. Hence an observed PF of less than unity for the VB location of the 12/13 configuration is in accord with very simple physical considerations.

From a rigorous viewpoint the PF considered here are dose PF. Consequently, use of dose PF for spectral adjustments, such as those carried out in Section 4.2, must obviously be justified. To this end, Figures 4.4.3 through 4.4.6 present the 1/4 T to 1/2 T and the 1/2 T to 3/4 T spectral ratios obtained from the 1981 PCA experiments for the 4/12 SSC and 12/13 configurations. These figures demonstrate that spectral changes within the PV block are small compared with intensity changes. Fluctuations arising in these spectral ratios can be attributed, in the main, to statistical uncertainties that exist in the unfolded gamma spectra. These statistical fluctuations can often be exacerbated in the neighborhood of peaks that arise above the general intensity level of the gamma continuum, such as near the 2.2-MeV peak that arises due to the capture gamma ray from hydrogen.

Table 4.4.2 compares the average of these spectral ratios with the corresponding Janus probe finite-size dose ratio. The quoted uncertainty in Table 4.4.2 is simply the standard deviation of the average spectral ratio. Three of the four comparisons in Table 4.4.2 agree within a 1σ uncertainty and all four agree within a 2σ uncertainty, even ignoring the uncertainty in the dose ratio. Hence it is clearly established that these dose PFs can be used for spectral adjustments. Moreover, the highest observed PF, $\sim$1.30, corresponds to a correction of $\sim$30%, which is at least an order of magnitude smaller than the dose ratios, $\sim$3.5 to $\sim$4.5, shown in Table 4.4.2. Thus, scaling the data in Table 4.4.2 down to the level of observed Janus probe PF would render any error introduced into a corrected spectrum by use of dose PFs considerably less than other sources of experimental uncertainty.

Finally, the effect of the finite size of the IC or TLD in these experiments must be considered, since detectors of finite size could possibly introduce a bias in the observed PF. However, the semi-voided region introduced by the

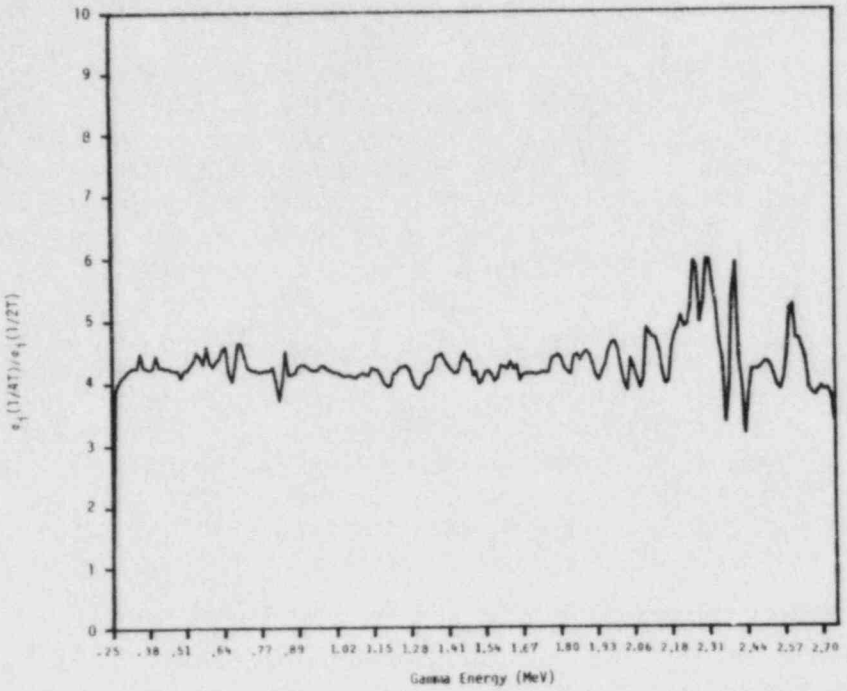

FIGURE 4.4.3. The Spectral Ratio of the 1/4 T to 1/2 T Locations of the 12/13 Configuration.

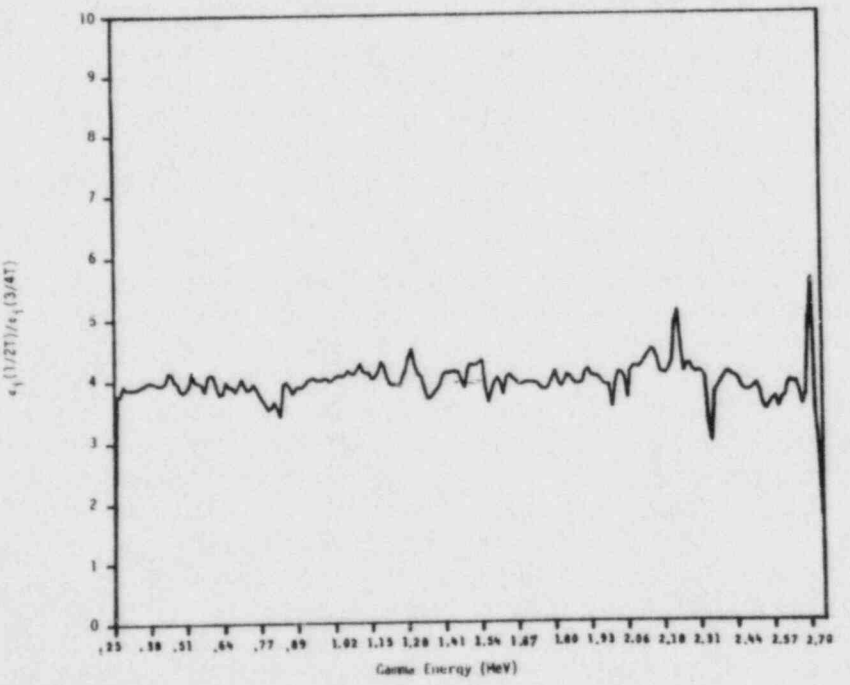

FIGURE 4.4.4. The Spectral Ratio of the 1/2 T to 3/4 T Locations of the 12/13 Configuration.

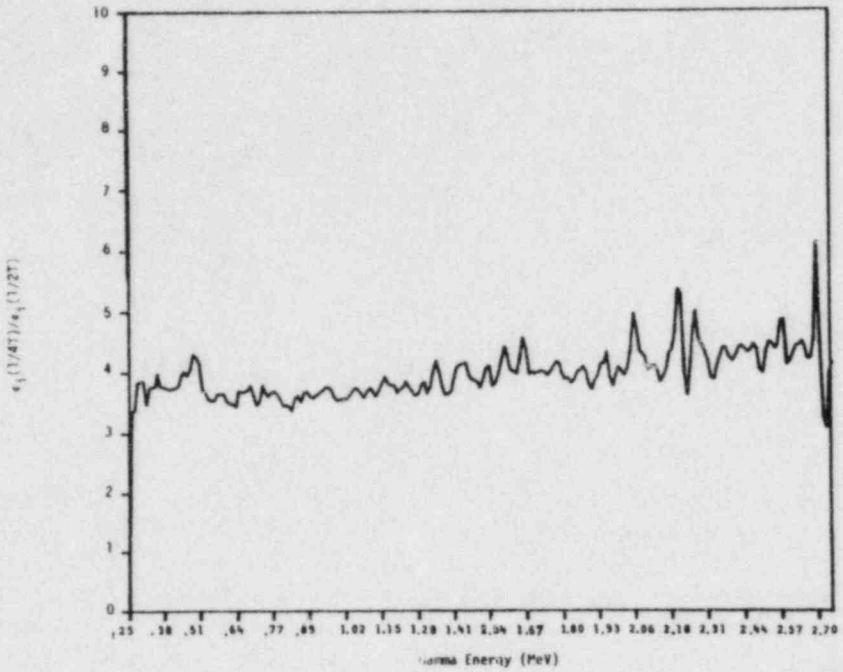

FIGURE 4.4.5. The Spectral Ratio of the 1/4 T to 1/2 T Locations of the 4/12 SSC Configuration.

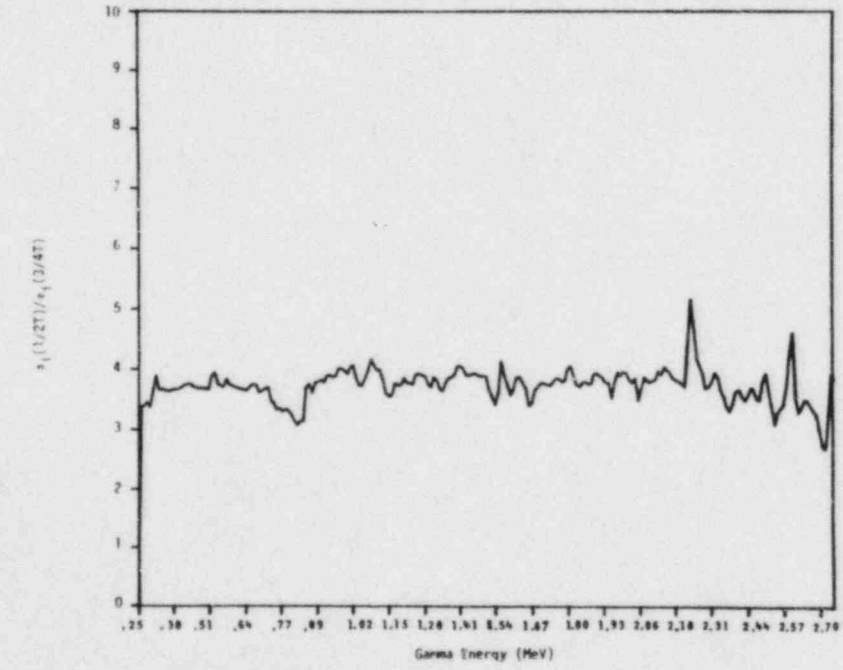

FIGURE 4.4.6. The Spectral Ratio of the 1/2 T to 3/4 T Locations of the 4/12 SSC Configuration.

TABLE 4.4.2

COMPARISON OF AVERAGE SPECTRAL RATIOS AND DOSE RATIOS

	(1/4 T)/(1/2 T)		(1/2 T)/(3/4 T)	
Configuration	Average Spectral Ratio	Dose Ratio	Average Spectral Ratio	Dose Ratio
4/12 SSC	3.98 ± 0.37	3.43	3.75 ± 0.26	3.51
12/13	4.29 ± 0.43	4.49	3.99 ± 0.26	4.05

miniature IC is easily an order of magnitude smaller than those introduced by the Janus probe. For the BeO TLD, the semi-voided region introduced is considerably smaller than those introduced by even the miniature IC. Hence, volume scaling of even the highest observed PF, ~1.30, renders any perturbation introduced by the IC or TLD negligible. This conclusion is also supported by the agreement, within experimental uncertainty, between the TLD and IC observed PF for the 1/4 T location of the 12/13 configuration, even though the semi-voided region produced by the TLD is roughly an order of magnitude smaller than that introduced by the miniature IC.

4.5 GAMMA-RAY RESPONSE OF INTEGRAL NEUTRON DOSIMETERS AND REVIEW OF MEASURED ^{235}U FISSION RATES

E. D. McGarry, C. M. Eisenhauer, G. Minsart, Raymond Gold, F. Ruddy, A. Fabry, and F. B. K. Kam

4.5.1 Current Status and Summary

Experimental results for the (n,f) and (n,n') neutron dosimetry reactions may include contributions from photofission reactions (γ,f) and other photon-initiated reactions (γ,γ'). To date most investigations of photofission for the LWR-PV program have been theoretical. HEDL has measured gamma-ray spectra in the PCA, and these data are presented in Section 4.2. Transport calculations of photofission use coupled cross-section libraries so that both neutron and gamma fluxes are derived. The fluxes are then convoluted with neutron and photonuclear cross sections to determine the fraction of the total reaction rate due to photonuclear effects.

This section presents calculated correction factors for the 4/12 SSC PCA configuration and reviews those for the 8/7 and 12/13 configurations. Further discussion of photofission corrections for the 8/7 and 12/13 configurations may be found in (Mc81).* Because of their predominent influence on gamma-ray generation, thermal and epithermal fluxes are examined by reviewing bare and cadmium-covered ^{235}U fission rates.

Neutron and gamma calculations for the 4/12 configuration (by G. Minsart, CEN/SCK) indicate that photoreaction effects are larger for the $^{238}U(n,f)$ reaction than for the $^{237}Np(n,f)$ and ^{235}U reactions, but all are smaller than the same three reactions in the 8/7 and 12/13 configurations (see, for example, Table 4.5.1).

TABLE 4.5.1

COMPARISON OF CALCULATED PHOTOFISSION IN ^{238}U IN THREE CONFIGURATIONS OF THE PCA/LWR PRESSURE VESSEL SIMULATOR

In Simulator Block Position	Percent Photofission in the $^{238}U(n,f)$ Reaction		
	8/7	12/13	4/12 SSC
1/4 T	2.4	3.7	2.1
1/2 T	1.5	1.9	1.3
3/4 T	5.4	4.0	1.5**

*Except for the $^{232}Th(n,f)$ reaction, which is given for all three configurations in Table 4.5.3 of this section.

**Revised later in this section to 2.6.

One immediately has questions about the apparent differences in the corrections for the 3/4 T position. NBS has rechecked the folding of spectra with the cross sections and found that the anomaly is due to differences in the gamma spectra, and these stem from differences in the calculational models of the cavity. Based upon examinations of the thermal and epithermal fission rates in ^{235}U and assuming that the trend of the 4/12 SSC data should be much like that of the other PCA configurations, the "1.5" values have been revised upward to 2.6 percent.

Photoreaction effects are geometrically and spatially dependent. Most of the photon-induced contributions far from the reactor originate from epithermal neutron capture in structural materials, mainly iron. Capture gamma rays in hydrogen (water) have too low an energy to induce photofission. However, the presence of water between the reactor and the structure tends to enhance the ratio of epithermal-to-fast neutrons, and this results in more photofission at the 1/4 T locations of the 12/13 configuration than for the 8/7 (or the 4/12 SSC, which has less water thickness than the 8/7 configuration because of the presence of the SSC on the back of the thermal shield). The photofission at the 3/4 T position of the PV simulator block is more difficult to explain. It is due to both neutron capture in the steel nearer the reactor and production locally from epithermal and thermal neutrons returning from the ex-vessel cavity walls. Because the photoreaction effect in the 3/4 T is generally larger, the cavity return contribution presents a problem. Cavities vary significantly in size even for the same type of reactor.

4.5.2 Photoreaction Effects in the 4/12 SSC Configuration

Table 4.5.2 summarizes the photofission contributions for the 4/12 SSC configuration. The effects are noticeably larger in the void box. These calculations were done by G. Minsart, CEN/SCK (Mol, Belgium). The gamma part of the EURLIB-3 library was linked to a 40-group fast plus thermal cross-section set, currently in use at Mol for study of the BR-3 PWR reactor. The calculated fluxes were folded with NBS photofission and ENDF/B-V neutron cross sections by C. Eisenhauer, NBS.

Table 4.5.3 summarizes the photofission contributions for $^{232}Th(n,f)$ for all the PCA configurations.

Similar calculations were done at ORNL for the 12/13 configuration. A comparison with the 12/13 CEN/SCK calculations is given in Tables 4.5.4 and 4.5.5. Also shown in the first two of these tables are comparisons with HEDL SSTR data. Note that two SSTR values are given to show the effect of a renormalization discussed and substantiated in Section 5. The agreement, except for the cadmium ratios, is less than for other measurements in this report; but no great effort has been devoted to the task of assessing high accuracies because thermal and epithermal neutron accuracies of 7% are considered satisfactory for PCA program objectives of the 8/7 and 12/13 investigations (see further data in Section 4.5.4 for the 4/12 SSC).

TABLE 4.5.2

SUMMARY OF PHOTOFISSION EFFECTS IN THE 4/12 SSC CONFIGURATION OF THE PCA-LWR PRESSURE VESSEL MOCKUP EXPERIMENT

	Relative Fluxes* x 10^5		
Position	Gamma (>6.5 MeV)	Neutron (>0.8 MeV)	$\frac{\phi_\gamma}{\phi_n}$
SSC	189.0	473.0	0.400
1/4 T	13.2	39.3	0.336
1/2 T	3.27	20.4	0.182
3/4 T	1.87	10.0	0.187
VB	3.37	3.14	1.070

Reaction Rate Ratios: $\frac{R(\gamma+n)}{R(n)}$

Position	^{235}U	^{238}U	^{237}Np
SSC	1.0002	1.026	1.007
1/4 T	1.0001	1.021	1.004
1/2 T	1.0001	1.013	1.002
3/4 T	1.0001	(1.026)**	(1.005)**
VB	1.0001	1.086	1.010

*Revised calculation by G. Minsart on June 24, 1980. The calculated fluxes are normalized. To obtain actual fluxes, in units of $(n/cm^2\text{-}s)/(n/s \text{ of PCA power})$, multiply by 8.86×10^{-4}.

**Revised.

TABLE 4.5.3

SUMMARY OF PHOTOFISSION EFFECTS FOR THE $^{232}Th(n,f)$ REACTION IN THE PCA-LWR PRESSURE VESSEL SIMULATOR

Reaction Rate Ratios: $\frac{R(\gamma+n)}{R(n)}$

Position	8/7 Configuration*	12/13 Configuration**
TSF	1.028	1.031
TSB	1.099	1.080
PVF	1.110	1.133
1/4 T	1.058	1.084
1/2 T	1.038	1.046
3/4 T	1.144	1.102

Reaction Rate Ratios: $\frac{R(\gamma+n)}{R(n)}$

Position	4/12 SSC Configuration
SSC	1.058
1/4 T	1.053
1/2 T	[illegible]
3/4 T	[illegible]
VB	1.232

*Actual calculations for a 8.4/6.7 configuration.
**Actual calculations for a 12.3/12.8 configuration.

TABLE 4.5.4

SUMMARY OF MEASURED AND CALCULATED $^{235}U(n,f)$ FISSION RATES IN THE PCA 12/13 IN FISSIONS/NUCLEUS/CORE NEUTRON

	A1	A3M	A4	A5	A6
Bare Meas.	2.45-26*	8.08-28	---	9.61-31	4.80-31
Bare Calc.	2.40-26	8.70-28	2.58-30	6.94-31	2.99-31
C/E	0.98	1.08	---	0.72	0.62
Cd-covered Meas.**	1.87-28	6.39-30	1.51-30	7.70-31	4.38-31
Cd-covered Calc.***	1.71-28	6.35-30	1.30-30	6.16-31	2.80-31
C/E	0.91	0.99	0.86	0.80	0.64
Cd Ratio Meas.**	1.87-28	6.39-30	1.31-30	6.70-31	3.81-31
Cd-covered Calc.***	1.71-28	6.35-30	1.30-30	6.16-31	2.80-31
C/E	0.91	0.99	0.99	0.92	0.73
Cd Ratio Meas.****	131	126	---	1.25	1.10
Cd Ratio Calc.***	140	137	1.98	1.13	1.07
C/E	1.07	1.07	---	0.90	0.97

*Read 2.45×10^{-26} fissions/nucleus/core neutron. Mol fission chamber results in the water, and HEDL SSTR results in the iron.

**Calculated assuming a cadmium cutoff of 0.414 eV. The corresponding values in water for a cutoff of 0.58 eV are about 10% less (10% more in the Cd ratio).

***The first set of calculated values refer to "as-measured" ^{235}U SSTR data. The second set are these data corrected by the (Oct'78)/(Nov'81) ^{237}Np SSTR fission rate ratio 1.149.

****Measured cadmium ratios are same for both data sets.

Table 4.5.5 summarizes $^{235}U(n,f)$ cadmium-covered fission rate measurements made with different chambers. Differences between the fission chamber results were noted very early in the program. The NBS fission chamber results are expected to be lower due to the presence of platinum deposit backings. For this reasons, the NBS ^{235}U measurements are discarded and no further measurements have been taken. The geometry of the fission chamber case is complex and the cadmium cutoff depends on the neutron spectrum. The effective Cd cutoff energies are different in all three cases due to differences in the Cd shields used and the sharper dropoff of the SSTR fission rates in the block is consistent with the lower effective Cd cutoff in the SSTR case.

TABLE 4.5.5

COMPARISON OF ^{235}U CADMIUM-COVERED FISSION RATES
IN PCA 8/7 CONFIGURATION

	Fission Chamber Data**			Ratios**		
				CEN/SCK	SSTR	CEN/SCK
Loc.	NBS	CEN/SCK	SSTR Data**	NBS	NBS	SSTR
1/4 T	9.20±2.5%	9.74±0.6%	10.06±2.6%	1.06±0.03	1.09±0.04	0.97±0.03
1/2 T	4.59±2.5%	5.03±3.0%	4.85±3.0%	1.10±0.04	1.06±0.04	1.04±0.04
3/4 T	2.30±2.5%	2.47±3.0%	2.26±2.3%	1.07±0.04	0.98±0.03	1.09±0.04
			Avg	1.08±0.02	1.04±0.06	1.03±0.06

*All data have been corrected to the geometrical configuration of the PCA used after June 1979.

**Units of [fission/(atom·s)] x 10^{15} at 9.75-kW absolute core power.

Finally, a comparison of gamma-ray with neutron fluxes for the present ORNL calculations as well as the earlier revised calculations of Mensart (Mol) os shown in Table 4.5.6.

TABLE 4.5.6

COMPARISON OF GAMMA-RAY FLUXES ABOVE 6.5 MeV
WITH NEUTRON FLUXES ABOVE 0.8 MeV
FOR ORNL AND MOL CALCULATIONS

	A1	A2	A3M	A4	A5	A6
Gammas >6.5 MeV, ORNL	1.72-6	3.57-7	2.26-7	3.14-8	7.53-9	1.89-9
Gammas >6.5 MeV, Mol	1.26-6	4.16-7	2.50-8	4.35-8	1.04-8	1.03-8
Neutrons >0.8 MeV, ORNL	3.95-6	4.40-7	1.43-7	5.01-8	2.42-8	1.09-8
Neutrons >0.8 MeV, Mol	4.41-6	5.23-7	1.70-7	6.37-8	3.31-8	1.61-8
ϕ_γ/ϕ_n, ORNL	0.435	0.811	1.58	0.627	0.311	0.173
ϕ_γ/ϕ_n, Mol	0.286	0.795	1.47	0.680	0.314	0.640

4.5.3 Estimates of Photofission in the Void Box Position and Near Cadmium Covers Throughout the PCA

Sufficient calculations have not been done to permit derivation of the calculated photofission corrections for the void box positions of the 8/7 and 12/13 configurations. Early planning and measurements tended to underestimate the importance of the void box and, consequently, so did the calculations. Table 4.5.7 reviews the relative behavior of the measurements in the PV block for all three configurations (8/7, 12/13, and 4/12 SSC) and then provides estimates proportional to that behavior and the calculated 4/12 SSC void box results.

Also, so far, photofission has been viewed as a result of photons from either the reactor core or from thermal and epithermal neutron capture in structural materials (primarily iron). There is also photofission from gammas produced by thermal neutron capture in the cadmium covers on the fission chambers. The following data will, however, show that it is a small effect even for the low count rate 3/4 T and void box positions.

NBS has measured fission rates of cadmium-covered, highly-depleted uranium in a thermal column with and without a surrounding shell of boron-10. The result is that there are only 10^{-9} fissions-per-second per milligram of uranium per unit of thermal fluence rate. For typical heavy mass deposits containing 800 micrograms of uranium in thermal fluxes of 10^8 n/cm^2·s, the neutron fission counting rate is about 5 counts per second while the gamma-induced photofission rate is at most 0.1 counts per second.

4.5.4 Investigations of the Effects of the Presence of Simulated Surveillance Capsule (SSC) on Thermal and Epithermal Fluxes

More extensive ^{235}U fission rate measurements have been made of the PCA 4/12 SSC configuration than previous configurations because it serves as the physics-dosimetry and calculational benchmarks for the high-flux Simulated Dosimetry Measurements Facility (SDMF) now operational at the Oak Ridge Research Reactor. The following results are most useful for at least two purposes:

1. Test the "synthesis" transport theory modeling of PCA: finite-size effects due to the simulated surveillance capsule (SSC) are sizeable, especially for cadmium-covered $^{235}U(n,f)$, see Figs. 4.5.1 and 4.5.3. In addition, Fig. 4.5.2 suggests finite-size effects (but of small importance) stemming from the thermal shield and pressure vessel simulator. Also, the upper part of Fig. 4.5.2 may lead one to believe that the SSC perturbation is no longer significant at approximately 275 mm above reactor midplane, but such is not the case, as Figs. 4.5.1 and 4.5.3 clearly show.

2. Test the adequacy of epithermal and thermal-neutron induced gamma-ray source terms in coupled neutron-gamma transport theory calculations of energy-deposition rates in steel.

TABLE 4.5.7

ESTIMATION AND COMPARISON OF PHOTOFISSION CORRECTIONS IN THE VOID BOX AND OTHER POSITIONS OF THE PCA SIMULATOR 4/12 SSC, 8/7, AND 12/13 CONFIGURATIONS

^{238}U Results*

Reaction Rate Ratios: $R(\gamma+n)/R(n)$

	4/12 SSC	8/7	12/13
1/4 T	1.021	1.024	1.037
1/2 T	1.013	1.015	1.019
3/4 T	1.026**	1.054	1.040
VB	1.086	(1.142)***	(1.115)***

^{237}Np Results*

Reaction Rate Ratios: $R(\gamma+n)/R(n)$

	4/12 SSC	8/7	12/13
1/4 T	1.004	1.006	1.010
1/2 T	1.002	1.003	1.004
3/4 T	1.005**	1.008	1.007
VB	1.010	(1.016)***	(1.012)***

^{232}Th Results

Reaction Rate Ratios: $R(\gamma+n)/R(n)$

	4/12 SSC	8/7	12/13
1/4 T	1.053	1.058	1.084
1/2 T	1.034	1/038	1.046
3/4 T	1.039	1.144	1.102
VB	1.232	(1.342)***	(1.285)***

*Numbers not in parentheses are from Minsart's calculation of spectra were then folded with photofission cross sections by Eisenhauer.
**Modification discussed early in this section.
***Estimated from 4/12 SSC behavior.

Whereas the graphs of Figures 4.5.1 and 4.5.2 demonstrate the effects of hanging a slab of steel (the SSC) on the back of the thermal shield, Figures 4.5.3 and 4.5.4 show the vertical variations of epithermal and thermal fluxes between the 1/4 T and 1/2 T locations of the 4/12 SSC configuration. Also, since the figures show ratios of measurements, Tables 4.5.8 through 4.5.11 are included to provide the actual data and precision for all measurements. These tables provide bare and cadmium-covered, absolute fission rates based on measurements with a miniature, cylindrical-geometry Mol chamber. This chamber has a ^{235}U mass of 4.72 (+1.5%) μg as measured at NBS (Mc81).

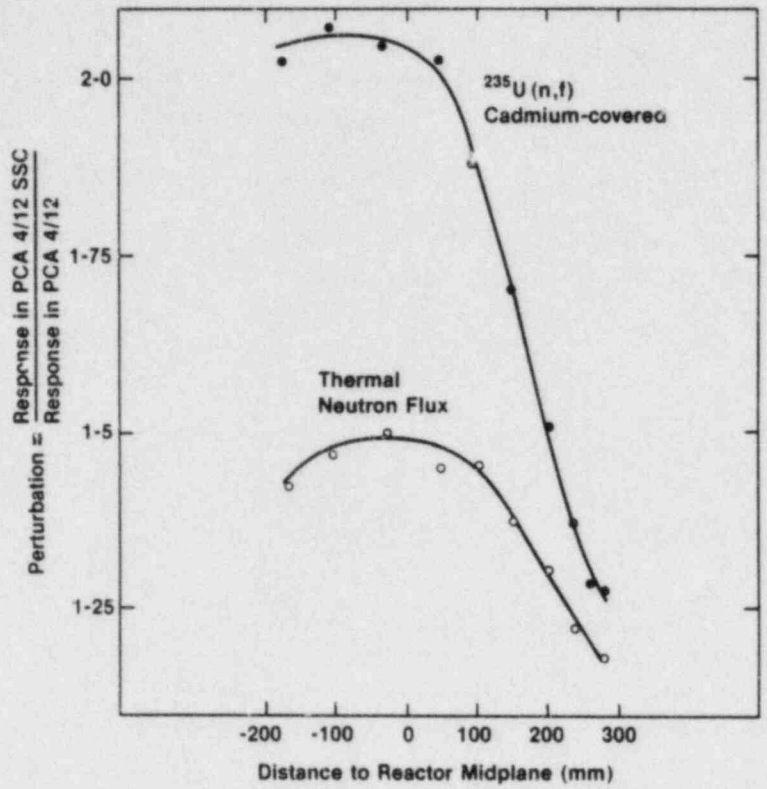

FIGURE 4.5.1. Perturbation Effects on Thermal and Epithermal Fluxes Associated with Adding a Simulated Surveillance Capsule to the 4/12 Configuration.

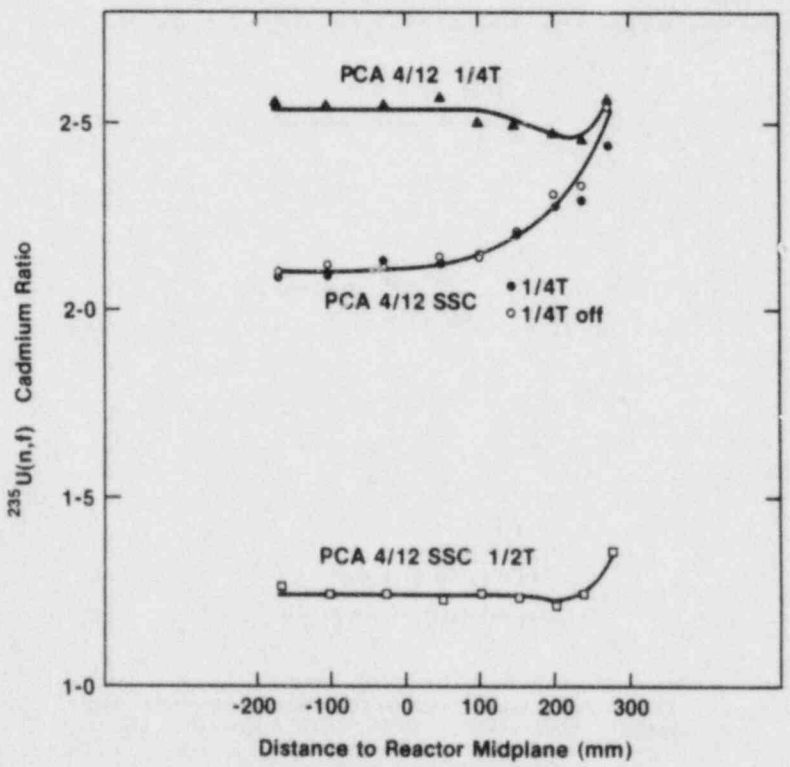

FIGURE 4.5.2. Cadmium Ratio Measurements in the 4/12 and 4/12 SSC Configurations.

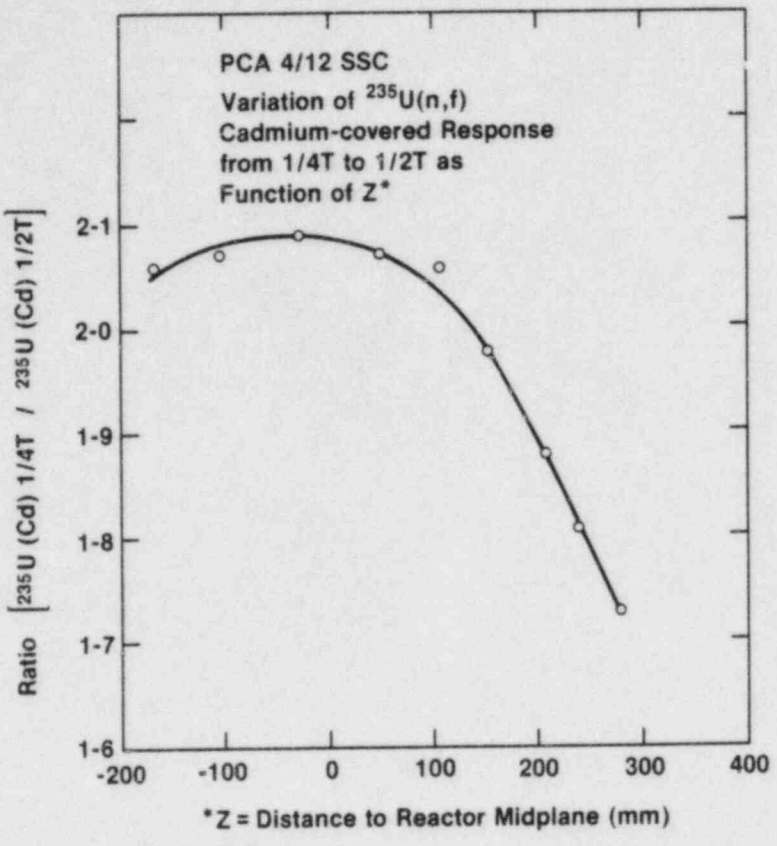

FIGURE 4.5.3. Epithermal ^{235}U Fission Rate Behavior in the 4/12 SSC.

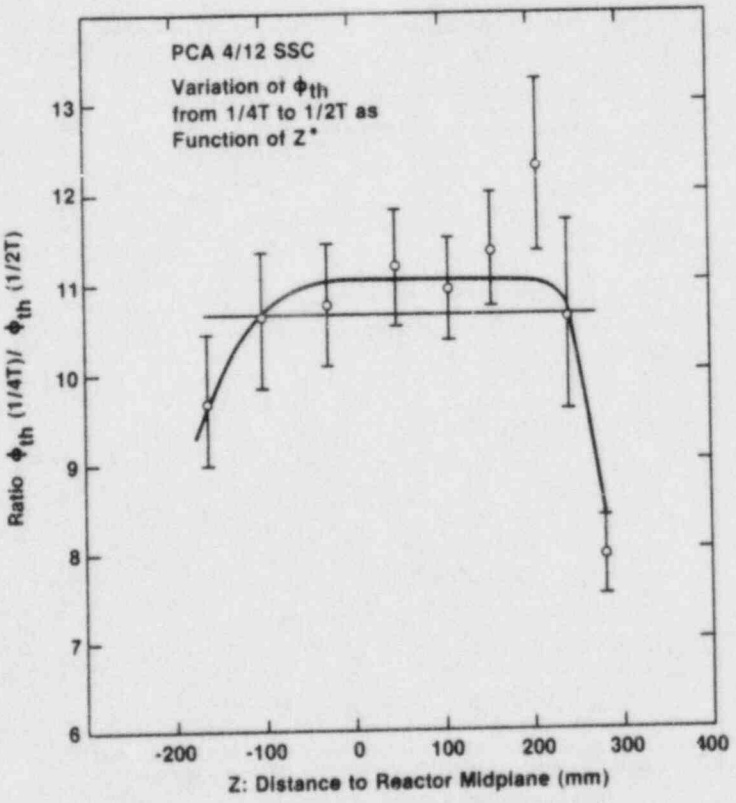

FIGURE 4.5.4. Thermal Flux Behavior in the 4/12 SSC.

TABLE 4.5.8

PCA 4/12 CONFIGURATION: 1/4 T LOCATION*

Distance[a] from midplane (mm)	$^{235}U(n,f)$ Fission rate[b][c] [fission/nucleus·s] Bare	Cadmium-covered	Cadmium ratio	Thermal[b][c][d] flux (cm^{-2} s^{-1})
-165	4.099,-14 (±0.9%)	1.602,-14 (±0.6%)	2.559 (±1.2%)	4.34,+7 (±1.5%)
-100	4.476 (±0.5%)	1.757 (±1.0%)	2.548 (±1.1%)	4.73 (±1.0%)
- 25	4.706 (±1.1%)	1.844 (±1.1%)	2.552 (±1.5%)	4.98 (±1.9%)
+ 51	4.524 (±1.0%)	1.757 (±0.8%)	2.575 (±1.3%)	4.81 (±1.7%)
+103	4.048 (±1.0%)	1.615 (±0.7%)	2.506 (±1.2%)	4.22 (±1.7%)
+154	3.533 (±1.0%)	1.411 (±1.0%)	2.503 (±1.4%)	3.68 (±1.8%)
+203	2.948 (±1.1%)	1.190 (±1.6%)	2.477 (±1.9%)	3.06 (±2.1%)
+240	2.432 (±2.5%)	0.989 (±1.7%)	2.460 (±3.0%)	2.51 (±4.4%)
+279	2.062 (±2.0%)	0.803 (±1.0%)	2.568 (±1.4%)	2.18 (±1.8%)

*Footnotes labeled as (a), (b),... are found after Table 4.5.11.

TABLE 4.5.9

PCA 4/12 SSC CONFIGURATION: 1/4 T LOCATION*

Distance[a] from midplane (mm)	$^{235}U(n,f)$ Fission rate[b][c] [fission/nucleus·s] Bare	Cadmium-covered	Cadmium ratio	Thermal[b][c][d] flux (cm^{-2} s^{-1})
-165	6.809,-14 (±0.7%)	3.247,-14 (±0.6%)	2.097 (±0.9%)	6.19,+7 (±1.4%)
-100	7.633 (±2.0%)	3.638 (±0.9%)	2.098 (±2.2%)	6.95 (±3.9%)
- 25	8.063 (±0.7%)	3.780 (±0.8%)	2.133 (±1.1%)	7.45 (±1.5%)
+ 51	7.574 (±0.7%)	3.560 (±0.9%)	2.127 (±1.1%)	6.98 (±1.5%)
+103	6.569 (±0.8%)	3.040 (±0.6%)	2.161 (±1.0%)	6.13 (±1.6%)
+154	5.315 (±0.9%)	2.404 (±0.9%)	2.211 (±1.3%)	5.06 (±1.8%)
+203	4.106 (±0.8%)	1.795 (±1.0%)	2.287 (±1.3%)	4.02 (±1.6%)
+240	3.124 (±0.8%)	1.356 (±1.4%)	2.304 (±1.6%)	3.07 (±1.8%)
+279	2.507 (±0.9%)	1.025 (±0.9%)	2.447 (±1.3%)	2.58 (±1.6%)

*Footnotes labeled as (a), (b),... are found after Table 4.5.11.

TABLE 4.5.10

PCA 4/12 SSC CONFIGURATION: 1/4 T_{off} LOCATION*

Distance[a] from midplane (mm)	$^{235}U(n,f)$ Fission rate[b][c] [fission/nucleus·s] Bare	Cadmium-covered	Cadmium ratio	Thermal[b][c][d] flux (cm^{-2} s^{-1})
-165	5.916,-14 (±0.5%)	2.809,-14 (±0.5%)	2.106 (±0.7%)	5.40,+7 (±1.0%)
-100	6.652 (±0.4%)	3.128 (±0.7%)	2.126 (±0.8%)	6.13 (±1.0%)
- 25	6.816 (±0.5%)	3.217 (±0.7%)	2.119 (±0.9%)	6.25 (±1.1%)
+ 51	6.341 (±0.7%)	2.948 (±0.4%)	2.150 (±0.8%)	5.90 (±1.4%)
+103	5.377 (±0.4%)	2.506 (±0.7%)	2.146 (±0.8%)	4.99 (±1.0%)
+154	4.300 (±0.3%)	1.940 (±0.4%)	2.216 (±0.5%)	4.10 (±0.7%)
+203	3.322 (±0.3%)	1.433 (±0.5%)	2.318 (±0.6%)	3.29 (±0.7%)
+240	2.600 (±0.5%)	1.110 (±0.3%)	2.342 (±0.6%)	2.59 (±1.0%)
+279	2.144 (±1.0%)	0.840 (±0.8%)	2.552 (±1.3%)	2.27 (±1.7%)

*Footnotes labeled as (a), (b),... are found after Table 4.5.11. The T_{off} location is an off-center location at the same depth into the PV simulator block as the 1/4 T location.

TABLE 4.5.11

PCA 4/12 SSC CONFIGURATION: 1/2 T LOCATION*

Distance[a] from midplane (mm)	$^{235}U(n,f)$ Fission rate[b][c] [fission/nucleus·s] Bare	Cadmium-covered	Cadmium ratio	Thermal[b][c][d] flux (cm^{-2} s^{-1})
-165	1.987,-14 (±1.6%)	1.577,-14 (±0.6%)	1.260 (±1.7%)	7.14,+7 (±8.1%)
-100	2.172 (±1.2%)	1.756 (±0.7%)	1.237 (±1.4%)	7.24 (±6.9%)
- 25	2.251 (±1.1%)	1.811 (±0.9%)	1.243 (±1.4%)	7.66 (±6.7%)
+ 51	2.114 (±1.0%)	1.720 (±0.7%)	1.230 (±1.2%)	6.86 (±6.2%)
+103	1.834 (±0.6%)	1.477 (±0.8%)	1.241 (±1.0%)	6.19 (±4.5%)
+154	1.496 (±0.6%)	1.216 (±1.1%)	1.231 (±1.2%)	4.88 (±5.7%)
+203	1.159 (±0.75%)	0.955 (±1.5%)	1.214 (±1.7%)	3.55 (±8.2%)
+240	0.933 (±1.6%)	0.749 (±1.8%)	1.245 (±2.4%)	3.19 (±11.0%)
+279	0.807 (±0.8%)	0.593 (±1.8%)	1.360 (±2.0%)	3.72 (±5.8%)

*Footnotes labeled as (a), (b),... are found after Table 4.5.11.

Footnotes to Tables

(a) Relative uncertainty from one vertical position to another estimated as ± 1 mm.

Absolute uncertainty: $\leq \pm 5$ mm.

(b) Corrected to a PCA core power of 10.0 kW, using the data compiled in Table 1.3.1 of report NUREG/CR-1861 (see "period B" of PCA program history). The runs were performed September 5-10, 1979; for some of them, the NBS run-to-run monitor was not in service and a sealed Mol fission chamber monitor in the pressure vessel simulator was used, but the uncertainty added by this does not exceed $\pm 0.4\%$. The actually "measured" run powers range from 9.21 kW to 9.39 kW.

(c) The quoted uncertainties are random (i.e., precision only) and given for a 68.3% confidence interval (1σ). They include power fluctuations, counting statistics, and reproducibility (measurements at a given distance from reactor midplane are generally always repeated, i.e., the traverse is taken with the chamber going down and then up). Electronic stability from run-to-run is verified daily and, if it causes any bias, this does not exceed 0.5%. The absolute fission rate and thermal neutron flux scales are based on a mass of uranium-235 of 4.72 µg ($\pm 1.5\%$) as measured at NBS (NUREG/CR-1861).

(d) Obtained by subtracting the cadmium-covered from the bare chamber response and dividing by an effective cross section $g\sigma_0 = 575$ b. This assumes that the thermal neutron spectrum is Maxwellian; considering such simplification and the neglect of other small corrections (which can only be applied through more extensive theoretical analysis accounting for the real spectrum shape at the thermal-to-epithermal joining), it is prudent to assign an additional systematic uncertainty of $\pm 3\%$ to these data.

5.0 TRANSPORT (NEUTRON AND GAMMA) RESULTS

F. B. K. Kam (ORNL)

SUMMARY

This section is in preparation and will be added during a future revision of this document.

5.1 ORNL ANALYSIS

5.1.1 Neutron and Gamma Transport Results for 12/13 Configuration

R. E. Maerker, M. L. Williams, F. B. K. Kam, and C. A. Baldwin

5.1.1.1 Introduction

The analysis and results presented in this section document the coupled neutron and gamma transport calculations performed at ORNL for the 12/13 configuration of the PCA. A modification to the existing 47n-20γ coupled SAILWR cross section library (Si80) was made to correct the thermal group cross sections for effects of upscattering. The resulting cross section library was used throughout the calculations. Broad group thermal cross section modifications were obtained by collapsing from a 127 group transport calculation, the lowest 35 groups of which were thermal. Slight adjustments were made in the broad group values to make them correspond to the same broad group structure as the SAILWR library. Changes were made in σ_a, $\sigma\nu_f$, and σ_t for groups 45, 46, and 47, and in the downscattering cross sections to each of the gamma groups from neutron groups 45, 46, and 47. The only changes important enough to incorporate (>4%) were for ^{235}U, Al, Cr, Mn, Ni, and Fe, the latter being divided into two zones, an inner 12.5 cm of the pressure vessel, and an outer 5 cm, front or back, which also can be used to represent the iron in this thermal shield. Perhaps surprisingly, no significant changes in the hydrogen thermal cross sections occurred. Changes at times amounted to 30% of the original SAILWR values.

The transport calculations were performed with DOT4.3, a two-dimensional discrete ordinates code, using the same general procedure for obtaining three-dimensional fluxes as was described in our analysis of the PCA several years ago (Ma81b), in which

$$\phi(x,y,z) = \phi(x,y)\phi(y,z)/\phi(y) \quad . \tag{5-1}$$

Although the source generation procedures utilized for the calculations cited in the previous reference and those utilized herein are somewhat different, both procedures yield the same resultant normalized fluxes. In particular, the sources for the xy, yz, and y calculations utilized herein are obtained by integrating the three-dimensional source in the appropriate transverse directions, and the sources for the above calculations are normalized to 1 n/s in the core and scaled based on the three-dimensional distribution.

Only two difficulties were experienced in the execution of the runs: one major and one minor. The minor difficulty occurred in the convergence of the thermal flux (group 47), where some 250 inner iterations were required before the flux converged to the preset criterion of 10^{-3}. Subsequent discussions of this problem with more experienced personnel have led to the conclusion that use of the diffusion acceleration option would have reduced the number of

iterations considerably. A more serious difficulty arose when comparisons of the denominator in Eq. 5-1 were made with $\Phi(y)$ determined by:

$$\Phi(y) = \int_{-\infty}^{\infty} \phi(y,z)dz \quad . \tag{5-2}$$

The range of z should have been sufficient to essentially produce a converged result (three feet on either side of the midplane), and indeed the discrepancy is small (<5%) for all neutron and gamma-ray fluxes out to and including detector A4 at 1/4 T. As the penetration depth increases through the pressure vessel, however, the discrepancy increases at detector A5 (1/2 T) from 9% for a few low energy neutron groups to 63% at detector A6 (3/4 T) for the thermal group. All remaining group fluxes still compare reasonably well in the pressure vessel (<10%). When the fluxes at A7 (void box) are compared, however, discrepancies in the 30-80% range are common for the lower energy neutron groups and all the gamma-ray groups. These discrepancies may be due to void effects associated with the calculations. The values used for the denominator of Eq. 5-1 in the flux synthesis are those calculated from the effectively one-dimensional DOT run, $\Phi(y)$, since they are not subject to the problem of integral convergence that integrating the two-dimensional fluxes might be.

5.1.1.2 Results

Fluxes using Eq. 5-1 were synthesized and written on tape for both the neutron and gamma ray groups at locations A1, A2, A3M, A4, A5, and A6. Comparisons of the saturated activities calculated by folding these 47 group neutron fluxes with END/B-V dosimetry cross sections with earlier calculations using a 51 neutron group to 171 neutron group scaling technique indicate that the present calculations reproduce the earlier results very well even though the group structure in the present calculation is much coarser.

The comparisons of the calculated $^{235}U(n,f)$ activities with measurements are, of course, unique to the present analysis since the earlier calculations did not stress the low energy portion of the neutron spectrum. These present comparisons should be a good indication of the accuracy of the calculated gamma-ray fluxes, since most of the high-energy gamma-ray flux comes from thermal and epithermal capture in the steel and aluminum window. The calculated $^{235}U(n,f)$ reaction rates presented in Table 5.1.1 were based on folding the thermal and epithermal fine group cross section in the 127 group structure with scaled fine group fluxes calculated through the iron in the collapsing procedure. (Recall that the modified thermal cross sections used to replace the original SAILWR values for ^{235}U were collapsed from fluxes calculated in the core.) A Maxwellian spectrum at T = 300°K with 1/E tail in the epicadmium region was used to collapse the $^{235}U(n,f)$ cross sections in water. These comparisons indicate absolute agreement to within about 10% at all locations where measurements have so far been reported so that there is every reason to anticipate similar agreement with the gamma-ray measurements when they become available. The treatment of the core gamma-ray source in the DOT calculations included only the contributions from prompt fission and capture. The gamma

production cross sections do not include the contribution from fission product gammas but there is little PCA fuel burnup so this omission should result in negligible error in the calculations.

TABLE 5.1.1

SUMMARY OF COMPARISONS OF MEASURED AND CALCULATED $^{235}U(n,f)$ REACTION RATES IN THE PCA 12/13 IN FISSIONS PER NUCLEUS PER CORE NEUTRON

	A1	A3M	A4	A5	A6
Bare meas.	2.45-26*	8.08-28		8.03-31	4.01-31
Bare calc.	2.40-26	8.70-28	2.58-30	6.94-31	2.99-31
C/E	0.98	1.08		0.86	0.75
Cd-covered meas.	1.87-28	6.39-30	1.26-30	6.43-31	4.01-31
Cd-covered calc.**	1.71-28	6.35-30	1.30-30	6.16-31	2.80-31
C/E**	0.91	0.99	1.03	0.96	0.77
Cd ratio meas.	131	126		1.25	1.10
Cd ratio calc.**	140	137	1.98	1.13	1.07
C/E**	1.07	1.09		0.90	0.97

*Read 2.45 x 10^{-26} fissions per nucleus per core neutron. CEN/SCK fission chamber results in the water, and HEDL SSTR results in the iron (Table 2.5.9).
**Calculated assuming a cadmium cutoff of 0.414 eV. The corresponding values in water for a cutoff of 0.58 eV are about 10% less (10% more in the Cd ratio). Iron values are little affected.

Table 5.1.2 presents the added effect of the photofission reactions to the neutron fissions calculated consistently with the present cross section library using photofission cross sections supplied by C. Eisenhauer of NBS. It is seen that the enhancement is small and that the effect is generally in good agreement with the revised calculations of G. Minsart (Mc81d).

Comparisons of the gamma-ray fluxes above 6.5 MeV and the neutron fluxes above 0.8 MeV for both the present calculations and the earlier revised calculations of Minsart (Ma82e) are shown in Table 5.1.3. A comparison of the gamma group fluxes is shown in Table 5.1.4.

5.1.1.3 Conclusions

There are significant discrepancies in the gamma calculations between ORNL and CEN/SCK. These discrepancies appear to be in the cross section libraries. Preliminary comparisons between calculations and measurements also indicate large discrepancies so that further studies will be necessary to resolve the problem.

TABLE 5.1.2

PHOTOFISSION ENHANCEMENT EFFECTS IN THE PCA 12/13

	^{238}U		^{237}Np	
	ORNL	CEN/SCK	ORNL	CEN/SCK
A1	1.02	1.02	1.01	1.01
A3M	1.06	1.06	1.03	1.03
A4	1.03	1.03	1.01	1.01
A5	1.02	1.02	1.00	1.00
A6	1.01	1.01	1.00	1.01

TABLE 5.1.3

COMPARISON OF ABSOLUTE NEUTRON AND GAMMA-RAY FLUXES IN UNITS OF PARTICLES·CM^{-2} PER CORE NEUTRON IN THE PCA 12/13 FOR TWO INDEPENDENT CALCULATIONS

	A1	A2	A3M	A4	A5	A6
Gammas > 6.5 MeV, ORNL	1.72-6	3.57-7	2.26-7	3.14-8	7.53-9	1.89-9
Gammas > 6.5 MeV, CEN/SCK	1.26-6	4.16-7	2.50-7	4.35-8	1.04-8	1.03-8
Neutrons > 0.8 MeV, ORNL	3.95-6	4.40-7	1.43-7	5.01-8	2.42-8	1.09-8
Neutrons > 0.8 MeV, CEN/SCK	4.41-6	5.23-7	1.70-7	6.37-8	3.31-8	1.61-8
Φ_γ/Φ_n, ORNL	0.435	0.811	1.58	0.627	0.311	0.173
Φ_γ/Φ_n, CEN/SCK	0.286	0.795	1.47	0.680	0.314	0.640

TABLE 5.1.4

COMPARISON OF CALCULATED GAMMA FLUXES FOR THE PCA 12/13 CONFIGURATION
IN PHOTONS·CM^{-2}·S^{-1}·MeV^{-1}·W^{-1}

Energy boundaries (MeV) lower-upper	1/4 T			1/2 T			3/4 T		
	ORNL	CEN/SCK	Ratio	ORNL	CEN/SCK	Ratio	ORNL	CEN/SCK	Ratio
10.0 -14.0	3.84-2	3.58-2	1.07	9.74-3	9.11-3	1.07	2.36-3	2.40-3	0.98
8.0 -10.0	1.78+2	3.04+2	0.59	4.00+1	7.16+1	0.59	9.02+0	3.85+1	0.23
5.0 - 8.0	1.14+3	1.47+3	0.78	2.89+2	3.68+2	0.79	6.74+1	3.54+2	0.19
4.0 - 5.0	1.71+3	1.84+3	0.93	4.53+2	4.95+2	0.92	5.08+2	3.04+2	0.36
3.0 - 4.0	2.76+3	3.49+3	0.79	7.31+2	9.10+2	0.80	1.74+2	4.30+2	0.40
2.0 - 3.0	7.24+3	9.13+3	0.79	1.65+3	2.07+3	0.80	3.61+2	8.75+2	0.41
1.0 - 2.0	1.31+4	1.91+4	0.69	3.09+3	4.27+3	0.72	6.86+2	1.52+3	0.45
0.8 - 1.0	2.38+4	3.58+4	0.66	6.02+3	8.46+3	0.71	1.51+3	3.01+3	0.50
0.6 - 0.8	2.90+4	4.52+4	0.64	6.80+3	9.77+3	0.70	1.55+3	3.34+3	0.46
0.4 - 0.6	5.93+4	6.66+4	0.89	1.40+4	1.41+4	1.00	3.19+3	4.82+3	0.66
0.2 - 0.4	9.74+4	1.29+5	0.76	2.28+4	2.73+4	0.84	5.17+3	9.77+3	0.53
0.1 - 0.2	1.19+5	1.43+5	0.83	2.78+4	2.98+4	0.93	6.32+3	1.08+4	0.59
0.02- 0.1	1.18+4	2.39+4	0.49	2.76+3	4.88+3	0.57	6.29+2	1.78+3	0.35

5.1.2 Calculations and Measurements for the PCA 4/12 and 4/12 SSC Configurations

C. A. Baldwin, F. B. Kam, L. F. Miller, and F. W. Stallmann

5.1.2.1 Introduction

Preliminary neutron transport calculations for the PCA 4/12 and PCA 4/12 SSC configurations are presented.

All neutronic calculations are performed with the DOT code (Rh79) using the measured source distribution for a fixed source calculation. All calculations use the VITAMIN-C cross section library (Ro82); however, the CEN/SCK calculations use a collapsed 17 broad group structure while the ORNL calculations maintain the original VITAMIN-C fine group structure. The CEN/SCK methodology (Mi81b) utilizes a variable vertical and transverse buckling technique in order to take into consideration three-dimensional effects whereas the ORNL methodology utilizes a flux density synthesis technique similar to that described by Maerker and Williams (Ma82e).

5.1.2.2 Results

Table 5.1.5 lists calculated results and comparisons for the 4/12 SSC and 4/12 configurations for the damage correlation parameters ($E > 1.0$ MeV), ($E > 0.1$ MeV), and displacements per atom (dpa) of iron. Measured and calculated reaction rates and comparisons for the 4/12 SSC configuration are listed in Table 5.1.6. Table 5.1.7 lists calculated reaction rates and comparisons for the 4/12 configuration. Tables 5.1.8 and 5.1.9 show the calculated perturbation effect of the SSC on damage correlation parameters and reaction rates, respectively. Results in Tables 5.1.5 through 5.1.9 are midplane values.

Comparisons show that the two calculations are in agreement with each other. Both 4/12 SSC calculations attenuate faster than the measurements. This discrepancy between measurements and calculations was also observed with previous results obtained in the PCA "Blind Test" (Mi81a).

The Np-237 reaction rates in the PCA 4/12 SSC and the 4/12 configurations at the 1/4 T location were calculated to determine the perturbation effect of the SSC. The Np-237 perturbation effect is defined as the ratio of the Np-237 reaction rate with the SSC divided by the reaction rate without the SSC. The calculated and measured ratios are shown in Table 5.1.10. The comparison indicates excellent agreement.

5.1.2.3 Conclusions

The neutron calculations and measurements are in good agreement with each other. More detailed comparisons will be made as more measurements become available in the future.

TABLE 5.1.5

COMPARISON OF CALCULATED DAMAGE CORRELATION PARAMETERS FOR
PCA-PVF 4/12 SSC AND 4/12 CONFIGURATIONS

Parameter*	Location	PCA-PVF 4/12 SSC			PCA-PVF 4/12		
		CEN/SCK (C1)	ORNL (C2)	C1/C2	CEN/SCK (C1)	ORNL (C2)	C1/C2
ϕ(E>1.0 MeV)	A0	1.671-4	1.754-4	0.95	1.671-4	1.754-4	0.95
	A1		2.389-5			2.381-5	
	A2	3.019-6	3.374-6	0.89		2.014-6	
	A3		8.657-7			7.032-7	
	A4	2.148-7	2.144-7	1.00	1.901-7	2.096-7	0.91
	A5	9.694-8	9.747-8	0.99		9.650-8	
	A6	4.090-8	4.139-8	0.99		4.119-8	
	A7	1.049-8	1.049-8	1.00		1.037-8	
ϕ(E>0.1 MeV)	A0	3.077-4	3.250-4	0.95	3.076-4	3.250-4	0.95
	A1		4.797-5			4.758-5	
	A2	9.678-6	1.075-5	0.90		4.601-6	
	A3		2.561-6			1.381-6	
	A4	9.364-7	9.017-7	1.04	6.107-7	6.663-7	0.92
	A5	6.034-7	5.728-7	1.05		4.294-7	
	A6	3.526-7	3.303-7	1.07		2.495-7	
	A7	1.066-7	9.163-8	1.16		7.031-8	
dpa (ASTM)	A0	2.297-25	2.339-25	0.98		2.339-25	
	A1		3.256-26			3.242-26	
	A2	4.852-27	5.188-27	0.93		2.851-27	
	A3		1.320-27			9.734-28	
	A4	4.094-28	3.816-28	1.07		3.295-28	
	A5	2.286-28	2.099-28	1.09		1.777-28	
	A6	1.208-28	1.091-28	1.11		9.071-29	
	A7		2.923-29			2.438-29	

*All results normalized to 1.0 source neutron.

TABLE 5.1.6

COMPARISON OF CALCULATED AND MEASURED REACTION RATES FOR THE 4/12 SSC CONFIGURATION

Parameter[a]	Location	Calculations		Experiment	Comparisons		
		CEN/SCK (C1)	ORNL (C2)		C1/C2	C1/E	C2/E
	A0	3.52-28	3.65-28		0.96		
	A2	8.30-30	9.05-30		0.92		
^{237}Np	A4	6.86-31	6.57-31	6.66-31[b]	1.04	1.03	0.99
(n,f)	A5	3.76-31	3.58-31	3.69-31[b]	1.05	1.02	0.97
F.P.	A6	1.93-31	1.83-31	1.93-31[b]	1.05	1.00	0.95
	A7		5.06-32	5.26-32[b]			0.96
	A0	4.25-29	4.44-29		0.96		
	A2	6.77-31	7.56-31	7.47-31[c]	0.90	0.91	1.01
^{115}In	A4	4.80-32	4.76-32	5.81-32[c]	1.01	0.83	0.82
(n,n')	A5	2.10-32	2.11-32		0.99		
^{115m}In	A6	8.77-33	8.86-33		0.99		
	A7		2.26-33				
	A0	1.83-28	1.87-28		0.98		
	A2	3.84-30	4.22-30	4.02-30[c]	0.91	0.96	1.05
^{103}Rh	A4	3.08-31	3.00-31	3.32-31[c]	1.03	0.93	0.90
(n,n')	A5	1.64-31	1.60-31	1.82-31[c]	1.02	0.90	0.88
^{103m}Rh	A6	8.24-32	8.04-32		1.02		
	A7		2.19-32				
	A0	7.10-29	7.41-29		0.96		
	A2	1.03-30	1.15-30		0.90		
^{238}U	A4	7.16-32	7.09-32	7.63-32[d]	1.01	0.94	0.93
(n,f)	A5	2.90-32	2.92-32	3.32-32[d]	0.99	0.87	0.88
F.P.	A6	1.11-32	1.13-32	1.36-32[d]	0.98	0.82	0.83
	A7		2.74-33	3.11-33[d]			0.88
	A0	2.35-29	2.42-29	2.40-29[e]	0.97	0.98	1.01
	A2	2.57-31	2.84-31	2.87-31[c]	0.90	0.89	0.99
^{58}Ni	A4	1.68-32	1.66-32	1.90-32[c]	1.01	0.88	0.87
(n,p)	A5	5.92-33	6.08-33	7.50-33[c]	0.97	0.79	0.81
^{58}Co	A6	1.98-33	2.12-33		0.93		
	A7		5.20-34				
	A0	1.58-31	1.58-31	1.51-31[e]	1.00	1.05	1.05
	A2	1.79-33	1.93-33	2.03-33[c]	0.93	0.88	0.95
^{27}Al	A4	1.58-34	1.50-34	1.68-34[c]	1.05	0.94	0.90
(n,α)	A5	5.52-35	5.64-35	6.70-35[c]	0.98	0.82	0.84
^{24}Na	A6	1.85-35	2.03-35		0.91		
	A7		5.99-36				

[a]Reactions per target atom per source neutron.
[b]Derived from Table 2.3.7 $\langle\sigma_{25}\rangle$Np 1312 mb.
[c]Derived from results given in Fa80a.
[d]Derived from Table 2.3.7 $\langle\sigma_{25}\rangle$U 305 mb.
[e]Derived from Table 8.3.1 $\langle\sigma_{25}\rangle$Ni 108.5 mb and $\langle\sigma_{25}\rangle$Al 0.705 mb (Mc81g).

TABLE 5.1.7

COMPARISON OF CALCULATED REACTION RATES FOR
THE 4/12 CONFIGURATION

Parameter*	Location	Calculations		Experiment	Comparisons		
		CEN/SCK (C1)	ORNL (C2)		C1/C2	C1/E	C2/E
	A0	3.52-28	3.65-28		0.96		
	A2		4.54-30				
^{237}Np	A4	5.15-31	5.60-31		0.92		
(n,f)	A5		3.06-31				
F.P.	A6		1.55-31				
	A7		4.30-32				
	A0		4.44-29				
	A2		4.99-31				
^{115}In	A4		4.83-32				
(n,n')	A5		2.14-32				
^{115m}In	A6		8.91-33				
	A7		2.24-33				
	A0		1.87-28				
	A2		2.26-30				
^{103}Rh	A4		2.62-31				
(n,n')	A5		1.39-31				
^{103m}Rh	A6		6.91-32				
	A7		1.88-32				
	A0	7.10-29	7.41-29		0.96		
	A2		8.22-31				
^{238}U	A4	6.90-32	7.58-32		0.91		
(n,f)	A5		3.15-32				
F.P.	A6		1.22-32				
	A7		2.95-33				
	A0	2.35-29	2.42-29		0.97		
	A2		2.59-31				
^{58}Ni	A4	1.92-32	2.05-32		0.94		
(n,p)	A5		7.55-33				
^{58}Co	A6		2.63-33				
	A7		6.37-34				
	A0		1.58-31				
	A2		2.19-33				
^{27}Al	A4		2.09-34				
(n,α)	A5		7.92-35				
^{24}Na	A6		2.85-35				
	A7		8.28-36				

*Reactions per target atom per source neutron.

TABLE 5.1.8

COMPARISON OF CALCULATED PERTURBATION EFFECTS OF THE SSC 0.4 DAMAGE CORRELATION PARAMETERS

Parameter	Location	$\left[\frac{4/12\ SSC}{4/12}\right]$ CEN/SCK (C1)	$\left[\frac{4/12\ SSC}{4/12}\right]$ ORNL (C2)	$\frac{C1}{C2}$
ϕ(E>1.0 MeV)	A0	1.00	1.00	1.00
	A1		1.00	
	A2		1.68	
	A3		1.23	
	A4	1.13	1.02	1.11
	A5		1.01	
	A6		1.00	
	A7		1.01	
ϕ(E>0.1 MeV)	A0	1.00	1.00	1.00
	A1		1.01	
	A2		2.34	
	A3		1.85	
	A4	1.53	1.35	1.13
	A5		1.33	
	A6		1.32	
	A7		1.30	
dpa (ASTM)	A0		1.00	
	A1		1.00	
	A2		1.82	
	A3		1.36	
	A4		1.16	
	A5		1.18	
	A6		1.20	
	A7		1.20	

TABLE 5.1.9

COMPARISON OF CALCULATED PERTURBATION EFFECTS
OF THE SSC ON REACTION RATES

Parameter	Location	Calculations		Experiment	Comparisons		
		CEN/SCK (C1)	ORNL (C2)		C1/C2	C1/E	C2/E
	A0	1.00	1.00		1.00		
	A2		1.99				
^{237}Np	A4	1.33	1.17		1.14		
(n,f)	A5		1.17				
F.P.	A6		1.18				
	A7		1.18				
	A0		1.00				
	A2		1.51				
^{115}In	A4		0.98				
(n,n')	A5		0.98				
^{115m}In	A6		0.99				
	A7		1.01				
	A0		1.00				
	A2		1.87				
^{103}Rh	A4		1.14				
(n,n')	A5		1.15				
^{103m}Rh	A6		1.16				
	A7		1.16				
	A0	1.00	1.00		1.00		
	A2		1.40				
^{238}U	A4	1.04	0.93		1.12		
(n,f)	A5		0.93				
F.P.	A6		0.93				
	A7		0.93				
	A0	1.00	1.00		1.00		
	A2		1.10				
^{58}Ni	A4	0.88	0.81		1.09		
(n,p)	A5		0.80				
^{58}Co	A6		0.81				
	A7		0.82				
	A0		1.00				
	A2		0.88				
^{27}Al	A4		0.72				
(n,α)	A5		0.71				
^{24}Na	A6		0.71				
	A7		0.72				

TABLE 5.1.10

COMPARISON OF CALCULATED TO MEASURED PERTURBATION EFFECT $\left[\frac{4/12\ SSC}{4/12}\right]$ FOR ^{237}Np REACTION RATE AT PCA 1/4 T POSITION

Z[a] (mm)	Np perturbation effect		
	ORNL Cal.	Exp.[b]	C/E
-101	1.167	1.219	0.96
- 25	1.167	1.238	0.94
+ 52	1.159	1.211	0.96
+102	1.148	1.195	0.96
+153	1.131	1.161	0.97
+204	1.103	1.146	0.96
+240	1.071	1.117	0.96
+280	1.011	1.114	0.91

[a]Distance from midplane.

[b]Private communication from A. Fabry (Mol) to F. B. K. Kam, ORNL, April 1983.

5.2 CEN/SCK ANALYSIS

J. Debrue (CEN/SCK)

This section is in preparation and will be added during a future revision of this document.

5.3 RR&A ANALYSIS

A. Dolan (Rolls-Royce & Associates Ltd., Derby, UK)

5.3.1 Introduction

This section presents the results of a recent recalculation of neutron spectra and detector reaction rates throughout the PCA 12/13 configuration performed using the Monte Carlo computer code McBEND (Be82).

The responses calculated using McBEND were compared with experiment, and two linear least squares data adjustments were made using the computer code LONDON recently developed at RR&A.

5.3.2 The Monte Carlo Calculation

The transport calculation was a modification of the RR&A/AEEW contribution to the PCA Calculational Blind Test (Mc81) and the changes to this original calculation are described here. The geometric modelling was simplified, but remained identical in all essential features; however the distances through the array were updated to the latest recommended values (Mc81, section 8). Some refinements were introduced into the energy group schemes used. The 'point' energy group library used for the McBEND transport calculation was a recent 8000 group version processed at the Atomic Energy Establishment, Winfrith, and used in place of the 300 group library reported in the original 'Blind Test', while the detector responses were included in the 620 group scheme in which they exist on the IRDF82 dosimetry cross-section library (largely compiled from ENDF/BV).

The responses scored are average ones over the McBEND regions which are 10cms square in cross-section and 2cm deep; these are corrected to centre line values using shape information obtained from a forward diffusion calculation (ADC, see Mc81). Correction factors of between 7% (at A1) and 2% (at the void box) were used.

In order to accelerate particle scoring it is necessary to supply an importance distribution in both space and energy. The results of the previous calculation indicated that improvements would result from biasing the importances towards high energies in order to score more particles in this energy range. A lower cut off energy of 0.11 MeV was again used in order to reduce the cost of the calculation, since this is sufficiently low in energy to cover the responses of all of the detectors used except ^{235}U. An inverse flux spectrum at the void box location was used as a source for the calculation to produce the required importances.

5.3.3 Results of the Monte Carlo Calculation

Table 5.3.1 shows a comparison of the measured and calculated detector responses. Since it is only possible to include up to seven responses in the calculation, the results for $^{237}Np(n,f)$, $^{232}Th(n,f)$ and $^{238}U(n,f)$ were obtained by folding 40 group condensations of the responses into the scored flux

TABLE 5.3.1

COMPARISON OF REACTION RATES CALCULATED USING THE MONTE CARLO CODE McBEND AND MEASURED FOR THE PCA 12/13 CONFIGURATION (REACTIONS/TARGET ATOM/CORE NEUTRON)

Location		^{237}Np (n,f) F.P.	^{232}Th (n,f) F.P.	^{238}U (n,f) F.P.	^{115}In (n,n') ^{115m}In	^{103}Rh (n,n') ^{103m}Rh	^{58}Ni (n,p') ^{58}Co	^{27}Al (n,α) ^{24}Na
A1	C	7.87E-6 ± 6%	4.59E-7 ± 6%	1.86E-6 ± 6%	1.04E-6 ± 3.4%	3.98E-6 ± 6.2%	6.45E-7 ± 3.0%	5.79E-9 ± 3.4%
	E	-	-	-	1.06E-6 ± 5.1%	4.06E-6 ± 5.2%	6.35E-7 ± 5.6%	5.55E-9 ± 5%
	C/E				0.98	0.98	1.02	1.04
A2	C	9.29E-7 ± 5%	4.86E-8 ± 5%	1.97E-7 ± 5%	1.14E-7 ± 4.4%	4.73E-7 ± 5.1%	6.92E-8 ± 3.1%	7.09E-10 ± 2.8%
	E	7.34E-7 ± 5.3%*	-	-	1.15E-7 ± 5.2%	-	6.74E-8 ± 5.7%	7.24E-10 ± 5.3%
	C/E	1.27			0.99		1.03	0.98
A3M	C	3.05E-7 ± 4%	1.67E-8 ± 4%	6.64E-8 ± 4%	3.96E-8 ± 4.1%	1.65E-7 ± 4.4%	2.63E-8 ± 3.1%	3.15E-10 ± 4.5%
	E	3.07E-7 ± 5.8%*	-	6.05E-8 ± 5.8%	3.69E-8 ± 5.1%	-	2.52E-8 ± 5.5%	3.18E-10 ± 5%
	C/E	0.99		1.10	1.07		1.04	0.99
A4	C	1.11E-7 ± 4%	4.39E-9 ± 4%	1.80E-8 ± 4%	1.07E-8 ± 3.9%	5.51E-8 ± 3.5%	5.39E-9 ± 3.3%	7.05E-11 ± 5.1%
	E	1.21E-7 ±10.5%*	3.59E-9 ± 4.9%*	1.78E-8 ± 11%	1.12E-8 ± 5.1%	5.67E-8 ± 5.3%	5.78E-9 ± 5.4%	7.24E-11 ± 5.3%
	C/E	0.92	1.22	1.01	0.96	0.97	0.93	0.97
A5	C	6.21E-8 ± 3%	1.88E-9 ± 3%	7.84E-9 ± 3%	4.95E-9 ± 2.9%	2.95E-8 ± 2.9%	2.08E-9 ± 3.3%	2.72E-11 ± 3.5%
	E	6.62E-8 ±11.2%*	1.57E-9 ± 5.1%*	7.83E-9 ± 10.9%	5.22E-9 ± 5.2%	3.19E-8 ± 7%	2.28E-9 ± 5.6%	2.91E-11 ± 5.4%
	C/E	0.94	1.20	1.00	0.95	0.92	0.91	0.93
A6	C	3.22E-8 ± 3%	7.20E-10 ± 3%	3.05E-9 ± 3%	2.07E-9 ± 3.8%	1.46E-8 ± 3.3%	7.63E-10 ± 3.5%	9.70E-12 ± 5.2%
	E	3.48E-8 ± 10.6%	6.00E-10 ± 4.9%	3.24E-9 ± 11.1%	2.25E-9 ± 5.8%	1.61E-8 ± 7%	8.10E-10 ± 5.7%	1.12E-12 ± 5.4%
	C/E	0.93	1.20	0.94	0.92	0.91	0.94	0.87
A7	C	9.71E-9 ± 5%	2.29E-10 ± 5%	9.70E-10 ± 5%	6.19E-10 ± 7.1%	4.30E-9 ± 4.6%	2.14E-10 ± 6.9%	2.94E-12 ± 5%
	E	9.65E-9 ± 7.3%	1.33E-10 ± 4.7%	8.60E-10 ± 4.9%	6.48E-10 ± 6.7%	-	-	4.36E-12 ± 7%
	C/E	1.01	1.72	1.13	0.96			0.67

* These are uncertainties on the measurements of equivalent fission flux only, but the uncertainties in fission average cross-section are small and do not apply to the SSTR measurements.

spectra. The uncertainties given in this table are stochastic only, and those quoted for the fission monitors do not take account of any uncertainty introduced by using a coarser group scheme. Table 5.3.2 gives a range of spectral indices calculated from the values given in Table 5.3.1 while Table 5.3.3 gives calculated values for damage exposure parameters. Experiment and calculation are compatible at all locations, except for $^{232}Th(n,f)$ at all measured locations, $^{237}Np(n,f)$ in the A2 location and $^{27}Al(n,\alpha)^{24}Na$ in the void box (A7) location.

5.3.4 The Linear Least-Squares Data Adjustment

The methodology used in LONDON is similar to that described in Ma81, but the scope is more limited, since the code was designed to use measured reaction rates in an RPV/PST cavity for the adjustment of calculated ones within the RPV. Fluxes are not adjusted explicitly, rather the effect of data adjustments are extrapolated in space and energy to modify reaction rates and damage exposure parameters at the same or other locations in the calculated array. The four classes of differential data adjusted, each of which is considered to be independent from the others, were the source distribution, transmission cross-sections, detector responses and Monte Carlo stochastic uncertainties. The sensitivities to the source distribution were obtained from source importance values, and the remaining sensitivities were obtained from the Monte Carlo calculation. The sensitivities of integral responses to the transmission data were obtained using a perturbation package included in McBEND (Mc81). Variance-covariance data was obtained from the published literature (Eu74, Zi83, Dr77, Mu81, St80a) and largely originates from ENDFBV.

The transmission cross-sections adjusted were Fe(N,N), Fe(N,X), O(N,N), O(N,α), O(N,N'), H(N,T), Cr(N,N), Cr(N,X), Ni(N,N) and Ni(N,X). A 15 energy group scheme was used for the adjustment of detector cross-sections (Ma81) while a 9 group scheme was used for the transmission data. Since adequate uncertainty data were not found for aluminium and uranium transmission cross-sections, these were not included. The exposure parameters were treated as standards and no uncertainties in responses were included.

Due to the highly correlated nature of the Watt fission spectrum (Ma81), a coarse 5 energy group scheme was used for this adjustment and the core was divided into 3 spatial regions only.

Two adjustment runs were made. Adjustment 1 used the measured $^{115}In(n,n')^{115m}In$ and $^{27}Al(n,\alpha)^{24}Na$ responses in the void box to adjust $^{115}In(n,n')^{115m}In$, $^{58}Ni(n,p)^{58}Co$, $^{103}Rh(n,n')^{103m}Rh$ and $^{27}Al(n,\alpha)^{24}Na$ responses and those for the damage exposure parameters, dpa, flux $>$ 1 MeV and flux $>$ 0.1 MeV, at the A4 location. This adjustment was intended to form part of the validation of a proposed method of estimation of exposure parameters to be used on power reactors. Adjustment 2 was run for the more academic reason of comparing the individual data adjustments obtained from a more representative sample of measurements, with those obtained from the previous adjustment, and to obtain values for the damage exposure parameters directly comparable with those obtained from 'in-situ' adjustment codes (e.g. McC79).

TABLE 5.3.2

COMPARISON OF REACTION RATE RATIOS FOR PCA 12/13 CONFIGURATION

Location	$^{238}U(n,f)FP/^{58}Ni(n,p)^{58}Co$			$^{27}Al(n,\alpha)^{24}Na/^{58}Ni(n,p)^{58}Co$		
	Calc.	Expt.	C/E	Calc.	Expt.	C/E
A1	2.88	-	-	8.98-3	8.74-3	1.03
A2	2.85	-	-	1.02-2	1.07-2	0.95
A3M	2.52	-	-	1.20-2	1.26-2	0.95
A4	3.34	3.23	1.03	1.30-2	1.25-2	1.04
A5	3.76	3.68	1.01	1.31-2	1.27-2	1.03
A6	3.99	4.24	0.94	1.27-2	1.35-2	0.94
	$^{237}Np(n,f)FP/^{58}Ni(n,n)^{58}Co$			$^{103}Rh(n,n')^{103m}Rh/^{58}Ni(n,p)^{58}Co$		
A1	12.2	13.8	0.88	6.2	6.4	0.97
A2	13.4	-	-	6.8	-	-
A3M	11.6	11.9	0.97	6.3	-	-
A4	20.6	21.2	0.97	10.2	9.9	1.04
A5	29.9	29.9	1.0	14.2	14.0	1.01
A6	42.2	43.9	0.96	19.1	19.8	0.96
	$^{115}In(n,n')^{115m}In/^{58}Ni(n,p)^{58}Co$					
A1	1.61	1.68	0.96			
A2	1.65	1.72	0.96			
A3M	1.51	1.50	1.01			
A4	1.99	1.93	1.03			
A5	2.38	2.30	1.03			
A6	2.71	2.74	0.99			

TABLE 5.3.3

RESULTS OF MONTE CARLO CALCULATION AND LEAST-SQUARES DATA ADJUSTMENTS FOR DAMAGE EXPOSURE PARAMETERS FOR THE PCA 12/13 CONFIGURATION (REACTIONS/TARGET ATOM/CORE NEUTRON)

Location		Flux Density > 1 MeV	Flux Density > 0.1 MeV	dpa (Iron) (ASTM)
A1	Calc.	3.92E-6 ± 7% +	5.18E-6 ± 10% +	5.00E-27 ± 6% +
A2	Calc.	4.44E-7 ± 5% +	7.06E-7 ± 8% +	5.93E-28 ± 5% +
A3M	Calc.	1.50E-7 ± 10%	2.85E-7 ± 10%	2.14E-28 ± 12%
	Adjustment 1	-	-	-
	Adjustment 2	1.40E-7 ± 6%	2.69E-7 ± 6%	2.00E-28 ± 6%
A4	Calc.	4.30E-8 ± 12%	1.36E-7 ± 13%	7.05E-29 ± 12%
	Adjustment 1	4.58E-8 ± 11%	1.40E-7 ± 10%	7.35E-29 ± 10%
	Adjustment 2	4.34E-8 ± 6%	1.31E-7 ± 6%	6.87E-29 ± 6%
A5	Calc.	2.11E-8 ± 12%	8.89E-8 ± 14%	3.85E-29 ± 12%
	Adjustment 1	-	-	-
	Adjustment 2	2.12E-8 ± 6%	8.63E-8 ± 6%	3.81E-29 ± 6%
A6	Calc.	8.80E-9 ± 13%	5.09E-8 ± 16%	1.93E-29 ± 11%
	Adjustment 1	-	-	-
	Adjustment 2	8.94E-9 ± 6%	4.94E-8 ± 6%	1.90E-29 ± 6%
A7	Calc.	2.62E-9 ± 7% +	1.51E-8 ± 5% +	5.69 E-30 ± 5% +

+ These uncertainties are stochastic only. Uncertainties on the adjusted values take into account those on the source and transmission cross-sections.

5.3.5 Results of the Linear Least-Squares Data Adjustment

The data adjustment code LONDON produces estimates of the uncertainty to be associated with individual calculated integral responses due to uncertainties in the differential data involved in the adjustments. Also calculated are the proportion of the overall uncertainties on integral responses at each location attributable to each class of differential data adjusted. The results of this latter analysis appear in Table 5.3.4.

The adjusted reaction rates appear in Table 5.3.5, where the total variances on the calculated data can be seen. The large reductions in variance seen on the calculated values of measured responses for adjustments 2 are a consequence of the inclusion of the measured data into this adjustment. Adjustment 1 represents a more testing use of the method, since data adjustments are extrapolated in space as well as energy and it can be observed that the

TABLE 5.3.4

% CONTRIBUTIONS TO TOTAL VARIANCE FOR PCA 12/13 CONFIGURATION AT THE A4 AND A7 LOCATIONS TAKEN FROM THE FIRST ADJUSTMENT

Location	Detector	Transmission	Source	M/C Stochastics	Measurement
A4	26%	65%	5%	4%	-
A7 (before adjustment)	14%	68%	11%	6%	-
A7 (after adjustment)	21%	42%	8%	20%	9%

TABLE 5.3.5

RESULTS OF LEAST-SQUARES DATA ADJUSTMENTS TO THE RADIOMETRIC RESPONSES FOR THE PCA 12/13 CONFIGURATION (REACTIONS/TARGET ATOM/CORE NEUTRON)

Location		$^{115}In(n,n')^{115m}In$	$^{58}Ni(n,p)^{58}Co$	$^{103}Rh(n,n')^{103m}Rh$	$^{27}Al(n,\alpha)^{24}Na$
A3M	Calc.	3.96E-8 ± 20%	2.63E-8 ± 11%	1.65E-7 ± 11%	3.15E-10 ± 11%
	Adjustment 1	-	-	-	-
	Adj/Exp.				
	Adjustment 2	3.92E-8 ± 5%*	2.61E-8 ± 5%*	1.64E-7 ± 6%	3.19E-10 ± 5%*
	Adj/Exp.	1.06	0.99	-	1.00
A4	Calc.	1.07E-8 ± 22%	5.39E-9 ± 17%	5.51E-8 ± 22%	7.05E-11 ± 14%
	Adjustment 1	1.08E-8 ± 10%	6.01E-9 ± 10%	5.70E-8 ± 11%	8.57E-11 ± 8.5%
	Adj/Exp.	0.96	1.04	1.01	1.18
	Adjustment 2	1.10E-8 ± 4%*	5.64E-9 ± 4%*	5.52E-8 ± 5%*	7.41E-11 ± 5%*
	Adj/Exp.	0.96	0.98	0.97	1.02
A5	Calc.	4.95E-9 ± 23%	2.08E-9 ± 21%	2.95E-8 ± 29%	2.72E-11 ± 14%
	Adjustment 1	-	-	-	-
	Adj/Exp.				
	Adjustment 2	5.15E-9 ± 4%*	2.22 E-9 ± 4%*	3.00E-8 ± 5%*	2.93E-11 ± 5%*
	Adj/Exp.	0.99	0.97	1.03	1.01
A6	Calc.	2.07E-9 ± 24%	7.63E-10 ± 25%	1.46E-8 ± 37%	9.70E-12 ± 14%
	Adjustment 1	-	-	-	-
	Adj/Exp.				
	Adjustment 2	2.19E-9 ± 5%*	8.27E-10 ± 5%*	1.47E-8 ± 5%*	1.08E-11 ± 6%*
	Adj/Exp.	0.97	1.02	0.91	0.96
A7	Calc.	6.19E-10 ± 26%	2.14E-10 ± 5%	4.30E-11	2.94E-12 ± 45%
	Adjustment 1	6.51E-10 ± 6.4%*			4.28E-12 ± 7%*
	Adj./Exp.	1.00			0.98
	Adjustment 2	-	-	-	-
	Adj./Exp.				

*These adjustments result from including measured values at locations in question.

var. ces of ~20% are reduced by a factor of two at the A4 location. Table 5.3.3 gives estimates of the adjusted damage exposure parameters. Adjustment 2 results in greater variance reduction due to the inclusion of additional measured data, and these results can be compared with those obtained from 'in-situ' adjustment codes (see section 7.1.3).

The overall consistency between measurement and calculation is extremely good. A χ^2 of 0.1 per degree of freedom is obtained for the four radiometric responses throug. ne PVS while at the void box the $^{27}Al(n,\alpha)^{24}Na$ and $^{115}In(n,n')^{115m}In$ responses give a corresponding value of 0.6.

Individual data adjustments are critically dependent on both the quality of the sensitivity and uncertainty information used in the adjustment and the extent to which the measured and calculated data used to drive the adjustment are representative of the overall agreement between calculation and measurement. Since the first adjustment does not involve a representative sample of measured data, (the A7 location being obviously subject to some inconsistency between measurements (see section 7.1.3)), the adjustments to the differential data must be regarded with some circumspection. Indeed the adjustments to individual differential data arising from the two LONDON calculations are on the whole very small and are not consistent between the two calculations. Only changes to the differential data common to both LONDON calculations are mentioned here.

The first adjustment results in a positive adjustment of ~10% to the iron elastic cross-section between 14 and 4 MeV with a corresponding negative one to the iron non-elastic cross-section. A small positive adjustment is made to the oxygen inelastic cross-section near its threshold (~1%). The second adjustments show the modifications to the iron cross-sections extending down to ~0.7 MeV but the adjustment over the 14 - 4 MeV range is now only ~5%. The adjustment to the oxygen inelastic cross-section is unchanged.

5.3.6 Conclusions

The overall consistency between the results of the repeated Monte Carlo calculation and measurement is good, except at the void box (A7) location and in the case of $^{232}Th(n,f)$, and in the case of $^{237}Np(n,f)$ at the A2 location. When these results are compared with those obtained from the original calculation (Mc81) it must be borne in mind that the latter were not corrected to allow for the variation in flux levels across a Monte Carlo scoring zone. Corrections of between 7% (at the A1 location) and 2% (at the A7 location) should be applied to correct the responses to centre line values. After this correction has been made the remaining differences between the two calculations can be accounted for by updates in the geometry which have occurred since the original calculational specification.'

The improved importance map is responsible for the reduction in stochastic uncertainties observed in this second calculation which was less costly in computer time than the original. Although the calculation still probably exhibits some tendency towards progressive underestimation with penetration through the PVS the effect is difficult to distinguish as it is of the same

order of magnitude as the uncertainties on the individual measured and calculated responses. Linear least squares data adjustments indicate that this effect, which is exhibited most strongly by the $^{27}Al(n,\alpha)^{24}Na$ reaction with its high threshold can be corrected for by decreasing the iron inelastic cross-section at high energy (14 - 4 MeV) at the expense of the elastic cross-section. The overall value of χ^2 which is 0.1 per degree of freedom suggests that there is some overestimation of the uncertainties in the differential data, but any reduction in these would leave the poorer consistency in the void box unexplained.

A data adjustment using the two measured radiometric responses in the void box (A7) to improve the estimation of parameters at the PVS (A4) location is of practical interest since such a method of adjustment could be used to correct calculated exposure damage parameters within the PVS of a power reactor. As a result of this adjustment the damage exposure parameters were increased by $\sim 2\%$ and the standard deviations of these were decreased by the same amount. Some gains would therefore be made from such an adjustment in setting limits for safety calculations at the 2σ or 3σ level. Consistency with experiment for the radiometric responses was improved except in the case of $^{27}Al(n,\alpha)^{24}Na$ which was over-adjusted to compensate for the low calculated value in the void box. A second adjustment to the 15 radiometric responses measured through the PVS resulted in small changes only to the damage exposure parameters, the largest movement being one of $\sim 2\%$ to flux > 1 MeV at the A6 location. These adjusted results had total variances of only $\sim 6\%$ and were comparable with the values obtained by using an 'in-situ' adjustment code (see section 7.1.3). The advantage of this, second, method over that of the 'in-situ' method is that the uncertainties of flux spectra in terms of standard deviations and VCV matrices are not required as input, but result implicitly from the input uncertainties on the differential data used for the Monte Carlo calculation.

5.4 BECHTEL POWER CORPORATION ANALYSIS

W. C. Hopkins (Bechtel Power Corporation)
W. L. Grove and T. E. Albert (Science Applications, Inc.)

5.4.1 Introduction

This section contains the neutron transport analyses and results performed at Bechtel Power Corporation for the PCA 8/7 and 12/13 configurations. Calculations for gamma transport and activity were not done; only total fluxes and fluxes with (E > 1 MeV) and (E > 0.11 MeV) were calculated throughout both configurations at the midplane. No attempt was made to optimize the nodalization of the source region or to correct for axial leakage.

The two-dimensional discrete ordinates transport code DOT 4.2 was used to obtain $\phi(x,y)$ in both cases. Cross sections were taken from the SAILWR cross-section library, which has a 47-neutron energy group structure. In both cases an S_6 quadrature set appropriate to x-y geometry was used. The source for the problems was input as a distributed source normalized to 1 neutron per second in the core region. The left boundary, i.e., the midline of each, was given the reflected boundary condition, while the void condition was used at the other boundaries.

The pointwise flux convergence criterion of 5×10^{-3} was met for the first 24-neutron energy groups in both analyses. A limit of 15 inner iterations was placed on the first 27-neutron energy groups. The last three energy groups, in both cases, were converged past 1×10^{-2}. It should be noted that the first 27-neutron energy groups of the 47-neutron energy group structure include all neutron energies greater than 0.1 MeV.

5.4.2 Neutron Transport Results for 8/7 and 12/13 Configurations

The flux spectra for each spatial mesh of each configuration were written on tapes. Table 5.4.1 compares the results of this analysis for fluxes with (E > 1 MeV) and (E > 0.1 MeV) to the PCA Blind Test calculated fluxes at surveillance locations A0 through A6 for the 12/13 configuration. Table 5.4.2 presents the corresponding comparison for the 8/7 configuration surveillance locations A1 through A6.

TABLE 5.4.1

COMPARISON OF CALCULATED DAMAGE CORRELATION PARAMETERS FOR PCA 12/13 CONFIGURATION

PARAMETER*	LOCATION	BECHTEL(A)	(B)**	A/B
	A0	1.28 (-4)	1.51 (-4)	0.85
ϕ(E>1.00 MeV)	A1	3.47 (-6)	3.47 (-6)	1.00
for (A) results	A2	2.83 (-7)	3.93 (-7)	0.72
	A3	8.83 (-8)	9.78 (-8)	0.90
ϕ(E>1.0 MeV)	A4	2.90 (-8)	3.87 (-8)	0.75
for (B) results	A5	1.34 (-8)	1.79 (-8)	0.75
	A6	6.07 (-9)	7.70 (-9)	0.79
ϕ(E>0.11 MeV)	A0	2.28 (-4)	2.83 (-4)	0.81
for (A) results	A1	6.08 (-6)	6.23 (-6)	0.98
	A2	6.25 (-7)	7.94 (-7)	0.79
ϕ(E>0.1 MeV)	A3	1.61 (-7)	2.05 (-7)	0.79
for (B) results	A4	9.92 (-8)	1.25 (-7)	0.79
	A5	6.66 (-8)	8.24 (-8)	0.81
	A6	3.98 (-8)	4.79 (-8)	0.83

*All results are normalized to 1.0 source neutron.
**(B) are the average results reported in Table 7.1.7 of (Mc81).

TABLE 5 4.2

COMPARISON OF CALCULATED DAMAGE CORRELATION PARAMETERS FOR PCA 8/7 CONFIGURATION

PARAMETER*	LOCATION	BECHTEL (A)	(B)**	A/B
ϕ(E>1.00 MeV)	A1	6.27 (-6)	7.42 (-6)	0.85
for (A) results	A2	6.32 (-7)	8.00 (-7)	0.79
	A3	5.06 (-7)	6.77 (-7)	0.75
ϕ(E>1.0 MeV)	A4	1.58 (-7)	2.18 (-7)	0.73
for (B) results	A5	7.37 (-8)	9.88 (-8)	0.75
	A6	3.27 (-8)	4.16 (-8)	0.79
ϕ(E>0.11 MeV)	A1	1.15 (-5)	1.41 (-5)	0.82
for (A) results	A2	1.47 (-6)	1.73 (-6)	0.85
	A3	1.13 (-6)	1.45 (-6)	0.78
ϕ(E>0.1 MeV)	A4	6.46 (-7)	7.95 (-7)	0.81
for (B) results	A5	4.31 (-7)	5.14 (-7)	0.84
	A6	2.56 (-7)	2.93 (-7)	0.87

*All results are normalized to 1.0 source neutron.
**(B) are the average results reported in Table 7.1.7 of (Mc81).

5.5 W-NTD ANALYSIS

S. Anderson (W-NTD)

This section is in preparation and will be added during a future revision of this document.

6.0 CURRENT PCA SPECIFICATIONS FOR TRANSPORT THEORY VALIDATION

E. P. Lippincott (HEDL) and F. B. K. Kam (ORNL)

This section contains the recommended measured PCA integral data to be used for comparisons with calculated results and as input for neutron spectral adjustment codes (as described in Section 7).

Section 6.1 contains recommended integral fission rates. For ^{237}Np and ^{238}U, these values are taken as an average of the fission chamber and SSTR values given in Section 2. For these two reactions, the recommended uncertainties are based on the difference from the average of the fission chamber and SSTR results; this results in nigher uncertainties than quoted for the fission chamber or SSTR results taken alone. More information is being developed on the causes of the SSTR-fission chamber differences, and this should allow these uncertainties to be reduced in the future.

Sections 6.2 and 6.3 give recommended integral reaction rate values for RM and NRE data, respectively. The radiometric results are the same as those given in Section 2.4 except that they are converted to reactions per second per core neutron. (Section 2.4 presents these results as equivalent fission rates.) The emulsion integral results duplicate those prescribed in Section 3.2.

Section 6.4 presents recommended gamma-ray dose results. The recommended results are an average of TLD results presented in (Mc81) and the Si(Li) results from Section 3.5. These two sets of results agree within experimental uncertainty.

All information necessary to calculate the PCA 8/7, 12/13, 4/12, and 4/12 SSC configurations is given in Sections 1.1 through 1.4 and 8.1 of Reference (Mc81) and Sections 1.0, 1.1, 1.2 and 5.0 of this report.

6.1 RECOMMENDED INTEGRAL RESULTS: FISSION RATE MEASUREMENTS

E. D. McGarry (NBS); F. H. Ruddy, Raymond Gold, J. H. Roberts, and C. C. Preston (HEDL); and A. Fabry (CEN/SCK)

The recommended integral fission rates for the PCA 8/7, 12/13, and 4/12 SSC configurations are contained in this section. Three measurement techniques were used, namely:

- SSTR measurements (HEDL).
- Dual fission chamber measurements (NBS).
- Miniature fission chamber measurements (CEN/SCK).

Comparisons between measurements have been made in Section 2.6. A 10% discrepancy exists between the NBS and HEDL measurements in the PVS block. Because this discrepancy cannot be resolved at this time, the block values have been linearly averaged and an additional 5% uncertainty has been added as recommended in Section 2.6. The results for ^{237}Np and ^{238}U are contained in Tables 6.1.1 and 6.1.2. In order to report SSTR fission rates as equivalent fission fluxes, the conversion factors 1.334×10^{-24} cm^2 for ^{237}Np and 3.08×10^{-25} cm^2 for ^{238}U have been used (see Section 3.2). Photofission corrections have been made (see Section 4.5).

In some locations, only SSTR or fission chamber measurements were made, and these have been included in Table 6.1.1. Unavoidably, location-to-location biases result when comparing these values with each other or the averaged values. The unaveraged fission chamber and SSTR values are contained in Sections 2.3 and 2.5, respectively.

Only SSTR fission rate measurements were made in the PCA for ^{232}Th. These results are contained in Table 6.1.2. Photofission corrections have been made using the calculations of Section 4.5. ^{237}Np and ^{238}U fission rates, corresponding to the equivalent fission fluxes of Table 6.1.1, are also included in Table 6.1.2.

TABLE 6.1.1

RECOMMENDED VALUES FOR ^{237}Np and ^{238}U (EQUIVALENT FISSION FLUXES)

Midplane Location	Distance from Core (cm)	Equivalent Fission Fluxes per PCA Core Neutron (x 10^8) ^{237}Np		^{238}U	
8/7 Configuration					
TSF (A1)	7.9	1460	(±6.2%)[a]		---
PVF (A3)	19.7	164	(±6.3%)[a]		---
1/4 T (A4)	29.5	55.4	(±10.8%)	31.2	(±10.8%)
1/2 T (A5)	34.7	31.1	(±11.1%)	13.8	(±10.9%)
3/4 T (A6)	40.1	15.7	(±10.8%)	5.5	(±11.1%)
12/13 Configuration					
TSB (A2)	23.8	54.7	(±5.3%)[b]		---
PVF (A3)	29.7	22.9	(±5.8%)[c]	19.2	(±5.8%)[b]
1/4 T (A4)	39.5	9.0	(±10.5%)	5.80	(±11.0%)
1/2 T (A5)	44.7	4.92	(±11.2%)	2.56	(±10.9%)
3/4 T (A6)	50.1	2.60	(±10.6%)	1.06	(±11.1%)
VB (A7)	59.1	0.72	(±7.3%)[c]	0.281	(±4.9%)
4/12 SSC Configuration					
SSC (A2)	15.6	626	(±4.8%)[b]	364.	(±4.8%)[b]
1/4 T (A4)	30.5	48.6	(±11.2%)	23.0	(±10.0%)
1/2 T (A5)	35.7	26.8	(±10.2%)	10.3	(±10.1%)
3/4 T (A6)	41.1	14.7	(±5.6%)[d]	4.28	(±10.3%)[d]
VB (A7)	50.1	4.01	(±5.8%)[a]	1.02	(±5.8%)[a]

[a] Only CEN/SCK fission chamber measurements were made at these locations.
[b] Only SSTR measurements were made at these locations.
[c] These were averaged CEN/SCK fission chamber and SSTR measurements (no detectable bias exists between the two measurements).
[d] Only NBS fission chamber measurements were made at these locations.

TABLE 6.1.2

RECOMMENDED VALUES FOR ^{237}Np, ^{238}U, AND ^{232}Th (FISSION RATES)

Midplane Location		Y* (cm)	Fission Rate per PCA Core Neutron (fissions/atom/neutron) x 10^{33} ^{237}Np		^{238}U		^{232}Th	
8/7 Configuration								
TSF	(A1)	7.9	19500	(±6.2%)		---		---
PVF	(A3)	19.7	2190	(±6.3%)		---		---
1/4 T	(A4)	29.5	739	(±10.8%)	96.1	(±10.8%)	21.5	(±4.8%)
1/2 T	(A5)	34.7	415	(±11.1%)	42.5	(±10.9%)	9.24	(±4.8%)
3/4 T	(A6)	40.1	209	(±10.8%)	17	(±11.1%)	3.46	(±4.8%)
VB	(A7)	49.1	---			---	0.782	(±5.0%)
12/13 Configuration								
TSB	(A2)	23.8	730	(±5.3%)		---		---
PVF	(A3)	29.7	305	(±5.8%)	59.1	(±5.8%)		---
1/4 T	(A4)	39.5	120	(±10.5%)	17.9	(±11.0%)	3.56	(±4.9%)
1/2 T	(A5)	44.7	65.6	(±11.2%)	7.88	(±10.9%)	1.55	(±5.1%)
3/4 T	(A6)	50.1	34.7	(±10.6%)	3.26	(±11.1%)	0.595	(±4.9%)
VB	(A7)	59.1	9.6	(±7.3%)	0.865	(±4.9%)	0.132	(±4.7%)
4/12 SSC Configuration								
SSC	(A2)	15.6	8350	(±4.8%)	1120	(±4.8%)		
1/4 T	(A4)	30.5	648	(±11.2%)	70.8	(±10.0%)		
1/2 T	(A5)	35.7	358	(±10.2%)	31.7	(±10.1%)		
3/4 T	(A6)	41.1	196	(±5.6%)	13.2	(±10.3%)		
VB	(A7)	50.1	53.5	(±5.8%)	3.14	(±5.8%)		

*Distance to inner face of core aluminum simulator (or window).

6.2 RECOMMENDED INTEGRAL RESULTS: RADIOMETRIC MEASUREMENTS

L. S. Kellogg (HEDL) and A. Fabry (CEN/SCK)

The recommended equivalent fission fluxes per unit core neutron source for the PCA 8/7 and 12/13 configurations and, to a limited extent, the 4/12 SSC configurations are gathered in Table 2.4.5; their relationship to absolute reaction rates is discussed in Fa81a. More extensive tabulations are found in Section 2.4. Because many experimenters are more familiar with and use reaction rates in their calculations, the data in Table 2.4.5 have been converted to reaction rates (see Table 6.2.1), using a consistent set of evaluated ^{235}U fission spectrum averaged cross sections (Gr78a); tabulated values are given at the bottom of Table 6.2.1. Validation of these conversion factors has been critically reviewed and discussed in Fa81a and in Section 2 of Mc81.

The evaluation of interlaboratory recommended values and uncertainties for radiometric measurements in PCA is rather straightforward because no significant bias is found between the results of the different experimenter teams (see Mc81, Tables 2.4.5 through 2.4.8) or between different periods of observations. This good consistency provides confidence in those data that were obtained by one team only and/or were within only one observation period. In the PVS, additional support for this consistency is obtained from the experimental evidence that fast flux gradients are independent of the specific water-steel configuration (Mc81b).

These radiometric results are recommended for use as input to PCA calculations of exposure parameters and uncertainties.

TABLE 6.2.1

RECOMMENDED VALUES FOR ^{103}Rh, ^{115}Im, ^{58}Ni, and ^{27}Al (REACTION RATES)

Midplane Location		Y[b] (mm)	Reaction Rate per PCA Core Neutron[a] $^{103}Rh(n,n')$	$^{115}In(n,n')$	$^{58}Ni(n,p)$[c]	$^{27}Al(n,\alpha)$
Core Center Configuration						
	(A0)	-205.7	(d)	(d)	2.40 E-30	1.51 E-31
4/12 SSC Configuration						
SSC	(A2)	156	2.95 E-30	7.35 E-31	2.87 E-31	2.20 E-33
1/4 T	(A4)	305	3.24 E-31	5.70 E-32	1.90 E-32	1.71 E-34
1/2 T	(A5)	357	1.80 E-31	2.73 E-32	7.64 E-33	1.53 E-34
8/7 Configuration						
TSF	(A1)	79.1	(d)	2.36 E-30	1.37 E-30	1.04 E-32
PVF	(A3M)	197.0	---	1.94 E-31	---	1.95 E-33
1/4 T	(A4)	295.0	3.46 E-31	6.41 E-32	2.65 E-32	2.48 E-34
1/2 T	(A5)	346.6	1.88 E-31	3.02 E-32	1.04 E-32	9.81 E-35
3/4 T	(A6)	401.2	9.51 E-32	1.35 E-32	3.79 E-33	3.66 E-35
VB	(A7)	491.2	2.73 E-32	3.44 E-33	9.29 E-34	1.06 E-35
12/13 Configuration						
TSF	(A1)	119.8	4.06 E-30	1.05 E-30	6.31 E-31	5.48 E-33
TSB	(A2)	238	4.50 E-31	1.14 E-31	6.72 E-32	7.16 E-34
PVF	(A3M)	297.1	1.47 E-31	3.68 E-32	2.50 E-32	3.13 E-34
1/4 T	(A4)	395.1	5.01 E-32	1.11 E-32	5.69 E-33	7.15 E-35
1/2 T	(A5)	446.7	3.24 E-32	5.20 E-33	2.25 E-33	2.92 E-35
3/4 T	(A6)	501.3	1.67 E-32	2.23 E-33	7.99 E-34	1.12 E-35
VB	(A7)	591.3	4.83 E-33	6.43 E-34	---	4.29 E-36
^{235}U Fission Spectrum-Averaged Cross Sections						
			733 ± 38 mb	189 ± 8 mb	108.5 ± 5.4 mb	0.705 ± 0.040 mb

(a) Uncertainty estimates are based on experimental precision only, as defined in Fa81a; and overall combined uncertainties are ~±6% for a precision of ±1% (see Mc81, Tables 2.4.8 and 2.4.9).

(b) Distance to inner face of core aluminum simulator (or window).

(c) All Mol nickel data were increased by 1.0% when deriving weighted best values by combination with HEDL data or whenever HEDL data were not available; this introduces 1% difference to all the nickel tabulations of Mc81, Section 2.

(d) Measurements are available, but analyses or evaluations are still in progress.

(e) Interpolated value.

6.3 RECOMMENDED INTEGRAL RESULTS: NUCLEAR RESEARCH EMULSION MEASUREMENTS

Raymond Gold, J. H. Roberts, C. P. Preston and F. H. Ruddy (HEDL)

As derived in earlier work (Go81d,Go81e,Go83), nuclear research emulsion (NRE) measurements can be used to determine two different absolute proton-recoil reaction rates, $I(E_{min})$ and $J(E_{min})$. These reaction rates are defined by the relations:

$$I(E_{min}) = \int_{E_{min}}^{\infty} \frac{\sigma_{n,p}(E)}{E} \phi(E)\, dE \qquad (1)$$

and

$$J(E_{min}) = \int_{E_{min}}^{\infty} \left(1 - \frac{E_{min}}{E}\right) \sigma_{n,p}(E)\, \phi(E)\, dE \qquad (2)$$

Here the hydrogen scattering cross section $\sigma_{n,p}(E)$ is given by (Ga61 and Ba73).

$$\sigma_{n,p}(E) = 3\pi\left[1.206\, E_n + \left(-1.860 + 0.941491\, E_n + 0.000130658\, E_n^{\,2}\right)^2\right]^{-1} + \pi\, 1.206\, E_n + (0.4223 + 0.1300\, E_n)^2\,^{-1} \qquad (3)$$

where E is in MeV and $\sigma_{n,p}$ is in barns.

It is evident from the least-squares' analysis given in Section 7.1.1 that an absolute bias of ~50% exists in the NRE results obtained from the 1981 irradiations in the PCA. Extensive efforts have now been launched to uncover the source of this systematic effect. In spite of this apparent bias, use of the 1981 integral mode NRE data in least squares' analysis of the 12/13 configuration produces a significant reduction in overall uncertainty (see Section 7.1.1). For the sake of convenience, these 1981 integral mode NRE results for the PCA are repeated, in Table 6.3.1 below. For use in least-squares' analyses of the PCA experiment, it is recommended that all NRE data given in Table 6.3.1 be decreased by 50%.

TABLE 6.3.1

RECOMMENDED I- AND J-INTEGRAL REACTION RATES FOR THE 1981 NRE EXPOSURES IN THE PCA

Emul No./ Config-uration	Location/ Distance from Core Center (cm)	I-Integral [protons/(MeV)(at.)(W-s)]				J-Integral [protons/(at.)(W-s)]			
		Energy (MeV)	Integral	Statistical Uncertainty (%)	Total* Uncertainty (%)	Energy (MeV)	Integral	Statistical Uncertainty (%)	Total* Uncertainty (%)
W9	TSB	0.4467	1.81×10^{-19}	6.61	8.10	0.4073	1.18×10^{-19}	3.19	5.67
		0.5198	1.73×10^{-19}	5.82	7.48	0.4837	1.05×10^{-19}	3.40	5.79
12/13	23.8	0.5877	1.59×10^{-19}	5.19	7.00	0.5540	9.37×10^{-20}	3.58	5.90
		0.6515	1.42×10^{-19}	5.36	7.12	0.6197	8.52×10^{-20}	3.76	6.01
		0.7119	1.21×10^{-19}	7.42	8.78	0.6197			
K4A	1/4 T	0.4467	4.58×10^{-20}	6.79	8.25	0.4073	2.15×10^{-20}	3.11	5.63
		0.5198	4.18×10^{-20}	4.55	6.53	0.4837	1.78×10^{-20}	3.41	5.80
12/13	39.5	0.5877	3.63×10^{-20}	5.17	6.98	0.5540	1.47×10^{-20}	3.77	6.02
		0.6515	2.96×10^{-20}	6.72	8.19	0.6197	1.27×10^{-20}	4.06	6.20
		0.7119	2.19×10^{-20}	7.47	8.82				
K5A	1/2 T	0.4467	3.31×10^{-20}	5.80	7.46	0.4073	1.21×10^{-20}	3.11	5.63
		0.5198	2.61×10^{-20}	4.42	6.44	0.4837	9.64×10^{-20}	3.50	5.85
12/13	44.7	0.5877	1.96×10^{-20}	5.39	7.14	0.5540	7.81×10^{-21}	3.88	6.09
		0.6515	1.47×10^{-20}	7.42	8.78	0.6197	6.53×10^{-21}	4.25	6.33
		0.7119	1.15×10^{-20}	7.94	9.22				
K6A	3/4 T	0.4467	1.99×10^{-20}	4.99	6.85	0.4073	6.61×10^{-21}	3.15	5.65
		0.5198	1.61×10^{-20}	4.00	6.17	0.4837	5.08×10^{-21}	3.59	5.91
12/13	50.1	0.5877	1.25×10^{-20}	5.50	7.23	0.5540	3.96×10^{-21}	4.07	6.21
		0.6511	9.40×10^{-21}	5.51	7.23	0.6197	3.14×10^{-21}	4.58	6.55
		0.7119	7.08×10^{-21}	7.00	8.43				
K7A	VB	0.4467	6.18×10^{-21}	5.23	7.02	0.4073	2.28×10^{-21}	4.21	6.30
		0.5198	5.62×10^{-21}	4.89	6.78	0.4837	1.81×10^{-21}	4.88	6.77
12/13	59.1	0.5877	4.87×10^{-21}	4.63	6.59	0.5540	1.41×10^{-21}	5.80	7.46
		0.6511	3.93×10^{-21}	4.62	6.58	0.6197	1.08×10^{-21}	6.74	8.21
		0.7119	2.84×10^{-21}	4.86	6.75				
K4B	1/4 T	0.4467	2.82×10^{-19}	6.60	8.10	0.4073	1.24×10^{-19}	3.11	5.63
		0.5198	2.47×10^{-19}	4.55	6.53	0.4837	1.01×10^{-19}	3.45	5.82
8/7	39.5	0.5877	2.09×10^{-19}	5.31	7.08	0.5540	8.48×10^{-20}	3.77	6.02
		0.6511	1.72×10^{-19}	6.86	8.31	0.6197	7.19×10^{-20}	4.10	6.23
		0.7119	1.36×10^{-19}	7.26	8.64				

*Does not include an estimated 6% for power normalization.

6.4 RECOMMENDED INTEGRAL RESULTS: GAMMA MEASUREMENTS

Raymond Gold (HEDL)

In the case of gamma-ray measurements, an integral reaction rate corresponds to an observed gamma-ray dose rate. The most comprehensive gamma-ray dose rate results have been obtained for the 4/12 SSC configuration. Measurements and calculations for this configuration have already been summarized in Table 4.3.2. These data reveal an inconsistency between calculated and experimental results, with good agreement attained at the 1/4 T and 3/4 T locations but poor agreement at the 1/2 T and VB locations.

In view of this inconsistency, the recommended gamma-ray dose rates given in Table 6.4.1 are based solely upon experimental results. These recommended values are simply the average obtained from the results of the two independent experimental techniques, namely TLD and Si(Li) dosimetry, which are in good agreement at all 4/12 SSC locations. Based on the experimental uncertainties of these two methods, as well as the uncertainty that exists in PCA power level measurements, the overall experimental uncertainty of these recommended values is estimated to be $\sim$10% (1σ).

TABLE 6.4.1

RECOMMENDED GAMMA-RAY DOSE RATES FOR THE 4/12 SSC CONFIGURATION

Midplane Location	Gamma-Ray Dose Rate*
1/4 T (A4)	233
1/2 T (A5)	66.7
3/4 T (A6)	20.3
VB (A7)	11.3

*Dose Rates in mrad/h at 1-W PCA power. To convert these values to mrad per hour per PCA core neutron per second, multiply by 1.324×10^{-11}.

7.0 COMPARISON AND EVALUATION OF EXPERIMENTAL AND DERIVED DATA

E. P. Lippincott (HEDL), F. W. Stallmann (ORNL), and
A. F. Thomas (RR&A)

In this section, recommended experimental data from Section 6.0 are used together with calculated neutron flux-spectra to produce best (in a least-squares sense) estimates of exposure parameter values and uncertainties. Three independent evaluations were carried out by HEDL, ORNL, and RR&A. Results of these evaluations have indicated that exposure parameters can be determined to accuracies down to the 5% range for the best situations, and elimination of some data inconsistencies could result in even lower uncertainties. These PCA physics-dosimetry studies and results provide users of the set of 21 ASTM standards (Figure S.1) and reference data obtained from benchmark facilities (Tables S.1 and S.2) with 1) significant information and guidelines to maintain and improve the accuracy of neutron exposure determinations for LWR surveillance programs and 2) reliably tested procedures and data for the quantification of uncertainties in these determinations.

7.1 CONSISTENCY OF EXPERIMENTAL AND DERIVED DATA

E. P. Lippincott (HEDL), F. W. Stallmann (ORNL), A. F. Thomas (RR&A)

Independent analyses and comparisons of the experimental data and calculations have been completed by HEDL, ORNL, and RR&A and are discussed in Sections 7.1.1 through 7.1.3, respectively. In general, the results of the three analyses indicate that the reactor physics calculations appear to be biased on the low side, and that the recommended experimental data are self-consistent within assigned uncertainties. It was not possible to reach any definitive conclusions with regard to the accuracy of the fission chamber versus the SSTR results. The chamber measurements appear to be more consistent with the radiometric measurements, but the SSTR results are closer to the calculation. Only HEDL looked at the proton recoil emulsion (NRE) integral results and found that the most recent experimental results appear to be significantly biased (on the high side) with repect to the other measurements, although the NRE values appear to be very self-consistent. Resolution and removal of this bias are important because the NRE provide step-wise (~0.1 MeV) absolute integral reaction rate data in the very important 0.4- to 0.8-MeV neutron energy region. It is expected that HEDL (NRE) and UKAEA [hydrogen proportional-counter techniques (covering the energy range 0.1 to 0.2 MeV) and NE213 spectrometer (covering the range 2 to 10 MeV)] results obtained in the Winfrith "PCA Replica" experiment will help in the resolution of this problem (Bu84,Mc84).

Derived exposure parameter values based on the results of the three independent least-squares analyses of the experimental data and reactor physics calculations are discussed and/or reported in Section 7.2.

7.1.1 Data Consistency -- HEDL Analysis

E. P. Lippincott (HEDL)

7.1.1.1 Introduction

In the previous PCA report (Mc81) least-squares analyses of the 12/13 and 8/7 configurations were reported. These least-squares analyses utilized the FERRET (Sc79) code to derive a "best fit" neutron flux spectrum at each location using as input a calculated neutron flux spectrum; integral solid state track recorder (SSTR), fission chamber (FC), radiometric (RM), and nuclear research emulsion (NRE) measurements, and neutron spectrum measurements, together with reaction cross sections and uncertainty estimates including covariances. In this first study, discrepancies were found in the data and, in general, data discrepancies larger than the quoted experimental uncertainty were prevalent.

In the present report, an updated least-squares analysis is discussed which focuses on the updated results reported in this document. Several modifications to the least-squares procedure have been made to simplify the analysis.

These include treating each spectrum separately (and not referencing the data to the fission spectrum) and collapsing cross-section correction factors for each spectrum to improve the broad group cross section accuracy. Differential data were not included in the present HEDL study.

7.1.1.2 Calculated Neutron Spectra

Calculated neutron spectra for the PCA 12/13 and 4/12 SSC configurations were obtained from ORNL. (See Section 5.1.) The 12/13 calculation was a 47 group calculation covering the entire neutron spectrum extending to thermal energies. However, the 4/12 calculation used 102 groups to cover only the energy range from 0.098 to 16.5 MeV (similar to the calculation for the PSF). This is an adequate procedure since no reactions used in the least-squares analysis had any significant response below ~0.4 MeV.

Although the absolute calculated flux has little impact on the least-squares result, it lends confidence to the result if the calculation and adjusted results are close. Comparisons of the calculated and adjusted flux >1.0 MeV are shown in Table 7.1.1.1. It is noted that the calculation is quite close to the measurements and variations from position to position are within ~5% to 20% for the 1/4 T, 1/2 T, and 3/4 T locations for both configurations.

7.1.1.3 Radiometric Data

The radiometric data were converted to reactions per second per core neutron for input to FERRET. Uncertainties were increased from the quoted measurement uncertainties to cover relative normalization and systematic effects. The radiometric uncertainties used were all 6% to 7%, and the data were found to be consistent within these uncertainties with the a priori input calculational results.

Cross sections for the radiometric and fission reactions were obtained from ENDF/B-V. The rhodium reaction was not used. Covariances were also obtained from ENDF/B-V or other sources and are the same as those being used for the PSF analyses. Cross-section uncertainties do not have a significant impact on the PCA results.

7.1.1.4 Fission Rate Data

The fission rates were taken as averages of the SSTR and fission chamber results, and the uncertainty in these average rates was taken to be 11%. These values were also converted to fissions per second per core neutron for input to FERRET. If only SSTR results were available, as with ^{232}Th, the SSTR fission rate value was used but the uncertainty was assumed to still be 11%.

TABLE 7.1.1.1

COMPARISON OF CALCULATED AND MEASURED FLUX >1.0 MeV

Midplane Location	Calculated Flux >1.0 MeV n/cm² per Core Neutron	FERRET Flux >1.0 MeV n/cm² per Core Neutron	FERRET/ Calculated Flux
	PCA 12/13 Configuration		
1/4 T	4.13 E-8	4.58 E-8	1.11
1/2 T	1.90 E-8	2.21 E-8	1.16
3/4 T	8.00 E-9	9.82 E-9	1.23
	PCA 4/12 SSC Configuration		
1/4 T	2.18 E-7	2.34 E-7	1.07
1/2 T	1.00 E-7	1.15 E-7	1.14
3/4 T	4.33 E-8	4.87 E-8	1.12

The fission rates for ^{237}Np and ^{238}U were found to be consistent with the radiometric data, but the ^{232}Th fission rate was consistently low (14% to 16% compared with the average fission rate data, and 6% compared with SSTR data). This could indicate a slight problem with the ^{232}Th cross section or may be in part due to an overestimation of the photofission contribution.

The input data are not adequate to unambiguously choose between the SSTR and fission chamber results. A comparison of results using SSTR data and averaged SSTR and fission chamber data is shown in Table 7.1.1.2. Use of the SSTR data result in a decrease in exposure parameter values of 4% to 7%. A corresponding effect in the opposite direction occurs if the fission chamber data are used. If the uncertainties in the fission rate data are lowered to 5% to 7% (as could be justified using each set of data alone), the uncertainty on flux (E > 1.0) is lowered from 7% to 5%, on flux (E > 0.1) from 14% to 13% and for dpa from 8% to 7% for he typical case.

7.1.1.5 Emulsion Data

The emulsion data are presented in the form of integral data. These data were converted to reactions per core neutron for input to FERRET. Group

TABLE 7.1.1.2

COMPARISON OF FERRET DERIVED EXPOSURE PARAMETER VALUES FOR AVERAGE* AND SSTR FISSION RATES FOR PCA 12/13 CONFIGURATION

Midplane Location	Value Based on Average Fission Rate	Value Based on SSTR Fission Rate	Difference (SSTR-Average) (%)
	ϕ(E > 1.0 MeV) n/cm^2 per Core Neutron		
1/4 T	4.58 E-8	4.36 E-8	-5
1/2 T	2.21 E-8	2.08 E-8	-6
3/4 T	9.82 E-9	9.39 E-9	-5
	ϕ(E > 0.1 MeV) n/cm^2 per Core Neutron		
1/4 T	1.44 E-7	1.39 E-7	-4
1/2 T	9.73 E-8	9.12 E-8	-7
3/4 T	5.93 E-8	5.63 E-8	-5
	dpa per Core Neutron		
1/4 T	7.45 E-29	7.16 E-29	-4
1/2 T	4.22 E-29	3.96 E-29	-7
3/4 T	2.25 E-29	2.14 E-29	-5

*Linear average of SSTR and fission chamber results given as recommended values in Section 6.

cross sections were constructed for FERRET for the I and J integral values. For energy groups above the threshold, the group-averaged cross section for the I integral is given by

$$\bar{\sigma}_i = \int_{E_1}^{E_2} \frac{\sigma_{np}}{E} \phi(E)dE \Big/ \int_{E_1}^{E_2} \phi(E)dE \quad . \qquad (1)$$

where E_1 and E_2 are the energy boundaries of group i and σ_{np} is the proton scattering cross section. The I integral is then calculated by summing $\sigma_j\phi_j$ over all groups (similar to the other reaction rates). The corresponding J integral group averaged cross section is

$$\bar{\sigma}_j = \int_{E_1}^{E_2} \frac{\sigma_{np}}{E} (E - E_{th})\ \phi(E)dE \Big/ \int_{E_1}^{E_2} \phi(E)dE \qquad (2)$$

where E_{th} is the energy threshold. For groups below the threshold, $\bar{\sigma}_j = 0$ and for the group including the threshold a suitable interpolation is used.

The emulsion data for the three 12/13 positions were found to be consistently biased with respect to the other data. Both the I and J integrals appeared self-consistent but high by about 50%. No explanation for this bias is currently available. In contrast, previously reported (Mc81) preliminary measured-perturbed* I and J integral results for the 1/4 T position for the 8/7 configuration were ~20% low. At the time this earlier analysis was performed, the 20% difference was concluded to be in reasonable agreement since this was about a 2σ error.

Because this result is not understood, the emulsion data were not used in the derivation of the recommended exposure parameter values given in Section 7.2.1. However, an investigation was carried out to determine the effect of the emulsion data on the exposure parameters and uncertainties. If the data were renormalized and the quoted experimental uncertainties are used, the emulsion data increases the flux (E > 1.0) by about 3% and decreases the flux (E > 0.1) by about the same margin. The dpa is not affected significantly. The uncertainties on flux (E > 1.0) and dpa are lowered significantly to ~3%, and the uncertainty on flux (E > 0.1) is lowered to 6%. Thus the emulsion data have the potential to make a very real contribution to measurement accuracy. It should be noted, however, that the improvement observed here may be overestimated since the nine emulsion integral results (for the approximate thresholds of 0.40, 0.45, 0.50, 0.60, 0.65 and 0.70) were treated as a set of independent measurements.

---

*No perturbation correction was made for the effect of the proton-recoil chamber (~2.5-cm diameter cylinder) in which the NREs were exposed. The British (Bu84) have studied the perturbation effect of rather large voids (4.7- and 6.6-cm diameter holes) for the "PCA 12/13 Replica" experiment at the 1/4 T position and find ratios of solid/hole for Rh of 0.92 ± 3% and 0.85 ± 3%, for In of 0.83 ± 3% and 0.80 ± 3%, and for S of 0.77 $\mp$ 3% and 0.76 $\mp$ 3%, respectively. The perturbation correction for the NRE measurements in the ~2.5-cm diameter cylindrical proton recoil chamber would be expected to be smaller. For the present series of NRE exposures discussed in this report, the irradiations were accomplished in small Cd boxes to further minimize perturbation effects.

7.1.1.6 Neutron Spectra

The a priori and adjusted neutron spectra and uncertainties for the 12/13 and 4/12 SSC configurations are given in Tables 7.1.1.3 through 7.1.1.8. Only the 22 energy groups above 0.0674 MeV are given. The uncertainties of the five to six lowest energy groups are higher since the reaction rates utilized have essentially no response below ~0.4 MeV. These uncertainties, therefore, are determined by the input assumptions rather than any real correlations.

7.1.1.7 Conclusions

The present status of the data allows for PCA exposure parameters to be determined to 1σ accuracies of 7% to 16%. Data inconsistencies are present that currently limit the improvement of this accuracy. If these inconsistencies can be removed, improvements in accuracy by a factor of 2 could be attained. The PCA data then could be applied to further improve the presently quoted 8% to 12% uncertainties for the PSF physics-dosimetry results as well as contribute to an improved overall accuracy for derived exposure parameter values for LWR surveillance programs.

TABLE 7.1.1.3

FERRET-SAND II RESULTS FOR PCA 12/13 CONFIGURATION, POSITION A4 (1/4 T)

Group	Energy* (MeV)	A Priori Flux (n/cm²/sec)**	Adjusted Flux (n/cm²/sec)**	% Uncertainty (1σ)
1	1.492 + 01	3.865 - 12	4.060 - 12***	20
2	1.350 + 01	9.444 - 12	9.968 - 12	18
3	1.162 + 01	4.301 - 11	4.560 - 11	16
4	1.000 + 01	1.076 - 10	1.145 - 10	14
5	8.607 + 00	2.594 - 10	2.771 - 10	12
6	7.408 + 00	4.622 - 10	4.965 - 10	12
7	6.065 + 00	1.131 - 09	1.227 - 09	12
8	4.966 + 00	1.610 - 09	1.772 - 09	12
9	3.679 + 00	2.972 - 09	3.279 - 09	12
10	2.865 + 00	3.144 - 09	3.423 - 09	12
11	2.231 + 00	6.018 - 09	6.475 - 09	12
12	1.738 + 00	6.978 - 09	7.387 - 09	12
13	1.353 + 00	8.305 - 09	8.717 - 09	13
14	1.108 + 00	7.648 - 09	8.081 - 09	15
15	8.208 - 01	1.251 - 08	1.315 - 08	16
16	6.393 - 01	1.354 - 08	1.414 - 08	18
17	4.979 - 01	1.455 - 08	1.514 - 08	20
18	3.877 - 01	9.589 - 09	9.959 - 09	22
19	3.020 - 01	1.618 - 08	1.679 - 08	23
20	1.832 - 01	1.581 - 08	1.641 - 08	25
21	1.111 - 01	1.478 - 08	1.536 - 08	26
22	6.738 - 02	9.220 - 09	9.597 - 09	28

*Lower bound of each energy group.

**Per core neutron per second.

***$4.060 - 12 \equiv 4.060 \times 10^{-12}$.

TABLE 7.1.1.4

FERRET-SAND II RESULTS FOR PCA 12/13 CONFIGURATION, POSITION A5 (1/2 T)

Group	Energy (MeV)	A Priori Flux (n/cm²/sec)*	Adjusted Flux (n/cm²/sec)*	% Uncertainty (1σ)
1	1.492 + 01	1.604 - 12	1.744 - 12	20
2	1.350 + 01	3.928 - 12	4.299 - 12	18
3	1.162 + 01	1.767 - 11	1.947 - 11	16
4	1.000 + 01	4.272 - 11	4.742 - 11	14
5	8.607 + 00	1.008 - 10	1.126 - 10	12
6	7.408 + 00	1.733 - 10	1.955 - 10	12
7	6.065 + 00	4.053 - 10	4.646 - 10	12
8	4.966 + 00	5.546 - 10	6.463 - 10	12
9	3.679 + 00	1.018 - 09	1.192 - 09	12
10	2.865 + 00	1.166 - 09	1.348 - 09	12
11	2.231 + 00	2.501 - 09	2.857 - 09	12
12	1.738 + 00	3.070 - 09	3.433 - 09	12
13	1.353 + 00	4.006 - 09	4.413 - 09	13
14	1.108 + 00	4.076 - 09	4.499 - 09	14
15	8.208 - 01	7.658 - 09	8.362 - 09	15
16	6.393 - 01	9.143 - 09	9.870 - 09	17
17	4.979 - 01	1.049 - 08	1.124 - 08	19
18	3.877 - 01	6.938 - 09	7.401 - 09	21
19	3.020 - 01	1.333 - 08	1.418 - 08	22
20	1.832 - 01	1.201 - 08	1.276 - 08	24
21	1.111 - 01	1.192 - 08	1.267 - 08	26
22	6.738 - 02	7.253 - 09	7.722 - 09	27

*Per core neutron per second.

TABLE 7.1.1.5

FERRET-SAND II RESULTS FOR PCA 12/13 CONFIGURATION, POSITION A6 (3/4 T)

Group	Energy (MeV)	A Priori Flux (n/cm²/sec)*	Adjusted Flux (n/cm²/sec)*	% Uncertainty (1σ)
1	1.492 + 01	6.373 - 13	7.176 - 13	20
2	1.350 + 01	1.562 - 12	1.768 - 12	18
3	1.162 + 01	6.925 - 12	7.876 - 12	16
4	1.000 + 01	1.611 - 11	1.843 - 11	14
5	8.607 + 00	3.706 - 11	4.267 - 11	12
6	7.408 + 00	6.130 - 11	7.133 - 11	12
7	6.065 + 00	1.369 - 10	1.618 - 10	12
8	4.966 + 00	1.806 - 10	2.170 - 10	13
9	3.679 + 00	3.306 - 10	4.003 - 10	12
10	2.865 + 00	4.031 - 10	4.856 - 10	12
11	2.231 + 00	8.727 - 10	1.046 - 09	12
12	1.738 + 00	1.233 - 09	1.457 - 09	12
13	1.353 + 00	1.727 - 09	2.018 - 09	12
14	1.108 + 00	1.913 - 09	2.249 - 09	14
15	8.208 - 01	4.104 - 09	4.792 - 09	15
16	6.393 - 01	5.302 - 09	6.125 - 09	16
17	4.979 - 01	6.380 - 09	7.317 - 09	18
18	3.877 - 01	4.204 - 09	4.800 - 09	20
19	3.020 - 01	8.559 - 09	9.732 - 09	22
20	1.832 - 01	7.570 - 09	8.587 - 09	23
21	1.111 - 01	7.708 - 09	8.731 - 09	25
22	6.738 - 02	4.282 - 09	4.848 - 09	26

*Per core neutron per second.

TABLE 7.1.1.6

FERRET-SAND II RESULTS FOR PCA 4/12 SSC CONFIGURATION,
POSITION A4 (1/4 T)

Group	Energy (MeV)	A Priori Flux (n/cm²/sec)*	Adjusted Flux (n/cm²/sec)*	% Uncertainty (1σ)
1	1.492 + 01	5.414 - 12	5.861 - 12	21
2	1.350 + 01	1.760 - 11	1.915 - 11	19
3	1.162 + 01	8.382 - 11	9.162 - 11	17
4	1.000 + 01	2.415 - 10	2.648 - 10	15
5	8.607 + 00	5.992 - 10	6.582 - 10	12
6	7.408 + 00	1.141 - 09	1.252 - 09	12
7	6.065 + 00	2.856 - 09	3.124 - 09	12
8	4.966 + 00	4.383 - 09	4.769 - 09	13
9	3.679 + 00	9.685 - 09	1.047 - 08	12
10	2.865 + 00	1.356 - 08	1.446 - 08	12
11	2.231 + 00	2.829 - 08	2.972 - 08	12
12	1.738 + 00	3.685 - 08	3.786 - 08	12
13	1.353 + 00	4.822 - 08	4.896 - 08	13
14	1.108 + 00	5.357 - 08	5.430 - 08	14
15	8.208 - 01	8.051 - 08	8.070 - 08	15
16	6.393 - 01	1.080 - 07	1.073 - 07	17
17	4.979 - 01	1.105 - 07	1.093 - 07	19
18	3.877 - 01	7.654 - 08	7.577 - 08	21
19	3.020 - 01	1.221 - 07	1.210 - 07	23
20	1.832 - 01	1.199 - 07	1.192 - 07	24
21	1.111 - 01	1.061 - 07	1.059 - 07	26
22	6.738 - 02	4.196 - 08	4.209 - 08	27

*Per core neutron per second.

TABLE 7.1.1.7

FERRET-SAND II RESULTS FOR PCA 4/12 SSC CONFIGURATION,
POSITION A5 (1/2 T)

Group	Energy (MeV)	A Priori Flux (n/cm²/sec)*	Adjusted Flux (n/cm²/sec)*	% Uncertainty (1σ)
1	1.492 + 01	2.141 - 12	2.361 - 12	21
2	1.350 + 01	6.952 - 12	7.725 - 12	19
3	1.162 + 01	3.352 - 11	3.753 - 11	17
4	1.000 + 01	9.387 - 11	1.059 - 10	15
5	8.607 + 00	2.280 - 10	2.589 - 10	12
6	7.408 + 00	4.188 - 10	4.787 - 10	12
7	6.065 + 00	1.005 - 09	1.157 - 09	12
8	4.966 + 00	1.477 - 09	1.710 - 09	13
9	3.679 + 00	3.243 - 09	3.757 - 09	12
10	2.865 + 00	4.830 - 09	5.550 - 09	12
11	2.231 + 00	1.089 - 08	1.238 - 08	12
12	1.738 + 00	1.564 - 08	1.737 - 08	12
13	1.353 + 00	2.237 - 08	2.444 - 08	12
14	1.108 + 00	2.810 - 08	3.043 - 08	14
15	8.208 - 01	4.701 - 08	4.993 - 08	15
16	6.393 - 01	6.771 - 08	7.059 - 08	16
17	4.979 - 01	7.735 - 08	7.975 - 08	18
18	3.877 - 01	5.286 - 08	5.432 - 08	20
19	3.020 - 01	9.323 - 08	9.538 - 08	22
20	1.832 - 01	8.349 - 08	8.534 - 08	23
21	1.111 - 01	7.642 - 08	7.821 - 08	25
22	6.738 - 02	2.638 - 08	2.709 - 08	26

*Per core neutron per second.

TABLE 7.1.1.8

FERRET-SAND II RESULTS FOR PCA 4/12 SSC CONFIGURATION,
POSITION A6 (3/4 T)

Group	Energy (MeV)	A Priori Flux (n/cm²/sec)*	Adjusted Flux (n/cm²/sec)*	% Uncertainty (1σ)
1	1.492 + 01	8.152 - 13	8.871 - 13	31
2	1.350 + 01	2.653 - 12	2.899 - 12	30
3	1.162 + 01	1.292 - 11	1.417 - 11	29
4	1.000 + 01	3.506 - 11	3.861 - 11	27
5	8.607 + 00	8.311 - 11	9.187 - 11	26
6	7.408 + 00	1.469 - 10	1.629 - 10	24
7	6.065 + 00	3.370 - 10	3.743 - 10	22
8	4.966 + 00	4.749 - 10	5.274 - 10	20
9	3.679 + 00	1.032 - 09	1.145 - 09	18
10	2.865 + 00	1.626 - 09	1.798 - 09	17
11	2.231 + 00	3.926 - 09	4.327 - 09	15
12	1.738 + 00	6.124 - 09	6.715 - 09	13
13	1.353 + 00	9.455 - 09	1.027 - 08	13
14	1.108 + 00	1.330 - 08	1.424 - 08	14
15	8.208 - 01	2.482 - 08	2.626 - 08	14
16	6.393 - 01	3.778 - 08	3.960 - 08	15
17	4.979 - 01	4.758 - 08	4.956 - 08	16
18	3.877 - 01	3.139 - 08	3.264 - 08	18
19	3.020 - 01	6.048 - 08	6.269 - 08	20
20	1.832 - 01	5.119 - 08	5.302 - 08	22
21	1.111 - 01	4.828 - 08	5.002 - 08	24
22	6.738 - 02	1.520 - 08	1.578 - 08	26

*Per core neutron per second.

7.1.2 Data Consistency -- ORNL Analysis

F. W. Stallmann (ORNL)

7.1.2.1 Summary

Experimental data combined with transport calculations were analyzed using the LSL-M2 adjustment procedure. This procedure allows simultaneous processing of several related neutron spectra with corresponding dosimetry data and gives estimates of exposure parameter values for any selected location with uncertainties. Dosimetry data were obtained from the recommended values in Sections 6.1, 6.2, and 4.5 for ^{235}U. The transport calculations of Section 5.1 were used for the PCA 12/13 and PCA 4/12 SSC configurations. The Blind Test calculations B and C were used for the PCA 8/7 configuration. The results for exposure parameter values are given in Table 7.1.2.1. These results are fairly insensitive against changes in the input correlations regarding the transport calculations as shown in Table 7.1.2.2.

The input data and uncertainties are consistent within statistical bounds with most values of chi-square below the expected values, indicating somewhat conservative input uncertainties. In particular, the analysis provides no clear cut indication in favor of either the fission chamber or SSTR measurements. Individually, only one adjustment clearly exceeds the assigned uncertainties, namely the $^{237}Np(n,f)$ measurement at TSB in PCA 12/13, which appears to be low by about 20%. Most $^{232}Th(n,f)$ measurements in PCA 12/13 appear also to be on the low side. Changes in the apparently inconsistent data do not affect the output exposure parameters by more than the output uncertainties. The only exception is TSB in PCA 12/13 in which the elimination of $^{237}Np(n,f)$ raises the values by about 8%. It is, therefore, recommended to use a mean value of the two outputs with and without ^{237}Np and to raise the standard deviation to 8%.

The new exposure parameter values are consistent with earlier ORNL results (Table 7.3.1 of Mc81) but with considerably smaller uncertainties, which reflect the better calculations and the more elaborate adjustment procedure.

7.1.2.2 Input Data and Uncertainties

The LSL-M2 adjustment procedure accepts both absolute and fission-equivalent dosimetry data. The latter requires as input a reference fission spectrum. The NBS ^{235}U fission spectrum in the IRDF-82 file was used for equivalent fission reactions of $^{103}Rh(n,n')$, $^{115}In(n,n')$, $^{58}Ni(n,p)$, $^{27}Al(n,\alpha)$, $^{237}Np(n,f)$, and $^{238}U(n,f)$. The $^{232}Th(n,f)$ and $^{235}U(n,f)$, bare and cadmium-covered, were available only as absolute reaction rates. The fission reactions were corrected for photofission according to the recommendations given in Section 4.5. A 6%, one standard deviation uncertainty was assigned to all non-fission reactions and 10% to the fission reactions.

The adjustment procedure was based on a 30-energy group structure, which was obtained from the calculation in Section 5.1.1 by condensing all groups below 0.1 MeV to 2 groups, one above and one below the cadmium cutoff at 0.414 eV. Dosimetry cross sections from the IRDF-82 file were processed and reduced to the above group structure using the PUFF processing code. Cross-section variances and covariances were obtained by the same code.

Calculations for the PCA 4/12 SSC (Section 5.1.2) and PCA 8/7 (Blind Test calculations B and C, found in Mc81) were interpolated to the same group structure. A 95% correlation was assumed between fluences of adjacent groups, except the 2 lowest ones, diminishing exponentially with the distance between groups. Correlations between spectra at different locations range from 95% to 75% depending on the distance between locations. Changing these correlations has very little influence on the results as can be seen in Table 7.1.2.2. Uncertainties for the group fluences individually were assigned as follows: for the PCA 12/13 and PCA 4/12 SSC 10%, one standard deviation above 1 MeV, 15% between 1 MeV and 0.1 MeV, and 50% for the 2 lowest energy groups. These values were increased to 30%, 40%, and 300%, respectively, for the PCA 8/7.

The LSL-M2 procedure includes an option for "scaling," i.e., the calculated spectrum may be multiplied by an unrestricted factor in order to better fit the dosimetry data. In other words, in this option only the shape of the calculated spectrum and not its magnitude is used. It can be assumed that the results of the procedure with scaling is somewhat more realistic; however, no large differences are found between scaled and non-scaled results (Table 7.1.2.2).

TABLE 7.1.2.1

RECOMMENDED EXPOSURE PARAMETER VALUES FOR THE PCA BENCHMARK CONFIGURATIONS BASED ON LSL-M2 ADJUSTMENT ANALYSIS

	Fluence > 1.0 MeV		Fluence > 0.1 MeV		dpa	
	Value	% Std.	Value	% Std.	Value	% Std.
PCA 12/13:						
TSF	3.55-6	4.4	6.33-6	5.2	5.52-27	4.0
TSB	3.85-7	8.0	7.66-7	8.0	5.98-28	8.0
PVF	1.24-7	4.3	2.19-7	5.0	1.96-28	4.0
1/4 T	4.22-8	3.9	1.35-7	5.3	7.03-29	4.0
1/2 T	2.03-8	4.0	9.24-8	5.5	4.00-29	4.2
3/4 T	8.91-9	4.1	5.55-8	5.7	2.11-29	4.5
PCA 4/12 SSC:						
core center	1.58-4	7.3	2.89-4	8.8	2.21-25	10.3
SSC	3.02-6	4.3	9.43-6	5.5	5.07-27	5.2
1/4 T	2.18-7	4.3	8.95-7	5.7	4.40-28	4.3
1/2 T	1.04-7	4.5	5.94-7	5.9	2.48-28	4.5
3/4 T	4.31-8	7.2	3.36-7	8.1	1.27-28	7.4
VB	1.04-8	8.1	9.08-8	8.6	3.28-29	8.5
PCA 8/7:						
TSF	8.64-6	5.6	1.60-5	8.7	1.40-26	6.8
PVF	7.60-7	5.6	1.61-6	8.4	1.39-27	6.5
1/4 T	2.62-7	4.8	8.98-7	8.8	4.46-28	5.2
1/2 T	1.25-7	5.1	5.92-7	9.4	2.50-28	5.8
3/4 T	5.44-8	5.6	3.47-7	10.0	1.31-28	6.5
VB	1.19-8	6.2	1.06-7	11.8	3.86-29	14.5

TABLE 7.1.2.2

COMPARISON OF RESULTS FROM LSL-M2 ADJUSTMENT ANALYSIS FOR DIFFERENT INPUT DATA (PCA 12/13 at 1/4 T)

Input data	Fluence > 1.0 MeV		Fluence > 0.1 MeV		dpa		χ^2/F
	Value ($\times 10^8$)	% Std.	Value ($\times 10^7$)	% Std.	Value ($\times 10^{29}$)	% Std.	
All reactions no scaling	4.23	3.3	1.36	4.9	7.08	3.5	0.72
All reactions individial scaling	4.22	3.9	1.35	5.3	7.03	4.0	0.57
As above but no correlations between positions	4.25	4.0	1.37	5.8	7.09	4.2	0.48
As above but no scaling	4.20	3.5	1.35	5.5	7.01	3.8	0.49
Inconsistent dosimeters removed with scaling	4.22	3.9	1.34	5.3	7.03	4.0	0.13
Inconsistent dosimeters removed no scaling	4.36	3.5	1.39	5.3	7.24	4.0	0.44
As above but with fission chamber measurements	4.41	3.5	1.41	5.3	7.35	4.0	0.53
As above but with SSTR measurements	4.30	3.5	1.36	5.3	7.13	4.0	0.45

7.1.3 Data Consistency -- RR&A Analysis

A F Thomas (Rolls-Royce and Associates)

7.1.3.1 Calculations

A consistency analysis of the recommended integral measurement data for the various PCA experimental configurations has been carried out using the SENSAK code (Mc79a) which uses a least squares data adjustment methodology. This analysis has been performed on the 8/7, 12/13, and 4/12 SSC configurations for the A2 (TSB/SSC), A4 (1/4 T PVS), A5 (1/2 T PVS), A6 (3/4 T PVS), and A7 (Void Box) locations.

Input Neutron Spectra

The input estimates of the neutron spectral shape were calculated using the ANISN neutron transport code (En67) from the dimensions given in Figures 8.1.1, 8.1.2 and 8.1.3 in (Mc81). The nuclear data library used was EURLIB-4, and the calculations were performed in 40 enegy groups between 14.9 MeV and 0.4 eV. The variance-covariances on the input spectra were based on previous experience from sensitivity analysis of transport calculational methods and a Gaussian distribution of correlation coefficients in which a full width half maximum (FWHM) of 5 flux groups was used.

Detector Cross Sections

Neutron detector cross sections were based on a condensation of the IRDF82 dosimetry cross section file which is largely ENDF/B-V based. Variance-covariance data was extracted from (Pr82), (Ma81), and (St80b) and appropriately regrouped.

Integral Measurements

The integral measurements used were the recommended data given on Tables 2.3.6, 2.3.7, 2.5.8, 2.5.9, 2.5.10, and 6.1.1, together with their uncertainties, which were separated into systematic and random errors. However, since thermal flux was not accurately calculated by the ANISN calculations the bare $^{235}U(n,f)$ reaction rates were not used in the analyses.

The $^{237}Np(n,f)$ and $^{238}U(n,f)$ reaction rates used were primarily those given in Table 6.1.1 which are average values of SSTR and fission chamber results due to the unresolved 10% discrepancy between reaction rates measured by these two techniques. However, in addition, analysis of the PCA 8/7(A4) detector location using the radiometric reaction rates, together first with the SSTR measurements only, and then with the fission chamber measurements only was also carried out in order to ascertain which if any of the methods gives the more consistent results.

7.1.3.2 Results

The results of the consistency analysis for all the PCA configurations and detector locations are summarised in Table 7.1.3.1.

The source scale factor reflects the average renormalisation of the ANISN calculated (c.f. the measured reaction rates) flux intensity which was required prior to data adjustment since the one-dimensional calculations of spectra were of unknown intensity discrepancy. These renormalisations were all within $\sim \pm$ 20% of the calculated intensities indicating that the ANISN calculations were of good quality.

The variance scale factor (VSF) is the value of χ^2 per degree of freedom, and reflects the degree of consistency between the calculated and measured reaction rates. For VSF<1.0, the implication is that the agreement is unlikely good given the size of the errors assigned to each of the integral quantities; for VSF>1.0, an inconsistency between calculated and measured reaction rates is implied. Generally the analysis of the PCA measurements showed VSF values less than 1.0 which, in the main, is a reflection of the over-estimations of the errors on the ANISN group fluxes, which were assumed to vary from about 30% in the I/E region and up to 50% in the near thermal and high-energy fission regions. (All the other data inputs were either physically measured or from evaluated data libraries). This conclusion was drawn since with the exception of the 8/7 and 12/13 Void Box locations no significant discrepancies between detector measurements were noted which would have otherwise caused an increase in the variance of the adjusted data.

The values of VSF for the 8/7 locations were significantly lower than those for the 12/13 locations but since the number of measurements made in these configurations was very similar, this may be ascribed to the better accuracy of the ANISN calculated spectra in the less dispersed configuration of the 8/7 array. However, the values of VSF in the 4/12 SSC array were considerably lower again than for the 8/7 array, which is almost certainly due to the number of detector measurements in the 4/12 SSC array being limited to ^{237}Np(n,f) and ^{238}U(n,f). In these circumstances, the degree of consistency between calculations and measurements can only be considered to be fortuitously good.

As indicated earlier and as can be seen in Table 7.1.3.1, the results of the consistency analysis of the void box measurements resulted in VSF values considerably higher than those for other locations on the same configuration. For the 8/7 configuration, this was primarily due to the inconsistency of the ^{235}U(n,f) (under cadmium) measurements in the void Box (N.B. for the 4/12 SSC configuration, no ^{235}U(n,f) measurements were made). However, the 12/13 void box location showed considerable discrepancies between all detectors. One possible cause for these discrepancies was considered to be the possibility that the ANISN-calculated spectrum in the void box was grossly inaccurate. In order

TABLE 7.1.3.1

SUMMARY OF RESULTS OF SENSAK CONSISTENCY ANALYSIS OF PCA DETECTOR MEASUREMENTS (SSTR + RM + FISSION CHAMBER)

LOCATION	DETECTOR POSITION	SOURCE SCALE FACTOR	VARIANCE SCALE FACTOR	NEUTRON FLUX (E > 1 Mev)* $n/cm^2/sec$	NEUTRON FLUX (E > 0.1 Mev)* $n/cm^2/sec$	DAMAGE IN IRON* dpa/sec
			8/7 CONFIGURATION			
TSB	A2(3)	0.92	0.57	8.51E-7 ± 8%	1.92E-6 ± 9%	1.25E-27 ± 7%
PVS($\frac{1}{4}$T)	A4	1.09	0.16	2.67E-7 ± 3%	8.97E-7 ± 5%	4.55E-28 ± 3%
PVS($\frac{1}{2}$T)	A5	1.16	0.21	1.29E-7 ± 4%	5.79E-7 ± 6%	2.56E-28 ± 4%
PVS($\frac{3}{4}$T)	A6	1.18	0.59	5.78E-8 ± 4%	3.39E-7 ± 12%	1.35E-28 ± 10%
Void Box	A7	0.88	1.98	1.54E-8 ± 26%	1.17E-7 ± 21%	4.24E-29 ± 22%
" "	A7 ($^{235}U(n,f)$ omitted)	0.97	1.03	1.41E-8 ± 7%	1.09E-7 ± 16%	4.10E-29 ± 13%
			12/13 CONFIGURATION			
TSB	A2	1.01	1.21	4.01E-7 ± 10%	7.42E-7 ± 15%	5.85E-28 ± 9%
PVS($\frac{1}{4}$T)	A4	1.11	0.81	4.50E-8 ± 6%	1.35E-7 ± 11%	7.41E-29 ± 8%
PVS($\frac{1}{2}$T)	A5	1.22	0.80	2.21E-8 ± 6%	9.01E-8 ± 12%	4.20E-29 ± 10%
PVS($\frac{3}{4}$T)	A6	1.23	1.06	9.73E-9 ± 8%	5.37E-8 ± 15%	2.22E-29 ± 13%
Void Box	A7	0.97	7.03	3.07E-9 ± 47%	1.71E-8 ± 45%	6.93E-30 ± 44%
" "	A7 $^{235}U(n,f)$ omitted	1.08	6.46	2.88E-9 ± 43%	1.70E-8 ± 47%	6.78E-30 ± 41%
			4/12 SSC CONFIGURATION			
SSC	A2	0.96	0.07	3.15E-6 ± 2%	9.36E-6 ± 4%	4.96E-27 ± 2%
PVS($\frac{1}{4}$T)	A4	0.98	0.04	2.11E-7 ± 1%	8.43E-7 ± 3%	3.92E-28 ± 2%
PVS($\frac{1}{2}$T)	A5	1.04	0.17	1.02E-7 ± 3%	5.41E-7 ± 7%	2.23E-28 ± 5%
PVS($\frac{3}{4}$T)	A6	1.11	0.19	4.65E-8 ± 7%	3.27E-7 ± 8%	1.24E-28 ± 5%
Void Box	A7	0.84	0.70	1.18E-8 ± 9%	9.15E-8 ± 16%	3.41E-29 ± 14%

* Values given are per PCA core neutron/second

to investigate this possibility, the NE213 spectrometer measurements of the neutron spectrum in the void box of the NESDIP PCA (12/13) Replica experiments at AEE Winfrith (UK) (Mc83c) were converted into the same 40 neutron energy group scheme as the ANISN calculation and used as a spectrum estimate in SENSAK. This spectrum was found to be very similar to the ANISN spectrum in the 10 MeV - 0.05 MeV energy region and resulted in no resolution of the detector discrepancies in the PCA (12/13) void box location.

In order to compare the SSTR and fission chamber measurements, a limited study was carried out on the PCA 8/7 (A4) location. The results are tabulated in Table 7.1.3.2. It appears on the basis of the values of VSF that the fission chamber measurements are more consistent with the radiometric measurements than the SSTR's but the consequences in terms of the determination of the dose parameters [i.e., neutron dose (E>1 MeV), neutron dose (E>0.1 MeV)and dpa] are not significantly different in terms of the parameter mean values or their errors.

TABLE 7.1.3.2

SUMMARY OF RESULTS OF SENSAK CONSISTENCY ANALYSIS: COMPARISON OF USE OF SSTR AND FISSION CHAMBER $^{237}Np(n,f)$ AND $^{238}U(n,f)$ MEASUREMENTS IN PCA 8/7 (A4) LOCATION

MEASUREMENTS USED	SOURCE SCALE FACTOR	VARIANCE SCALE FACTOR	NEUTRON FLUX (E > 1 MeV)* (n/cm²/sec)	NEUTRON FLUX (E > 0.1 MeV)* n/cm²/sec	DAMAGE IN IRON* dpa/sec
Fission Chamber and Radiometric	1.14	0.10	2.82E-7 ± 2%	8.96E-7 ± 4%	4.68E-28 ± 2%
SSTR +Radiometric	1.09	0.32	2.61E-7 ± 2%	8.92E-7 ± 7%	4.53E-28 ± 5%
Mean (SSTR + Fission Chamber)+ Radiometric	1.09	0.16	2.67E-7 ± 3%	8.97E-7 ± 5%	4.55E-28 ± 3%

* Values given are per PCA core neutron/second.

7.1.3.3 Conclusions

The radiometric, SSTR, and fission chamber measurements in the PCA(8/7), PCA(12/13) and PCA(4/12 SSC) configurations are generally consistent and produce errors on exposure parameters in the order of 5-15% (1σ). The exceptions to this generalisation are the void box locations in the PCA(8/7)and PCA(12/13) configurations. Significant improvement in the consistency of the PCA(8/7)void box location measurements can be achieved by omitting the $^{235}U(\ ,f)$ (under cadmium) SSTR measurement. However, in the PCA(12/13) void box location there is generally poor consistency between all measurements.

The discrepancy of 10% between the SSTR and fission chamber $^{237}Np(n,f)$ and $^{238}U(n,f)$ measurements appears to make little material difference in terms of estimates of exposure parameters and their errors.

7.2 DERIVED EXPOSURE PARAMETERS

E. P. Lippincott (HEDL), F. W. Stallmann (ORNL), A. F. Thomas (RR&A)

The derived exposure parameter values [$\phi(E > 1)$, $\phi(E > 0.1)$, and dpa] are given in Sections 7.2.1 through 7.2.3 as calculated by HEDL, ORNL, and RR&A, respectively. These values are calculated using the recommended fission rates and radiometric reaction rates given in Section 6.0 and the specific methods and assumptions used are discussed in Section 7.1. Although all three laboratories used a least-squares procedure to derive the exposure parameters from a calculated neutron flux spectrum and the same integral data, differences outside the derived 1σ uncertainties were observed in some cases.

Comparisons of derived exposure parameter values in the block show differences between the three laboratories of up to 12%. No consistent bias between the results exists, when all the configurations are considered. These differences will have to be investigated and understood to further increase confidence in the least-squares derived uncertainties.

Uncertainties in the exposure parameters also differ between the three laboratories. ORNL has the lowest uncertainty estimates which reflect the application of a more sophisticated approach and/or tighter tolerances on the input spectrum shape. RR&A has the largest range of uncertainty values; for example, for $\phi(E > 1)$, the RR&A uncertainties range from 5% to 16% in the block compared to HEDL values of 6% to 9% and ORNL values of 4% to 7%.

A comparison of the present results with those previously reported by HEDL and ORNL (Table 7.3.1 of Mc81), indicates improved and closer agreement (previous differences ranged as high as 22%). Improved methods and different assumptions have enabled ORNL to reduce their error estimates by a factor of 2 or more. HEDL uncertainty estimates are now higher because the results of each measurement location were handled individually and the proton recoil data were neglected.

7.2.1 Exposure Parameters -- HEDL Analysis

E. P. Lippincott (HEDL)

The HEDL derived exposure parameter results for three PCA configurations are given in Table 7.2.1.1. As discussed in Section 7.1.1, these values are based on a least squares analysis using as input calculated neutron flux-spectra supplied by ORNL and consensus radiometric reaction rate and consensus fission rate values as given in Section 6.1. The NRE data were not used to derive the results in this section because of an unresolved significant absolute bias (see Section 7.1.1.5).

The following assumptions were made:

1) Conservative estimates of data uncertainties were used but normalization error was only partly included since this uncertainty is extensively correlated in the independent data measurements. The normalization uncertainty should therefore be combined with the uncertainty values in Table 7.2.1.1 if a total uncertainty is desired. Uncertainties in fission rates were not taken from estimated uncertainties in the measurements but rather from the difference between the SSTR and fission chamber results. When only one set of measurements was available (e.g., ^{232}Th fission rates), the uncertainty was increased accordingly.

2) The input flux-spectra were assumed to have a large normalization uncertainty (100%) and the input group fluxes were assigned an uncertainty of 25% with a short-range correlation of 0.8 extending over a width of six groups (details of this formulation are discussed in Section 4.2 of Mc81). Using these assumptions, the flux magnitude was typically changed 5% to 15% and group fluxes were relatively shifted up to about 15%. These results provide confidence that the uncertainties in Table 7.2.1.1 are realistic.

TABLE 7.2.1.1

RECOMMENDED EXPOSURE PARAMETER VALUES FOR PCA BENCHMARK CONFIGURATIONS BASED ON FERRET SAND II ANALYSIS

Location	Flux >1.0 MeV (n/cm^2 per Core Neutron)	Flux >0.1 MeV (n/cm^2 per Core Neutron)	dpa per Core Neutron
	8/7 Configuration		
1/4 T	2.56 E-7 (±6%)	8.56 E-7 (±14%)	4.26 E-28 (±8%)
1/2 T	1.23 E-7 (±7%)	5.66 E-7 (±15%)	2.42 E-28 (±10%)
3/4 T	5.65 E-7 (±8%)	3.19 E-7 (±16%)	1.25 E-28 (±11%)
	12/13 Configuration		
1/4 T	4.58 E-8 (±7%)	1.44 E-7 (±14%)	7.45 E-29 (±8%)
1/2 T	2.21 E-8 (±7%)	9.73 E-8 (±15%)	4.22 E-29 (±10%)
3/4 T	9.82 E-9 (±7%)	5.93 E-8 (±15%)	2.25 E-29 (±11%)
	4/12 SSC Configuration		
1/4 T	2.34 E-7 (±7%)	9.34 E-7 (±14%)	4.06 E-28 (±10%)
1/2 T	1.15 E-7 (±7%)	6.17 E-7 (±14%)	2.37 E-28 (±11%)
3/4 T	4.87 E-8 (±9%)	3.57 E-7 (±14%)	1.23 E-28 (±11%)

7.2.2 Exposure Parameters -- ORNL Analysis
F. Stallmann

The ORNL derived exposure parameter results for three PCA configurations are given in Table 7.1.2.1. The reader is referred to Section 7.1.2 for summary information and a discussion of input data and related uncertainties.

7.2.3 Exposure Parameters -- RR&A Analysis
A. F. Thomas

The RR&A recommended exposure parameters for the PCA 8/7, 12/13, and 4/12 SSC configurations (based on the analysis described in Section 7.1.3) are shown in Table 7.2.3.1. For the purpose of defining the errors on these exposure parameters, no variance scaling has been employed except in the case of PCA 12/13 void box parameters. For these parameters, the values are based on analyses that omitted the apparently discrepant $^{235}U(n,f)$ (under cadmium) measurements. Since the response of this detector is principally below the energy level at which the exposure parameters require a contribution, this is considered justified.

The uncertainties on the exposure parameters are generally in the 5% to 15% (1σ) region.

TABLE 7.2.3.1

RECOMMENDED EXPOSURE PARAMETERS FOR PCA BENCHMARK CONFIGURATIONS BASED ON SENSAK ANALYSIS

LOCATION	DETECTOR POSITION	NEUTRON FLUX (E>1 Mev) n/cm²/sec	NEUTRON FLUX (E>0.1 Mev) n/cm²/sec	DAMAGE IN IRON dpa/sec
		8/7 CONFIGURATION		
TSB	A2(3)	8.51E-7 ± 11%	1.92E-6 ± 12%	1.25E-27 ± 9%
PVS(¼T)	A4	2.67E-7 ± 8%	8.97E-7 ± 13%	4.55E-28 ± 8%
PVS(¼T)	A5	1.29E-7 ± 9%	5.79E-7 ± 13%	2.56E-28 ± 9%
PVS(¼T)	A6	5.78E-8 ± 5%	3.39E-7 ± 16%	1.35E-28 ± 13%
Void Box	A7	1.41E-8 ± 7%	1.09E-7 ± 16%	4.10E-29 ± 13%
		12/13 CONFIGURATION		
TSB	A2	4.01E-7 ± 9%	7.47E-7 ± 14%	5.85E-28 ± 8%
PVS(¼T)	A4	4.50E-8 ± 7%	1.35E-7 ± 12%	7.41E-29 ± 9%
PVS(¼T)	A5	2.21E-8 ± 7%	9.01E-8 ± 12%	4.20E-29 ± 11%
PVS(¼T)	A6	9.73E-9, ± 8%	5.37E-8 ± 15%	2.22E-29 ± 13%
Void Box	A7	2.88E-9 ± 43%	1.70E-8 ± 47%	6.78E-30 ± 41%
		4/12 SSC CONFIGURATION		
SSC	A2	3.15E-6 ± 8%	9.36E-6 ± 15%	4.96E-27 ± 8%
PVS(¼T)	A4	2.11E-7 ± 5%	8.43E-7 ± 15%	3.92E-28 ± 10%
PVS(¼T)	A5	1.02E-7 ± 7%	5.41E-7 ± 17%	2.23E-28 ± 12%
PVS(¼T)	A6	4.65E-8 ± 16%	3.27E-7 ± 18%	1.24E-28 ± 11%
Void Box	A7	1.18E-8 ± 11%	9.15E-8 ± 19%	3.41E-29 ± 17%

B I B L I O G R A P H Y

FOR LWR-PV-SDIP REPORTS

3.0 BIBLIOGRAPHY FOR LWR-PV-SDIP REPORTS

(Ad70) F. Adams and R. Dams, Applied Gamma-Ray Spectrometry, Pergamon Press, New York, NY, 1970.

(Ad75) H. L. Adair and E. H. Kobisk, "Preparation and Characterization of Neutron Dosimeter Materials," Nucl. Technol. 25, (2), p. 224, February 1975.

(Ad78) H. L. Adair, E. H. Kobisk, J. A. Setaro, T. C. Quinby and J. M. Dailey, "Dosimeter Sample Preparation, Quality Assurance, and Materials Development for ILRR, FRMDC, and FFTF Dosimetry Programs," Proc. of the 2nd ASTM-EURATOM Symposium on Reactor Dosimetry, Palo Alto, CA, October 3-7, 1977, NUREG/CP-0004, NRC, Washington, DC, Vol. 3, pp. 987-1001, 1978.

(Ad80) H. L. Adair, E. H. Kobisk, J. A. Setaro, T. C. Quinby, J. A. Carter, J. F. Emery, R. Walker and J. H. Cooper, "Neutron Dosimeter Materials Development and Characterization," Proc. of the 3rd ASTM-EURATOM Symposium on Reactor Dosimetry, Ispra, Italy, October 1-5, 1979, EUR 6813, Commission of the European Communities, Vol. II, pp. 1091-1103, 1980.

(Al77) A. A. Alberman et al., "Damage Function for the Mechanical Properties of Steels, "Nucl. Technol. 36, p. 336, 1977.

(Al79) A. A. Alberman et al., "The Miniaturized Tungsten Damage Detector," Proc. of the 3rd ASTM-EURATOM Symposium on Reactor Dosimetry, Ispra, Italy, October 1-5, 1979, EUR 6813, Commission of the European Communities, Vol. II, pp. 1104, 1980.

(Al82) A. A. Alberman et al., "Nouveaux Developpements de la Dosimetrie des Dommages par Technique Tungstene," Proc. of the 4th ASTM-EURATOM Symposium on Reactor Dosimetry, Gaithersburg, MD, March 22-26, 1982, NUREG/CP-0029, NRC, Washington, DC, Vol. 1, pp. 321-329, July 1982.

(Al82a) A. A. Alberman et al., "Influence des Neutrons Thermiques sur la Fragilisation de l'Acier de Peau d'Etancheite des Reacteurs a Haute Temperature (H.T.R.)," Proc. of the 4th ASTM-EURATOM Symposium on Reactor Dosimetry, Gaithersburg, MD, March 22-26, 1982, NUREG/CP-0029, NRC, Washington, DC, Vol. 2, p. 839, July 1982.

(Al82b) A. A. Alberman et al., "Mesure et Interpretation des Flux de Dommages dans le Simulateur de Cuve P.W.R. d'Oak Ridge (ORR-PSF)," Proc. of the 4th ASTM-EURATOM Symposium on Reactor Dosimetry, Gaithersburg, MD, March 22-26, 1982, NUREG/CR-0029, NRC, Washington, DC, Vol. 2, pp. 1051-1060, July 1982.

(Al83) A. A. Alberman et al., DOMPAC Dosimetry Experiment Neutron Simulation of the Pressure Vessel of a Pressurized-Water Reactor, Characterization of Irradiation Damage, CEA-R-5217, Centre d'Etudes Nucleaires de Saclay, France, May 1983.

(An78) S. L. Anderson, "Characterization of the Neutron Environment for Commercial LWR Pressure Vessel Surveillance Programs," Proc. of the 2nd ASTM-EURATOM Symposium on Reactor Dosimetry, Palo Alto, CA, October 3-7, 1977, NUREG/CP-0004, NRC, Washington, DC, Vol. 3, pp. 1093-1107, 1978.

(An80) S. L. Anderson, "Data Correlation Between Surveillance Measurements in the Predicted Vessel Neutron Exposure," Paper presented at the 3rd ASTM-EURATOM Symposium on Reactor Dosimetry, Ispra, Italy, October 1-5, 1979, preprint available.

(An82) S. L. Anderson, "Sensitivity of Vessel Exposure to Power Distribution Uncertainties," Paper presented at the 4th ASTM-EURATOM Symposium on Reactor Dosimetry, Gaithersburg, MD, March 22-26, 1982, preprint available.

(An83) S. L. Anderson and C. Whitmarsh, "Pressure Vessel Fluence Dependence on Core Configuration Design," Proc. of the 11th WRSR Information Meeting, Gaithersburg, MD, October 24-28, 1983, NUREG/CP-0048, NRC, Washington, DC.

(Ar83) A. L. Aronson et al., Evaluation of Methods for Reducing Pressure Vessel Fluence, BNL-NUREG-32876, NRC, Washington, DC, March 1983.

(As77) ASTM A370-77, "Methods and Definitions for Mechanical Testing of Steel Products," 1977 Annual Book of ASTM Standards, American Society for Testing and Materials, Philadelphia, PA, 1977.

(As78) ASME Boiler and Pressure Vessel Code, Section III, Nuclear Power Plant Components, Subsection NF, July 1, 1974, Summer 1975 Addenda, current edition.

(As79a) 1979 Annual Book of ASTM Standards, Part 45, "Nuclear Standards," American Society for Testing and Materials, Philadelphia, PA, p. 999, 1979.

(As79b) ASTM E21-79, "Practice for Short-Time Elevated-Temperature Tension Tests of Materials," 1979 Annual Book of ASTM Standards, American Society for Testing and Materials, Philadelphia, PA, 1979.

(As79c) ASTM E185-79, "Practice for Surveillance Tests for Nuclear Reactor Vessels," 1979 Annual Book of ASTM Standards, American Society for Testing and Materials, Philadelphia, PA, Part 45, 1979.

(As79d) ASTM E693-79, "Practice for Characterizing Neutron Exposures in Ferritic Steels in Terms of Displacements per Atom (dpa)," 1979 Annual Book of ASTM Standards, American Society for Testing and Materials, Philadelphia, PA, 1979.

(As81) 1981 Annual Book of ASTM Standards, Part 45, "Nuclear Standards," American Society for Testing and Materials, Philadelphia, PA, 1981.

(As82) ASTM E706-81a, "Master Matrix for LWR Pressure Vessel Surveillance Standards," 1982 Annual Book of ASTM Standards, American Society for Testing and Materials, Philadelphia, PA, Part 45, 1982.

(As82a) ASTM E706 (IID), "Standard Guide for Application of Neutron Transport Methods for Reactor Vessel Surveillance," 1982 Annual Book of ASTM Standards, American Society for Testing and Materials, Philadelphia, PA, Part 45, 1982.

(As82b) ASTM E854-81, "ASTM Standard Method for Application and Analysis of Solid State Track Recorder (SSTR) Monitors for Reactor Surveillance," 1982 Annual Book of ASTM Standards, American Society for Testing and Materials, Philadelphia, PA, Part 45, 1982.

(As82c) ASTM E8-82, "Standard Method of Tension Testing of Metallic Materials," 1982 Annual Book of ASTM Standards, American Society for Testing and Materials, Philadelphia, PA, Part 10, 1982.

(As82d) ASTM E23-82, "Standard Methods for Notched Bar Impact Testing of Metallic Materials," 1982 Annual Book of ASTM Standards, American Society for Testing and Materials, Philadelphia, PA, Part 10, 1982.

(As82e) ASTM E208-82, "Standard Methods for Conducting Drop-Weight Test to Determine Nil Ductility Transition Temperature of Ferritic Steels," 1982 Annual Book of ASTM Standards, American Society for Testing and Materials, Philadelphia, PA, Part 10, 1982.

(As83) 1983 Annual Book of ASTM Standards, Section 12, Volume 12.02, "Nuclear (II), Solar, and Geothermal Energy," American Society for Testing and Materials, Philadelphia, PA, 1983.

(As83a) ASTM 910-82, "Standard Method for Application and Analysis of Helium Accumulation Fluence Monitors for Reactor Vessel Surveillance," 1983 Annual Book of ASTM Standards, American Society for Testing and Materials, Philadelphia, PA, Section 12, Volume 12.02, pp. 761-774, 1983.

(As83b) ASTM E844-81, "ASTM Standard Guide for Sensor Set Design and Irradiation for Reactor Surveillance," 1983 Annual Book of ASTM Standards, American Society for Testing and Materials, Philadelphia, PA, Volume 12.02, 1983.

(As83c) ASTM E263-82, "ASTM Standard Method for Determining Fast-Neutron Flux Density by Radioactivation of Iron," 1983 Annual Book of ASTM Standards, American Society for Testing and Materials, Philadelphia, PA, Volume 12.02, 1983.

(At68) F. H. Attix and W. C. Roesch, Radiation Dosimetry, 2nd ed., Academic Press, New York, NY, 1968.

(Au82) M. Austin, "Description and Status of the NESTOR Dosimetry Improvement Programme (NESDIP)," Proc. of the 10th WRSR Information Meeting, Gaithersburg, MD, October 12-15, 1982, NUREG/CP-0041, Vol. 4, NRC, Washington, DC, pp. 228-231, January 1983.

(Au82a) M. Austin, "Sense of Direction: An Observation of Trends in Materials Dosimetry in the United Kingdom," Proc. of the 4th ASTM-EURATOM Symposium on Reactor Dosimetry, Gaithersburg, MD, March 22-26, 1982, NUREG/CP-0029, NRC, Washington, DC, Vol. 1, p. 461-469, July 1982.

(Au83) M. Austin et al., "The NESTOR Shielding and Dosimetry Improvement Programme (NESDIP): The Replica Experiment (Phase 1)," Proc. of the 11th WRSR Information Meeting, Gaithersburg, MD, October 24-28, 1983, NUREG/CP-0048, NRC, Washington, DC.

(Ax77) E. J. Axton, "Accuracies and Corrections in Neutron Bath Techniques," Proc. of a Symposium on Neutron Standards and Applications, NBS Special Publication 493, p. 237, 1977.

(Ba63) W. H. Barkas, "Techniques and Theories," Nuclear Research Emulsions, Vol. I, Academic Press, New York, NY, 1963.

(Ba73) W. H. Barkas, Nuclear Research Emulsions, Vol. II, Academic Press, New York, NY, 1973.

(Ba75) J. F. Bates and T. K. Bierlein, "Characterization of the In-Reactor Environment of Subassemblies X-216 and X-223," Cladding and Structural Materials Semi-Annual Progress Report January 1975 to July 1975, HEDL-TME 75-77, Hanford Engineering Development Laboratory, Richland, WA, pp. 127-147, October 1975.

(Ba83) C. A. Baldwin, Neutron Spectral Characterization Calculations for the Fourth Nuclear Regulatory Commission Heavy Section Steel Technology TT-CT Irradiation Experiments, NUREG/CR-3311, ORNL/TM-8782, Oak Ridge National Laboratory, Oak Ridge, TN, June 1983.

(Be66) E. F. Bennett, R. Gold and R. J. Huber, "Spectrum Measurements in a Large Dilute Plutonium-Fueled Fast Reactor," Proc. of the International Conference on Fast Critical Experiments and Their Analysis, ANL-7320, Argonne National Laboratory, Argonne, IL, p. 477, 1966.

(Be67) E. F. Bennett and R. Gold, "Neutron Spectrum Measurements in ZPR-3, -6 and -9 Using Hydrogen-Recoil Proportional Counters," Trans. Am. Nucl. Soc. 10, p. 577, 1967.

(Be67a) R. A. Bennett and P. L. Hofmann, "Rationale and Plans for the FTR Critical Experiments Program," BNWL-490, Battelle Pacific Northwest Laboratory, Richland, WA, June 1967.

(Be67b) S. Berg and W. N. McElroy, A Computer Automated Iterative Method for Neutron Flux Spectra Determination by Foil Activation, AFWL-TR-67-41, Vol. 1, Air Force Weapons Laboratory, Kirkland AFB, NM, July 1967.

(Be71) E. F. Bennett and T. J. Yule, Technique and Analyses of Fast Reactor Neutron Spectroscopy with Proton-Recoil Proportional Counters, ANL-7763, Argonne National Laboratory, Argonne, IL, August 1971.

(Be72) G. E. Belovitiskii et al., "Measurement of the Spectra of Fast Neutrons (~14 MeV) with High-Energy Resolution with the Aid of Nuclear Emulsions - Automation of the Measurements," Proc. (Trudy) of the P.N. Lebedev Physics Institute, Nuclear Reactions and Interaction of Neutrons and Matter 63, Nanka Press, Moscow, USSR, pp. 109-119, 1972.

(Be80) E. V. Benton et al., "Proton- and Alpha-Particle Response Characteristics of CR-39 Polymer for Reactor and Dosimetry Applications," Proc. of the 10th International Conference on Solid State Track Detectors, Lyons, France, July 2-7, 1979, Pergamon Press, Oxford, UK, p. 459, 1980.

(Be81) E. F. Bennett and T. J. Yule, Summary of Neutron Spectrum Measurement Results at the Fast Test Reactor, ZPR-TM-392, Argonne National Laboratory, Argonne, IL, 1981.

(Be82) D. E. Bendall and R. J. Brissenden, "McBend Program User Guide WRS Modular Code," Trans. Am. Nucl. Soc. 41, pp. 332-333, 1982.

(Be83) R. G. Berggren and F. W. Stallmann, "Statistical Analysis of Pressure Vessel Steel Embrittlement Data," from the ANS Special Session on Correlations and Implications of Neutron Irradiation Embrittlement of Pressure Vessel Steels, Detroit, MI, June 12-16, 1983, Trans. Am. Nucl. Soc. 44, p. 225, 1983.

(Bh60) A. T. Bharucha-Reid, Elements of the Theory of Markov Processes and Their Applications, McGraw-Hill, New York, NY, 1960.

(Bi78) T. K. Bierlein, Ed., "Energy-Dependent Damage Functions," Nuclear Systems Materials Handbook, TID-26666, Vol. 2, Appendix E, DOE Technical Information Center, Oak Ridge, TN, December 1, 1978.

(Bl80) L. D. Blackburn et al., "Strength and Ductility of Austenitic Stainless Steels Irradiated in Various Fast Reactor Spectra," Proc. of the 3rd ASTM-EURATOM Symposium on Reactor Dosimetry, Ispra, Italy, October 1-5, 1979, EUR 6813, Commission of the European Communities, Vol. I, pp. 326-333, p. 236, 1980.

(Bo70) R. D. Bourquin, TIMH - A Computer Program for the Determination of Fluence with a Time-Varying Flux, BNWL-1492, Battelle Pacific Northwest Laboratory, Richland, WA, August 1970. (TIMWH is a modified version of the TIMH program.)

(Bo72) E. T. Boulette and D. R. Marr, "Diffusion Theory Analyses for Fast Reactor Shield Design," Proc. of ANS National Topical Meeting on New Developments in Reactor Physics and Shielding, September 12-15, 1972, CONF-720901, US Department of Energy, Washington, DC, 1973.

(Bo77) C. D. Bowman, C. M. Eisenhauer and D. M. Gilliam, "Photofission Effects in Reactor Pressure Vessel Dosimetry," Proc. of the 2nd ASTM-EURATOM Symposium on Reactor Dosimetry, Palo Alto, CA, October 3-7, 1977, NUREG/CP-0004, NRC, Washington, DC, Vol. 2, pp. 575-582, 1978.

(Bo79) J. W. Bolderman, D. Culley and R. J. Cawley, "The Fission Neutron Spectrum from the Spontaneous Fission of ^{252}Cf," Trans. Am. Nucl. Soc. 32, p. 733, 1979.

(Br60) G. T. Brown and R. T. Allsop, "Embrittlement of a 12%Cr-4%Ni Steel," J. Iron & Steel Institute 196, p. 435, April 1960.

(Br82) J. G. Bradley, B. M. Oliver, H. Farrar IV and E. P. Lippincott, "Threshold Response Helium Accumulation Fluence Monitors for Fast Reactor Dosimetry," Proc. of the 4th ASTM-EURATOM Symposium on Reactor Dosimetry, Gaithersburg, MD, March 22-26, 1982, NUREG/CP-0029, NRC, Washington, DC, Vol. 1, pp. 195-209, July 1982.

(Br82a) W. E. Brandon et al., "Neutron Dosimetry in the Pressure Vessel Cavity of Two Pressurized Water Reactors," Proc. of the 4th ASTM-EURATOM Symposium on Reactor Dosimetry, Gaithersburg, MD, March 22-26, 1982, NUREG/CP-0029, NRC, Washington, DC, Vol. 1, pp. 533-554, July 1982.

(Bu82) W. L. Bunch, "FFTF Gamma-Ray Measurements," Proc. of the 4th ASTM-EURATOM Symposium on Reactor Dosimetry, Gaithersburg, MD, March 22-26, 1982, NUREG/CP-0029, NRC, Washington, DC, Vol. 1, pp. 183-193, July 1982.

(Bu84) J. Butler, M. D. Carter, I. J. Curl, M. R. March, A. K. McCracken, M. F. Murphy and A. Packwood, The PCA Replica Experiment Part I: Winfrith Measurements and Calibrations, NUREG/CR-324, AEEW-R1736, Part I, NRC, Washington, DC, January 1984.

(By80) S. T. Byrne, Omaha Public Power District Fort Calhoun Station Unit No. 1: Post-Irradiation Evaluation of Reactor Vessel Surveillance Capsule W-225, TR-0-MCM-001, Rev. 1, Combustion Engineering Inc., August 1980.

(Ca75) L. L. Carter and E. D. Cashwell, "Particle Transport Simulation with the Monte Carlo Method," ERDA Critical Review Series, TID-26607, DOE Technical Information Center, Oak Ridge, TN, 1975.

(Ca81) K. Carlson, G. Guthrie and G. R. Odette, "Embrittlement of Compression Specimens in the PSF," LWR-PV-SDIP, Quarterly Progress Report, NUREG/CR-2345, Vol. 1, HEDL-TME 81-33, Hanford Engineering Development Laboratory, Richland, WA, October 1981.

(Cf83) Code of Federal Regulations, 10CFR50, "Domestic Licensing of Production and Utilization Facilities," "General Design Criteria for Nuclear Power Plants," Appendix A; "Fracture Toughness Requirements," Appendix G; "Reactor Vessel Material Surveillance Program Requirements," Appendix H; US Government Printing Office, Washington, DC, current edition.

(Cf83a) Code of Federal Regulations, 10CFR21, "Reporting of Defects and Noncompliance," US Government Printing Office, Washington, DC, current edition.

(Ch82) R. D. Cheverton, "A Brief Account of the Effect of Overcooling Accidents on the Integrity of PWR Pressure Vessels," Proc. of the 4th ASTM-EURATOM Symposium on Reactor Dosimetry, NUREG/CP-0029, NRC, Washington, DC, Vol. 2, pp. 1061-1070, July 1982.

(Ch83) R. D. Cheverton, S. K. Iskander and G. D. Whitman, "The Integrity of PWR Pressure Vessels During Overcooling Accidents," Proc. of the 10th WRSR Information Meeting, Gaithersburg, MD, October 12-15, 1982, NUREG/CP-0041, Vol. 4, NRC, Washington, DC, pp. 232-241, January 1983.

(Co69) C. E. Cohn, R. Gold and T. W. Pienias, "Computer-Controlled Microscope for Scanning Fission Track Plates," Trans. Am. Nucl. Soc. 12, p. 68, 1969.

(Co70) F. J. Congel et al., "Automatic System for Counting Etched Holes in Thin Dielectric Plastics," Trans. Am. Nucl. Soc. 13, p. 419, 1970.

(Co72) C. E. Cohn and R. Gold, "Computer-Controlled Microscope for Automatic Scanning of Solid-State Nuclear Track Recorders," Rev. Sci. Instrum. 42, pp. 12-17, 1972.

(Co72a) F. J. Congel et al., "Automatic System for Counting Etched Holes in Thin Dielectric Plastics," Nucl. Instrum. Methods 100, pp. 247-252, 1972.

(Co75) C. E. Cohn and R. J. Armani, "Automatic Scanning of Mica Track Recorders," Rev. Sci. Instrum. 46, p. 18, 1975.

(Cr69) N. G. Cross and L. Tommasino, Proc. of the International Topical Conf. on Nuclear Track Registration in Insulating Solids and Applications, University of Clermont, Clermont-Ferrand, France, Vol. I, p. 73, 1969.

(Cu74) G. W. Cunningham, "Advanced Breeder Fuel Development Program 1975-1985," Trans. Am. Nucl. Soc. 19, p. 83, October 1974.

(Cu74a) G. W. Cunningham, "LMFBR Fuels and Materials Development," Nucl. Eng. Int. 19, (221), p. 840, October 1974.

(Cu78) J. G. Cuninghame, "Status of Fission Product Yield Data," Fission Product Nuclear Data - 1977, IAEA-213, International Atomic Energy Agency, Vienna, Austria, Vol. I, pp. 351-419, 1978.

(Cu82) D. E. Cullen et al., "The IAEA International Reactor Dosimetry File (IRDF-82)," Proc. of the 4th ASTM-EURATOM Symposium on Reactor Dosimetry, Gaithersburg, MD, March 22-26, 1982, NUREG/CP-0029, NRC, Washington, DC, Vol. 2, pp. 917-927, July 1982.

(Da59) W. C. Davidon, Variable Metric Method (VMM) for Minimization, ANL-5990, Argonne National Laboratory, Argonne, IL, 1959.

(Da77) J. A. Davidson, S. L. Anderson and K. V. Scott, Analysis of Capsule V from Northern States Power Company Prairie Island Unit No. 1 Reactor Vessel Radiation Surveillance Program, WCAP-8916, Westinghouse Electric Corp., Pittsburgh, PA, August 1977.

(Da78) J. W. Daughtry, R. A. Bennett, W. L. Bunch, W. N. McElroy and T. J. King, "FFTF Reactor Characterization Program," Proc. of the 2nd ASTM-EURATOM Symposium on Reactor Dosimetry, Palo Alto, CA, October 3-7, 1977, NUREG/CP-0004, NRC, Washington, DC, Vol. 1, pp. 69-83, 1978.

(Da78a) J. A. Davidson, S. L. Anderson and R. P. Shogan, Analysis of Capsule T from the Wisconsin Electric Power Company Point Beach Nuclear Plant Unit No. 2 Reactor Vessel Radiation Surveillance Program, WCAP-9331, Westinghouse Electric Corp., Pittsburgh, PA, August 1978.

(Da79) J. A. Davidson, S. L. Anderson and W. T. Kaiser, Analysis of Capsule T from the Indian Point Unit 3 Reactor Vessel Radiation Surveillance Program, WCAP-9491, Westinghouse Electric Corp., Pittsburgh, PA, April 1979.

(Da83) L. M. Davies et al., "Analysis of the Behavior of Advanced Reactor Pressure Vessel Steels Under Neutron Irradiation - The UK Programme," Report from the UK for the IAEA Coordinated Research Programme on the Analysis of the Behavior of Advanced Reactor Pressure Vessel Steels Under Neutron Irradiations," Unnumbered UKAEA-Harwell Report, Harwell, UK, April 1983.

(De82) S. De Leeuw and R. Menil, "Silicon P.I.N. Diode Neutron Damage Monitors," Proc. of the 4th ASTM-EURATOM Symposium on Reactor Dosimetry, Gaithersburg, MD, March 22-26, 1982, NUREG/CP-0029, NRC, Washington, DC, Vol. 1, pp. 387-412, July 1982.

(Di82) W. J. Dircks, Pressurized Thermal Shock (PTS), and Enclosure A, "NRC Staff Evaluation of PTS," SECY-82-465, NRC, Washington, DC, November 1982.

(Do72) D. G. Doran and R. W. Burnett, "Computer Simulation of the Short-Term Annealing of Displacement Cascades," Interatomic Potentials and Simulation of Lattice Defects, P. C. Gehlen, J. R. Beeler Jr and R. I. Jaffee, Eds., Plenum Press, New York, NY, p. 403, 1972.

(Do73) D. G. Doran, J. R. Beeler, Jr., N. D. Dudey and M. J. Fluss, Report of the Working Group on Displacement Models and Procedure for Damage Calculations, HEDL-TME 73-76, Hanford Engineering Development Laboratory, Richland, WA, December 1973.

(Do74) D. G. Doran, R. L. Simons and W. N. McElroy, "Spectral Effects in Neutron and Charged-Particle Irradiations," Proc. of the ASTM Symposium on the Effects of Radiation on Structural Materials, ASTM STP 570, Gatlinburg, TN, June 11-13, 1974, American Society for Testing and Materials, Philadelphia, PA, February 1976.

(Do75) E. J. Dowdey, E. J. Lozito and E. A. Plassmann, "The Central Neutron Spectrum of the Fast Critical Assembly BIG-10," Nucl. Technol. 25, p. 381, 1975.

(Do76) D. G. Doran and N. J. Graves, "Neutron Displacement Damage Cross Sections for Structural Metals," Irradiation Effects on the Microstructure and Properties of Metals, ASTM STP 611, American Society for Testing and Materials, Philadelphia, PA, p. 463, 1976.

(Do81) K. D. Dobbin, J. P. McNeece, J. A. Rawlins and J. W. Daughtry, "Summary of the FFTF Traversable Fission Chamber Experiment Results," Trans. Am. Nucl. Soc. 39, p. 899, December 1981.

(Dr77) J. D. Drichler and C. R. Weisbin, Compilation of Multigroup Cross-Section Covariance Matrices for Several Important Reactor Materials, ORNL-5318 (ENDF-235), Oak Ridge National Laboratory, Oak Ridge, TN, 1977.

(Du74) N. D. Dudey et al., "Measurement and Calculation of Integral Heavy-Element Cross-Section Ratios in the Fast Breeder Reactor EBR-II," Nucl. Sci. Eng. 53, 1974.

(Du75) N. D. Dudey, R. J. Popek, R. C. Greenwood, R. G. Heimer, J. W. Rogers, L. S. Kellogg and W. H. Zimmer, "Fission-Product-Rate Measurements and Yields," Nucl. Technol. 25, (2), p. 294, February 1975.

(Ei77) N. Von Eichselpasch and R. Seepolt, "Experimentelle Ermittung der Neutronendosis des KRB - Druckgefässes und deren Betriebliche Bedeutung," Atomkernenergie 29, 1977.

(Em74) J. F. Emery and F. F. Dyer, "Replacement of Chemistry in Isotope Calibration, Activity Analysis and Fuel Element Analysis by Instrumental Alpha-Ray Spectrometry," Proc. of the 2nd International Conference on Nuclear Materials in Environmental Research, July 29-31, 1974, University of Missouri, Columbia, MO, 1974.

(En66) R. L. Engel, M. M. Hendrickson and J. Greenborg, ISOSHLD - A Computer Code for General Purpose Shielding Analysis, BNWL-236, Battelle Pacific Northwest Laboratory, Richland, WA, June 1966.

(En67) W. W. Engle, A User's Manual for ANISN, A One-Dimensional Discrete Ordinates Transport Code with Anisotropic Scattering, K-1693, Union Carbide Corp., Oak Ridge, TN, 1967.

(En75) T. R. England and R. E. Schenter, ENDF/B-IV Fission-Product Files: Summary of Major Nuclide Data, LA-6116-MS (ENDF-223), Los Alamos National Laboratory, Los Alamos, NM, October 1975.

(En81) G. W. R. Endres et al., Neutron Dosimetry at Commercial Nuclear Plants - Final Report of Subtask A: Reactor Containment Measurements, NUREG/CR-1769, PNL-3585, NRC, Washington, DC, May 19, 1981.

(En82) T. R. England, W. B. Wilson, R. E. Schenter and F. M. Mann, "Delayed Neutron Spectral Calculation Using Augmented ENDF/B-V Data," Trans. Am. Nucl. Soc. 41, pp. 567-569, June 1982.

(Et77) E. W. Etherington, "The Calculation of Atomic Displacement Dose in Fast Reactors," Proc. of the 1st ASTM-EURATOM Symposium on Reactor Dosimetry, Petten, Netherlands, September 22-26, 1975, EUR 5667, Commission of the European Communities, Vol. I, pp. 375-413, 1977. (This paper discusses uncertainties of thermal power balances in DFR and PFR.)

(Eu74) European-American Nuclear Data Committee, Compilation of Threshold Reaction Neutron Cross Sections for Neutron Dosimetry and Other Applications, EANDC 93 U, Organization for Economic Cooperation and Development, Paris, France, February 1974.

(Ev83) Evaluated Nuclear Data File (ENDF/B), available from and maintained by the National Nuclear Data Center (NNDC) at Brookhaven National Laboratory, Upton, NY, current edition.

(Fa75) A. Fabry, G. De Leeuw and S. De Leeuw, "The Secondary Intermediate-Energy Standard Neutron Field at the Mol-ΣΣ Facility," Nucl. Technol. 25, (2), p. 349, February 1975.

(Fa75a) H. Farrar IV, W. N. McElroy and E. P. Lippincott, "Helium Production Cross Section of Boron for Fast-Reactor Neutron Spectra," Nucl. Technol. 25, (2), p. 305, February 1975.

(Fa77) A. Fabry, H. Ceulemans, P. Vandeplas, W. N. McElroy and E. P. Lippincott, "Reactor Dosimetry Integral Reaction Rate Data in LMFBR Benchmark and Standard Neutron Fields: Status, Accuracy and Implications," Proc. of the 1st ASTM-EURATOM Symposium on Reactor Dosimetry, Petten, Netherlands, September 22-26, 1975, EUR 5667, Commission of the European Communities, Vol. II, pp. 112-130, 1977.

(Fa77a) H. Farrar IV, D. W. Kneff, R. A. Britten and R. R. Heinrich, "Fluence Mapping of RTNS-I by Helium Accumulation and Foil Activation Methods," Proc. of a Symposium on Neutron Cross Sections from 10 to 40 MeV, BNL-NCS-50681, M. R. Bhat and S. Pearlstein, Eds., National Nuclear Data Center, Brookhaven National Laboratory, Upton, NY, pp. 175-184, July 1977.

(Fa77b) H. Farrar IV, E. P. Lippincott and W. N. McElroy, "Dosimetry for Fluence Applications," Proc. of the 1st ASTM-EURATOM Symposium on Reactor Dosimetry, Petten, Netherlands, September 22-26, 1975, EUR 5667, Commission of the European Communities, Vol. I, pp. 675-699, 1977.

(Fa78) H. Farrar IV and E. P. Lippincott, "Helium Production Measurements for Neutron Dosimetry and Damage Correlations," Proc. of the 2nd ASTM-EURATOM Symposium on Reactor Dosimetry, Palo Alto, CA, October 3-7, 1977, NUREG/CP-0004, NRC, Washington, DC, Vol. 2, pp. 725-738, 1978.

(Fa79) A. Fabry and F. B. K. Kam, "Towards Adequate Evaluation of LWR Pressure Vessel Steel Irradiation Exposures," Proc. of an IAEA Specialist's Meeting on Accuracies in Correlation Between Property Change and Exposure Data from Reactor Pressure Vessel Steel Irradiations, Jülich, Federal Republic of Germany, September 24-27, 1979, Unnumbered IAEA Report, International Atomic Energy Agency, Vienna, Austria, 1979.

(Fa80) H. Farrar IV, B. M. Oliver and E. P. Lippincott, "Helium Generation Reaction Rates for ^{6}Li and ^{10}B in Benchmark Facilities," Proc. of the 3rd ASTM-EURATOM Symposium on Reactor Dosimetry, Ispra, Italy, October 1-5, 1979, EUR 6813, Commission of the European Communities, Vol. I, pp. 552-570, 1980

(Fa80a) A. Fabry et al., "Results and Implications of the Initial Neutronic Characterization of Two HSST Irradiation Capsules and the PSF Simulated LWR Pressure Vessel Irradiation Facility," Proc. of the 8th WRSR Information Meeting, Gaithersburg, MD, October 27-31, 1980, NUREG/CP-0023, NRC, Washington, DC, March 1982.

(Fa81) A. Fabry, R. Gold, F. H. Ruddy, J. H. Roberts, E. D. McGarry and F. W. Stallman, "Comparison Between Solid State Track Recorder and Fission Chamber Measurements," LWR-PV-SDIP: PCA Experiments and Blind Test, W. N. McElroy, Ed., NUREG/CR-1861, HEDL-TME 80-87, NRC, Washington, DC, pp. 4.3-1 - 4.3-8, July 1981.

(Fa81a) A. Fabry, F. Cops and L. S. Kellogg, "Radiometric Measurements," LWR-PV-SDIP: PCA Experiments and Blind Test, W. N. McElroy, Ed., NUREG/CR-1861, HEDL-TME 80-87, NRC, Washington, DC, p. 2.4-1 - 2.4-31, July 1981.

(Fa81b) A. Fabry, N. Maene, R. Menil, G. Minsart and J. Tissot, "Validation of Gamma-Ray Field Calculations by TLD Measurements," LWR-PV-SDIP: PCA Experiments and Blind Test, NUREG/CR-1861, HEDL-TME 80-87, NRC, Washington, DC, Sec. 5.4, July 1981.

(Fa81c) A. Fabry and L. S. Kellogg, "Recommended Integral Results - Radiometric Measurements," LWR-PV-SDIP: PCA Experiments and Blind Test, NUREG/CR-1861, HEDL-TME 80-87, NRC, Washington, DC, Sec. 8.3, July 1981.

(Fa81d) A. Fabry, G. Minsart, F. B. K. Kam and C. A. Baldwin, "Implications of PCA Blind Test Results," LWR-PV-SDIP: PCA Experiments and Blind Test, NUREG/CR-1861, HEDL-TME 80-87, NRC, Washington, DC, p. 7.2-3, July 1981.

(Fa82) A. Fabry et al., "Improvement of LWR Pressure Vessel Steel Embrittlement Surveillance: Progress Report on Belgian Activities in Cooperation with the USNRC and other R&D Programs," Proc. of the 4th ASTM-EURATOM Symposium on Reactor Dosimetry, Gaithersburg, MD, March 22-26, 1982, NUREG/CP-0029, NRC, Washington, DC, Vol. 1, pp. 45-77, July 1982.

(Fa82a) A. Fabry et al., "The Mol Cavity Fission Spectrum Standard Neutron Field and Its Applications," Proc. of the 4th ASTM-EURATOM Symposium on Reactor Dosimetry, Gaithersburg, MD, March 22-26, 1982, NUREG/CP-0029, NRC, Washington, DC, Vol. 2, pp. 665-687, July 1982.

(Fa82b) A. Fabry et al., "Workshop on Nuclear Data and Benchmarks," Proc. of the 4th ASTM-EURATOM Symposium on Reactor Dosimetry, Gaithersburg, MD, March 22-26, 1982, NUREG/CP-0029, NRC, Washington, DC, Vol. 2, pp. 1231-1232, July 1982.

(Fa83) A. Fabry et al., "VENUS Dosimetry Program," Paper presented at the 10th WRSR Information Meeting, Gaithersburg, MD, October 12-15, 1982, preprint available.

(Fa83a) A. Fabry et al., "The Belgium Characterization Program and the Venus Program for Core Source to PV Wall Fluence Verification," Proc. of the 11th WRSR Information Meeting, Gaithersburg, MD, October 24-28, 1983, NUREG/CP-0048, NRC, Washington, DC.

(Fe66) W. Feller, An Introduction to Probability Theory and Its Applications, Vols. I and II, John Wiley and Sons, New York, NY, 1966.

(Fl75) R. L. Fleischer, P. B. Price and R. M. Walker, Nuclear Tracks in Solids, University of California Press, Berkeley, CA, 1975.

(Fo76) W. E. Ford, C. C. Webster and R. M. Westfall, A 218-Group Neutron Cross-Section Library in the AMPX Master Interface Format for Criticality Safety Studies, ORNL/CSD/TM-4, Oak Ridge National Laboratory, Oak Ridge, TN, July 1976.

(Fo82) W. E. Ford et al., CSRL-V: Processed ENDF/B-V 227-Neutron Group and Pointwise Cross-Section Libraries for Criticality Safety, Reactor and Shielding Studies, NUREG/CR-2306, NRC, Washington, DC, June 1982.

(Fr71) D. G. Franklin and W. E. Ruther, "A Reactor In-Core Temperature Monitor," Trans. Am. Nucl. Soc. 14, p. 632, 1971.

(Fr78) Fracture Control Corp., Nuclear Pressure Vessel Steel Data Base, EPRI NP-933, Electric Power Research Institute, Palo Alto, CA, December 1978.

(Ga61) J. L. Gammel, Fast Neutron Physics, Part II, J. B. Marion and J. L. Fowler, Eds., Wiley (Interscience), New York, NY, 1961.

(Ga75) J. M. Gasidlo, M. M. Bretcher and D. W. Madison, Measurement of the Breeding Ratio and Its Components in ZPPR Assembly 4, Phase 1, ANL-RDP-40, Argonne National Laboratory, Argonne, IL, May 1975.

(Ga76) T. A. Gabriel, J. D. Gurney and N. M. Greene, Radiation-Damage Calculations: Primary Recoil Spectra, Displacement Rates, and Gas-Production Rates, ORNL/TM-5160, Oak Ridge National Laboratory, Oak Ridge, TN, March 1976.

(Ga83) D. M. Galliani, Nuclear Power Plant of Caorso Pressure Vessel Surveillance Program: Fast Neutron Flux Measurement, Performed at the End of the First Operating Cycle (January 1983), DPT/SN-158/R/83, ENEL - Italian Atomic Power Authority, National Electric Energy Agency, Rome, Italy, July 1983.

(Ge74) J. P. Genthon, B. W. Hasenclever et al., Recommendations on the Measurement of Irradiation Received by the Structural Materials of Reactors, EUR 5274, Commission of the European Communities, 1974.

(Ge75) J. P. Genthon and L. Salon, "G.A.M.I.N. Technique and Applications," Nucl. Eng. and Design 33, p. 2, 1975.

(Ge82) D. S. Gelles and L. E. Thomas, "Microstructural Examination of HT-9 and 9Cr-1Mo Contained in the AD-2 Experiment," Alloy Development for Irradiation Performance, Semiannual Report, DOE/ER-0045/8, US Department of Energy, Office of Fusion Energy, p. 343, March 1982.

(Gi78) D. M. Gilliam et al., "Reference and Standard Benchmark Field Consensus Fission Yields for U.S. Reactor Dosimetry Programs," Proc. of the 2nd ASTM-EURATOM Symposium on Reactor Dosimetry, Palo Alto, CA, October 3-7, 1977, NUREG/CP-0004, NRC, Washington, DC, p. 1507, 1978.

(Gi81) D. M. Gilliam et al., "Absolute Fission Rates in the FFTF," Trans. Am. Nucl. Soc. 39, p. 901, December 1981.

(Go68) R. Gold, R. J. Armani and J. H. Roberts, "Absolute Fission Rate Measurements with Solid-State Track Recorders," Nucl. Sci. Eng. 34, p. 13-34, 1968.

(Go68a) R. Gold, "Compton Continuum Measurements for Continuous Gamma-Ray Spectroscopy," Bull. Am. Phys. Soc. 13, p. 1405, 1968.

(Go68b) R. Gold and E. F. Bennett, "Effects of Finite Size in 4π-Recoil Proportional Counters," Nucl. Instrum. Methods 63, p. 285, 1968.

(Go70) R. Gold and I. K. Olson, Analysis of Compton Continuum Measurements, ANL-7611, Argonne National Laboratory, Argonne, IL, 1970.

(Go70a) R. Gold, "Compton Recoil Gamma-Ray Spectroscopy," Nucl. Instrum. Methods 84, p. 173, 1970.

(Go70b) R. Gold, "Compton Recoil Measurements of Continuous Gamma-Ray Spectra," Trans. Am. Nucl. Soc. 13, p. 421, 1970.

(Go70c) R. Gold, R. J. Armani and J. H. Roberts, "Spontaneous-Fission Decay Constants of ^{241}Am," Phys. Rev. C, I, p. 738, 1970.

(Go70d) R. Gold and A. M. Strash, "Gamma-Ray Dosimetry for the Natural Environment," Trans. Am. Nucl. Soc. 13, p. 502, 1970.

(Go71) R. Gold and C. E. Cohn, "Analysis of Automatic Fission Track Scanning Data," Trans. Am. Nucl. Soc. 14, p. 500, 1971.

(Go71a) R. Gold, "Gamma-Continuum at the Air-Land Interface," Health Phys. 21, p. 79, 1971.

(Go71b) R. Gold, Gamma Spectrum in ZPR-6 Assembly No. 6, ANL-ZPR-TM-63, Argonne National Laboratory, Argonne, IL, 1971.

(Go71c) R. Gold and A. M. Strash, "Preoperational Measurement of Environmental Gamma Rays at the Monticello Site with a Continuum Spectrometer," Trans. Am. Nucl. Soc. 14, p. 31, 1971.

(Go72) R. Gold and C. E. Cohn, "Analysis of Automatic Fission Track Scanning in Solid-State Nuclear Track Recorders," Rev. Sci. Instrum. 43, pp. 18-28, 1972.

(Go72a) R. Gold, F. J. Congel, J. H. Roberts and A. M. Strash, "Gamma Continuum at a Fossile-Fuel Site," Trans. Am. Nucl. Soc. 15, p. 639, 1972.

(Go73) R. Gold, A. M. Strash, F. J. Congel and J. H. Roberts, "Continuous Gamma-Ray Spectroscopy in the Natural Environment," Trans. IEEE NS-20, (1), p. 48, February 1973.

(Go74) R. Gold, B. G. Oltman, K. F. Eckerman and A. M. Strash, "Environmental Radiation at the EBR-II Site," Trans. IEEE NS-21, (1), pp. 596-601, February 1974.

(Go75) R. Gold, Status of Gamma-Ray Heating Characterization in LMFBR, HEDL-TME 75-126, Hanford Engineering Development Laboratory, Richland, WA, November 1975.

(Go77a) R. Gold, "Critical Requirements of the SSTR Method," Proc. of the 1st ASTM-EURATOM Symposium on Reactor Dosimetry, Petten, Netherlands, September 22-26, 1975, EUR 5667, Commission of the European Communities, Vol. II, pp. 175-188, 1977.

(Go77b) R. Gold, "Mass and Charge Dependence of SSTR Asymptotic Sensitivity," Proc. of the 1st ASTM-EURATOM Symposium on Reactor Dosimetry, Petten, Netherlands, September 22-26, 1975, EUR 5667, Commission of the European Communities, Vol. II, pp. 189-196, 1977.

(Go77c) R. Gold, "Neutron Spectrometry for Reactor Applications: Status Limitations and Future Directions," Proc. of the 1st ASTM-EURATOM Symposium on Reactor Dosimetry, Petten, Netherlands, September 22-26, 1975, EUR 5667, Commission of the European Communities, Vol. I, pp. 119-147, 1977.

(Go78) R. Gold, "Gamma-Ray Heating in Breeder Reactors," Interlaboratory Reaction Rate Program 11th Progress Report, November 1975 - October 1976, HEDL-TME 77-34, Hanford Engineering Development Laboratory, Richland, WA, Vol. 2, pp. HEDL-85 - HEDL-95, May 1978.

(Go78a) R. Gold, "Overview of Gamma-Ray Energy Deposition and Spectra in Fast Reactor Environments," Proc. of the 2nd ASTM-EURATOM Symposium on Reactor Dosimetry, Palo Alto, CA, October 3-7, 1977, NUREG/CP-0004, NRC, Washington, DC, Vol. 1, pp. 101-140, 1978.

(Go78b) R. Gold, "Estimates of High-Energy Gamma and Neutron Flux from Continuous Gamma-Ray Spectrometry," LWR-PV-SDIP Quarterly Progress Report - July-September 1983, NUREG/CP-0551, HEDL-TME 78-8, NRC, Washington, DC, December 1978.

(Go79) R. Gold, F. H. Ruddy and J. H. Roberts, "Applications of Solid State Track Recorders in US Nuclear Reactor Energy Programs," Proc. of the 10th International Conference on Solid State Nuclear Track Detectors, Lyons, France, July 2-7, 1979, Pergamon Press, Oxford, UK, 1980.

(Go79a) R. Gold, J. H. Roberts and F. H. Ruddy, "Solid State Track Recorder Materials for Use in Light Water Reactor Pressure Vessel Surveillance Exposures," Effects of Radiation on Structural Materials: Proc. of the 9th International Symposium, J. S. Sprague and D. Kramer, Eds., ASTM STP 683, American Society for Testing and Materials, Philadelphia, PA, pp. 402-423, 1979.

(Go79b) R. Gold and B. J. Kaiser, "Status of Compton Recoil Gamma-Ray Spectroscopy," Trans. Am. Nucl. Soc. 33, p. 692, 1979.

(Go79c) R. Gold, E. P. Lippincott, W. N. McElroy and R. L. Simons, "Radiation Damage Function Analysis," Effects of Radiation on Structural Materials: Proc. of the 9th International Symposium, J. A. Sprague and D. Kramer, Eds., ASTM STP 683, American Society for Testing and Materials, Philadelphia, PA, pp. 380-401, 1979.

(Go79d) R. Gold, "Estimates of High Energy Gamma and Neutron Flux from Continuous Gamma Ray Spectrometry," LWR-PV-SDIP Quarterly Progress Report, July - September 1978, NUREG/CR-0551, HEDL-TME 78-8, NRC, Washington, DC, 1979.

(Go80) R. Gold, J. H. Roberts and F. H. Ruddy, "Advances in SSTR Techniques for Dosimetry and Radiation Damage Measurements," Proc. of the 3rd ASTM-EURATOM Symposium on Reactor Dosimetry, Ispra, Italy, October 1-5, 1979, EUR 6813, Commission of the European Communities, Vol. II, pp. 1172-1187, 1980.

(Go80a) R. Gold, F. H. Ruddy and J. H. Roberts, "Buffon Needle Method of Track Scanning at High Track Density," Bull. Am. Phys. Soc. 25, p. 484, 1980.

(Go80b) R. Gold, R. B. Kaiser, F. S. Moore Jr, W. L. Bunch, W. N. McElroy and E. M. Sheen, "Continuous Gamma-Ray Spectrometry in the Fast Flux Test Facility," HEDL-SA-2166, Proc. of the ANS Topical Meeting on 1980 Advances in Reactor Physics and Shielding, Sun Valley, ID, September 14-17, 1980, ISDN 0-89448-107-X, p. 803, 1980.

(Go80c) R. Gold, E. P. Lippincott, W. N. McElroy and J. A. Rawlins, "FTR Measurement Plan for Interlaboratory Calibrations and Fission Product Yields," Interlaboratory Reaction Rate Program 12th Progress Report, November 1976 - October 1979, HEDL-TME 79-58, Hanford Engineering Development Laboratory, Richland, WA, p. HEDL-1, September 1980.

(Go80d) R. Gold and B. J. Kaiser, "Reactor Gamma-Ray Spectrometry: Status," Proc. of the 3rd ASTM-EURATOM Symposium on Reactor Dosimetry, Ispra, Italy, October 1-5, 1979, EUR 6813, Commission of the European Communities, Vol. II, pp. 1160-1171, 1980.

(Go80e) R. Gold, F. H. Ruddy and J. H. Roberts, "Solid State Track Recorder Applications in United States Nuclear Reactor Energy Programs," Trans. Am. Nucl. Soc. 34, p. 146, 1980.

(Go80f) R. Gold, F. H. Ruddy and J. H. Roberts, "Applications of Solid-State Track Recorders in US Nuclear Reactor Energy Programs," Proc. of the 10th International Conference on Solid-State Nuclear Track Detectors, Lyons, France, July 2 - 7, 1979, Pergamon Press, Oxford, UK, pp. 533-547, 1980.

(Go81) R. Gold and J. H. Roberts, "Nuclear Emulsion Neutron Spectrometry in the FFTF," Trans. Am. Nucl. Soc. 39, p. 896, December 1981.

(Go81b) R. Gold, "Gamma-Ray Data," LWR-PV-SDIP: PCA Experiments and Blind Test, NUREG/CR-1861, HEDL-TME 80-87, NRC, Washington, DC, Sec. 5.1 - 5.4, July 1981.

(Go81c) R. Gold and B. J. Kaiser, "Gamma-Ray Spectrometry," LWR PV-SDIP: PCA Experiments and Blind Test, NUREG/CR-1861, HEDL-TME 80-87, NRC, Washington, DC, Sec. 5.3, July 1981.

(Go81d) R. Gold, J. H. Roberts, F. H. Ruddy, C. C. Preston and C. A. Hendricks, "Proton-Recoil Emulsion Observations for Integral Neutron Dosimetry," Proc. of the IAEA Advisory Group Meeting on Nuclear Data for Radiation Damage Assessment and Related Safety Aspects, Vienna, October 12-18, 1981, IAEA-TECDOC-263, International Atomic Energy Agency, Vienna, Austria, pp. 115-121, 1982.

(Go81e) R. Gold, J. H. Roberts, C. C. Preston and F. H. Ruddy, "Neutron Spectrometry with Nuclear Research Emulsions," LWR-PV-SDIP: PCA Experiments and Blind Test, NUREG/CR-1861, HEDL-TME 80-87, NRC, Washington, DC, Sec. 3.3, July 1981.

(Go81f) R. Gold, "Experimental Program: Neutron Spectrometry," LWR-PV-SDIP: PCA Experiments and Blind Test, NUREG/CR-1861, HEDL-TME 80-87, NRC, Washington, DC, Chap. 3, July 1981.

(Go82) R. Gold, F. H. Ruddy and J. H. Roberts, "Buffon Needle Method of Track Counting," Proc. of the 11th International Conference on Solid State Nuclear Track Detectors, Bristol, UK, 1981, Pergamon Press, Oxford, UK, pp. 891-897, 1982.

(Go82a) R. Gold et al., "Computer-Controlled Scanning Systems for Quantitative Track Measurements," Proc. of the 4th ASTM-EURATOM Symposium on Reactor Dosimetry, Gaithersburg, MD, March 22-26, 1982, NUREG/CP-0029, NRC, Washington, DC, Vol. 1, pp. 281-292, July 1982.

(Go82b) R. Gold, B. J. Kaiser and J. P. McNeece, "Gamma-Ray Spectrometry in Light Water Reactor Environments," Proc. of the 4th ASTM-EURATOM Symposium on Reactor Dosimetry, Gaithersburg, MD, March 22-26, 1982, NUREG/CP-0029, NRC, Washington, DC, Vol. 1, pp. 267-279, July 1982.

(Go82c) R. Gold, F. H. Ruddy and J. H. Roberts, "Photofission Observations in Reactor Environments Using Selected Fission Product Yields," Proc. of the 4th ASTM-EURATOM Symposium on Reactor Dosimetry, Gaithersburg, MD, March 22-26, 1982, NUREG/CP-0029, NRC, Washington, DC, Vol. 1, pp. 345-353, July 1982.

(Go83) R. Gold et al., "Interactive System for Scanning Tracks in Nuclear Research Emulsions," Rev. Sci. Instrum. 54, pp. 183-192, 1983.

(Go83a) R. Gold, B. J. Kaiser and J. P. McNeece, "Continuous Energy Gamma-Ray Spectrometry," Trans. Am. Nucl. Soc. 45, pp. 228-230, 1983 (invited paper).

(Go83b) R. Gold, J. H. Roberts, J. P. McNeece, B. J. Kaiser, F. H. Ruddy, C. C. Preston, J. A. Ulseth and W. N. McElroy, "Fuel Debris Assessment for Three Mile Island Unit 2 (TMI-2) Reactor Recovery by Gamma-Ray and Neutron Dosimetry," 6th International Conf. on Nondestructive Evaluation in the Nuclear Industry, Zurich, Federal Republic of Germany, November 27-December 2, 1983.

(Gr75) R. C. Greenwood, R. G. Helmer, J. W. Rogers, N. D. Dudey, R. J. Popek, L. S. Kellogg and W. H. Zimmer, "Nonfission Reaction Rate Measurements," Nucl. Technol. 25, (2), p. 274, February 1975.

(Gr75a) J. A. Grundl, D. M. Gilliam, N. D. Dudey and R. J. Popek, "Measurement of Absolute Fission Rates," Nucl. Technol. 25, (2), p. 237, February 1975.

(Gr75b) J. A. Grundl and C. M. Eisenhauer, "Fission Spectrum Neutrons for Cross-Section Validation and Neutron Flux Transfer," Proc. of a Conference on Nuclear Cross Sections and Technology, NBS Special Publication 425, National Bureau of Standards, Washington, DC, Vol. 1, pp. 250-257, 1975.

(Gr77) J. A. Grundl, "Fission Rate Measurements and Their Interpretation for Reactor Materials," Proc. of the 1st ASTM-EURATOM Symposium on Reactor Dosimetry, Petten, Netherlands, September 22-26, 1975, EUR 5667, European Atomic Energy Community, 1977.

(Gr77a) J. A. Grundl and A. Fabry, "Workshop on Reactor Dosimetry Benchmarks," Proc. of the 1st ASTM-EURATOM Symposium on Reactor Dosimetry, Petten, Netherlands, September 22-26, 1975, EUR 5667, European Atomic Energy Community, 1977.

(Gr77b) J. A. Grundl, V. Spiegel, C. M. Eisenhauer, H. T. Heaton, D. M. Gilliam and J. Bigelow, "A Californium-252 Fission Spectrum Irradiation Facility for Neutron Reacton Rate Measurements," Nucl. Technol. 32, p. 315, 1977.

(Gr78) J. A. Grundl and C. M. Eisenhauer, "Benchmark Neutron Fields for Reactor Dosimetry," Neutron Cross Sections for Reactor Dosimetry, IAEA-208, International Atomic Energy Agency, Vienna, Austria, Vol. I, pp. 53-104, 1978.

(Gr78a) J. A. Grundl, C. M. Eisenhauer and E. D. McGarry, "Benchmark Neutron Fields for Pressure Vessel Surveillance Dosimetry," Compendium of Benchmark and Test Region Neutron Fields for Pressure Vessel Irradiation Surveillance, NUREG/CR-0551, NRC, Washington, DC, p. NBS-3, December 1978.

(Gr78b) N. M. Greene et al., AMPX-II: A Modular Code System for Generating Coupled Multigroup Neutron-Gamma-Ray Cross-Section Libraries from Data in ENDF Format, ORNL/TM-3706, Oak Ridge National Laboratory, Oak Ridge, TN, 1978.

(Gr81) J. A. Grundl et al., "NRC-EPRI Studies of Pressure-Vessel-Cavity Neutron Fields," Proc. of the 9th Water Reactor Safety Information Meeting, Gaithersburg, MD, October 26-30, 1981, NUREG/CP-0024, Vol. 1-3, NRC, Washington, DC, March 1982.

(Gr82) J. A. Grundl et al., "NBS Compendium of Benchmark Neutron Fields for Reactor Dosimetry," 1982 Annual Book of ASTM Standards, Part 45, "Nuclear Standards," American Society for Testing and Materials, Philadelphia, PA, p. 1266, 1982.

(Gr83) J. A. Grundl, C. M. Eisenhauer and E. D. McGarry, "Neutron Flux Measurements in the Pressure Vessel Cavity of an Operating US Power Reactor, LWR-PV-SDIP Quarterly Progress Report, January 1982 - March 1982, NUREG/CR-2805, Vol. 1, HEDL-TME 82-18, pp. NBS-3 - NBS-52, January 1983.

(Gr83a) J. A. Grundl and D. M. Gilliam, "Fission Cross-Section Measurements in Reactor Physics and Dosimetry Benchmarks," Trans. Am. Nucl. Soc. 44, p. 533, 1983.

(Gr83b) P. W. Gray, "Random Sampling in the Scanning of Solid-State Track Recorders," Thesis, Imperial College, University of London, Silwood Park, Ascot, UK, 1983.

(Gu68) R. O. Gumprecht, Mathematical Basis of Computer Code RIBD, DUN-4136, Douglas United Nuclear, Inc., Richland, WA, June 1968.

(Gu72) R. Gunnink and J. B. Nidday, Computerized Quantitative Analysis by Gamma-Ray Spectrometry: The GAMANAL Program, UCRL-51567, Vol. 1, Lawrence Livermore National Laboratory, Livermore, CA, March 1972.

(Gu80) G. L. Guthrie, "Reanalysis of the Existing Data Base Relating Irradiation Embrittlement and Neutron Exposure of Pressure Vessel Steels," LWR-PV-SDIP Quarterly Progress Report, January 1980 - March 1980, NUREG/CR-1241, Vol. 1, HEDL-TME 80-4, Hanford Engineering Development Laboratory, Richland, WA, December 1980.

(Gu82) G. L. Guthrie, W. N. McElroy and S. L. Anderson, "A Preliminary Study of the Use of Fuel Management Techniques for Slowing Pressure Vessel Embrittlement," Proc. of the 4th ASTM-EURATOM Symposium on Reactor Dosimetry, Gaithersburg, MD, March 22-26, 1982, NUREG/CP-0029, NRC, Washington, DC, Vol. 1, pp. 111-120, July 1982.

(Gu82a) G. L. Guthrie, W. N. McElroy and S. L. Anderson, "Investigations of Effects of Reactor Core Loadings on PV Neutron Exposure," LWR-PV-SDIP Quarterly Progress Report, October 1981 - December 1981, NUREG/CR-2345, Vol. 4, HEDL-TME 81-36, Section E and Appendix, pp. HEDL-35 - HEDL-36 & HEDL-A1 - HEDL-A46, Hanford Engineering Development Laboratory, Richland, WA, October 1982.

(Gu82b) G. L. Guthrie, "Development of Trend Curve Formulas Using Surveillance Data," LWR-PV-SDIP Quarterly Progress Report, January 1982 - March 1982, NUREG/CR-2805, Vol. 1, HEDL-TME 82-18, Hanford Engineering Development Laboratory, Richland, WA, pp. HEDL-3 - HEDL-18, December 1982.

(Gu82c) G. L. Guthrie, "Development of Trend Curve Formulas Using Surveillance Data-II," LWR-PV-SDIP Quarterly Progress Report, April - June 1982, NUREG/CR-2805, Vol. 2, HEDL-TME 82-19, Hanford Engineering Development Laboratory, Richland, WA, pp. HEDL-3 - HEDL-13, December 1982.

(Gu82d) C. Guionnet, B. Houssin et al., Radiation Embrittlement of PWR Reactor Vessel Weld Metals - Nickel and Copper Synergism Effects, ASTM STP 782, American Society for Testing and Materials, Philadelphia, PA, 1982.

(Gu83) G. L. Guthrie, "Charpy Trend Curve Formulas Derived from an Expanded Surveillance Data Base," LWR-PV-SDIP Quarterly Progress Report, October 1982 - December 1982, NUREG/CR-2805, Vol. 4, HEDL-TME 82-21, Hanford Engineering Development Laboratory, Richland, WA, pp. HEDL-3 - HEDL-13, July 1983.

(Gu83a) G. L. Guthrie, "Pressure Vessel Steel Irradiation Embrittlement Formulas Derived from PWR Surveillance Data," from the ANS Special Session on Correlations and Implications of Neutron Irradiation Embrittlement of Pressure Vessel Steels, Detroit, MI, June 12-16, 1983, Trans. Am. Nucl. Soc. 44, p. 222, January 1983.

(Gu83b) G. L. Guthrie, "Error Estimations in Applications of Charpy Trend Curve Formulas," LWR-PV-SDIP Quarterly Progress Report, January 1983 - March 1983, NUREG/CR-3391, Vol. 1, HEDL-TME 83-21, Hanford Engineering Development Laboratory, Richland, WA, pp. HEDL-3 - HEDL-13, November 1983.

(Gu83c) G. L. Guthrie, "Charpy Trend-Curve Development Based on PWR Surveillance Data," Proc. of the 11th WRSR Information Meeting, Gaithersburg, MD, October 24-28, 1983, NUREG/CP-0048, NRC, Washington, DC.

(Gu84) G. L. Guthrie, "Charpy Trend Curves Based on 177 PWR Data Points," LWR-PV-SDIP Quarterly Progress Report, April 1983 - June 1983, NUREG/CR-3391, Vol. 2, HEDL-TME 83-22, Hanford Engineering Development Laboratory, Richland, WA, HEDL-3 - HEDL-15, April 1984.

(Gu84a) G. L. Guthrie, W. N. McElroy and R. L. Simons, "Effect of Thermal Neutrons in Irradiation Embrittlement of PWR Pressure Vessel Plates and Welds," LWR-PV-SDIP Quarterly Progress Report, April 1983 - June 1983, NUREG/CR-3391, Vol. 2, HEDL-TME 83-22, Hanford Engineering Development Laboratory, Richland, WA, HEDL-16 - HEDL-21, April 1984.

(Ha68) R. W. Hardie and W. W. Little Jr, 1DX, A One-Dimensional Diffusion Code for Generating Effective Nuclear Cross Sections, BNWL-954, Battelle Pacific Northwest Laboratory, Richland, WA, September 1968.

(Ha70) R. W. Hardie and W. W. Little Jr, 3 hree-Dimensional Diffusion Theory Burnup Code, BNWL-1264, Battelle Pacific Northwest Laboratory, Richland, WA, March 1970.

(Ha79) J. R. Hawthorne and J. A. Sprague, Radiation Effects to Reactor Vessel Support Structures, Report by Task C of Interagency Agreement NRC-03-79-148, NRC, Washington, DC, October 22, 1979.

(Ha81) M. G. C. Hall, "DUCKPOND: A Perturbation Monte Carlo Code and Its Applications," Proc. of NEA Specialists Meeting on Nuclear Data and Benchmarks for Reactor Shielding, Paris, France, October 1980, Organization for Economic Cooperation and Development, 1981.

(Ha82) W. O. Harms et al., National Program Plan for Mechanical Properties Design Data, Materials and Structures Technology Management Center, Oak Ridge National Laboratory, Oak Ridge, TN, current edition.

(Ha82a) J. R. Hawthorne, "Irradiation and Annealing Sensitivity Studies," MEA-2009, Materials Engineering Associates, Inc., Oxen Hill, MD, October 1982, and Proc. of the 10th WRSR Information Meeting, Gaithersburg, MD, October 12-15, 1982, NUREG/CR-0041, Vol. 4, NRC, Washington, DC, January 1983.

(Ha83) J. R. Hawthorne, "Evaluation of Reimbrittlement Rate Following Annealing and Related Investigations on RPV Steels," MEA-2032, Materials Engineering Associates, Inc., Oxen Hill, MD, and Proc. of the 11th WRSR Information Meeting, Gaithersburg, MD, October 24-28, 1983, NUREG/CP-0048, NRC, Washington, DC.

(Ha84) J. R. Hawthorne, B. H. Menke and A. L. Hiser, LWR-PV-SDIP: Notch Ductility and Fracture Toughness Degradation of A302-B and A533-B Reference Plates from PSF Simulated Surveillance and Through-Wall Irradiation Capsules, NUREG/CR-3295, MEA-2017, NRC, Washington, DC, 1984.

(Ha84a) J. R. Hawthorne and B. H. Menke, LWR-PV-SDIP: Postirradiation Notch Ductility and Tensile Strength Determinations for PSF Simulated Surveillance and Through-Wall Specimen Capsules, NUREG/CR-3457, MEA-2026, NRC, Washington, DC, 1984.

(He74) D. Heck, H. Borner, J. A. Pinston and R. Roussille, "Neutron Capture Cross Section of ^{147}Nd," Atomkernenergie 24, p. 141, 1974.

(He75) R. G. Helmer and R. C. Greenwood, "Evaluated Decay Scheme Data," Nucl. Technol. 25, (2), p. 258, February 1975.

(He78) R. G. Helmer and R. C. Greenwood, "Evaluated Decay Scheme Data," Interlaboratory Reaction Rate Program 11th Progress Report, November 1975 - October 1976, HEDL-TME 77-34, Vol. 1, Hanford Engineering Development Laboratory, Richland, WA, pp. EGG-1 - EGG-6, May 1978.

(He82) P. D. Hedgecock and J. S. Perrin, "Standards for Materials Behavior Under Neutron Irradiation," Proc. of the 4th ASTM-EURATOM Symposium on Reactor Dosimetry, Gaithersburg, MD, March 22-26, 1982, NUREG/CP-0029, NRC, Washington, DC, Vol. 2, pp. 829-837, July 1982.

(Hi66) B. S. Hickman and D. G. Walker, "The Effect of Neutron Irradiation on Aluminum Oxide," J. Nucl. Mater. 18, p. 197, 1966.

(Ho78) W. C. Hopkins, "Suggested Approach for Fracture-Safe RPV Support Structure Design in Neutron Environments," Trans. Am. Nucl. Soc. 30, p. 187, November 1978.

(Ho79) N. E. Holden, "Atomic Weights of the Elements, 1977," Pure & Appl. Chem. 51, pp. 405-433, 1979.

(Ir70) D. R. Ireland and V. G. Scotti, Examination and Evaluation of Capsule A for the Connecticut Yankee Reactor Pressure Vessel Surveillance Program, Battelle Memorial Institute, Columbus Laboratories, Columbus, OH, October 30, 1970.

(Ja73) J. L. Jackson, W. N. McElroy, J. A. Ulseth and L. S. Kellogg, EBR-II Dosimetry Test (Reactor Runs 50G and 50H), HEDL-TME 73-62, Hanford Engineering Development Laboratory, Richland, WA, July 1973.

(Ja73a) J. L. Jackson, W. N. McElroy, J. A. Ulseth and L. S. Kellogg, "EBR-II Dosimetry Tests," Proc. of ANS Topical Meeting on Irradiation Experimentation in Fast Reactors, Jackson, WY, September 10-12, Unnumbered ANS Report, American Nuclear Society, Hinsdale, IL, pp. 383-400, 1973.

(Ji78) S. H. Jiang and H. Werle, "Fission Neutron-Induced Gamma Fields in Iron," Nucl. Sci. Eng. 66, p. 354, 1978.

(Ka75) F. B. K. Kam and F. W. Stallman, "Damage Function Analysis," J. Testing & Eval. 3, (3), p. 220, 1975.

(Ka81) B. J. Kaiser, R. Gold and J. P. McNeece, "Si(Li) Gamma-Ray Dosimetry," LWR-PV-SDIP: PCA Experiments and Blind Test, NUREG/CR-1861, HEDL-TME 80-87, NRC, Washington, DC, pp. 5.3-1 - 5.3-8, July 1981.

(Ka82) F. B. K. Kam, Ed., Proc. of the 4th ASTM-EURATOM Symposium on Reactor Dosimetry, Gaithersburg, MD, March 22-26, 1982, NUREG/CP-0029, NRC, Washington, DC, Vols. 1 and 2, July 1982.

(Ka82a) F. B. K. Kam, "Characterization of the Fourth HSST Series of Neutron Spectral Metallurgical Irradiation Capsules," Paper presented at the 4th ASTM-EURATOM Symposium on Reactor Dosimetry, Gaithersburg, MD, March 22-26, 1982, preprints available.

(Ka82b) F. B. K. Kam et al., "Neutron Exposure Parameters for the Fourth HSST Series of Metallurgical Irradiation Capsules," Proc. of the 4th ASTM-EURATOM Symposium on Reactor Dosimetry, Gaithersburg, MD, March 22-26, 1982, NUREG/CP-0029, NRC, Washington, DC, Vol. 2, pp. 1023-1033, July 1982.

(Ka83) F. B. K. Kam, F. W. Stallmann, R. E. Maerker and M. L. Williams, "Light Water Reactor Pressure Vessel (LWR-PV) Benchmark Facilities (PCA, ORR-PSF, ORR-SDMF) at ORNL," LWR-PV-SDIP Quarterly Progress Report, April 1982 - June 1982, HEDL-TME 82-19, Hanford Engineering Development Laboratory, Richland, WA, pp. ORNL-1 - ORNL-19, January 1983.

(Ke70) L. S. Kellogg and W. Zimmer, EBR-II Dosimetry Test Reaction Rate Measurements (Reactor Runs 31E and 31F), BNWL-1403, Battelle Pacific Northwest Laboratory, Richland, WA, 1970.

(Ke76) L. S. Kellogg, W. Y. Matsumoto, C. J. Ambrose and J. M. Ruggles, "EBR-II Derived Fission Yields from Vanadium Encapsulated Fission Monitors," LMFBR Reaction Rate and Dosimetry 10th Progress Report, June 1974 - October 1975, HEDL-TME 75-130, Hanford Engineering Development Laboratory, Richland, WA, August 1976.

(Ke78) L. S. Kellogg, A. I. Davis, E. P. Lippincott and J. M. Ruggles, "EBR-II Validated, Key Fission Product Yields for Fast Reactor Application," Proc. of the 2nd ASTM-EURATOM Symposium on Reactor Dosimetry, Palo Alto, CA, October 3-7, 1977, NUREG/CP-0004, NRC, Washington, DC, Vol. 3, pp. 1307-1321, 1978.

(Ke82) L. S. Kellogg and E. P. Lippincott, "PSF Interlaboratory Comparison," Proc. of the 4th ASTM-EURATOM Symposium on Reactor Dosimetry, Gaithersburg, MD, March 22-26, 1982, NUREG/CP-0029, NRC, Washington, DC, Vol. 1, pp. 929-945, July 1982.

(Ki71) R. B. Kidman and R. E. Schenter, FTR Set 300S Multigroup Cross Sections for FTR Shielding Calculations, HEDL-TME 71-84, Hanford Engineering Development Laboratory, Richland, WA, December 1971.

(Ki79) R. Kinsey, ENDF-201, ENDF/B Summary Documentation, BNL-NCS-17541 (ENDF/B-V), 3rd ed., Brookhaven National Laboratory, Upton, NY, 1979.

(Kn70) J. R. Knight and F. R. Mynatt, MUG, A Program for Generating Multigroup Photon Cross Sections, CTC-17, Computing Technology Center, Oak Ridge, TN, January 1970.

(Kn79) D. W. Kneff and H. Farrar IV, "Helium Accumulation Fluence Dosimetry for Fusion Reactor Materials Irradiations," J. Nucl. Mater. 85 & 86, p. 479, 1979.

(Ko75) H. E. Korn, Measurement of the Energy Distribution of the Gamma Field in a Fast Reactor, KFK 2211, Karlsruhe Nuclear Research Center, Karlsruhe, Federal Republic of Germany, 1975.

(Ko82) N. P. Kocherov, "Highlights from the IAEA Advisory Group Meeting on Nuclear Data for Radiation Damage Assessment and Related Safety Aspects," Proc. of the 4th ASTM-EURATOM Symposium on Reactor Dosimetry, Gaithersburg, MD, March 22-26, 1982, NUREG/CP-0029, NRC, Washington, DC, Vol. 2, pp. 873-875, July 1982.

(Kr82) R. C. Kryter et al., Evaluation of Pressurized Thermal Shock, Initial Phase Study, NUREG/CR-2083, ORNL/TM-8072, Oak Ridge National Laboratory, Oak Ridge, TN, 1982.

(La65) K. D. Lathrop, DTV-IV, A FORTRAN-IV Program for Solving the Multigroup Transport Equation with Anisotropic Scattering, LA-3373, Los Alamos National Laboratory, Los Alamos, NM, July 1965.

(La69) N. L. Lark, "Spark Scanning for Fission Fragment Tracks in Plastic Foils," Nucl. Instrum. Methods 67, pp. 137-140, 1969.

(La82) M. Lammer, Comp., Progress in Fission Product Nuclear Data, INDC(NDS)-130/G+P, No. 8, International Atomic Energy Agency, Vienna, Austria, July 1982.

(Le83) T. A. Lewis, "Use of Beryllium-Oxide Thermoluminescence Dosimeters for Measuring Gamma Exposure Rates in Graphite-Moderated Reactors," Needs Lab TPRD/B/0349/N83, October 1983.

(Li68) W. W. Little and R. W. Hardie, 2DB, A Two-Dimensional Diffusion-Burnup Code for Fast Reactor Analysis, BNWL-640, Battelle Pacific Northwest Laboratory, Richland, WA, January 1968.

(Li68a) W. W. Little and R. W. Hardie, 2DB User's Manual, BNWL-831, Rev. 1, Battelle Pacific Northwest Laboratory, Richland, WA, July 1968.

(Li75) E. P. Lippincott, J. A. Ulseth, L. S. Kellogg, A. I. Davis and W. N. McElroy, EBR-II 75D High Power Dosimetry Test, HEDL-TME 75-86, Hanford Engineering Development Laboratory, Richland, WA, December 1975.

(Li75a) E. P. Lippincott, W. N. McElroy and H. Farrar IV, "Helium Production in Reactor Materials," Proc. of the Conference on Nuclear Cross Sections and Technology, Washington, DC, March 3-7, 1975, COM-75-11469, Air Force Ballistic Missile Division, Englewood, CA, Vol. 1, p. 375, October 1975.

(Li78) E. P. Lippincott and J. A. Ulseth, "High Flux-Fluence Measurements in Fast Reactors," Proc. of the 2nd ASTM-EURATOM Symposium on Reactor Dosimetry, Palo Alto, CA, October 3-7, 1977, NUREG/CP-0004, NRC, Washington, DC, Vol. 1, pp. 271-283, 1978.

(Li80) E. P. Lippincott, W. N. McElroy and C. C. Preston, Interlaboratory Reaction Rate Program 12th Progress Report, November 1976 - October 1979, HEDL-TME 79-58, Hanford Engineering Development Laboratory, Richland, WA, September 1980.

(Li81) E. P. Lippincott, W. M. McElroy, L. S. Kellogg et al., Fabrication Data Package for HEDL Dosimetry in the ORNL Poolside Facility LWR Pressure Vessel Mock-Up Irradiation, HEDL-TC-2065, Cleared 2/23/82, Hanford Engineering Development Laboratory, Richland, WA, September 1981.

(Li82) E. P. Lippincott and W. N. McElroy, "ASTM Standard Recommended Guide on Application of ENDF/A Cross Section and Uncertainty File: Establishment of the File," Proc. of the 4th ASTM-EURATOM Symposium on Reactor Dosimetry, Gaithersburg, MD, March 22-26, 1982, NUREG/CP-0029, NRC, Washington, DC, Vol. 2, pp. 705-710, July 1982.

(Lo75) A. L. Lowe Jr et al., Analysis of Capsule OCI-F from Duke Power Company, Oconee Unit No. 1 Reactor Vessel Materials Surveillance Program, BAW-1421, Babcock & Wilcox, Lynchburg, VA, August 1975.

(Lo77) A. L. Lowe Jr et al., Analysis of Capsule OCI-E from Duke Power Company, Oconee Nuclear Station - Unit 1, BAW-1436, Babcock & Wilcox, Lynchburg, VA, September 1977.

(Lo77a) A. L. Lowe Jr et al., Analysis of Capsule OCII-C from Duke Power Company, Oconee Nuclear Station - Unit 2, BAW-1437, Babcock & Wilcox, Lynchburg, VA, May 1977.

(Lo77b) A. L. Lowe Jr et al., Analysis of Capsule OCII-A from Duke Power Company, Oconee Nuclear Station - Unit 3, BAW-1438, Babcock & Wilcox, Lynchburg, VA, July 1977.

(Lo77c) A. L. Lowe Jr et al., Analysis of Capsule TMI-1E from Metropolitan Edison Company, Three Mile Island Nuclear Station - Unit 1, BAW-1439, Babcock & Wilcox, Lynchburg, VA, January 1977.

(Lo77d) A. L. Lowe Jr et al., Analysis of Capsule ANI-E from Arkansas Power & Light Company, Arkansas Nuclear Station - Unit 1, BAW-1440, Babcock & Wilcox, Lynchburg, VA, April 1977.

(Lo79) C. L. Long, J. A. Ulseth, E. P. Lippincott and N. J. Graves, EBR-II Spectral Parameters, Run 75D, HEDL-TME 78-84, Hanford Engineering Development Laboratory, Richland, WA, March 1979.

(Lo81) A. L. Lowe Jr et al., Analysis of Capsule CR3-B from Florida Power Corporation, Crystal River - Unit 3, BAW-1679, Babcock & Wilcox, Lynchburg, VA, June 1981.

(Lo81a) A. L. Lowe Jr et al., Analysis of Capsule ANI-B from Arkansas Power & Light Company, Arkansas Nuclear Station - Unit 1, BAW-1698, Babcock & Wilcox, Lynchburg, VA, December 1981.

(Lo81b) A. L. Lowe Jr et al., Analysis of Capsule OCII-A from Duke Power Company, Oconee Nuclear Station - Unit 2, BAW-1699, Babcock & Wilcox, Lynchburg, VA, December 1981.

(Lo81c) A. L. Lowe Jr et al., Analysis of Capsule OCIII-B from Duke Power Company, Oconee Nuclear Station - Unit 3, BAW-1697, Babcock & Wilcox, Lynchburg, VA, October 1981.

(Lo81d) A. L. Lowe Jr et al., Analysis of Capsule V Virginia Electric and Power Company, North Anna Unit No. 1 Reactor Vessel Materials Surveillance Program, BAW-1638, Babcock & Wilcox, Lynchburg, VA, March 1981.

(Lo82) A. L. Lowe Jr et al., Analysis of Capsule TEI-F from the Toledo Edison Company, Davis-Besse Nuclear Station - Unit 1, BAW-1701, Babcock & Wilcox, Lynchburg, VA, January 1982.

(Lo82a) A. L. Lowe Jr et al., Analysis of Capsule RSI-B from Sacramento Muncipal Utility District, Rancho Seco - Unit 1, BAW-1702, Babcock & Wilcox, Lynchburg, VA, February 1982.

(Lo82b) F. J. Loss, B. H. Menke and A. L. Hiser, "Fracture Toughness Characterization of Irradiated, Low-Upper Shelf Welds," Proc. of the 10th WRSR Information Meeting, Gaithersburg, MD, October 12-15, 1982, NUREG/CP-0041, Vol. 4, NRC, Washington, DC, pp. 168-183, January 1983.

(Lu81) A. T. Luksic, W. L. Bunch and G. Felgate, "In-Reactor Thimble System for FTR Characterization," Trans. Am. Nucl. Soc. 39, p. 893, 1981.

(Lu83) G. E. Lucas et al., "Preliminary Observations of the Chemistry and Temperature Dependence of Radiation Hardening in Pressure Vessel Steels," from the ANS Special Session on Correlations and Implications of Neutron Irradiation Embrittlement of Pressure Vessel Steels, Detroit, MI, June 12-16, 1983, Trans. Am. Nucl. Soc. 44, p. 231, 1983.

(Ly72) J. H. Lynch, "Correlation of Irradiation Data Using Activation Fluences and Irradiation Temperatures," Nucl. Technol. 3, pp. 411-421, September 1972.

(Ma63) D. W. Marquardt, "An Algorithm for Least-Squares Estimation of Non-Linear Parameters," J. Soc. Indust. Appl. Math. 11, pp. 431-441, 1963.

(Ma70) D. R. Marr, A User's Manual for 2DBS, A Diffusion Theory Shielding Code, BNWL-1291, Battelle Pacific Northwest Laboratory, Richland, WA, February 1970.

(Ma71) B. R. Martin, Statistics for Physicists, Academic Press, New York, NY, Sec. 8.1.2, 1971.

(Ma73) W. J. Maeck, R. P. Larsen and J. E. Rein, Burnup Determination for Fast Reactor Fuels: A Review and Status of the Nuclear Data and Analytical Chemistry Methodology Requirements, TIC-26209, Allied Chemical Corp., 1973.

(Ma73a) T. R. Mager et al., Analysis of Capsule V from the Rochester Gas and Electric Company, R. E. Ginna Unit No. 1 Reactor Vessel Radiation Surveillance Program, FP-RA-1, Westinghouse Electric Corp., Pittsburgh, PA, April 1973.

(Ma74) W. J. Maeck, Fission Product Nuclear Data Requirements for the Determination of Nuclear Fuel Burnup: A Review, ICP-1040, US Department of Energy, Washington, DC, January 1974.

(Ma75) B. A. Magurno and O. Ozer, "ENDF/B File for Dosimetry Applications," Nucl. Technol. 25, (2), p. 376, February 1975.

(Ma76) W. J. Maeck, W. A. Emel, L. L. Dickerson, J. E. Delmore, J. H. Keller, F. A. Duce and R. L. Tromp, Discrepancies and Comments Regarding ^{235}U and ^{239}Pu Thermal Fission Yields and the Use of ^{148}Nd as a Burnup Monitor, CP-1092, Idaho National Engineering Laboratory, Idaho Falls, ID, 1976.

(Ma78) W. J. Maeck, W. A. Emel and J. E. Delmore, "Fast Reactor Fission Yield Measurement Program at the Idaho National Engineering Laboratory," Proc. of the 2nd ASTM-EURATOM Symposium on Reactor Dosimetry, Palo Alto, CA, October 3-7, 1977, NUREG/CP-0004, NRC, Washington, DC, Vol. 3, pp. 1267-1278, 1978.

(Ma78a) W. J. Maeck, "Studies Relative to the Correlation of Fission Yields with Neutron Energy," Proc. of the 2nd ASTM-EURATOM Symposium on Reactor Dosimetry, Palo Alto, CA, October 3-7, 1977, NUREG/CP-0004, NRC, Washington, DC, Vol. 3, pp. 1279-1287, 1978.

(Ma78b) T. U. Marston and K. E. Stahlkopf, "Radiation Embrittlement: Significance of Its Effects on Integrity and Operation of LWR Pressure Vessels," Nuclear Safety 2, (6), p. 724, November - December 1978.

(Ma80) W. J. Maeck and R. L. Tromp, "Fast Reactor Fission Yield Measurements in FFTF," Interlaboratory Reaction Rate Program 12th Progress Report, November 1976 - October 1979, HEDL-TME 79-58, Hanford Engineering Development Laboratory, Richland, WA, p. EXXON-1, September 1980.

(Ma80a) R. E. Maerker and J. J. Wagschal, "Uncertainties and Biases Arising from Methods Approximations," Proc. of an IAEA Technical Meeting Held at KFA, Jülich, Federal Republic of Germany, September 24-27, 1979, Jul-CONF-37, International Atomic Energy Agency, Vienna, Austria, May 1980.

(Ma80b) B. A. Magurno, "Status of Data Testing of ENDF/B-V Reactor Dosimetry File," Proc. of the 3rd ASTM-EURATOM International Symposium on Reactor Dosimetry, Ispra, Italy, October 1-5, 1979, EUR 6813, Commission of the European Communities, Vol. II, pp. 903-913, 1980.

(Ma81) R. E. Maerker, J. J. Wagschal and B. L. Broadhead, Development and Demonstration of an Advanced Methodology for LWR Dosimetry Applications, EPRI NP-2188, (Project 1399-1, Interim Report), Electric Power Research Institute, Palo Alto, CA, December 1981.

(Ma81a) W. Mannhart, "Progress in Integral Data and Their Accuracy: Average Neutron Cross Sections in the Californium-252 Benchmark Field," Nucl. Sci. Eng. 77, p. 40, 1981.

(Ma81b) R. E. Maerker, "Analysis of Participant A," LWR-PV-SDIP: PCA Experiments and Blind Test, NUREG/CR-1861, HEDL-TME 80-87, NRC, Washington, DC, pp. 6.10-1 - 6.10-8, July 1981.

(Ma81c) G. C. Martin and H. A. Till, "Brown's Ferry Unit 3 Cavity Neutron Spectral Analysis," Proc. of the 4th ASTM-EURATOM Symposium on Reactor Dosimetry, Gaithersburg, MD, March 22-26, 1982, NUREG/CP-0029, NRC, Washington, DC, Vol. 1, pp. 555-564, July 1982.

(Ma81d) G. C. Martin, Brown's Ferry Unit-3 Cavity Neutron Spectral Analysis, EPRI NP-1997, Electric Power Research Institute, Palo Alto, CA, August 1981.

(Ma81e) R. E. Maerker and P. J. Maudlin, Supplementary Neutron Flux Calculations for the ORNL Pool Critical Assembly Pressure Vessel Facility, ORNL/TM-7602, Oak Ridge National Laboratory, Oak Ridge, TN, 1981.

(Ma82) N. Maene, R. Menil, G. Minsart and L. Ghoos, "Gamma Dosimetry and Calculations," Proc. of the 4th ASTM-EURATOM Symposium on Reactor Dosimetry, Gaithersburg, MD, March 22-26, 1982, NUREG/CP-0029, NRC, Washington, DC, Vol. 1, pp. 355-363, July 1982.

(Ma82a) R. E. Maerker and M. Austin, "Workshop on Neutron and Gamma-Ray Transport Methods," Proc. of the 4th ASTM-EURATOM Symposium on Reactor Dosimetry, Gaithersburg, MD, March 22-26, 1982, NUREG/CP-0029, NRC, Washington, DC, Vol. 2, pp. 1235-1237, July 1982.

(Ma82b) P. Mas and R. Perdreau, "Caracterisation d' Emplacements d'Irradiation en Spectres Neutroniques et en Dommages," Proc. of the 4th ASTM-EURATOM Symposium on Reactor Dosimetry, Gaithersburg, MD, March 22-26, 1982, NUREG/CP-0029, NRC, Washington, DC, Vol. 2, pp. 847-854, July 1982.

(Ma82c) J. A. Mason, "Development of Sensitive Microcalorimeters for Absorbed Dose Measurements in Benchmark ıdiation Fields," Proc. of the 4th ASTM-EURATOM Symposium on Reactor Dosimetry, Gaithersburg, MD, March 22-26, 1982, NUREG/CP-0029, NRC, Washington, DC, Vol. 1, pp. 365-378, July 1982.

(Ma82d) F. M. Mann, FTR Set 500, A Multigroup Cross-Section Set for FTR Analysis, HEDL-TME 81-31, Hanford Engineering Development Laboratory, Richland, WA, February 1982.

(Ma82e) R. E. Maerker and M. L. Williams, "Calculations of the Westinghouse Perturbation Experiment at the Poolside Facility," Proc. of the 4th ASTM-EURATOM Symposium on Reactor Dosimetry, Gaithersburg, MD, March 22-26, 1982, NUREG/CP-0029, NRC, Washington, DC, Vol. 1, pp. 131-141, July 1982.

(Ma82f) P. J. Maudlin and R. E. Maerker, "Supplementary Neutron Flux Calculations for the ORNL PCA-PV Facility," Proc. of the 4th ASTM-EURATOM Symposium on Reactor Dosimetry, Gaithersburg, MD, March 22-26, 1982, NUREG/CP-0029, NRC, Washington, DC, Vol. 2, pp. 689-698, July 1982.

(Ma82g) T. R. Mager et al., Feasibility of and Methodology for Thermal Annealing of Embrittled Reactor Vessel - Vol. 2: Detailed Technical Description of the Work, EPRI NP-2712, (Final Report, Project 1021-1), Electric Power Research Institute, Palo Alto, CA, November 1982.

(Ma82h) T. U. Marston and T. R. Mager, "EPRI Thermal Anneal Program RP1021-1," Report to ASME Section XI Subcommittee on Repairs and Replacements and to NRC, February 1982.

(Ma83) T. U. Marston, "A Brief on the Assessment of Relative Uncertainties," from the ANS Special Session on Correlations and Implications of Neutron Irradiation Embrittlement of Pressure Vessel Steels, Detroit, MI, June 12-16, 1983, Trans. Am. Nucl. Soc. 44, p. 221, 1983.

(Ma83a) R. E. Maerker and M. L. Williams, "Validation of Neutron Transport Calculations in Benchmark Facilities for Improved Vessel Fluence Estimations," Proc. of the 11th WRSR Information Meeting, Gaithersburg, MD, October 24-28, 1983, NUREG/CP-0048, NRC, Washington, DC.

(Ma84) R. E. Maerker et al., "Neutron and Gamma Transport Results for 12/13 Configurations," PCA Dosimetry in Support of the PSF Physics-Dosimetry-Metallurgy Experiments, NUREG/CR-3318, HEDL-TME 84-1, NRC, Washington, DC, January 1984.

(Mc67) W. N. McElroy, S. Berg and T. Crocket, A Computer-Automated Iterative Method of Neutron Flux Spectra Determined by Foil Activation, AFWL-TR-67-41, Vol. I-IV, Air Force Weapons Laboratory, Kirkland AFB, NM, July 1967.

(Mc69) W. N. McElroy, R. E. Dahl Jr and C. Z. Serpan Jr, "Damage Functions and Data Correlation," Nucl. Appl. Technol. 7, (6), pp. 561-571, December 1969.

(Mc70) W. N. McElroy, J. L. Jackson, J. A. Ulseth and R. L. Simons, EBR-II Dosimetry Test Data Analysis (Reactor Runs 31E and 31F), BNWL-1402, Battelle Pacific Northwest Laboratory, Richland, WA, 1970.

(Mc70a) W. N. McElroy and R. E. Dahl, "Neutron Dosimetry for Fast Reactor Applications," Irradiation Effects on Structural Alloys for Nuclear Reactor Applications, ASTM STP 484, American Society for Testing and Materials, Philadelphia, PA, pp. 375-399, 1970.

(Mc70b) W. N. McElroy, R. E. Dahl Jr and E. R. Gilbert, "Neutron Energy-Dependent Damage Function for Analysis of Austenitic Steel Creep Data," Nucl. Eng. & Design 14, (1), pp. 319-331, October 1970.

(Mc71) W. N. McElroy and H. Farrar IV, "Helium Production in Stainless Steel and Its Constituents as Related to LMFBR Development Programs," Proc. of Conference on Radiation-Induced Voids in Metals, Albany, NY, June 9-11, 1971.

(Mc72) W. N. McElroy, R. L. Simons, D. G. Doran and J. L. Straalsund, "Damage Function for Swelling in Type 304 Stainless Steel," Trans. Am. Nucl. Soc. 15, (1), p. 249, 1972.

(Mc73) W. N. McElroy, "Fast Reactor Flux-Spectral Characterization, Proc. of ANS Topical Meeting on Irradiation Experimentation in Fast Reactors, Jackson, WY, September 10-12, Unnumbered ANS Report, American Nuclear Society, Hinsdale, IL, pp. 333-354, 1973.

(Mc75) W. N. McElroy, R. L. Simons, D. G. Doran and G. R. Odette, "Damage Function Analysis," J. Test. & Eval. 3, (3), pp. 220-229, May 1975.

(Mc75a) W. N. McElroy, "ENDF/B-IV Dosimetry Cross Section File Benchmark Neutron Flux-Spectral Uncertainties," Proc. of the Conference on Nuclear Cross Sections and Technology, Washington, DC, March 3-7, 1975, COM-75-11469, Air Force Ballistic Missile Division, Englewood, CA, Vol. 1, p. 189, October 1975.

(Mc75c) W. N. McElroy and L. S. Kellogg, "Fuels and Materials Fast-Reactor Dosimetry Data Development and Testing," Nucl. Technol. 25, (2), pp. 180-223, 1975.

(Mc76a) W. N. McElroy, Ed., "EBR-II Derived Fission Yields from Vanadium Encapsulated Fission Monitors," LMFBR Reaction Rate and Dosimetry 10th Progress Report, June 1974 Through October 1975, HEDL-TME 75-130, Hanford Engineering Development Laboratory, Richland, WA, p. HEDL 21 - HEDL-25, August 1976.

(Mc77) W. N. McElroy, R. A. Bennett and D. L. Johnson, "Neutron Environmental Characterization Requirements for Reactor Fuels and Materials Development and Surveillance Programs," HEDL-SA-911, Proc. of the 1st ASTM-EURATOM Symposium on Reactor Dosimetry, Petten, Netherlands, September 22-26, 1975, EUR 5667, Commission of the European Communities, Vol. I, pp. 1-26, 1977.

(Mc78) W. N. McElroy et al., "Spectral Characterization by Combining Neutron Spectroscopy, Analytical Calculations, and Integral Measurements," Proc. of a Consultants' Meeting on Integral Cross-Section Measurement in Standard Neutron Fields for Reactor Dosimetry, Vienna, November 1976, IAEA-208, International Atomic Energy Agency, Vienna, Austria, 1978.

(Mc78a) W. N. McElroy et al., "Standardization of Dosimetry and Damage Analysis Work for U.S. LWR, FBR and MFR Development Programs," Proc. of the 2nd ASTM-EURATOM Symposium on Reactor Dosimetry, Palo Alto, CA, October 3-7, 1977, NUREG/CP-0004, NRC, Washington, DC, Vol. 1, pp. 17-60, 1978.

(Mc79) W. N. McElroy et al., "Development and Testing of Standardized Procedures and Reference Data for LWR Surveillance," HEDL-SA-1719 and Proc. of the IAEA Specialists' Meeting on Irradiation Embrittlement, Thermal Annealing and Surveillance Reactor Pressure Vessels, Vienna, Austria, February 26-March 1, 1979, IWG-RRPC-79/2, December 1979.

(Mc79a) A. K. McCracken, "Few Channel Unfolding in Shielding - The SENSAK Code," Proc. of the 3rd ASTM-EURATOM Symposium on Reactor Dosimetry, Ispra, Italy, October 1-5, 1979, EUR 6813, Commission of the European Communities, Vol. II, p. 732, 1980.

(Mc80) W. N. McElroy et al., LWR-PV-SDIP: 1979 Annual Report, NUREG/CR-1291, HEDL-SA-1949, NRC, Washington, DC, February 1980.

(Mc80a) W. N. McElroy et al., "NRC Metallurgy and Materials Research Branch LWR-PV-SDIP Review Graphics," HEDL-SA-2225, and Proc. of the 8th WRSR Research Information Meeting, Gaithersburg, MD, October 27-31, 1980.

(Mc81) W. N. McElroy, Ed., LWR-PV-SDIP: PCA Experiments and Blind Test, NUREG/CR-1861, HEDL-TME 80-87, NRC, Washington, DC, July 1981.

(Mc81a) W. N. McElroy et al., LWR-PV-SDIP: 1980 Annual Report, NUREG/CR-1747, HEDL-TME 80-73, NRC, Washington, DC, April 1981.

(Mc81b) E. D. McGarry and A. Fabry, "Fission Chamber Measurements," LWR-PV-SDIP: PCA Experiments and Blind Test, W. N. McElroy, Ed., NUREG/CR-1861, HEDL-TME 80-87, NRC, Washington, DC, pp. 2.3-1 - 2.3-38, July 1981.

(Mc81c) E. D. McGarry et al., LWR-PV-SDIP: PCA Experiments and Blind Test, NUREG/CR-1861, HEDL-TME 80-87, Tables 2.3.4 and 5.5.2, NRC, Washington, DC, July 1981.

(Mc81d) E. D. McGarry et al., LWR-PV-SDIP: PCA Experiments and Blind Test, NUREG/CR-1861, HEDL-TME 80-87, Table 5.5.1, NRC, Washington, DC, July 1981.

(Mc81e) E. D. McGarry et al., "Benchmark Field Referencing," LWR-PV-SDIP: PCA Experiments and Blind Test, W. N. McElroy, Ed., NUREG/CR-1861, HEDL-TME 80-87, NRC, Washington, DC, pp. 2.2-1 - 2.2-27, July 1981.

(Mc81f) E. D. McGarry and A. Fabry, "Recommended Integral Results - Fission Chamber Measurements," LWR-PV-SDIP: PCA Experiments and Blind Test, NUREG/CR-1861, HEDL-TME 80-87, NRC, Washington, DC, pp. 8.2-1 - 8.2-2, July 1981.

(Mc81g) W. N. McElroy, E. P. Lippincott, A. Fabry, F. W. Stallman and F. B. K. Kam, "Overview Analysis of Neutronic Calculations and Measurements," LWR-PV-SDIP: PCA Experiments and Blind Test, NUREG/CR-1861, HEDL-TME 80-87, NRC, Washington, DC, pp. 7.0-1 - 7.0-3, July 1981.

(Mc82) W. N. McElroy et al., "Surveillance Dosimetry of Operating Power Plants," Proc. of the 4th ASTM-EURATOM Symposium on Reactor Dosimetry, Gaithersburg, MD, March 22-26, 1982, NUREG/CP-0029, NRC, Washington, DC, pp. 3-43, July 1982. (Serves as the LWR Pressure Vessel Surveillance Dosimetry Improvement Program 1981 Annual Report.)

(Mc82a) W. N. McElroy et al., LWR-PV-SDIP: 1982 Annual Report, NUREG/CR-2805, Vol. 3, HEDL-TME 82-20, NRC, Washington, DC, December 1982.

(Mc82b) W. N. McElroy et al., "Verification of Effects of Fuel Management Schemes on the Condition of Pressure Vessels and Their Support Structures," HEDL-SA-2791 and Proc. of the 10th WRSR Information Meeting, Gaithersburg, MD, October 12-15, 1982, NUREG/CP-0041, Vol. 4, pp. 184-227, January 1983.

(Mc82c) P. McConnell et al., Irradiated Nuclear Pressure Vessel Steel Data Base, EPRI NP-2428, Electric Power Research Institute, Palo Alto, CA, June 1982.

(Mc83) J. P. McNeece, R. Gold, D. D. Preston and J. H. Roberts, "Automated Scanning of Solid-State Track Recorders: Computer-Controlled Microscope, Nucl. Tracks 7, pp. 137-140, 1983.

(Mc83a) W. N. McElroy, Ed., LWR Power Reactor Surveillance Physics-Dosimetry Data Base Compendium, NUREG/CR-3319, HEDL-TME 84-2, NRC, Washington, DC, January 1984.

(Mc83b) W. N. McElroy et al., Proc. of the 10th WRSR Information Meeting, Gaithersburg, MD, October 12-15, 1982, NUREG/CP-0041, Vol. 4, NRC, Washington, DC, January 1983.

(Mc83c) J. P. McNeece, B. J. Kaisar, R. Gold and W. W. Jenkins, Fuel Content of the Three Mile Island Unit 2 Makeup Demineralizers, HEDL-7285, Hanford Engineering Development Laboratory, Richland, WA, February 1983.

(Mc83d) W. N. McElroy and F. B. K. Kam, PSF Blind Test Instructions and Data Packages, HEDL-7448, Hanford Engineering Development Laboratory, Richland, WA, April 1983.

(Mc84) W. N. McElroy et al., LWR-PV-SDIP 1983 Annual Report, NUREG/CR-3391, Vol. 3, HEDL-TME 83-23, NRC, Washington, DC, January 1984.

(Mc84a) E. D. McGarry et al., "Gamma-Ray Response of Integral Neutron Dosimeters and Review of Measured ^{235}U Fission Rates," LWR-PV-SDIP: PCA Dosimetry in Support of the PSF Physics-Dosimetry-Metallurgy Experiments, NUREG/CR-3318, Section 4.5, NRC, Washington, DC, 1984.

(Mc84b) W. N. McElroy and F. B. K. Kam, eds., PSF Blind Test SSC, SPVC, and SVBC Physics-Dosimetry-Metallurgy Data Packages, HEDL-7449, Hanford Engineering Development Laboratory, Richland, WA, February 1984.

(Mc84c) W. M. McElroy et al., LWR-PV-SDIP Semiannual Progress Report, NUREG/CR-3746, Vol. 1, HEDL-TME 84-20, NRC, Washington, DC, 1984.

(Mc84d) W. N. McElroy et al., LWR-PV-SDIP Quarterly Progress Report April - June 1983, NUREG/CR-3391, Vol. 2, HEDL-TME 83-22, NRC, Washington, DC, April 1984.

(Mc84e) W. N. McElroy, G. L. Guthrie and R. L. Simons, "Thermal-Relative-to-Fast-Neutron Contribution to Charpy Shift for PWR and BWR Surveillance Capsule Weld Materials," LWR-PV-SDIP Quarterly Progress Report, April 1983 - June 1983, NUREG/CR-3391, Vol. 2, HEDL-TME 83-22, Hanford Engineering Development Laboratory, Richland, WA, HEDL-22 - HEDL-33, April 1984.

(Mc84f) A. K. McCracken, Ed., The PCA Replica Experiment, Part I: Winfrith Measurements and Calculations, NUREG/CR-3324, Vol. I; AEEW-R 1736, UK Atomic Energy Establishment, Winfrith, UK, January 1984.

(Mc84g) J. P. McNeece, R. Gold, A. Fabry, S. DeLeeuw and P. Gubel, "Nondestructive Measurement of Neutron Exposure in the BR-3 Pressure Vessel by Continuous Gamma-Ray Spectrometry," HEDL-SA-3124 and 5th International ASTM-EURATOM Symposium on Reactor Dosimetry, September 24-28, 1984, Geesthact, Federal Republic of Germany.

(Me73) W. Mendenhall and R. L. Schaeffer, Mathematical Statistics with Applications, Duxbury Press, London, UK, Section 11.10, 1973.

(Me75) D. Meneghetti, E. R. Ebersole and P. Walker, "Analysis of Burnups in EBR-II Driver-Fuel Elements," Nucl. Technol. 25, (2), p. 406, February 1975.

(Me75a) D. Meneghetti and J. R. Honekamp, "Impact of EBR-II Tests and Operational Data on Analyses," Advanced Reactors: Physics, Design and Economics, Pergamon Press, New York, NY, 1975.

(Me75b) W. D. Metz, "European Breeders (I): France Leads the Way," Science 190, p. 1279, 1975.

(Me76) W. D. Metz, "European Breeders (II): The Nuclear Parts Are Not the Problem," Science 191, p. 368, 1976.

(Me76a) W. D. Metz, "European Breeders (III): Fuels and Fuel Cycle Are Keys to Economy," Science 191, p. 551, 1976.

(Me82) S. H. Merriman, A Computerized Process Control System for the ORR-PSF Irradiation Experiment Part 1: Overall View of the Control System, NUREG/CR-1710, Vol. 1, ORNL/NUREG/TM-405/P1, NRC, Washington, DC, 1982.

(Mi80) L. F. Miller, A Computerized Process Control System for the ORR-PSF Irradiation Experiment Part 2: Mathematical Basis and Computer Implementation of the Temperature Control Algorithm, NUREG/CR-1710, Vol. 2, ORNL/NUREG/TM-405/P2, NRC, Washington, DC, 1980.

(Mi81) L. F. Miller, Analysis of the Temperature Data from the ORR-PSF Irradiation Experiment: Methodology and Computer Software, NUREG/CR-2273, ORNL/TM-7766, NRC, Washington, DC, 1981.

(Mi81a) L. F. Miller and F. B. K. Kam, "Neutronic Calculation Methods," LWR-PV-SDIP: PCA Experiments and Blind Test, NUREG/CR-1861, HEDL-TME 80-87, NRC, Washington, DC, pp. 6.0-1 - 6.0-5, July 1981.

(Mi81b) G. Minsart, "Analysis of Participant B," LWR-PV-SDIP: PCA Experiments and Blind Test, NUREG/CR-1861, HEDL-TME 80-87, NRC, Washington, DC, pp. 6.2-1 - 6.2-16, July 1981.

(Mo75) W. C. Morgan, "Long-Term Dosimetry," J. Test. & Eval. 3, (3), p. 217, 1975.

(Mo78) W. C. Morgan, Ed., Proc. of the 2nd ASTM-EURATOM Symposium on Reactor Dosimetry, Palo Alto, CA, October 3-7, 1977, NUREG/CP-0004, NRC, Washington, DC, Vols 1, 2 & 3, 1978.

(Mp79) MPC Subcommittee 6 on Nuclear Materials, "Prediction of the Shift in the Brittle-Ductile Transition Temperature of LWR Pressure Vessel Materials," Final Report to ASTM Subcommittee E10.02, June 1979.

(Mu76) S. F. Mughabghab and D. I. Garber, Neutron Cross Sections, BNL-325, 3rd ed., Brookhaven National Laboratory, Upton, NY, Vol. I, 1973, Vol. II, 1976.

(Mu81) D. W. Muir and R. J. LaBauve, COVFILS - A 30-Group Covariance Library Based on ENDF/B-V, LA-8733-MS, Los Alamos National Laboratory, Los Alamos, NM, March 1981.

(My69) F. R. Mynatt, A User's Manual for DOT, A Two-Dimensional Discrete Ordinates Transport Code with Anisotropic Scattering, K-1674, Union Carbide Corp., Oak Ridge, TN, 1969.

(Ne77) J. V. Nelson, E. P. Lippincott, R. A. Bennett, W. N. McElroy and J. W. Daughtry, Measurement and Calculation of Neutron Spectra in the FTR Engineering Mock-Up Critical, HEDL-TME 76-88, Hanford Engineering Development Laboratory, Richland, WA, February 1977.

(No63) R. H. Noyce, E. R. Mosburg Jr, S. Garfinkel and R. S. Caswell, "Absolute Calibration of the National Bureau of Standards Photoneutron Source III. Absorption in a Heavy Water Solution of Manganous Sulphate," J. Nucl. Energy, A/B 17, p. 313, 1963.

(No67) E. B. Norris, Influence of Neutron Irradiation on the Properties of Steels and Welds Typical of the ERR Pressure Vessel, SwRI 1228 P4-28, Southwest Research Institute, San Antonio, TX, January 1967.

(No68) D. R. Ireland and E. B. Norris, Influence of Neutron Irradiation on the Properties of Steels and Welds Typical of the ERR Pressure Vessel After Two Power Years Operation, SwRI 1228 P9-15, Southwest Research Institute, San Antonio, TX, March 1968.

(No71) E. B. Norris, Analysis of First Surveillance Material Capsule from San Onofre Unit 1, SwRI Project 07-2892, Southwest Research Institute, San Antonio, TX, May 1971.

(No72) E. B. Norris, Analysis of Second Surveillance Material Capsule from San Onofre Unit 1, Final Report, SwRI Project 07-2892, Southwest Research Institute, San Antonio, TX, June 1972.

(No73) E. B. Norris, Analysis of the First Vessel Material Surveillance Capsule Withdrawal from LaCrosse Boiling Water Reactor, Topical Report No. 1, SwRI Project 02-3467, Southwest Research Institute, San Antonio, TX, March 1973.

(No73a) E. B. Norris, Analysis of the First Material Surveillance Capsule from H. B. Robinson Unit No. 2, Final Report, SwRI Project 02-3574, Southwest Research Institute, San Antonio, TX, July 1973.

(No74) E. B. Norris, Vessel Material Surveillance Program for Pilgrim Nuclear Power Station, Topical Report No. 1, SwRI Project 02-3812-001, Southwest Research Institute, San Antonio, TX, August 1974.

(No75) E. B. Norris, Vessel Material Surveillance Program for Vermont Yankee Nuclear Power Station, Final Report, SwRI Project 02-4032, Southwest Research Institute, San Antonio, TX, May 1975.

(No76) E. B. Norris, Reactor Vessel Material Surveillance Program for Turkey Point Unit No. 4 -- Analysis of Capsule T, Final Report, SwRI Project 02-4221, Southwest Research Institute, San Antonio, TX, June 1976.

(No76a) E. B. Norris and J. F. Unruh, Pressure-Temperature Limitations for the Turkey Point Unit Nos. 3 and 4 Nuclear Power Plants, SwRI Project 02-4383-039, Southwest Research Institute, San Antonio, TX, June 1976.

(No76b) E. B. Norris, Reactor Vessel Material Surveillance Program for H. B. Robinson Unit No. 2 -- Analysis of Capsule V, Final Report, SwRI Project 02-4397, Southwest Research Institute, San Antonio, TX, October 1976.

(No77) E. B. Norris, Analysis of the Vessel Material Surveillance Capsules Withdrawn from LaCrosse Boiling Water Reactor During the 1975 Refueling, Final Report, SwRI Project 02-4074-001, Southwest Research Institute, San Antonio, TX, April 1977.

(No77a) E. B. Norris, Reactor Vessel Material Surveillance Program for Indian Point Unit No. 2 -- Analysis of Capsule T, Final Report, SwRI Project 02-4531, Southwest Research Institute, San Antonio, TX, June 1977.

(No77b) E. B. Norris, Reactor Vessel Material Surveillance Program for Donald C. Cook Unit No. 1 -- Analysis of Capsule T, Final Report, SwRI Project 02-4770, Southwest Research Institute, San Antonio, TX, December 1977.

(No78) E. B. Norris, Analysis of the Vessel Wall Neutron Dosimeter from Browns Ferry Unit 1 Pressure Vessel, Final Report, SwRI Project 02-4884-001, Southwest Research Institute, San Antonio, TX, August 1978.

(No79) E. B. Norris, Reactor Vessel Material Surveillance Program for Capsule S -- Turkey Point Unit No. 3; Capsule S -- Turkey Point Unit No. 4, Final Report, SwRI Projects 02-5131 and 02-5380, Southwest Research Institute, San Antonio, TX, May 1979.

(No79a) E. B. Norris, Analysis of the Vessel Wall Neutron Dosimeter from Browns Ferry Unit 2 Pressure Vessel, Final Report, SwRI Project 02-4884-002, Southwest Research Institute, San Antonio, TX, September 1979.

(No79b) E. B. Norris, Analysis of the Vessel Wall Neutron Dosimeter from Browns Ferry Unit 3 Pressure Vessel, Final Report, SwRI Project 02-4884-003, Southwest Research Institute, San Antonio, TX, September 1979.

(No80) E. B. Norris, Reactor Vessel Material Surveillance Program for KO-RI Unit No. 1 -- Analysis of Capsule V, Final Report, SwRI Project 17-5759-201, Southwest Research Institute, San Antonio, TX, June 1980.

(No80a) E. B. Norris, Reactor Vessel Material Surveillance Program for Indian Point Unit No. 2 -- Analysis of Capsule Y, Final Report, SwRI Project 02-5212, Southwest Research Institute, San Antonio, TX, November 1980.

(No80b) E. B. Norris, Reactor Vessel Material Surveillance Program for Indian Point Unit No. 2 -- Analysis of Capsule T, Supplement to Final Report, SwRI Project 02-4531, Southwest Research Institute, San Antonio, TX, December 1980.

(No81) E. B. Norris, Reactor Vessel Material Surveillance Program for Donald C. Cook Unit No. 1 -- Analysis of Capsule X, Final Report, SwRI Project 02-6159, Southwest Research Institute, San Antonio, TX, June 1981.

(No81a) E. B. Norris, Pilgrim Nuclear Power Station Unit 1 Reactor Vessel Irradiation Surveillance Program, Final Report, SwRI Project 02-5951, Southwest Research Institute, San Antonio, TX, July 1981.

(No81b) E. B. Norris, Reactor Vessel Material Surveillance Program for Donald C. Cook Unit No. 2 -- Analysis of Capsule T, Final Report, SwRI Project 02-5928, Southwest Research Institute, San Antonio, TX, September 1981.

(No81c) E. B. Norris, Analysis of the Vessel Material Surveillance Capsules Withdrawn from LaCrosse Boiling Water Reactor During the 1980 Refueling, Final Report, SwRI Project 02-6208-001, Southwest Research Institute, San Antonio, TX, October 1981.

(No81d) E. B. Norris, Evaluation of the Response of Ferritic Materials to an Elevated Temperature Radiation Environment, Final Report, SwRI Project 02-9247, Southwest Research Institute, San Antonio, TX, September 30, 1981.

(Nr80) NRC Staff, Presentation to Advisory Committee on Reactor Safeguards, Metal Components Subcommittee, Transcribed Proceedings of Meeting, Washington, DC, January 24, 1980.

(Nr81) NRC, Task Action Plan A-11 Report: Resolution of the Reactor Vessel Materials Toughness Safety Issue, NUREG-0744, NRC, Washington, DC, September 1981.

(Nr82) NRC Staff, Presentation to Advisory Committee on Reactor Safeguards, Metal Components Subcommittee, Meeting on Reactor Vessel Integrity (RVI), Washington, DC, May 11-12, 1982.

(OaXX) CASK-40-Group Coupled Neutron and Gamma Ray Cross-Section Data, RSIC-DLC-23, Radiation Shielding Information Center, Oak Ridge, TN.

(OaSA) Coupled, Self-Shielded, 47 Neutron, 20 Gamma-Ray, P_3, Cross-Section Library for Light Water Reactors, SAILWR, RSIC-DLC-76, Radiation Shielding Information Center, Oak Ridge, TN.

(Od72) G. R. Odette and T. O. Ziebold, "The Yield Stress Radiation Damage Function of Iron," Nucl. Sci. Eng. 49, (1), pp. 72-81, 1972.

(Od78) G. R. Odette, W. L. Server, W. Oldfield, R. O. Ritchie and R. A. Wullaert, Analysis of Radiation Embrittlement Reference Toughness Curves, FCC 78-11, Fracture Control Corp., Goleta, CA, November 14, 1978.

(Od79) G. R. Odette, "Neutron Exposure Dependence of the Embrittlement of Reactor Pressure Vessel Steels: Correlation Models and Parameters," Proc. of an IAEA Specialists' Meeting on Z Accuracies in Correlation Between Property Change and Exposure Data from Reactor Pressure Vessel Steel Irradiations, Jülich, Federal Republic of Germany, September 24-27, 1979, ISSN0344-5798, p. 310, May 1980.

(Od83) G. R. Odette and P. Lombrozo, "A Physically Statistically Based Correlation for Transition Temperature Shifts in Pressure Vessel Steel Surveillance Welds," from the ANS Special Session on Correlations and Implications of Neutron Irradiation Embrittlement of Pressure Vessel Steels, Detroit, MI, June 12-16, 1983, Trans. Am. Nucl. Soc. 44, p. 224, 1983.

(Od83a) G. R. Odette, "On the Dominant Mechanism of Irradiation Embrittlement of Reactor Pressure Vessel Steels, Scripta Met. 17, pp. 1183-1188, 1983.

(0170) A. P. Olson, RABID: An Integral Transport Theory Code for Neutron Slowing Down in Slab Cells, ANL-7645, Argonne National Laboratory, Argonne, IL, 1970.

(0182) B. M. Oliver, H. Farrar IV and E. P. Lippincott, "Spectrum-Integrated Helium Generation Cross Sections for ^{6}Li and ^{10}B in the Sigma Sigma and Fission Cavity Standard Neutron Fields," Proc. of the 4th ASTM-EURATOM Symposium on Reactor Dosimetry, Gaithersburg, MD, March 22-26, 1982, NUREG/CP-0029, NRC, Washington, DC, Vol. 2, pp. 889-901, July 1982.

(0183) B. M. Oliver, Helium Analysis of Samples from Maine Yankee and HFBR, Informal Report 83ESG-5544, Rockwell International, Energy Systems Group, Canoga Park, CA, September 22, 1983.

(0184) B. M. Oliver and H. Farrar, "Application of Helium Accumulation Fluence Monitors (HAFM) to LWR Surveillance, LWR-PV-SDIP Quarterly Progress Report, April 1983 - June 1983, NUREG/CR-3391, Vol. 2, HEDL-TME 83-22, Hanford Engineering Development Laboratory, Richland, WA, pp. RI-3 - RI-5, April 1984.

(Os76) C. A. Oster, W. N. McElroy, R. L. Simons, E. P. Lippincott and G. R. Odette, A Modified Monte Carlo Program for SAND-II with Solution Weighting and Error Analysis, HEDL-TME 76-60, Hanford Engineering Development Laboratory, Richland, WA, August 1976.

(Pa83) D. Pachur, "Mechanical Properties of Neutron-Irradiated Reactor Pressure Vessel Steel Dependent on Radiation Mechanisms," from the ANS Special Session on Correlations and Implications of Neutron Irradiation Embrittlement of Pressure Vessel Steels, Detroit, MI, June 12-16, 1983, Trans. Am. Nucl. Soc. 44, p. 229, 1983.

(Pe72) J. S. Perrin, J. W. Sheckherd and V. G. Scotti, Examination and Evaluation of Capsule F for the Connecticut Yankee Reactor Pressure Vessel Surveillance Program, NRC, Public Document Room, Washington, DC, March 30, 1972.

(Pe75) J. S. Perrin et al., Surry Unit No. 1 Pressure Vessel Irradiation Capsule Program: Examination and Analysis of Capsule T, Docket 50280-462, NRC, Public Document Room, Washington, DC, June 24, 1975.

(Pe75a) J. S. Perrin et al., Surry Unit No. 2 Pressure Vessel Irradiation Capsule Program: Examination and Analysis of Capsule X, NRC, Public Document Room, Washington, DC, September 2, 1975.

(Pe75b) J. S. Perrin et al., Point Beach Unit No. 2 Pressure Vessel Surveillance Program: Evaluation of Capsule V, NRC, Public Document Room, Washington, DC, June 10, 1975.

(Pe77) F. G. Perey, The Data Covariance Files for ENDF/B-V, ORNL/TM-5839, Oak Ridge National Laboratory, Oak Ridge, TN, July 1977.

(Pe77a) F. G. Perey, Least Squares Dosimetry Unfolding: The Program STAY'SL, ORNL/TM-6062, Oak Ridge National Laboratory, Oak Ridge, TN, 1977.

(Pe78) J. S. Perrin et al., Zion Nuclear Plant Reactor Pressure Vessel Surveillance Program: Unit No. 1 Capsule T and Unit No. 2 Capsule U, BCL-585-4, Battelle Memorial Institute, Columbus Laboratories, Columbus, OH, March 1978.

(Pe78a) P. Petrequin and P. Soulat, Etude de la Fragilisation par Irradiation des Aciers de Cuve Type A508 cl 3 et A533-B cl 1, SM218/21, International Atomic Energy Agency, Vienna, Austria, 1978.

(Pe79) G. P. Pells and D. C. Phillips, "Radiation Damage of α-Al_2O_3 in the HVEM: I. Temperature Dependence of the Displacement Threshold," J. Nucl. Mater. 80, p. 207, 1979.

(Pe79a) G. P. Pells and D. C. Phillips, "Radiation Damage of α-Al_2O_3 in the HVEM: II. Radiation Damage at High Temperature and High Dose," J. Nucl. Mater. 80, p. 215, 1979.

(Pe79b) J. S. Perrin et al., Palisades Nuclear Plant Reactor Pressure Vessel Surveillance Program: Capsule A-240, BCL-585-12, Battelle Memorial Institute, Columbus Laboratories, Columbus, OH, March 13, 1979.

(Pe80) J. S. Perrin et al., Maine Yankee Nuclear Plant Reactor Pressure Vessel Surveillance Program: Capsule 263, BCL-585-21, Battelle Memorial Institute, Columbus Laboratories, Columbus, OH, December 21, 1980.

(Pe82) G. P. Pells, A. J. Fudge, M. J. Murphy and M. Wilkins, "An Investigation into the Use of Sapphire as a Fast Neutron Damage Monitor," Proc. of the 4th ASTM-EURATOM Symposium on Reactor Dosimetry, Gaithersburg, MD, March 22-26, 1982, NUREG/CP-0029, NRC, Washington, DC, Vol. 1, pp. 331-344, July 1982.

(Pe82a) H. Petitcolas et al., "Ameliorations des Calorimetres pour la Mesure des Puissances Specifiques Deposees dans les Reacteurs Nucleaires," Proc. of the 4th ASTM-EURATOM Symposium on Reactor Dosimetry, Gaithersburg, MD, March 22-26, 1982, NUREG/CP-0029, NRC, Washington, DC, Vol. 1, pp. 303-320, July 1982.

(Pe82b) M. Petilli, "A New Analysis of the Experiment for Measurement of $\Phi > 1$ MeV in Pressure Vessel Cavity of U.S. Light Water Power Reactor Arkansas," Proc. of the 4th ASTM-EURATOM Symposium on Reactor Dosimetry, Gaithersburg, MD, March 22-26, 1982, NUREG/CP-0029, NRC, Washington, DC, Vol. 1, pp. 545-554, July 1982.

(Pe82c) M. Petilli, "Tashi Results for Multigroup Cross Sections and Their Uncertainties," Proc. of the IAEA Advisory Group Meeting on Nuclear Data for Radiation Damage Assessment and Related Safety Aspects, Vienna, Austria, October 12-16, 1981, IAEA-TECDOC-263, International Atomic Energy Agency, Vienna, Austria, p. 57, 1982.

(Pe84) J. S. Perrin, R. A. Wullaert, G. R. Odette and M. P. Lombroso, Physically Based Regression Correlations of Embrittlement Data from Reactor PV Surveillance Programs, EPRI NP-3319, Electric Power Research Institute, Palo Alto, CA, January 1984.

(Pi75) M. Pinter et al., "Interlaboratory Comparison of Absolute Fission Rate and Uranium-238 Capture Rate Measurements in the MOL-ΣΣ Secondary Intermediate-Energy Standard Neutron Field," Proc. of the Conference on Nuclear Cross Sections and Technology, Washington, DC, March 3-7, 1975, COM-75-11469, Air Force Ballistic Missile Division, Englewood, CA, Vol. 1, p. 258, October 1975.

(Pr58) W. Primak, "Fast Neutron Induced Changes in Quartz and Vitreous Silica," Phys. Rev. 110, (6), p. 1240, 1958.

(Pr58a) W. J. Price, Nuclear Radiation Detection, McGraw-Hill, New York, NY, 1958.

(Pr71) Proc. of a Consultants' Meeting on Prompt-Fission-Neutron Spectra, IAEA Press, International Atomic Energy Agency, Vienna, Austria, 1971.

(Pr73) C. C. Price, D. G. Franklin and A. Gopalakrishnan, "In-Core Monitoring in the Experimental Breeder Reactor-II," Proc. of ANS Topical Meeting on Irradiation Experimentation in Fast Reactors, Jackson, WY, September 10-12, 1973, Unnumbered ANS Report, American Nuclear Society, Hindsale, IL, pp. 401-411, 1973.

(Pr74) "Fission Product Nuclear Data (FPND)," Proc. of a Panel on Fission Product Nuclear Data, Bologna, Italy, November 26-30, 1973, IAEA-169, International Atomic Energy Agency, Vienna, Austria, 1974.

(Pr77) Proc. of the 1st ASTM-EURATOM Symposium on Reactor Dosimetry, Petten, Netherlands, September 22-26, 1975, EUR 5667, Commission of the European Communities, Volumes I and II, 1977.

(Pr82) Proc. of the IAEA Advisory Group Meeting on Nuclear Data for Radiation Damage Assessment and Related Safety Aspects, Vienna, October 12-16, 1981, IAEA-TECDOC-263, International Atomic Energy Agency, Vienna, Austria, 1982.

(Pr83) C. C. Preston, R. Gold, J. P. McNeece, J. H. Roberts and F. H. Ruddy, "Progress in Automated Scanning Electron Microscopy for Track Counting," Nucl. Tracks 7, pp. 53-61, 1983.

(Ra79) P. N. Randall, "Regulatory Aspects of Radiation Embrittlement of Reactor Vessel Steels," Proc. of an IAEA Specialists' Meeting on Irradiation Embrittlement, Thermal Annealing, and Surveillance of Reactor Pressure Vessels, Vienna, Austria, February 26 - March 1, 1979, IWG-RRPC-79/2, December 1979.

(Ra81a) J. A. Rawlins, R. S. McBeath, D. W. Wootan, E. P. Lippincott and A. I. Davis, "Reaction Rates and Neutron Flux Spectra in the FFTF," Trans. Am. Nucl. Soc. 39, p. 902, December 1981.

(Ra81b) P. N. Randall, "The Status of Trend Curves and Surveillance Results in USNRC Regulatory Activities," Proc. of an IAEA Specialists' Meeting, Vienna, Austria, October 20, 1981.

(Ra82) J. A. Rawlins, J. W. Daughtry and R. A. Bennett, "FFTF Reactor Characterization Program Review," Proc. of the 4th ASTM-EURATOM Symposium on Reactor Dosimetry, Gaithersburg, MD, March 22-26, 1982, NUREG/CP-0029, NRC, Washington, DC, Vol. 1, pp. 245-263, July 1982.

(Ra82a) P. N. Randall, "Status of Regulatory Demands in the U.S. on the Application of Pressure Vessel Dosimetry," Proc. of the 4th ASTM-EURATOM Symposium on Reactor Dosimetry, Gaithersburg, MD, March 22-26, 1982, NUREG/CP-0029, NRC, Washington, DC, Vol. 2, pp. 1011-1022, July 1982.

(Ra83) P. N. Randall, "NRC Perspective of Safety and Licensing Issues Regarding Reactor Vessel Steel Embrittlement," from the ANS Special Session on Correlations and Implications of Neutron Irradiation Embrittlement of Pressure Vessel Steels, Detroit, MI, June 12-16, 1983, Trans. Am. Nucl. Soc. 44, p. 220, 1983.

(Re73) W. H. Reed, T. R. Hill, F. W. Brinkley and K. D. Lathrop, TRIPLET: A Two-Dimensional, Multigroup, Triangular Mesh, Planar Geometry, Explicit Transport Code, LA-5428-M5, Los Alamos National Laboratory, Los Alamos, NM, October 1973.

(Re77) Regulatory Guide 1.99, Effects of Residual Elements on Predicted Radiation Damage to Reactor Vessel Materials, Rev. 1, NRC, Washington, DC, April 1977.

(Re81) Regulatory Guide 1.150, Ultrasonic Testing of Reactor Vessel Welds During Preservice and In-Service Examinations, NRC, Washington, DC, June 1981.

(Rh79) W. A. Rhoades, D. B. Simpson, R. L. Childs and W. W. Engle, The DOT-IV Two-Dimensional Discrete Ordinates Transport Code with Space-Dependent Mesh and Quadrature, ORNL/TM-6529, Oak Ridge National Laboratory, Oak Ridge, TN, 1979.

(Ri80) B. F. Rider et al., Evaluation of Fission Product Yields for the US National Nuclear Data Files, Workshop on Evaluation Methods and Procedures for Applied Data, Upton, NY, September 22-26, 1980 (Available as ENDF-292).

(Ro53) L. Rosen, "Nuclear Emulsion Techniques for the Measurement of Neutron Energy Spectra," Nucleonics 11, p. 32, and 12, p. 38, 1953.

(Ro57) J. H. Roberts, "Absolute Flux Measurements of Anisotropic Neutron Spectra with Proton Recoil Tracks in Nuclear Emulsions," Rev. Sci. Instrum. 28, p. 667, 1957.

(Ro63) A. D. Rossin, "Significance of Neutron Spectrum on Radiation Effects Studies," ASTM STP 341, Symposium on Radiation Effects on Metals and Neutron Dosimetry, October 2-3, 1962, Los Angeles, CA, pp. 115-132, 1963.

(Ro65) A. D. Rossin, "Comparison of Neutron Embrittlement of Steel in Different Reactor Spectra," Nucl. Struct. Eng. 1, pp. 76-82, 1965.

(Ro68) J. H. Roberts and A. N. Behkami, "Measurement of Anisotropic Fast Neutron Spectra with Nuclear Emulsion Techniques," Nucl. Technol. 4, p. 182, 1968.

(Ro68a) J. H. Roberts, R. Gold and R. J. Armani, "Spontaneous-Fission Decay Constant of ^{238}U," Phys. Rev. 174, pp. 1482-1484, 1968.

(Ro75) J. W. Rogers, D. A. Millsap and Y. D. Harker, "CFRMF Neutron Field Flux Spectral Characterization," Nucl. Technol. 25, p. 330, 1975.

(Ro76) J. W. Rogers, Y. D. Harker and D. A. Millsap, "The Coupled Fast Reactivity Measurements Facility (CFRMF)," Neutron Cross Sections for Reactor Dosimetry: Proc. of a Consultants' Meeting, Vienna, Austria, IAEA-208, International Atomic Energy Agency, Vol. II, p. 117, November 1976.

(Ro77) J. H. Roberts and R. Gold, "Nuclear Emulsion Techniques and Data Needs for Fast Neutron Angular Spectrometry," Proc. of the Symposium on Neutron Cross Sections 10-40 MeV, BNL-NCS-5068, Brookhaven National Laboratory, Upton, NY, p. 287, May 1977.

(Ro77a) J. W. Rogers, Y. D. Harker and D. A. Millsap, "Fast Neutron Spectrum and Dosimetry Studies in the Coupled Fast Reactivity Measurements Facility," Proc. of the 1st ASTM-EURATOM Symposium on Reactor Dosimetry, Petten, Netherlands, September 22-26, 1975, EUR 5667, Commission of the European Communities, Vol. II, pp. 277-295, 1977.

(Ro78) J. H. Roberts and R. Gold, "SSTR and Emulsion Techniques and Their Applications for FBR, LWR, and MFER Programs," Proc. of the 2nd ASTM-EURATOM Symposium on Reactor Dosimetry, Palo Alto, CA, October 3-7, 1977, NUREG/CP-0004, NRC, Washington, DC, Vol. 2, p. 739-774, 1978.

(Ro79) J. H. Roberts, R. Gold and F. H. Ruddy, "Thermal Annealing Studies in Muscovite and in Quartz," Proc. of the 10th International Conference on Solid State Nuclear Track Detectors, Lyons, France, July 2-7, 1979.

(Ro80) H. Röttger, Ed., Proc. of the 3rd ASTM-EURATOM Symposium on Reactor Dosimetry, Ispra, Italy, October 1-5, 1979, EUR 6813, Commission of the European Communities, Vols. I and II, 1980.

(Ro81) J. W. Rogers, "Gas Proton-Recoil Spectrometry," LWR-PV-SDIP: PCA Experiments and Blind Test, NUREG/CR-1861, HEDL-TME 80-87, NRC, Washington, DC, pp. 3.2-1 - 3.2-31, July 1981.

(Ro82) R. W. Roussin et al., VITAMIN-C: 171 Neutron, 36 Gamma-Ray Group Cross Sections in AMPX and CCCC Interface Formats for Fusion and LMFBR Neutronics, ORNL/RSIC-37, Radiation Shielding Information Center, Oak Ridge, TN, 1982.

(Ro82a) G. C. Robinson, "Small-Scale Clad Effects Study," Proc. of the 10th WRSR Information Meeting, Gaithersburg, MD, October 12-15, 1982, NUREG/CP-0041, Vol. 4, NRC, Washington, DC, pp. 272-281, January 1983.

(Ro83) J. H. Roberts, F. H. Ruddy, J. P. McNeece and R. Gold, "Automatic Scanning of Solid State Track Recorders: Calibration," Nucl. Tracks 7, 1983.

(Ro83a) J. H. Roberts, F. H. Ruddy and R. Gold, "Optical Efficiency for Fission Fragment Track Counting in Muscovite Solid State Track Recorders," Proc. of the 12th International Conference on Solid State Nuclear Track Detectors, Acapulco, Mexico, September 1983.

(Ru78) F. H. Ruddy, R. Gold and J. H. Roberts, "Preparation of Fissionable Deposits for SSTR Dosimetry in the LWR-PV Surveillance Program," LWR-PV-SDIP Quarterly Progress Report, April - July 1978, NUREG/CR-0550, HEDL-TME 78-7, Hanford Engineering Development Laboratory, Richland, WA, Washington, DC, pp. HEDL-27 - HEDL-35, June 1979.

(Ru80) F. H. Ruddy et al., "CR-39 Polymer, A Promising New Solid State Track Recorder for High Energy Neutron Applications," Proc. of a Symposium on Neutron Cross Sections 10-50 MeV, BNL-NCS-51245, Brookhaven National Laboratory, Upton, NY, Vol. II, pp. 599-616, 1980.

(Ru80a) F. H. Ruddy, R. Gold and J. H. Roberts, "Solid State Track Recorder Measurements in the Poolside Critical Assembly," Dosimetry Methods for Fuels, Cladding, and Structural Materials: Proc. of the 3rd ASTM-EURATOM Symposium on Reactor Dosimetry, Ispra, Italy, October 1-5, 1979, EUR 6813, European Atomic Energy Community, Vol. II, pp. 1069-1075, 1980.

(Ru81) F. H. Ruddy, R. Gold and J. H. Roberts, "Solid State Track Recorder Measurements," LWR-PV-SDIP: PCA Experiments and Blind Test, W. N. McElroy, Ed., NUREG/CR-1861, HEDL-TME 80-87, NRC, Washington, DC, pp. 2.5-1 - 2.5-13, July 1981.

(Ru82) F. H. Ruddy, R. Gold and J. H. Roberts, "Light Water Reactor - Pressure Vessel Neutron Spectrometry with Solid State Tracks Recorders," Proc. of the 4th ASTM-EURATOM Symposium on Reactor Dosimetry, Gaithersburg, MD, March 22-26, 1982, NUREG/CP-0029, Vol. 1, pp. 293-301, July 1982.

(Sa72) L. Salmon and D. V. Booker, FATAL - A General Purpose Computer Program for Fitting Experimental Data to Any Required Function, AERE-R-7129, Atomic Energy Research Establishment, Harwell, UK, 1972.

(Sc69) R. E. Schenter, J. L. Baker and R. B. Kidman, ETOX, A Code to Calculate Group Constants for Nuclear Reactor Calculations, BNWL-1002, Battelle Pacific Northwest Laboratory, Richland, WA, May 1969.

(Sc79) F. A. Schmittroth, FERRET Data Analysis Code, HEDL-TME 79-40, Hanford Engineering Development Laboratory, Richland, WA, September 1979.

(Sc79a) R. E. Schenter, F. Schmittroth and F. M. Mann, "Evaluation of the $^{54}Fe(n,/)^{59}Fe$ and $^{54}Fe(n,p)^{54}Mn$ Reactions for the ENDF/B-V File," HEDL-SA-1908, Proc. of the International Conference on Nuclear Cross Sections for Technology, Knoxville, TN, October 1979.

(Sc80) W. Schneider, Ed., "CAPRICE 79: Correlation Accuracy in Pressure Vessel Steel as Reactor Component Investigation of Change of Material Properties with Exposure Data," Proc. of the IAEA Technical Committee Meeting, Jülich, Federal Republic of Germany, Jul-CONF-37, International Atomic Energy Agency, Vienna, Austria, May 1980.

(Sc82) F. Schmittroth, "FERRET Adjustment Code - Status/Use," Proc. of the 4th ASTM-EURATOM Symposium on Reactor Dosimetry, Gaithersburg, MD, March 22-26, 1982, NUREG/CP-0029, NRC, Washington, DC, Vol. 2, pp. 1129-1139, July 1982.

(Sc83) F. a. Schmittroth and E. P. Lippincott, "Adjusted Cross Sections in Neutron Spectrum Unfolding," Trans. Am. Nucl. Soc., p. 606, November 1983.

(Se69) C. Z. Serpan Jr and W. N. McElroy, Damage Function Analysis of Neutron Energy and Spectrum Effects Upon the Radiation Embrittlement of Steels, NRL 6925, Naval Research Laboratory, Washington, DC, July 1969.

(Se71) C. Z. Serpan Jr, "Reliability of Fluence-Embrittlement Projections for Pressure Vessel Surveillance Analysis," Nucl. Technol. 12, pp. 108-118, September 1971.

(Se72) C. Z. Serpan Jr, Ed., Proc. of the IAEA Specialists' Meeting on Radiation Damage Units for Ferritic and Stainless Steels, Seattle, WA, October 31 - November 1, 1972, Unnumbered IAEA Report, International Atomic Energy Agency, Vienna, Austria, 1972.

(Se72a) C. Z. Serpan Jr and W. N. McElroy, "Elevated-Temperature Damage Functions for Neutron Embrittlement in Pressure Vessel Steels," Nucl. Technol. 13, February 1972.

(Se73) B. R. Sehgal and D. Meneghetti, "Analyses of Dosimetry Spectrometry in EBR-II Systems," Proc. of the ANS Topical Meeting on Irradiation Experimentation in Fast Reactors, Jackson, WY, September 10-12, 1973, Unnumbered ANS Report, American Nuclear Society, Hinsdale, IL.

(Se73a) M. G. Seitz et al., "Improved Methods for Measurement of Thermal Neutron Dose by the Fission Track Technique," J. Appl. Phy. 44, p. 510, 1973.

(Se73b) C. Z. Serpan Jr, "Damage Function Analysis of Neutron-Induced Embrittlement in A302-B Steel at 550°F (288°C)," Effects of Radiation on Substructure and Mechanical Properties of Metals and Alloys, ASTM STP 529, American Society for Testing and Materials, Philadelphia, PA, pp. 92-106, 1973.

(Se75) B. R. Sehgal and R. H. Rempert, "Analysis of Dosimetry Measurements in EBR-II," Nucl. Technol. 25, (2), p. 390, February 1975.

(Se75a) C. Z. Serpan Jr, "Engineering Damage Cross Sections for Neutron Embrittlement of A302B Pressure Vessel Steel," Nucl. Eng. Design 33, pp. 19-29, 1975.

(Se80) C. Z. Serpan Jr, "Standardization of Dosimetry-Related Procedures for the Prediction and Verification of Changes in LWR Pressure Vessel Steel Fracture Toughness During Reactor Service Life: Status and Recommendations," Proc. of the 3rd ASTM-EURATOM Symposium on Reactor Dosimetry, Ispra, Italy, October 1-5, 1979, EUR 6813, Commission of the European Communities, Vol. II, pp. 1266-1274, 1980.

(Se81) W. Seelmann-Eggebert, G. Pfennig et al., Karlsruher Nuklidkarte, 5th ed., KfK, Karlsruhe, Federal Republic of Germany, 1981.

(Se82) W. E. Selph and J. MacKenzie, Passive Neutron Dosimetry for Measurements at the McGuire Reactor, EPRI NP-2570, Electric Power Research Institute, Palo Alto, CA, September 1982.

(Sh82) R. A. Shaw, "Brown's Ferry and Arkansas Nuclear One Pressure Vessel Neutron Fluence Benchmarks," Proc. of the 4th ASTM-EURATOM Symposium on Reactor Dosimetry, Gaithersburg, MD, March 22-26, 1982, NUREG/CP-0029, NRC, Washington, DC, Vol. 1, pp. 513-518, July 1982.

(Si59) E. C. H. Silk and R. S. Barnes, "Examination of Fission Fragment Tracks with an Electron Microscope," Philos. Mag. 4, p. 970, 1959.

(Si68) M. G. Silk, Iterative Unfolding of Compton Spectra, AERE-R-5653, Atomic Energy Research Establishment, Harwell, UK, 1968.

(Si69) M. G. Silk, "Energy Spectrum of the Gamma Radiation in the DAPHINE Core," J. Nucl. Energy 23, p. 308, 1969.

(Si70) R. L. Simons et al., "A Comparison of Measured and Calculated Integral Fluxes and Spectra in a Pressure Vessel Mock-up," Trans. Am. Nucl. Soc. 1970 Winter Meeting, November 15-19, 1970, Vol. 13, p. 884.

(Si71) R. L. Simons, Damage Functions for Determining Irradiation Effectiveness, HEDL-TME 71-189, Hanford Engineering Development Laboratory, Richland, WA, November 1971.

(Si72) R. L. Simons, W. N. McElroy and L. D. Blackburn, "Damage Function Analysis of Austenitic-Steel Neutron-Induced Mechanical Property Change Data," Nucl. Technol. 16, pp. 14-24, 1972.

(Si73) J. M. Simmons and J. E. Fox, "Fast Flux Irradiation Program in the United States," Proc. of the ANS Topical Meeting on Irradiation Experimentation in Fast Reactors, Jackson, WY, September 10-12, 1973, Unnumbered ANS Report, American Nuclear Society, Hinsdale, IL.

(Si75) B. Sicard et al., "Fuel Management Codes for Fast Reactors," Proc. of European Nuclear Conference, Paris, France, April 21-25, 1975.

(Si79) G. L. Simmons, V. V. Verbinski, W. K. Hagan and C. G. Cassapekis, Measurement and Analysis of Gamma-Ray Induced Contamination of Neutron Dosimetry Procedures Used for Reactor Pressure Vessel Applications, EPRI NP-1056, Electric Power Research Institute, Palo Alto, CA, 1979.

(Si80) G. L. Simmons and R. W. Roussin, "A New Cross Section Library for Light Water Reactor Shielding and Pressure Vessel Dosimetry Applications," Proc. of the Conference on 1980 Advances in Reactor Physics and Shielding, Sun Valley, CA, September 14-19, 1980, American Nuclear Society, Hinsdale, IL, 1980.

(Si81) R. L. Simons, "Re-evaluation of Dosimetry for 19 PWR Surveillance Capsules - II," LWR-PV-SDIP Quarterly Progress Report, October 1980 - December 1980, NUREG/CR-1241, Vol. 4, HEDL-TME 80-6, Hanford Engineering Development Laboratory, Richland, WA, pp. HEDL-3 - HEDL-8, November 1981.

(Si81a) R. L. Simons," Re-evaaluation of Dosimetry for 19 PWR Surveillance Capsules." LWR-PV-SDIP Quarterly Progress Report, April 1980 - June 1980, NUREG/CR-1241, Vol. II, HEDL-TME 80-5, Hanford Engineering Development Laboratory, Richland, WA, pp. HEDL-3 - HEDL-7, May 1981.

(Si82) R. L. Simons, "Correlation of Macroscopic Material Properties with Microscopic Nuclear Data," Nuclear Data for Radiation Damage Assessment and Related Safety Aspects, IAEA-TECDOC-263, International Atomic Energy Agency, Vienna, Austria, p. 241, 1982.

(Si82a) R. L. Simons et al., "Re-evaluation of the Dosimetry for Reactor Pressure Vessel Surveillance Capsules," Proc. of the 4th ASTM-EURATOM Symposium on Reactor Dosimetry, Gaithersburg, MD, March 22-26, 1982, NUREG/CP-0029, NRC, Washington, DC, Vol. 2, pp. 903-916, July 1982.

(Si81) W. R. Sloan et al., "Proton Recoil Proportional Counter Measurements in the FFTF," Trans. Am. Nucl. Soc. 39, p. 896, December 1981.

(Sm80) J. D. Smith III and B. L. Broadhead, Processing of ENDF/B-V Uncertainty Data Multigroup Covariance Matrices, ORNL/TM-7221, Radiation Shielding Information Center, Oak Ridge, TN, June 1980.

(So70) R. G. Soltesz, R. K. Disney, J. Jedruch and S. L. Ziegler, "Nuclear Rocket Shielding Methods, Modification, Updating and Input Data," Two-Dimensional Discrete Ordinates Transport Technique, WANL-PR(LL)-034, Vol. 5, Westinghouse Electric Corp., Pittsburgh, PA, August 1970.

(St70) E. A. Straker, P. N. Stevens, D. C. Irving and V. R. Cain, The MORSE Code - A Multigroup Neutron and Gamma Ray Monte Carlo Transport Code, ORNL-4584, Oak Ridge National Laboratory, Oak Ridge, TN, 1970.

(St71) A. M. Strash and R. Gold, "Absolute Gamma-Ray Dosimetry by Recoil Electron Spectroscopy," Nature 234, p. 260, 1971.

(St75) J. M. Steichen and R. A. Moen, Fast Flux Test Facility Coupon Surveillance Program, HEDL-TME 72-106, Rev. 3, Hanford Engineering Development Laboratory, Richland, WA, December 1975.

(St78) L. Stewart et al., "Status of the ENDF/B Special Applications Files," Proc. of the 2nd ASTM-EURATOM Symposium on Reactor Dosimetry, Palo Alto, CA, October 3-7, 1977, NUREG/CR-0004, NRC, Washington, DC, p. 843, 1978.

(St79) L. E. Steele, "Review of the IAEA Specialists' Meeting," Proc. of IAEA Specialist's Meeting on Irradiation Embrittlement, Thermal Annealing and Surveillance of Reactor Pressure Vessels, Vienna, Austria, February 26 - March 1, 1979, IWG-RRPC-79/2, International Atomic Energy Agency, December 1979.

(St79a) K. E. Stahlkopf and T. U. Marston, "A Comprehensive Approach to Radiation Embrittlement Analysis," Proc. of IAEA Specialists' Meeting on Irradiation Embrittlement, Thermal Annealing and Surveillance of Reactor Pressure Vessels, Vienna, Austria, February 26 - March 1, 1979, IWG-RRPC-79/2, International Atomic Energy Agency, December 1979.

(St80) J. Strosnider and C. Monseprate, with Appendix Prepared by L. D. Kenworthy and C. D. Tether, MATSURV -- Computerized Reactor Pressure Vessel Materials Information System, NUREG-0688, NRC, Washington, DC, October 1980.

(St80a) L. E. Steele, "Review of IAEA Specialists' Meeting on Irradiation Embrittlement, Thermal Annealing and Surveillance of Reactor Vessels," Proc. of the 3rd ASTM-EURATOM Symposium on Reactor Dosimetry, Ispra, Italy, October 1-5, 1979, EUR 6813, Commission of the European Communities, Vol. I, pp. 476-481, 1980.

(St80b) Strohmaier, S. Tagesen and H. Voniach, "Evaluation of the Cross Sections for the Reaction $^{19}F(n,2n)^{18}F$, $^{31}P(n,p)^{31}Si$; $^{93}Nb(n,n')^{93m}Nb$, and $^{103}Rh(n,n')^{103m}Rh$," Physik Daten 13-2, Karlsruhe, Federal Republic of Germany, 1980.

(St81) Standard Review Plan and Branch Technical Position MTEB 5.2: Fracture Toughness Requirements, NUREG-75/087, NRC, Washington, DC, 1981.

(St81a) W. F. Stallmann, Theory and Practice of General Adjustment and Model Fitting Procedures, NUREG/CR-2222, ORNL/TM-8976, Oak Ridge National Laboratory, Oak Ridge, TN, December 1981.

(St81b) F. W. Stallmann and F. B. K. Kam, "Compilation and Appraisal of PCA Blind Test C/E Data," LWR-PV-SDIP: PCA Experiments and Blind Test, NUREG/CR-1861, HEDL-TME 80-87, NRC, Washington, DC, pp. 7.1-1 - 7.1-56, July 1981.

(St81c) F. W. Stallmann, F. B. K. Kam, J. F. Eastham and C. A. Baldwin, Reactor Calculation "Benchmark" PCA Blind Test Results, ORNL/NUREG/TM-428, Oak Ridge National Laboratory, Oak Ridge, TN, 1981.

(St82) F. W. Stallmann, "Workshop on Adjustment Codes and Uncertainties," Proc. of the 4th ASTM-EURATOM Symposium on Reactor Dosimetry, Gaithersburg, MD, March 22-26, 1982, NUREG/CP-0029, NRC, Washington, DC, Vol. 2, pp. 1219-1220, July 1982.

(St82a) F. W. Stallmann, Curve Fitting and Uncertainty Analysis of Charpy Impact Data, NUREG/CR-2408, NRC, Washington, DC, 1982.

(St82b) F. W. Stallmann, "LSL - A Logarithmic Least Squares Adjustment Method," Proc. of the 4th ASTM-EURATOM Symposium on Reactor Dosimetry, Gaithersburg, MD, March 22-26, 1982, NUREG/CP-0029, NRC, Washington, DC, Vol. 2, pp. 1123-1128, July 1982.

(St82c) F. W. Stallmann, "Uncertainties in the Estimation of Radiation Damage Parameters," Proc. of the 4th ASTM-ERATOM Syumposium on Reactor Dosimetry, Gaithersburg, MD, March 22-26, 1982, NUREG/CP-0029, NRC, Washington, DC, Vol. 2, pp. 1155-1163, July 1982.

(St82d) F. W. Stallmann, "Evaluation and Uncertainty Estimates of Charpy Impact Data," Proc. of the 4th ASTM-EURATOM Symposium on Reactor Dosimetry, Gaithersburg, MD, March 22-26, 1982, NUREG/CP-0029, NRC, Washington, DC, Vol. 2, pp. 855-859, July 1982.

(St82e) F. W. Stallmann, "Pressure Vessel Benchmark Facility to Study Fracture Toughness of Irradiated Pressure Vessel Materials (BSR-HSST)," LWR-PV-SDIP Quarterly Progress Report, April 1982 - June 1982, NUREG/CR-2805, Vol. 2, HEDL-TME 82-19, Hanford Engineering Development Laboratory, Richland, WA, p. ORNL-17, December 1982.

(St83) F. W. Stallmann, C. A. Baldwin and F. B. K. Kam, Neutron Spectral Characterization of the 4th Nuclear Regulatory Commission Heavy Section Steel Technology IT-CT Irradiation Experiment: Dosimetry and Uncertainty Analysis, NUREG/CR-3333, ORNL/TM-8789, Oak Ridge National Laboratory, Oak Ridge, TN, July 1983.

(St83a) L. E. Steele, Ed., Status of USA Nuclear Reactor Pressure Vessel Surveillance for Radiation Effects, ASTM STP 784, American Society for Testing and Materials, Philadelphia, PA, January 1983.

(St83b) L. E. Steele, Ed., Radiation Embrittlement and Surveillance of Nuclear Reactor Pressure Vessels: An International Study, ASTM STP 819, American Society for Testing and Materials, Philadelphia, PA, November 1983.

(St84) F. W. Stallmann, Determination of Damage Exposure Parameter Values in the PSF Metallurgical Irradiation Experiment, ORNL/TM-9166, Oak Ridge National Laboratory, Oak Ridge, TN, 1984.

(Su82) S. Suzuki et al., "PNC/DOE Collaborative Dosimetry Test in JOYO," Proc. of the 4th ASTM-EURATOM Symposium on Reactor Dosimetry, Gaithersburg, MD, March 22-26, 1982, NUREG/CP-0029, NRC, Washington, DC, Vol. 1, pp. 171-182, July 1982.

(Ta82) S. W. Tagert et al., Structural Mechanics Program: Progress in 1981, EPRI NP-2705-SR, Electric Power Research Institute, Palo Alto, CA, October 1982.

(Th67) R. P. Thorne and V. C. Howard, "Radiation-Induced Changes in Porous Cubic Silicon Carbide," Proc. of Brit. Ceram. Soc. 7, p. 439, 1967.

(Th70) D. H. Thompson and T. M. Traver, BMC-I: The Battelle Monte Carlo Code, BNWL-1433, Battelle Pacific Northwest Laboratory, Richland, WA, June 1970.

(Ti80) H. Till, "Neutron Radiometric and Calculation Benchmarking for LWR Pressure Vessel Radiation Effects," Proc. of the 3rd ASTM-EURATOM Symposium on Reactor Dosimetry, Ispra, Italy, October 1-5, 1979, EUR 6813, Commission of the European Communities, Vol. II, pp. 1275-1287, 1980.

(To67) B. J. Toppel, A. L. Rago and D. M. O'Shea, MC^2, A Code to Calculate Multigroup Cross Sections, ANL-7318, Argonne National Laboratory, Argonne, IL, June 1967.

(To77) H. Tourwé, "Neutron Dosimetry Programme in the BR-3 Reactor Core 4B," Neutron Calculations: Geometrical Description and Composition of the Outer Regions, CEN/SCK 313/77-12/C, Centre d'Etude de l' Energie Nucleaire Studiecentrum voor Kernenergie, Mol, Belgium, September 29, 1977.

(To80) H. Tourwé and N. Maene, "Fast Neutron Fluence Measurement with the $^{93m}Nb(N,n')^{93}Nb$ Reaction," Proc. of the 3rd ASTM-EURATOM Symposium on Reactor Dosimetry, Ispra, Italy, October 1-5, 1979, EUR 6813, Commission of the European Communities, 1980.

(To82) H. Tourwé and G. Minsart, "Surveillance Capsule Perturbation Studies in the PSF 4/12 Configuration," Proc. of the 4th ASTM-EURATOM Symposium on Reactor Dosimetry, Gaithersburg, MD, March 22-26, 1982, NUREG/CR-0029, NRC, Washington, DC, Vol. 1, pp. 471-480, July 1982.

(To82a) H. Tourwé et al., "Interlaboratory Comparison of Fluence Neutron Dosimeters in the Frame of the PSF Start-Up Measurement Programme," Proc. of the 4th ASTM-EURATOM Symposium on Reactor Dosimetry, Gaithersburg, MD, March 22-26, 1982, NUREG/CP-0029, Vol. 1, pp. 159-168, NRC, Washington, DC, July 1982.

(Ts82) N. Tsoulfaniqis et al., "Calculation of Neutron Spectra at the Pressure Vessel and Cavity of a PWR," Proc. of the 4th ASTM-EURATOM Symposium on Reactor Dosimetry, Gaithersburg, MD, March 22-26, 1982, NUREG/CP-0029, Vol. 1, NRC, Washington, DC, pp. 519-532, July 1982.

(Ul75) G. Ullrich and B. Bürgisser, Nachbestrahlungsuntersuchungen an NOK-Reaktordruckgefäss Material der Kernkraftwerke Beznau II/1, Kapsel V, PB-ME-75/01, Nordostschweizerische Kraftwerke AG (NOK), Baden, Switzerland, October 1975.

(Ul80) G. Ullrich, B. Bürgisser and F. Hegedüs, Nachbestrahlungs-untersuchungen an NOK-Reaktordruckgefäss Material der Kern-kraftwerke Beznau II/2, Kapsel R, PB-ME-80/5, Nordostschweizerische Kraftwerke AG (NOK), Baden, Switzerland, April 1980.

(Va81) J. D. Varsik, "Evaluation of Irradiation Response of Reactor Pressure Vessel Materials," Semi-Annual Progress Report No. 3, July - December 1980, EPRI RP-1553-1, TR-MCM-110, Combustion Engineering Inc., Windsor, CT, 1981.

(Va82) J. D. Varsik, S. M. Schloss and J. M. Koziol, Evaluation of Irradiation Response of Reactor Pressure Vessel Materials, EPRI NP-2720, Electric Power Research Institute, Palo Alto, CA, 1982.

(Va83) J. D. Varsik, "An Empirical Evaluation of a Transition Temperature Shift in LWR-PV-SDIP Steels," from the ANS Special Session on Correlations and Implications of Neutron Irradiation Embrittlement of Pressure Vessel Steels, Detroit, MI, June 12-16, 1983, Trans. Am. Nucl. Soc. 44, p. 223, 1983.

(Ve80) V. V. Verbinski, C. G. Cassapakis, W. K. Hagen and G. L. Simmons, "Photointerference Corrections in Neutron Dosimetry for Reactor Pressure Vessel Lifetime Studies," Nucl. Sci. & Eng. 75, p. 159, 1980.

(Vi82) R. Viswanathan and R. I. Jaffee, "2-1/4Cr-1Mo Steels for Coal Conversion Pressure Vessels," J. Eng. Mater. & Tech., July 1982.

(Vl73) M. Vlasov and C. Dunford, Proc. of a Consultants' Meeting on Nuclear Data for Reactor Neutron Dosimetry, INDC(NDS)-56/U, International Atomic Energy Agency, Vienna, Austria, 1973.

(Vo77) D. R. Vondy, T. B. Fowler and G. W. Cunningham, VENTURE: A Code Block for Solving Multigroup Neutronics Problems Appliyng the Finite-Different Diffusion-Theory Approximation to Neutron Transport, Version II, ORNL-5016R2, Oak Ridge National Laboratory, Oak Ridge, TN, 1977.

(Wa74) J. Watanabe, "Temper Embrittlement of 2-1/4Cr-1Mo Pressure Vessel Steel," Paper presented at ASME 29th Petroleum Mech. Eng. Conf., Dallas, TX, September 15-18, 1974.

(Wa75) S. R. Wagner, "The Treatment of Systematic Errors Which Cannot Be Quantitatively Assessed with the Aim to Characterize the Accuracy of a Measurement," Proc. of the Symposium on Measurement Theory-Measurement Error Analysis, Enschede, The Netherlands, December 11-13, 1975, International Measurement Confederation, IMEKO Secretariat, Budapest, Hungary.

(We83) L. Weise, Neutron Spectra Unfolding from Measured Detector Activations, Jül-1837, in German, KFA, Jülich, Federal Republic of Germany, 1983.

(Wh83) G. D. Whitman and R. W. McCulloch, "Pressurized-Thermal-Shock Experiments," Proc. of the 10th WRSR Information Meeting, Gaithersburg, MD, October 12-15, 1982, NUREG/CP-0041, NRC, Washington, DC, Vol. 4, pp. 262-271, January 1983.

(Wi65) R. S. Wilks, J. A. Desport and R. Bradley, Transmission Electron Microscopy of Neutron Irradiated α-Al_2O_3 Single Crystals, AERE-R-5103, Atomic Energy Research Establishment, Harwell, UK, 1965.

(Wi68) R. S. Wilks, "Neutron-Induced Damage in BeO, Al_2O_3 and MgO - A Review," J. Nucl. Mater. 26, p. 137, 1968.

(Wi82) M. L. Williams and R. E. Maerker, "Calculations of the Startup Experiments at the Poolside Facility," Proc. of the 4th ASTM-EURATOM Symposium on Reactor Dosimetry, Gaithersburg, MD, March 22-26, 1982, NUREG/CP-0029, NRC, Washington, DC, Vol. 1, pp. 149-158, July 1982.

(Wi83) M. L. Williams et al., "Validation of Neutron Transport Calculations in Benchmark Facilities for Improved Damage Fluence Predictions," Proc. of the 11th WRSR Information Meeting, Gaithersburg, MD, October 24-28, 1983, NUREG/CP-0048, Vol. 1-6, NRC, Washington, DC.

(Wi83a) M. L. Williams, Report of Foreign Travel to CEN/SCK, Mol, Belgium, ORNL/FTR-1481, Oak Ridge National Laboratory, Oak Ridge, TN, April 11, 1983.

(Wi84) F. W. Wiffen et al., "Production Rate of Helium During Irradiation of Nickel in Thermal Spectrum Fission Reactors," J. Nucl. Mater., 1984.

(Wo81) D. W. Wootan, J. A. Rawlins, E. P. Lippincott, L. S. Kellogg, W. Y. Matsumoto and J. W. Daughtry, "Fission Rate Assessments in the FFTF Using Passive Techniques," Trans. Am. Nucl. Soc. 39, p. 901, December 1981.

(Wo82) D. W. Wootan, K. D. Dobbin, F. A. Schmittroth and J. H. Roberts, "Neutron Flux Spectra in the FFTF In-Reactor Thimble," HEDL-SA-2819, Hanford Engineering Development Laboratory, Richland, WA, December 1982.

(Wo83) S. Wood et al., "Microstructural and Microchemical Characterization of Irradiated Pressure Vessel Steels," from the ANS Special Session on Correlations and Implications of Neutron Irradiation Embrittlement of Pressure Vessel Steels, Detroit, MI, June 12-16, 1983, Trans. Am. Nucl. Soc. 44, p. 228, 1983.

(Wu75) R. A. Wullaert and J. W. Shuckherd, Evaluation of the First Maine Yankee Accelerated Surveillance Capsule, CR75-317, Effects Technology, Inc., Goleta Heights, CA, August 15, 1975.

(Ya67) S. E. Yanichko, Connecticut Yankee Reactor Vessel Radiation Surveillance Program, WCAP-7036, Westinghouse Electric Corp., Pittsburgh, PA, April 1967.

(Ya73) S. E. Yanichko et al., Analysis of Capsule S from Carolina Power and Light Company, H. B. Robinson Unit No. 2 Reactor Vessel Radiation Surveillance Program, WCAP-8249, Westinghouse Electric Corp., Pittsburgh, PA, December 18, 1973.

(Ya74) S. E. Yanichko, T. R. Mager and S. Kang, Analysis of Capsule R from the Rochester Gas and Electric Corporation, R. E. Ginna Unit No. 1 Reactor Vessel Radiation Surveillance Program, WCAP-8421, Westinghouse Electric Corp., Pittsburgh, PA, November 1974.

(Ya75) S. E. Yanichko, J. H. Phillips and S. L. Anderson, Analysis of Capsule T from the Florida Power and Light Company, Turkey Point Unit No. 3 Reactor Vessel Radiation Surveillance Program, WCAP-8631, Westinghouse Electric Corp., Pittsburgh, PA, December 1975.

(Ya76) S. E. Yanichko and S. L. Anderson, Analysis of Capsule S from the Wisconsin Electric Power Company and Wisconsin-Michigan Power Company, Point Beach Nuclear Plant Unit No. 1 Reactor Vessel Radiation Surveillance Program, WCAP-8739, Westinghouse Electric Corp., Pittsburgh, PA, 1976.

(Ya77) S. E. Yanichko, S. L. Anderson and K. V. Scott, Analysis of Capsule V from the Wisconsin Public Service Corporation, Kewaunee Nuclear Plant Reactor Vessel Radiation Surveillance Program, WCAP-8908, Westinghouse Electric Corp., Pittsburgh, PA, January 1977.

(Ya78) S. E. Yanichko and S. L. Anderson, Analysis of Capsule R from the Wisconsin Electric Power Company, Point Beach Nuclear Plant Unit No. 1 Reactor Vessel Radiation Surveillance Program, WCAP-9357, Westinghouse Electric Corp., Pittsburgh, PA, August 1978.

(Ya79) S. E. Yanichko, S. L. Anderson and W. T. Kaiser, Analysis of Capsule F from the Southern California Edison Company, San Onofre Reactor Vessel Radiation Surveillance Program, WCAP-9520, Westinghouse Electric Corp., Pittsburgh, PA, May 1979.

(Ya79a) S. E. Yanichko et al., Analysis of Capsule R from the Wisconsin Electric Power Company, Point Beach Nuclear Plant Unit No. 2 Reactor Vessel Radiation Surveillance Program, WCAP-9635, Westinghouse Electric Corp., Pittsburgh, PA, December 1975.

(Ya80) S. E. Yanichko et al., Analysis of Capsule T from the Salem Unit 1 Reactor Vessel Surveillance Program, WCAP-9678, Westinghouse Electric Corp., Pittsburgh, PA, February 1980.

(Ya81) S. E. Yanichko, S. L. Anderson and W. T. Kaiser, Analysis of Capsule V from Northern States Power Company, Prairie Island Unit No. 2 Reactor Vessel Radiation Surveillance Program, WCAP-9877, Westinghouse Electric Corp., Pittsburgh, PA, March 1981.

(Ya81a) S. E. Yanichko et al., Analysis of Capsule U from the Commonwealth Edison Company, Zion Nuclear Plant Unit No. 1 Reactor Vessel Radiation Surveillance Program, WCAP-9890, Westinghouse Electric Corp., Pittsburgh, PA, March 1981.

(Ya81b) S. E. Yanichko et al., Analysis of the Maine Yankee Reactor Vessel Second Accelerated Surveillance Capsule, WCAP-9875, Westinghouse Electric Corp., Pittsburgh, PA, March 1981.

(Ya81c) S. E. Yanichko et al., Analysis of the Third Capsule from the Commonwealth Edison Company, Quad-Cities Unit 1 Nuclear Plant Reactor Vessel Radiation Surveillance Program, WCAP-9920, Westinghouse Electric Corp., Pittsburgh, PA, August 1981.

(Ya82) S. E. Yanichko et al., Analysis of the Fourth Capsule from the Commonwealth Edison Company, Dresden Unit 3 Nuclear Plant Reactor Vessel Radiation Surveillance Program, WCAP-10030, Westinghouse Electric Corporation, Pittsburgh, PA, January 1982.

(Ya82a) S. E. Yanichko et al., Analysis of the Third Capsule from the Commonwealth Edison Company, Quad Cities Unit 2 Nuclear Plant Reactor Vessel Radiation Surveillance Program, WCAP-10064, Westinghouse Electric Corporation, Pittsburgh, PA, April 1982.

(Yo58) D. A. Young, "Etching of Radiation Damage in Lithium Fluoride," Nature 182, p. 375, 1958.

(Yo73) H. H. Yoshikawa, "Materials Performance Prediction from Irradiation Test Data," Effects of Radiation on Substructure and Mechanical Properties of Metals and Alloys, ASTM STP 529, American Society for Testing and Materials, Philadelphia, PA, pp. 337-348, 1973.

(Zi75) W. H. Zimmer, R. R. Heinrich, L. S. Kellogg and W. Y. Matsumoto, "High Flux Level Reaction Rate Measurements," Nucl. Technol. 25, (2), p. 289, February 1975.

(Zi79) W. L. Zijp and J. H. Baard, Nuclear Data Guide for Reactor Neutron Metrology, Parts I and II, EUR 7167, Energieonderzoek Centrum Nederland, Petten, Netherlands, August 1979.

(Zi82) W. L. Zijp et al., "Comparison of Measured and Evaluated Spectrum-Averaged Cross-Section Data," Proc. of the 4th ASTM-EURATOM Symposium on Reactor Dosimetry, Gaithersburg, MD, March 22-26, 1982, NUREG/CP-0029, NRC, Washington, DC, Vol. 2, pp. 725-743, July 1982.

(Zi82a) W. L. Zijp and F. W. Stallmann, "Workshop on Spectrum Adjustment Procedures," Proc. of the 4th ASTM-EURATOM Symposium on Reactor Dosimetry, Gaithersburg, MD, March 22-26, 1982, NUREG/CP-0029, NRC, Washington, DC, Vol. 2, pp. 1221-1230, July 1982.

(Zi82b) W. L. Zijp et al., "Status Report on the REAL-80 Exercise," Proc. of the 4th ASTM-EURATOM Symposium on Reactor Dosimetry, Gaithersburg, MD, March 22-26, 1982, NUREG/CP-0029, NRC, Washington, DC, Vol. 2, pp. 1089-1110, July 1982.

(Zi83) W. L. Zijp et al., Final Report of REAL-80 Exercise, ECN-128, Netherlands Energy Research Foundation, Petten, The Netherlands, February 1983.

DISTRIBUTION

R5

DOE-HQ/Office of Converter
Reactor Deployment
Nuclear Regulation & Safety Division
NE-12
Washington, DC 20545

JD Griffith, Deputy Director

DOE-HQ/Office of Breeder
Technology Projects (8)
NE-53
Washington, DC 20545

H. Alter, Asst Director, Safety
DF Bunch, Director, Office of Breeder Technology Projects
PB Hemmig, Asst Director, Reactor Physics Technology
JW Lewellen, Manager, Core Analysis Technology
DK Magnus, Director, Fuels & Core Materials
RJ Neuhold, Director, Safety & Physics
CM Purdy, Asst Director, Materials & Structures Tech
A. Van Echo, Manager, Metallurgy, Absorbers & Standards

DOE-RL/AME
Breeder Technology Division
Technology Development Branch
P.O. Box 550, FED/210
Richland, WA 99352

KR Absher, Chief

Arizona State University (2)
College of Eng & Appl Sciences
Tempe, AZ 85287

JW McKlveen
B. Stewart

Argonne National Laboratory (2)
9700 South Cass Avenue
Argonne, IL 60439

RJ Armani
RR Heinrich, Bldg 316

Babcock & Wilcox Co
Lynchburg Research Center (4)
P.O. Box 1260
Lynchburg, VA 24505

LB Gross AA Lowe Jr
RH Lewis CL Whitmarsh

Battelle
Pacific Northwest Laboratory
P.O. Box 999
Richland, WA 99352

EP Simonen

Battelle Memorial Institute
505 King Avenue
Columbus, OH 43201

MP Manahan

Bechtel Power Corporation
15740 Shady Grove Road
Gaithersburg, MD 20760

WC Hopkins

Brookhaven National Laboratory (3)
National Neutron Cross-Section Center
Upton, Long Island, NY 11973

JF Carew BA Magurno
S. Pearlstein, Bldg T-197

Burns & Roe Inc
633 Industrial Avenue
Paramus, NJ 07672

J. Celnik

DISTRIBUTION (Cont'd)

Carolina Power & Light Co
P.O. Box 1551
Raleigh, SC 27602

SP Grant

Centre d'Etude de l'Energie Nucléaire
Studiecentrum voor Kernenergie (6)
Boeretang 200
B-2400 Mol, Belgium

J. Debrue
G. DeLeeuw
S. DeLeeuw
A. Fabry
G. Minsart
Ph Van Asbroeck

Combustion Engineering Inc (5)
1000 Prospect Hill Road
Windsor, CT 06095

S. Byrne
G. Cavanaugh
JJ Koziol
RG Shimko
D. Stephen

Comitato Nazional per Energia Nucléare
Centro di Studi Nucleari della Casaccia
Casella Postale 2400
Santa Maria di Galeria
I-00060 Rome, Italy

U. Farinelli

Commissariat a l'Energie Atomique
Centre d'Etudes Nucleaires de Saclay (6)
Boite Postale 2
91190 Gif-sur-Yvette, France

AA Alberman
C. Buchalet
(Framatome)
JM Cerles
JP Genthon
P. Mas
(Grenoble)
P. Petrequin

Commonwealth Edison
P.O. Box 767
Chicago, IL 60690

E. Steeve

EG&G Idaho Inc (3)
P.O. Box 1625
Idaho Falls, ID 83415

RC Greenwood
Y. Harker
JW Rogers

EG&G Ortec Inc
100 Midland Road
Oak Ridge, TN 37830

W. Zimmer

Electric Power Research Institute (7)
3412 Hillview Avenue
P.O. Box 10412
Palo Alto, CA 94304

TU Marston
O. Ozer
T. Passell
AD Rossin
R. Shaw
K. Stahlkopf
JJ Taylor

Energieonderzoek Centrum Nederland
Westerdionweg 3
Postfach 1
NL-1755 ZG, Petten, The Netherlands

WL Zijp

Engineering Services Associates
3320 Bailey
Buffalo, NY 14215

M. Haas

EURATOM
Joint Research Center Ispra (2)
I-21020 Ispra, Varese, Italy

R. Dierckx
H. Rief

DISTRIBUTION (Cont'd)

Fracture Control Corporation
5951 Encina Road, No. 105
Goleta, CA 93117

P. McConnell

Fracture Control Corporation
2041 Willowick Drive
Columbus, OH 43229

JS Perrin

General Electric Co
Vallecitos Nuclear Center
P.O. Box 460
Pleasanton, CA 94566

GC Martin

IKE-Stüttgart (2)
Institüt für Kernenergetik
und Energiesysteme
Pfaffenwaldring 31, Postfach 801140
D-7000, Stüttgart 80 (Vaihingen)
Federal Republic of Germany

G. Hehn
G. Prillinger

International Atomic Energy Agency (2)
Wagramerstrasse 5
Postfach 100
A-1400 Vienna, Austria

A. Sinev
JJ Schmidt

IRT Corporation (3)
P.O. Box 80817
San Diego, CA 92183

NA Lurie WE Selph
C. Preskitt

Italian Atomic Power Authority
National Electric Energy Agency (2)
Viale Regina Margherita 137
Rome, Italy

M. Galliani
F. Remondino

Japan Atomic Energy Research Institute (2)
Tokai Research Establishment
Tokai-mura, Naka-gun
Ibaraki-ken, Japan

S. Mizazono
K. Sakurai

Kernforschungsanlage Jülich GmbH (3)
Postfach 1913
D-517 Jülich 1,
Federal Republic of Germany

D. Pachur L. Weise
W. Schneider

Kraftwerk Union Aktiengesellschaft (5)
Postfach 3220
D-8520 Erlangen,
Federal Republic of Germany

A. Gerscha J. Koban
U. Groschel C. Leitz
W. Hofmann

Los Alamos National Laboratory (2)
P.O. Box 1663
Los Alamos, NM 87545

GE Hansen, Group N-2
L. Stewart

Maine Yankee Atomic Power Co
Edison Drive
Augusta, MA 04336

HF Jones Jr

DISTRIBUTION (Cont'd)

Materials Engineering Associates Inc
111 Mel-Mara Drive
Oxen Hill, MD 20021

JR Hawthorne

Max-Planck-Institüt
für Plasma Physik
The NET Team
D-8046 Garching bei München,
Federal Republic of Germany

DR Harries, Technology

National Bureau of Standards
Center of Radiation Research (6)
Washington, DC 20234

RS Caswell
CM Eisenhauer
DM Gilliam
JA Grundl
G. Lamaze
ED McGarry

Naval Research Laboratory
Engineering Materials Division
Thermostructural Materials Branch
Code 6390
Washington, DC 20375

LE Steele

Nuclear Regulatory Commission (17)
Office of Nuclear Regulatory Research
Division of Engineering Technology
Materials Engineering Branch
NL-5650
Gaithersburg, MD 20899

Chief
Public Doc Rm (3)
M. Bolotski
M. Dunenseld
R. Gamble
W. Hazelton
KG Hoge
RE Johnson
L. Lois
S. Pawlicki
PN Randall
CZ Serpan
D. Sieno
A. Taboada
M. Vagin

Oak Ridge National Laboratory (8)
P.O. Box X
Oak Ridge, TN 37830

CA Baldwin, Bldg 3091
RG Berggren
FBK Kam
AL Lotts
RE Maerker
LS Miller
R. Nanstad
FW Stallmann

Radiation Research Associates (2)
3550 Hulen Street
Fort Worth, TX 76107

RM Rubin
MB Wells

Rockwell International
Energy Systems Group (2)
P.O. Box 309
Canoga Park, CA 91304

H. Farrar IV
BM Oliver

Rolls-Royce & Associates Ltd (4)
P.O. Box 31
Derby DE2 8BJ, UK

M. Austin
P. Burch
AF Thomas
TJ Williams

S.A. Cockerill-Ougree
Recherches et Developments
Division de la Construction Mecanique
B-4100 Seraing, Belgium

J. Widart

Science Applications Inc (3)
P.O. Box 2325
La Jolla, CA 92037

W. Hagan
GL Simmons
VV Verbinski

DISTRIBUTION (Cont'd)

Ship Research Institute
Tokai Branch Office
Tokai-mura, Naka-gun
Ibaraki-ken, Japan

K. Takeuchi

Southwest Research Institute
8500 Calebra Road
P.O. Box 28510
San Antonio, TX 78284

EB Norris

Swiss Federal Institute
for Reactor Research
CH-5303 Würenlingen, Switzerland

F. Hegedus

United Kingdom Atomic Energy Authority
Atomic Energy Research Establishment (2)
Harwell, Oxon OX11 ORA, UK

LM Davies
AJ Fudge

United Kingdom Atomic Energy Authority
Atomic Energy Establishment (4)
Winfrith, Dorchester, Dorset, UK

J. Butler
CG Campbell
AK McCracken
J. Sanders

University of Arkansas (2)
Dept of Mechanical Engineering
Fayetteville, AR 72701

CO Cogburn
L. West

University of California
at Santa Barbara (2)
Dept of Chem & Nucl Engineering
Santa Barbara, CA 93106

G. Lucas
GR Odette

Univ of London Reactor Center
Silwood Park, Sunnyhill,
Ascot, Berkshire SL5 7PY, UK

JA Mason

University of Tokyo (2)
Dept of Nuclear Engineering
7-3-1, Hongo
Bunkyo-ku, Tokyo, 113 Japan

M. Nakazawa
J. Sekiguchi

Westinghouse
Nuclear Energy Systems (4)
P.O. Box 355
Pittsburgh, PA 15230

SL Anderson
TR Mager
RC Shank
SE Yanichko

Westinghouse
Research and Development Center
1310 Beulah Road
Pittsburgh, PA 15235

JA Spitznagel

University of Missouri at Rolla (2)
Dept of Nucl Engineering
Building C
Rolla, MO 65401

DR Edwards
N. Tsoulfanidis

DISTRIBUTION (Cont'd)

HEDL (46)
c/o Supervisor, Documentation
P.O. Box 1970, W/C-123
Richland, WA 99352

HJ Anderson	W/C-28	JP McNeece	W/A-56
RA Bennett	W/D-3	JE Nolan	W/B-65
LD Blackburn	W/A-40	RE Peterson	W/B-66
DG Doran	W/A-57	CC Preston	W/C-39
EA Evans	W/C-23	JH Roberts	W/C-39
DS Gelles	W/A-65	FH Ruddy	W/C-39
R. Gold	W/C-39	JM Ruggles	W/C-33
GL Guthrie	W/A-40	RE Schenter	W/A-58
BR Hayward	W/C-44	FA Schmittroth	W/A-58
LA James	W/A-40	WF Sheely	W/C-44
LS Kellogg	W/C-39	FR Shober	W/E-3
NE Kenny	W/C-115	RL Simons	W/A-65
RL Knecht	W/A-40	HH Yoshikawa	W/C-44
JJ Laidler	W/B-107	Program Files (10)	W/C-39
EP Lippincott (2)	W/C-39	Central Files (2)	W/C-110
WY Matsumoto	W/C-33	Microfilm Services	W/C-123
WN McElroy (2)	W/C-39		

NRC FORM 335 (2-84) NRCM 1102, 3201, 3202

U.S. NUCLEAR REGULATORY COMMISSION

BIBLIOGRAPHIC DATA SHEET

SEE INSTRUCTIONS ON THE REVERSE

1. REPORT NUMBER (Assigned by TIDC, add Vol. No., if any)

NUREG/CR-3318
HEDL-TME 84-1

2. TITLE AND SUBTITLE

LWR PRESSURE VESSEL SURVEILLANCE DOSIMETRY IMPROVEMENT PROGRAM: PCA EXPERIMENTS, BLIND TEST, AND PHYSICS-DOSIMETRY SUPPORT FOR THE PSF EXPERIMENTS

3. LEAVE BLANK

4. DATE REPORT COMPLETED

MONTH	YEAR
August	1984

5. AUTHOR(S)

Edited by W. N. McElroy

6. DATE REPORT ISSUED

MONTH	YEAR
September	1984

7. PERFORMING ORGANIZATION NAME AND MAILING ADDRESS (Include Zip Code)

Hanford Engineering Development Laboratory
P.O. Box 1970
Richland, WA 99352

8. PROJECT/TASK/WORK UNIT NUMBER

9. FIN OR GRANT NUMBER

B5988

10. SPONSORING ORGANIZATION NAME AND MAILING ADDRESS (Include Zip Code)

Division of Engineering Technology
Office of Nuclear Regulatory Research
U.S. Nuclear Regulatory Commission
Washington, D.C. 20555

11a. TYPE OF REPORT

Technical

b. PERIOD COVERED (Inclusive dates)

12. SUPPLEMENTARY NOTES

13. ABSTRACT (200 words or less)

This report was prepared to: 1) Serve as a general reference document containing benchmarked experimental and theoretical data and information required to determine and certify the accuracy of the experimental and analytical methods and data that are recommended in a series of ASTM LWR pressure vessel surveillance standards; 2) Provide detailed experimental and theoretical results to determine the limiting accuracy of transport theory calculations for predicting dosimetry sensor reaction rates and derived values of neutron exposure parameters (total fluence, fluence greater than 0.1 and 1.0 MeV, and dpa) for LWR pressure vessel benchmark fields simulating steel-water configurations of commercial power reactors; 3) Assess the accuracy of the methodology used to translate measured pressure vessel steel damage and exposure data (and the corresponding uncertainties) obtained at surveillance locations to the pressure vessel beltline region; 4) Provide PCA 4/12 and 4/12 SSC configurations' experimental and theoretical physics-dosimetry results in support of the "PSF Experiments and Blind Test."

After an executive summary, a description of the PCA experimental test facility is provided in Section 1 followed by the presentation and discussion of experimental measurements and data in Sections 2, 3 and 4. The results of neutronic calculations by participants are given and referenced in Section 5. Current PCA specifications for transport theory validation are given in Section 6. The comparison and evaluation of measured and derived data are considered in Section 7.

14. DOCUMENT ANALYSIS - a. KEYWORDS/DESCRIPTORS

LWR pressure vessel surveillance
PCA experiments

b. IDENTIFIERS/OPEN-ENDED TERMS

15. AVAILABILITY STATEMENT

Unlimited

16. SECURITY CLASSIFICATION

(This page) Unclassified

(This report) Unclassified

17. NUMBER OF PAGES

18. PRICE